

# **Investigating MeCP2 Isoform-Specific Expression and Function**

By

**Robby Mathew Zachariah**

A Thesis submitted to the Faculty of Graduate Studies of

The University of Manitoba

In partial fulfillment of the requirements of the degree of

**DOCTOR OF PHILOSOPHY**

Department of Biochemistry and Medical Genetics

University of Manitoba

Winnipeg, Manitoba, Canada

Copyright © 2016 by Robby Mathew Zachariah

## Abstract

Methyl CpG Binding Protein 2 (MeCP2) is an epigenetic regulator capable of recognizing and binding to methylated DNA. Mutations in *MECP2* are the primary cause of Rett Syndrome (RTT) and *MECP2* Duplication Syndrome (MDS). RTT is a neurodevelopmental disorder that mainly affects young females. MDS on the other hand is 100% penetrant in males and is rarely reported in females. The two disorders, although caused by extremely different etiologies, exhibit many similarities in their phenotypes including but not limited to autistic features, learning impairments and seizures. However, the molecular basis of this phenotypic similarity remains unknown. No cure has been identified to date for RTT and MDS. Alternative splicing of *Mecp2/MECP2* leads to the generation of two isoforms, MeCP2E1 and MeCP2E2. Limited knowledge exists on the expression patterns and function of the two isoforms. In this thesis, I have attempted to address this knowledge gap by taking part in the validation of custom-made MeCP2 isoform-specific antibodies that are capable of differentially recognizing MeCP2E1 and MeCP2E2. Using the custom-made MeCP2E1-specific antibody, I also demonstrate that MeCP2E1 is expressed at much higher levels in neurons, as compared to astrocytes. My studies into the functional role of MeCP2 isoforms in neurons suggest that overexpression of both *MECP2E1* and *MECP2E2* leads to reduced *rRNA* levels in neurons. The potential role of MeCP2 as a negative regulator of neuronal *rRNA* biogenesis is further corroborated by direct binding of MeCP2 to the *rDNA* promoter, specifically the methylated fraction of *rDNAs*. Preliminary evidence from my studies suggests that *MECP2* duplication in mice leads to brain region-specific alterations in *rRNA* levels, specifically in the cerebellum. Thus, the data presented in this thesis addresses two important knowledge gaps in the field of MeCP2 research: the higher levels of

MeCP2E1 in neurons compared to astrocytes and the molecular consequences of *MECP2E1* and *MECP2E2* overexpression in neurons.

## **Acknowledgements**

My deepest and heartiest gratitude is offered to everybody who supported me and who were there for me during these past seven years. First and foremost, I express my sincere gratitude to my graduate advisor, Dr. Mojgan Rastegar for the continuous support, guidance and motivation she provided throughout my graduate studies. I joined her lab as a very inexperienced researcher and her steadfast support has been pivotal for my progress as a student and a scientist. I should especially thank her for encouraging me to think ‘outside the box’ and supporting me to develop those ideas to scientifically valid investigations. Thank you very much for giving me this wonderful opportunity and I strongly believe that I am very lucky to have you as my mentor.

My sincere thanks also goes to the members of my thesis advisory committee Dr. James Davie, Dr. Kirk McManus and Dr. Benedict Albensi for their insightful advice to improve my project and keeping me focused. I highly appreciate the support and guidance they provided in and outside committee meetings. I would also like to thank Dr. Paul Fernyhough for his mentorship as my committee member from 2009-2011.

Special thanks to Dr. Louise Simard, who mentored and guided me during my thesis revisions. Dr. Simard went above and beyond her responsibilities to help me and I will be thankful forever for her support. I would also like to express my heartfelt gratitude towards Dr. Mark Nachtigal, and Dr. Geoff Hicks for their support through a very stressful time. Their guidance was critical for the completion of this thesis in its present form, and will always be remembered.

Special thanks goes to Carl Olson from our lab. I have pestered Carl a lot with my daily barrage of queries, especially in the beginning of my studies. Carl’s patience and professionalism will always be an inspiration to me. I would also like to thank Benjamin Barber, whose friendship

and support will not be forgotten. I owe both Ben and Carl a lot for helping me avoid many faux pas when I first came to this country. Carl, Ben and Vichitra Liyanage from our lab have been a great support in my lab life and they made it a second home for me. We were a great team and together we achieved a lot. I would also like to acknowledge Chinelo Ezeonwuka, Dr. Wenjun Zhou and Prabhpreet Bassi for their support.

I thank Dr. Huda Zoghbi and her lab members for providing the RNA samples from *MECP2* Tg1 mice. Without their collaboration, the completion of the MDS mouse model part of the thesis would not have been possible.

I would also like to thank Dr. James Ellis, at the Hospital for Sick Children for providing cell lines (NIH3T3, Phoenix, and HEK293T cell lines), retroviral vectors (Retro-EF1 $\alpha$ -*MECP2E1*, and Retro-EF1 $\alpha$ -*MECP2E2*) and lentiviral vectors (Lenti-EF1 $\alpha$ -*MECP2E1* and Lenti-EF1 $\alpha$ -*MECP2E2*).

I gratefully acknowledge the financial support for the research of my thesis awarded to Dr. Rastegar by International Rett Syndrome Foundation (IRSF) (Award # 3212); Scottish Rite Charitable Foundation of Canada-10110 (SRCFC) (2010-2013); Natural Sciences and Engineering Research Council of Canada (NSERC DG-372405-2009) and (NSERC-DG 2016-06035); Manitoba Institute of Child Health (MICH) / Children's Hospital Research Institute of Manitoba (CHRIM) [seed funding for MeCP2E1-E2 antibody production, grant entitled: Generating MeCP2 Isoform-Specific Antibodies] (2009-2010); MICH/CHRIM consecutive Operating Grants 2009-2012); Manitoba Health Research Council (MHRC) Establishment Grant (2009-2012) and Health Sciences Centre Foundation Grant. I would also like to acknowledge the scholarship support from MHRC/Research Manitoba (2009-2011; 2012-2014).

The office staff of the Department of Biochemistry and Medical Genetics, especially Mrs. Cathy Webber, have helped me on many occasions to navigate the various intricate channels of administrative regulations. I would also like to acknowledge the former office staff of the Department, including Mrs. Tuntun Sarkar, Mrs. Jan Middleton, and Mrs. Nadia Burtniak for their support in the first few years of my studentship.

I owe a lot to my fun-loving friend circle. Sumi, Rony, and little angel Suri have been a second family to me away from my home. I cannot thank enough Biswajit, Ariff, Kannan, Vasu, Manoj and the whole ‘gang’ for all the fun we had. I would also like to Dr. Santhosh Thomas for all his help during the past seven years.

My deepest gratitude is offered to my parents, my brother Bobby and his family for being there for me and for their love which kept me strong during good and bad times.

I can state without any hesitation that without the unwavering support and unconditional love of my soulmate Vichy, I would not be writing this thesis. Her strengths have always complemented my weaknesses and have made me the man I am today, personally and professionally. Thank you Vichy for always being there for me, and for having faith in me at times that I had none. I know I have sacrificed our personal life quite a bit for my graduate studies, but I will make amends for it for the rest of our lives.

## **Dedication**

**Dedicated to my loving parents**

Mr. and Mrs. Zachariah Mathew

## TABLE OF CONTENTS

<b>ABSTRACT</b> .....	<b>II</b>
<b>ACKNOWLEDGEMENTS</b> .....	<b>IV</b>
<b>DEDICATION</b> .....	<b>VII</b>
<b>LIST OF TABLES</b> .....	<b>XVI</b>
<b>LIST OF FIGURES</b> .....	<b>XVIII</b>
<b>LIST OF ABBREVIATIONS</b> .....	<b>XXI</b>
<b>COPYRIGHT AND CONTRIBUTIONS</b> .....	<b>XXVII</b>
<b>Copyright Acknowledgement</b> .....	<b>xxvii</b>
Chapter 1 .....	xxvii
Chapter 3 .....	xxviii
<b>Acknowledgement of Contributions</b> .....	<b>xxx</b>
<b>THESIS OVERVIEW</b> .....	<b>XXXI</b>
<b>CHAPTER 1: INTRODUCTION</b> .....	<b>1</b>
<b>1.1 Chromatin and Epigenetics - Introduction and History</b> .....	<b>1</b>
1.1.1 Chromatin Remodeling .....	5
1.1.2 Histone Post-Translational Modifications .....	6
1.1.3 Non-Coding RNAs .....	7
<b>1.2 DNA methylation</b> .....	<b>8</b>
1.2.1 CpG methylation .....	10
1.2.2 Five (5)-Hydroxymethylcytosine .....	11
1.2.3 Non-CpG methylation .....	11
1.2.4 Writers of DNA methylation .....	13



1.2.4.1 DNA methyltransferases (DNMTs).....	13
1.2.5 DNA methyl-erasers and DNA demethylation.....	14
1.2.6 Readers of DNA methylation .....	15
1.2.6.1 MBD Protein Family.....	16
<b>1.3 MeCP2 .....</b>	<b>19</b>
1.3.1 <i>Mecp2/MECP2</i> gene and MeCP2 protein structure .....	19
1.3.2 MeCP2 functional domains .....	22
1.3.3 MeCP2 isoforms: expression and regulation.....	24
1.3.4 MeCP2 functions and target genes .....	25
<b>1.4 Rett Syndrome (RTT) .....</b>	<b>32</b>
1.4.1 RTT prevalence and phenotypes .....	32
1.4.2 MeCP2 and Rett Syndrome .....	33
1.4.3 <i>Mecp2</i> mouse models of RTT .....	33
1.4.4 Challenges for RTT therapy .....	34
<b>1.5 MECP2 Duplication Syndrome (MDS) .....</b>	<b>35</b>
1.5.1 Causes of MDS.....	35
1.5.2 Prevalence and phenotypes of MDS.....	36
1.5.3 Mouse models of MDS.....	37
1.5.3.1 <i>MECP2 Tg1</i> model.....	39
1.5.3.2 <i>Tau-Mecp2</i> mouse model .....	41
<b>1.6 Phenotypic overlap between RTT and MDS .....</b>	<b>42</b>
<b>1.7 Ribosomal RNA genomic organization, <i>rDNA</i> transcription, and processing .....</b>	<b>44</b>
1.7.1 Ribosomal RNA genomic organization.....	44

1.7.2 RNA polymerase I-mediated <i>rDNA</i> transcription .....	45
1.7.3 Epigenetic regulation of ribosome biogenesis.....	47
1.7.4 Ribosomal RNA processing .....	49
1.7.4.1 5'ETS processing.....	51
1.7.4.2 18S rRNA maturation.....	52
1.7.4.3 Maturation of 5.8S rRNA and 28S rRNA.....	53
<b>1.8 Role of epigenetics in neural differentiation and neuronal disorders .....</b>	<b>53</b>
1.8.1 The role of epigenetics in neurogenesis and neural cell function.....	54
1.8.2 Epigenetics and neurodevelopment (neurogenesis and brain development).....	56
1.8.3 Epigenetic modifiers involved in neuronal disorders .....	58
<b>1.9 MeCP2 and rRNA synthesis .....</b>	<b>59</b>
<b>1.10 Summary .....</b>	<b>60</b>
<b>1.11 Rationale, Hypotheses, and Research Aims.....</b>	<b>61</b>
1.11.1 Rationale.....	61
1.11.2 Hypotheses .....	63
1.11.3 Research aims .....	63
<b>CHAPTER 2: MATERIALS AND METHODS .....</b>	<b>64</b>
<b>2.1 Ethics statement.....</b>	<b>64</b>
<b>2.2 MeCP2 isoform-specific antibody production.....</b>	<b>64</b>
2.2.1 Peptide selection for antibody synthesis.....	64
2.2.2 Chicken anti-MeCP2E1 antibody generation .....	69
2.2.3 Rabbit anti-MeCP2E1 antibody generation.....	69
2.2.4 Chicken anti-MeCP2E2 antibody development .....	69

<b>2.3 Cell Culture.....</b>	<b>70</b>
2.3.1 Culture and maintenance of cell lines .....	70
2.3.2 Primary cortical neuron isolation .....	70
2.3.2.1 <i>Embryo harvest and preparation</i> .....	71
2.3.2.2 <i>Embryonic Forebrain dissection</i> .....	71
2.3.2.3 <i>Coating plates for neuron seeding</i> .....	71
2.3.2.4 <i>Dissociation, plating and initial culturing of the cortices</i> .....	72
2.3.2.5 <i>Maintenance of primary neuron culture</i> .....	72
2.3.3 Primary cortical astrocytes isolation and culture.....	73
2.3.3.1 <i>Dissociation, plating and initial culturing of the cortices</i> .....	73
2.3.3.2 <i>Maintenance of primary astrocyte culture</i> .....	74
<b>2.4 Lentiviral Transduction.....</b>	<b>74</b>
2.4.1 Plasmid amplification and purification.....	74
2.4.2 Generation of lentiviral particles .....	75
2.4.3 Transduction of primary neurons .....	75
<b>2.5 Retroviral Transduction.....</b>	<b>76</b>
2.5.1 Plasmid amplification and purification.....	76
2.5.2 Generation of retroviral particles.....	76
2.5.3 Transduction of NIH3T3 cells.....	76
<b>2.6 Immunocytochemistry (ICC) .....</b>	<b>76</b>
2.6.1 Fixation of cells .....	76
2.6.2 Primary/Secondary antibody addition .....	77
2.6.3 Imaging.....	80

2.6.4 Quantification of nuclear and nucleolar size .....	80
<b>2.7 Western blot.....</b>	<b>81</b>
2.7.1 Extraction and quantification of total cell lysates and nuclear fractions .....	81
2.7.2 Sodium dodecyl sulfate polyacrylamide gel electrophoresis (SDS-PAGE) and WB ..	82
2.7.3 Development of blots and quantification of signal intensity .....	83
<b>2.8 Quantitative reverse transcription real-time PCR (qRT-PCR).....</b>	<b>83</b>
<b>2.9 Chromatin immunoprecipitation (ChIP) and quantitative real-time PCR (qPCR) ...</b>	<b>86</b>
2.9.1 Calculation of ChIP percentage input.....	88
<b>2.10 ChIP-CHOP Assay .....</b>	<b>89</b>
<b>2.11 CHOP assay .....</b>	<b>90</b>
<b>2.12 MeCP2 ChIPseq data mining using CistromeDB .....</b>	<b>91</b>
<b>2.13 Statistical analysis .....</b>	<b>91</b>
<b>CHAPTER 3: ANALYSIS OF MECP2 ISOFORM-SPECIFIC EXPRESSION IN MURINE NEURAL CELLS USING CUSTOM-MADE ANTIBODIES.....</b>	<b>93</b>
<b>3.1 Background.....</b>	<b>93</b>
<b>3.2 General model for testing antibody specificity .....</b>	<b>94</b>
<b>3.3 Validation of anti-MeCP2E1 antibodies .....</b>	<b>95</b>
3.3.1 Peptide selection for the MeCP2E1 antibodies .....	96
3.3.2 Validation of the Chicken anti-MeCP2E1 antibody.....	96
3.3.3 Validation of the Rabbit anti-MeCP2E1 antibody .....	100
<b>3.4 Analysis of MeCP2 expression and localization in embryonic primary cortical neurons and astrocytes .....</b>	<b>103</b>

3.4.1 Characterization of total MeCP2 localization within the nucleus of primary embryonic cortical neurons.....	103
3.4.2 Determination of MeCP2E1 expression patterns in embryonic primary cortical neurons and astrocytes .....	105
<b>3.5 Validation of the Chicken anti-MeCP2E2 antibody .....</b>	<b>108</b>
3.5.1 Identification of a peptide to generate an anti-Chicken MeCP2E2 antibody .....	108
3.5.2 Validation of Chicken anti-MeCP2E2 antibody.....	108
<b>3.6 Discussion.....</b>	<b>113</b>
<b>CHAPTER 4: ANALYZING THE EFFECT OF NEURONAL <i>MECP2E1</i> AND <i>MECP2E2</i> OVEREXPRESSION ON <i>RRNA</i> BIOGENESIS.....</b>	<b>117</b>
<b>4.1 Background.....</b>	<b>117</b>
<b>4.2 Overexpression of <i>MECP2</i> isoforms in primary neurons.....</b>	<b>119</b>
<b>4.3 Analysis of <i>45S pre-rRNA</i> levels in <i>MECP2E1</i>- and <i>MECP2E2</i>-overexpressing neurons</b>	<b>121</b>
<b>4.4 Analysis of mature <i>rRNA</i> levels in <i>MECP2E1</i> and <i>MECP2E2</i> overexpressing neurons</b>	<b>122</b>
<b>4.5 Deregulation of <i>rRNA</i> synthesis in <i>MECP2</i> Tg1 mice.....</b>	<b>124</b>
<b>4.6 Summary of findings.....</b>	<b>126</b>
<b>4.7 Discussion.....</b>	<b>127</b>
<b>CHAPTER 5: EXPLORING THE POTENTIAL BINDING OF MECP2 TO <i>RDNA</i>.....</b>	<b>132</b>
<b>5.1 Introduction .....</b>	<b>132</b>
<b>5.2 Potential localization of MeCP2 within the neuronal nucleolus .....</b>	<b>132</b>
5.2.1 Localization of MeCP2 to the neuronal perinucleolar chromocenters .....	132

<b>5.3 Direct binding of MeCP2 to <i>rDNA</i>.....</b>	<b>136</b>
5.3.1 Analyzing direct binding of MeCP2 to the <i>rDNA</i> promoter .....	136
5.3.2 Analyzing direct binding of MeCP2 to the methylated/unmethylated fraction of <i>rDNAs</i> .....	140
<b>5.4 Analysis of DNA methylation at the <i>rDNA</i> promoters .....</b>	<b>141</b>
<b>5.5 Alterations in nucleolar and nuclear parameters by <i>MECP2E1</i> and <i>MECP2E2</i> overexpressing neurons.....</b>	<b>142</b>
5.5.1 Number of nucleoli (nucleolar coefficient) .....	143
5.5.2 Size of nucleoli .....	145
5.5.3 Size of nuclei in primary neurons.....	146
5.5.4 Nucleolar size normalized to nuclear size .....	147
<b>5.6 Discussion.....</b>	<b>148</b>
<b>CHAPTER 6: CONCLUSION AND FUTURE DIRECTIONS.....</b>	<b>152</b>
<b>6.1 Development of MeCP2 isoform-specific antibodies allowed the investigation of cell- type specific, spatial, and temporal expression patterns of MeCP2E1 and MeCP2E2 ..</b>	<b>152</b>
<b>6.2 Overexpression of MeCP2 isoforms is associated with downregulation of neuronal <i>rRNA</i> levels.....</b>	<b>154</b>
<b>6.3 MeCP2 binds to the methylated promoter of the <i>rDNA</i> .....</b>	<b>157</b>
6.3.1 Does MeCP2 bind to methylated <i>rDNA</i> promoter <i>in vivo</i> ? .....	157
6.3.2 Does MeCP2 bind to the methylated CpG -133 of the <i>rDNA</i> promoter?.....	159
6.3.3 Does MeCP2 bind to 5mC, 5hmC or both modifications at the <i>rDNA</i> promoters? ...	159
6.3.4 Do both MeCP2 isoforms bind to the <i>rRNA</i> promoter? .....	160

<b>6.4 Overexpression of MeCP2E1, but not MeCP2E2 leads to decreased methylation of the <i>rDNA</i> promoter</b> .....	<b>161</b>
6.4.1 Can the decrease in <i>rDNA</i> promoter methylation by MeCP2E1 be replicated?.....	161
6.4.2 What could be the potential mechanism/s for MeCP2 mediated demethylation?.....	162
6.4.3 Does overexpression of MeCP2 in MDS mice cerebellum lead to changes in <i>rDNA</i> methylation? .....	163
<b>6.5 Overexpression of MeCP2 leads to a decrease in <i>45S pre-rRNA</i> levels</b> .....	<b>164</b>
6.5.1 Does the decrease in <i>45S pre-rRNA</i> levels following the overexpression of MeCP2 isoforms correlate with alterations in <i>rDNA</i> transcription?.....	164
<b>6.6 Overexpression of MeCP2 leads to altered levels of mature <i>rRNAs</i></b> .....	<b>165</b>
6.6.1 Does the alteration in mature <i>rRNA</i> levels following the overexpression of MeCP2 isoforms correlate with alterations in <i>rRNA</i> processing? .....	165
<b>6.7 Does the alterations in mature <i>rRNA</i> levels following the overexpression of MeCP2 lead to decreased ribosome biogenesis?</b> .....	<b>165</b>
<b>6.8 Does MeCP2 overexpression lead to reduced protein synthesis?</b> .....	<b>166</b>
<b>6.9 Can change in mature <i>rRNA</i> levels by MeCP2 overexpression lead to compromised neuronal functions?</b> .....	<b>167</b>
<b>6.10 Summary</b> .....	<b>168</b>
<b>CHAPTER 7: REFERENCES</b> .....	<b>169</b>
<b>APPENDIX A: REAGENTS AND MATERIALS LIST</b> .....	<b>234</b>
<b>A1. Cortical Neuron Isolation</b> .....	<b>234</b>
Materials used.....	234
Other Materials .....	235

Reagent Preparation.....	235
<b>A2. Primary astrocyte isolation and culture.....</b>	<b>237</b>
Materials Used.....	237
Other Materials .....	238
Preparation of solutions and media .....	239
<b>A3. Salt shock total cell extraction buffer .....</b>	<b>240</b>



## List of Tables

### Chapter 1

Table 1.1 History of epigenetics.....	4
Table 1.2 A list of known MeCP2 target genes.....	28
Table 1.3 Mouse models of <i>MECP2</i> Duplication Syndrome.....	38
Table 1.4 Comparison of RTT ( <i>Mecp2<sup>tm1.1Bird-/y</sup></i> ) and MDS ( <i>MECP2</i> Tg1) mouse models.....	42

### Chapter 2

Table 2.1 Identification of peptide sequence for MeCP2 isoform-specific antibodies using Antigen Profiler Peptide Tool.....	68
Table 2.2 Primary antibodies used in ICC, WB and ChIP .....	78
Table 2.3 Secondary antibodies used in ICC and WB.....	79
Table 2.4 Primers used for qRT-PCR experiments.....	84
Table 2.5 Primers used for ChIP-qPCR experiments.....	88
Table 2.6 Primers used for ChIP-CHOP experiments.....	89
Table 2.7 ChIPseq datasets analyzed from CistromeDB.....	91

### Chapter 4

Table 4.1 Summary of findings of the <i>MECP2</i> overexpression and <i>MECP2</i> duplication mice studies.....	127
-----------------------------------------------------------------------------------------------------------------	-----

### Appendix

Table A1. Reagents used in cortical neuron isolation.....	235
-----------------------------------------------------------	-----

Table A2. Other materials used in cortical neuron isolation.....	236
Table A3. ACSF preparation.....	238
Table A4. Reagents used in primary astrocyte isolation and culture.....	239
Table A5. Other materials used in astrocyte culture.....	239

## List of Figures

### Chapter 1

Figure 1.1 Generation of different types of DNA methylation marks.....	9
Figure 1.2 Structural comparison of the members of Methyl CpG Binding Protein (MBP) family.....	18
Figure 1.3 Genome map of human and mouse <i>MECP2/Mecp2</i> genes.....	20
Figure 1.4 <i>MECP2/Mecp2</i> gene and protein isoforms MeCP2E1 and MeCP2E2.....	24
Figure 1.5 Multiple functions of MeCP2 in the brain.....	26
Figure 1.6 Phenotypic progression of <i>MECP2</i> Duplication Syndrome (MDS) in <i>MECP2</i> Tg1 mice .....	40
Figure 1.7 Phenotypic overlap of Rett Syndrome and <i>MECP2</i> Duplication Syndrome.....	43
Figure 1.8 Ribosome biogenesis and protein synthesis.....	44
Figure 1.9 Ribosomal RNA ( <i>rRNA</i> ) processing in mammalian cells.....	50

### Chapter 2

Figure 2.1 Amino acid sequence alignments of human and mouse MeCP2 isoforms.....	66
Figure 2.2 Selection of peptide sequence for anti-MeCP2E1 and anti-MeCP2E2 antibodies.....	67
Figure 2.3 Primer locations for 45S <i>pre-rRNA</i> , 18S <i>rRNA</i> and 28S <i>rRNA</i> .....	85
Figure 2.4 Schematic representation of ChIP-ChOP Assay.....	90

### Chapter 3

Figure 3.1 Validation of the newly developed chicken anti-MeCP2E1 antibody.....	98
Figure 3.2 Controls for MeCP2 overexpression in NIH3T3 cells.....	99

Figure 3.3 Validation of the custom-made rabbit MeCP2E1 antibody.....	102
Figure 3.4 Nuclear localization of total MeCP2 and heterochromatin marks in primary neurons.	104
Figure 3.5 Expression of total MeCP2 and MeCP2E1 in primary neurons and astrocytes.....	107
Figure 3.6 Validation of the chicken anti-MeCP2E2 antibody .....	110
Figure 3.7. Additional controls for chicken anti-MeCP2E2 antibody validation.....	111

## Chapter 4

Figure 4.1 Lentiviral <i>MECP2E1</i> , <i>MECP2E2</i> overexpression vectors and <i>EGFP</i> control vector..	119
Figure 4.2 Confirmation of neuronal overexpression of <i>MECP2</i> isoforms.....	120
Figure 4.3 Effect of <i>MECP2</i> overexpression on <i>45S pre-rRNA</i> levels.....	122
Figure 4.4 Effect of <i>MECP2</i> overexpression on mature <i>rRNA</i> levels.....	123
Figure 4.5 Analysis of <i>45S pre-rRNA</i> levels in brain regions of <i>MECP2</i> Tg1 mice (Tg).....	124
Figure 4.6 Analysis of processed <i>rRNAs</i> in brain regions of <i>MECP2</i> Tg1 mouse model (Tg).....	125

## Chapter 5

Figure 5.1 Localization of MeCP2 to perinucleolar chromocenters in primary neurons.....	134
Figure 5.2 Co-localization of MeCP2 and 5mC in the nucleus of primary neurons.....	135
Figure 5.3 MeCP2 binding to the promoter of the <i>rDNA</i> .....	137
Figure 5.4 Enrichment of MeCP2 at the <i>rDNA</i> in mouse embryonic stem cells, neurons and cerebellum.....	139
Figure 5. Determination of MeCP2 binding to the methylated <i>rDNA</i> fraction in primary cortical neurons.....	141
Figure 5.6 CHOP assay for <i>rDNA</i> promoters in neurons overexpressing <i>MECP2</i> .....	142

Figure 5.7 Analysis of the nucleolar coefficient in neurons overexpressing *MECP2* isoforms.....144

Figure 5.8 Analysis of the nucleolar size in *MECP2*-overexpressing neurons.....145

Figure 5.9 Analysis of nuclear size in *MECP2*-overexpressing neurons.....146

Figure 5.10 Nucleolar size normalized against nuclear size in *MECP2*-overexpressing neurons.....147

**Chapter 6**

Figure 6.1 Proposed model for *MeCP2*'s effect on neuronal *rRNA* levels and its potential downstream role.....157

## List of Abbreviations

Standard gene symbols were not considered as abbreviations and therefore not included here.

<b>Abbreviation</b>	<b>Full Form</b>
5caC	5-carboxycytosine
5fC	5-formylcytosine
5hmC	5-hydroxymethylcytosine
5hmU	5-hydroxymethyluracil
5mC	5-methylcytosine
ACSF	Artificial Cerebrospinal Fluid
ADP	Adenosine Diphosphate
ANOVA	Analysis of Variance
AP	Apurinic/Apyrimidinic sites
ATP	Adenosine Triphosphate
ATRX	Alpha-thalassemia mental retardation syndrome
BER	Base Excision Repair
BSA	Bovine Serum Albumin
BTB/POZ	Broad-Complex, Tramtrack and Bric a brac/ POxvirus and Zinc finger domain.
CA	Cytosine Arabinoside
CDD	Conserved Domain Database
cDNA	complementary DNA
CH <sub>3</sub>	Methyl
CHD	Chromodomain-Helicase-DNA binding
ChIP	Chromatin Immunoprecipitation

cHS4	chicken $\beta$ -globin locus Hypersensitive Site 4
cPPT	central Poly Purine Tract
Ct	Threshold cycle
CTD	C-terminal domain
CTS	Central Terminal Sequence
CXXC	Zinc-finger motifs
DAPI	4',6-diamidino-2-phenylindole
DMEM	Dulbecco's Modified Eagle Medium
DNA	Deoxyribonucleic acid
DNase	Deoxyribonuclease
DNMTs	DNA methyl transferases
E	Embryonic Day
E-repeats	Glutamic Acid Repeats
EBSS	Earle's Balanced Salt Solution
EGFP	Enhanced Green Fluorescent Protein
EMBOSS	European Molecular Biology Open Software Suite
ENCODE	Encyclopedia of DNA Elements
ESCs	Embryonic Stem Cells
EST	Expressed Sequence Tags
ETS	External Transcribed Sequence
FBS	Fetal Bovine Serum
FITC	Fluorescein Isothiocyanate
GR	Glycine and arginine residues

h	Hours
HBSS	Hank's Balanced Salt Solution
HDACs	Histone Deacetylases
hMeDIP	Hydroxymethylated DNA Immunoprecipitation
HPLC	High Performance Liquid Chromatography
hPTM	Histone Post-translational modifications
ICC	Immunocytochemistry
ICF	Immunodeficiency, Centromere Instability, Facial Anomalies
ID	Interdomain
IF	Immunofluorescence
IGSs	Intergenic Spacers
IHC	Immunohistochemistry
INO80	Inositol Requiring 80
ISW1	Imitation SWItch
ITS	Internal Transcribed Sequence
KAT	Lysine Acetyltransferase
KMT	Lysine Methyltransferase
LB	Luria-Bertani
lncRNA	Long non-coding RNAs
MBD	Methyl Binding Domain
MBP	Methyl Binding Protein
mCG	CpG dinucleotides
MDS	<i>MECP2</i> Duplication Syndrome



MeCP2	Methyl CpG Binding Protein 2
MeDIP	Methylated DNA Immunoprecipitation
MEM	Minimum Essential Medium
MeP	<i>Mecp2</i> Endogenous Promoter
mHC	non-CpG methylation
min	Minutes
miRNAs	microRNAs
NATs	Natural antisense transcripts
ncRNAs	non-coding RNAs
NGS	Normal Goat Serum
NoRC	Nucleolar Remodelling Complex
NORs	Nucleolar Organizer Regions
NSCs	Neural Stem Cells
NTD	N-terminal domain
NURD	Nucleosome Remodeling and Deacetylase
O <sub>2</sub>	Oxygen
PAC	P1-derived artificial chromosome
PBS	Phosphate Buffered Saline
PD	Parkinson's Disorder
PFA	Paraformaldehyde
PIC	Pre-initiation complex
piRNAs	piwi-interacting RNAs
PoII	RNA Polymerase I

PRFs	Pre-Ribosomal Factors
pRNA	promoter-associated RNA
PTM	Post-translational Modifications
PTRF	RNA Polymerase I associated Transcript Release Factor
qPCR	quantitative Real-time PCR
qRT-PCR	Quantitative Reverse Transcription Real-time PCR
RNA	Ribonucleic acid
ROI	Region of Interest
RPs	Ribosomal Proteins
RRDX	Rhodamine Red-X
RRE	Rev-Responsive Element
<i>rRNA</i>	Ribosomal RNA
RTT	Rett Syndrome
SAM	S-adenosyl methionine
SANT	Swi3, Ada2, N-Cor, TFIIB
SDS-PAGE	Sodium Dodecyl Sulfate Polyacrylamide Gel Electrophoresis
SEM	Standard Error of Mean
shRNA	short hairpin RNA
SLIDE	SANT-like ISWI domain
snoRNA	small nucleolar RNAs
snoRNPs	small nucleolar Ribonucleoprotein Particles
snRNA	small nuclear RNAs
SOC	Super Optimal Broth with Catabolite Repression

SWI/SNF	switching defective/sucrose non-fermenting
TAF	TBP-associated Factors
TALEN	Transcription activator-like effector nucleases
TBP	TATA-box binding protein
TBST	Tris-Buffered Saline (TBS) Solution with 0.2% Detergent Tween 20
TDG	DNA glycosylase
TET	Ten Eleven Translocation
TLC	Thin-layer Chromatography
TRD	Transcription Repression Domain
tRNA	transfer RNAs
TTF1	Transcription Termination Factor for PolII
TSS	Transcription Start Sites
UBF	Upstream Binding Factor
UCE	Upstream Control Element
UCSC	University Of California Santa Cruz
UD	Undigested DNA
UTR	Untranslated Region
WB	Western Blot
WT	Wild type
XCI	X-chromosome Inactivation

## Copyright and Contributions

### Copyright Acknowledgement

#### Chapter 1

- Figure 1.5 and Table 1.2 is taken from Zachariah RM, Rastegar M (2012) Linking epigenetics to human disease and Rett syndrome: the emerging novel and challenging concepts in MeCP2 research. *Neural Plast* 2012: 415825

Copyright permission to include the figure and table was obtained from Hindawi publishers. The email communication indicating the permission to re-use the material is shown below.

“I apologize for not replying earlier. Open-access authors retain the copyrights of their papers, and all open-access articles are distributed under the terms of the Creative Commons Attribution License, which permits unrestricted use, distribution and reproduction in any medium, provided that the original work is properly cited.

Please feel free to contact me if you have further inquiries.”

Best regards,

Radwa Ibrahim

Editorial Office

Hindawi Publishing Corporation

<http://www.hindawi.com/>

- Figure 1.9 and its figure legend is taken from Henras AK, Plisson-Chastang C, O'Donohue MF, Chakraborty A and Gleizes PE (2015). An overview of pre-ribosomal RNA processing in eukaryotes, Wiley Interdiscip Rev RNA 6: 225-242.

Copyright permission to include the figure was obtained from Wiley.com and is detailed below.

11/27/2016 Rightslink® by Copyright Clearance Center



**WILEY**

**RightsLink®**

Home Create Account Help 

**Title:** An overview of pre ribosomal RNA processing in eukaryotes

**Author:** Anthony K. Henras, Célia Plisson Chastang, Marie Françoise O'Donohue, Anirban Chakraborty, Pierre Emmanuel Gleizes

**Publication:** WILEY INTERDISCIPLINARY REVIEWS: RNA

**Publisher:** John Wiley and Sons

**Date:** Oct 27, 2014

© 2014 The Authors. WIREs RNA published by John Wiley & Sons, Ltd.

LOGIN

If you're a copyright.com user, you can login to RightsLink using your copyright.com credentials. Already a RightsLink user or want to [learn more?](#)

**Open Access Article**

This article is available under the terms of the Creative Commons Attribution Non-Commercial License CC BY-NC (which may be updated from time to time) and permits non-commercial use, distribution and reproduction in any medium, provided the original work is properly cited.

For an understanding of what is meant by the terms of the Creative Commons License, please refer to [Wiley's Open Access Terms and Conditions](#).

Permission is not required for non-commercial reuse. For commercial reuse, please hit the "back" button and select the most appropriate commercial requestor type before completing your order.

### Chapter 3

- The results presented in Chapter 3 are adapted from two publications of which I am an equally contributing first author (\*).
  - Zachariah RM\*, Olson CO\*, Ezeonwuka C, Rastegar M (2012) Novel MeCP2 isoform-specific antibody reveals the endogenous MeCP2E1 expression in murine brain, primary neurons and astrocytes. PLOS ONE 7: e49763.

- Olson CO\*, Zachariah RM\*, Ezeonwuka CD\*, Liyanage VR, Rastegar M (2014) Brain region-specific expression of MeCP2 isoforms correlates with DNA methylation within *Mecp2* regulatory elements. PLOS ONE 9: e90645.

I have obtained copyright permission to include the sections I have contributed to these two studies.

The email communication indicating the permission to re-use the material is shown below.

“Thank you for your message. PLOS ONE publishes all of the content in the articles under an open access license called “CC-BY.” This license allows you to download, reuse, reprint, modify, distribute, and/or copy articles or images in PLOS journals, so long as the original creators are credited (e.g., including the article’s citation and/or the image credit). Additional permissions are not required. You can read about our open access license here: <https://www.plos.org/open-access/>. There are many ways to access our content, including HTML, XML, and PDF versions of each article. Higher resolution versions of figures can be downloaded directly from the article. Thank you for your interest in PLOS ONE and for your continued support of the Open Access model. Please do not hesitate to be in touch with any additional questions.

Kind Regards,

Jodie Elgey, Staff EO, PLOS ONE”

- Figures 3.1, 3.2, 3.4 and 3.5 are taken from Zachariah *et al.*, 2012 [1].
- Figures 3.3 and 3.7 are taken from Olson *et al.*, 2014 [2].
- Figure 3.6 is adapted from Olson *et al.*, 2014 [corrected figure] [3].

## **Acknowledgement of Contributions**

Mr. Carl Olson (Rastegar Lab) performed the mouse dissections required for the primary neuron cultures used in Chapters 3-5. Mr. Olson also prepared the Phoenix cell protein extracts, and paraformaldehyde-fixed NIH3T3 cells required for the experiments detailed in Figure 3.6 and 3.7.

## Thesis Overview

Chapter 1 consists of an in-depth literature review and rationale for my PhD project. It is mainly focused on MeCP2, its association with Rett Syndrome (RTT), *MECP2* Duplication Syndrome (MDS), and *rRNA* synthesis. Chapter 1 also contains the project aims and hypotheses. The general materials and methods are represented in Chapter 2. The two major research aims and results are included as Chapters 3, 4 and 5. Chapter 3 is on ‘Analysis of MeCP2 isoform-specific expression in murine neural cells using custom-made antibodies’, which will report and discuss the development of MeCP2 isoform-specific antibodies and their applications in studying expression and localization of MeCP2 in murine brain cell types. Chapter 4 is focused on ‘analyzing the effect of neuronal *MECP2E1/MECP2E2* overexpression on *rRNA* synthesis, which will connect overexpression of MeCP2, MDS, and *rRNA* synthesis. Each chapter contains its own discussion and conclusion. Chapter 5 is used to establish the binding of MeCP2 to the methylated fraction of the mouse *rDNA* promoter. A general discussion summarizing the overall implications and significance of the findings as well as future directions are included in Chapter 6. References for all cited reports are included in Chapter 7.



## Chapter 1: Introduction

### 1.1 Chromatin and Epigenetics - Introduction and History

In 1879, German cytologist Walther Flemming coined the term ‘chromatin’ to describe stainable threads observed within the nucleus through microscopic studies. At the time, Flemming believed that “The word chromatin may serve until its chemical nature is known, and meanwhile stands for that substance in the cell nucleus which is readily stained” [4]. However, the discovery of chromatin was an underappreciated milestone that later led to the establishment of ‘*epigenetics*’ as a fundamental molecular mechanism that governs the development of eukaryotic organisms. The term epigenetics was initially coined by Conrad Waddington in 1942, who defined it as “the branch of biology which studies the causal interactions between genes and their products which bring the phenotype into being” [5]. The era of epigenetic research shed light on to the complexity of gene expression and its regulation that was previously underappreciated by genetic studies alone.

In eukaryotes, genomic DNA is organized by histones to form chromatin. Nucleosomes are the fundamental subunits of chromatin, consisting of a nucleosome octamer core and linker DNA. The nucleosome core includes a 147 bp segment of DNA and two copies each of four core histone proteins (H2A, H2B, H3 and H4), a feature that is relatively conserved from yeast to metazoans [6,7]. The four core histones are basic proteins that are highly conserved among eukaryotes. Each core histone has a mostly  $\alpha$ -helical C-terminal domain that facilitates histone-histone interactions to form octamers around which DNA is wrapped. The C-terminal domain of histones possess a ‘histone-fold’ motif, which forms a protein–protein interface that facilitates heterodimerization of histones H2A with H2B, and H3 with H4 [8-10]. All core histones also have

## Chapter 1

evolutionarily conserved ‘tail domains’ found at their N-terminal portions, with the only exception being the C-terminus of histone H2A [11]. The core histone N-terminal sequences contain a high proportion of lysine (K), arginine (R), glycine (G), alanine (A), and threonine (T) residues that undergo post-translational modifications (PTMs), which are known as histone post-translational modifications (hPTMs) and are critical for their epigenetic functions (discussed later). Sequence analysis of the tail domains identifies them as intrinsically disordered structures. However, when bound with chromatin, tail domains are considered to adopt specific structures [12-14].

Linker histone H1 is less conserved than core histones, varying in both sequence homology and number of non-allelic variants among eukaryotes. Studies have indicated that the presence of histone H1 protects an additional 20 bp of DNA from nuclease digestion, symmetrically positioned on either side of the 147 bp core DNA shielded by the nucleosome core [15]. The globular domain of histone H1 is considered sufficient to protect the 20 bp DNA from nuclease digestion. However, the full-length H1 is required for chromatin compaction [16]. The N-terminal domain of histone H1 is considered to serve as an anchor for its positioning, sealing off DNA entering and exiting the nucleosome [17,18]. The C-terminal domain is made up of highly basic residues and functions to stabilize higher order chromatin structure *via* neutralization of DNA charge mostly within the linker DNA, as well as a determinant of H1 binding to chromatin [19-22]. The arrays of nucleosomes, connected by the linker DNA, termed ‘nucleosomal arrays’ or 10 nm fibers represent the basic level of chromatin organization. The 10 nm fibers can also fold into chromatin fibers with 30 nm diameter, and can be detected in special cells such as chicken erythrocytes and starfish sperm (reviewed in [23]).

Chromatin is the epicenter of epigenetic-mediated regulation of eukaryotic gene expression. The direct modulation of chromatin structure and re-positioning of nucleosomes by

## Chapter 1

chromatin remodelers are an important epigenetic mechanism (discussed in Section 1.1.1). The hPTMs within the core nucleosomal histones are associated with specific transcriptional states (discussed in Section 1.1.2). Genomic DNA also encodes several hundreds of non-coding RNAs that can control chromatin structure (discussed in Section 1.1.3). Moreover, hPTMs are also known to crosstalk with specific methyl marks present within genomic DNA, i.e. DNA methylation (discussed in 1.2), creating another layer of the epigenetic code that further determines gene expression [24,25].

The history of epigenetics and epigenetic mechanisms are often depicted as a linear sequence of events. In reality however, most epigenetic mechanisms were discovered by separate groups in an overlapping manner. **Table 1.1** attempts to highlight this collective historical effort that has led to the concept of the epigenome.

**Table 1.1 History of Epigenetics**

<b>TIMELINE</b>	<b>1870-1950</b>	<b>1950-1960</b>	<b>1960-1970</b>	<b>1970-1980</b>	<b>1980-1990</b>	<b>1990-2000</b>	<b>2000-Present</b>
<b>Chromatin</b>	Discovery of nucleic acids [26], histones [27], chromatin [4]	DNA double-helical structure [28]	Fractionation of histones [29]	Discovery of the nucleosome [30,31]	Nucleosome crystal structure to 7.0 Å [32]	Nucleosome crystal structure determined to 2.8 Å [7]	
<b>Histone PTMs</b>			Link between histone modifications and chromatin [33]	Isolation of the first protein fraction with Lysine Acetyl transferase (KAT) [34]		Discovery of KAT [35], histone deacetylase HDAC [36], Lysine Methyl transferase KMT [37]	Histone code [38]
<b>DNA Methylation</b>		DNA methylation linked to X-chromosome inactivation [39,40]	Target of DNA methylation is CpG dinucleotide [41]	Methylation of endogenous CpG sites [42]		Discovery of Methyl Binding Domains (MBD) proteins [43]	Discovery of Ten Eleven Translocation methylcytosine dioxygenase 1 TET1 [44]
<b>Non-coding RNA</b>			Discovery of heterogeneous nuclear RNA [45]	Discovery of Intronic non-coding RNA elements [46,47]	Self-Splicing catalytic RNAs [48,49]	Discovery of H19, Xist, Lin-4 [50-53] RNA interference (RNAi) [54,55]	Discovery of Dicer, Drosha, piRNA, Enhancer RNA [56-59]

### 1.1.1 Chromatin Remodeling

Chromatin remodelers utilize the energy from ATP hydrolysis to restructure/reposition the nucleosomes to facilitate cellular processes such as gene transcription, DNA repair, DNA replication, and DNA recombination. Previous reports have identified a specific subset of proteins and protein complexes that are capable of modulating gene expression by nucleosome repositioning [60]. Chromatin remodelers act by shifting nucleosomes to either alter the spacing between nucleosomes or to allow/hinder access for transcription factors. In general, chromatin remodellers act through three main mechanisms: altering chromatin organization (spacing of nucleosomes), facilitating chromatin access (nucleosome movement or ejection) and chromatin restructuring (insertion of histone variants) [61,62].

Chromatin remodelers can be categorized into four different groups based on the presence of specific functional domains: the SWI/SNF (switching defective/sucrose non-fermenting) family, the ISWI (Imitation SWItch) family, the CHD (Chromodomain-Helicase-DNA binding) family and INO80 (inositol requiring 80) family [60]. All four chromatin remodelling groups share a similar ATPase domain. In addition, they also harbor 2 to 20 non-catalytic subunits that confer functional specificity. The SWI/SNF family has a C-terminally located bromo domain, which allows it to recognize and bind to acetylated lysine residues within histones. This family of chromatin remodelers are involved in facilitating chromatin access but do not function in chromatin assembly [63]. The ISWI family possesses a SANT domain (Swi3, Ada2, N-Cor, TFIIB) and SLIDE (SANT-like ISWI domain) domain, which forms a nucleosome recognition module allowing it to bind to DNA and unmodified H4 N-terminal tails. Members of this family are mostly involved in transcriptional repression, but also facilitate chromatin assembly, nucleosome spacing and chromatin compaction [61]. The CHD family has two chromo domains,

which allows it to bind to methylated lysines at the N-terminus. The characterized member of CHD family is the NURD (nucleosome remodeling and deacetylase) complex, which is involved in transcriptional repression [64]. The INO80 complex exhibits DNA helicase activity and functions in homologous recombination and DNA replication [65,66].

### 1.1.2 Histone Post-Translational Modifications

Histone PTMs along with DNA methylation marks encompass a basic epigenetic framework in eukaryotic genomes. Although most hPTMs occur in the N-terminal tails of histones, hPTMs have also been identified within the histone core and C-terminal tails [67-69]. Some of the most common hPTMs include acetylation, phosphorylation, methylation, sumoylation, ubiquitination and ADP-ribosylation [25,70]. Even though a multitude of hPTMs have been discovered, they are mostly confined to a few residues. For instance, lysine residues are the target for acetylation, methylation, ubiquitination and sumoylation, whereas arginine residues can be methylated and ADP-ribosylated [71]. These marks are subsequently read by effector proteins or “readers,” which in turn can recruit other co-activator or co-repressor complexes, and regulate the chromatin structure and transcriptional activity of genes [72,73].

The site of hPTMs with respect to its position within the nucleosome often influences its action on chromatin structure [74]. For instance, hPTMs within the nucleosome DNA entry/exit region such as H3K56ac, H4K77ac and H4K79ac (hPTM nomenclature based on [75]) are known to enhance DNA unwrapping from the nucleosome [76,77]. The hPTMs occurring within the nucleosome dyad symmetry axis such as phosphorylation of H3T118, however, mediates nucleosome destabilization based on *in vitro* studies [78,79]. Acetylation of H4K91 positioned at histone-histone interfaces, regulates nucleosome assembly and disassembly [80,81]. In addition to

these direct functions, hPTMs often act as guides for chromatin remodelers, leading to alterations in chromatin structure [82].

### 1.1.3 Non-Coding RNAs

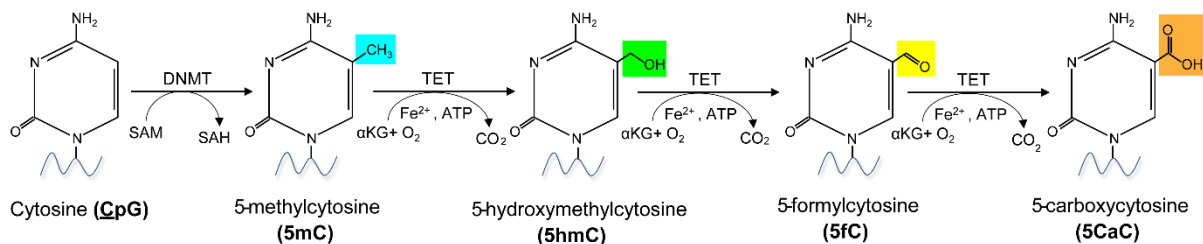
Previous studies on the eukaryotic transcriptome have revealed that up to 90% of the human genome undergoes transcription [83]. However, ENCODE-annotated (Encyclopedia of DNA Elements) exons for protein-coding genes encompass only 2.94% the genome, with the remaining transcribed fraction being non-coding RNAs (ncRNAs) [84]. The ncRNAs can be divided into two sub-categories, namely small RNAs and long non-coding RNAs (lncRNA). Small ncRNAs are usually 20-30 nucleotides in length and include small nuclear RNAs (snRNA), small nucleolar RNAs (snoRNA), microRNAs (miRNAs), transfer RNAs (tRNA) and piwi-interacting RNAs (piRNAs). LncRNAs, on the other hand, have more than 200 nucleotides and consist of ribosomal RNAs (rRNAs) and other ncRNAs [85,86].

Several studies have revealed the vast and significant functions on ncRNAs [87,88]; some of these are mediated by the effects of lncRNA on chromatin structure. LncRNAs can influence gene expression by interacting with chromatin modelers. For instance, the lncRNA second chromosome locus associated with prostate-1 (*SChLAP1*) physically interacts with and antagonizes the SWI/SNF complex, resulting in substantial alterations in gene expression which have important implications for certain types of cancer [89]. Additionally, miRNAs such as miR-302 have been linked to modulating chromatin structure through interactions between chromatin remodeling complexes [90].

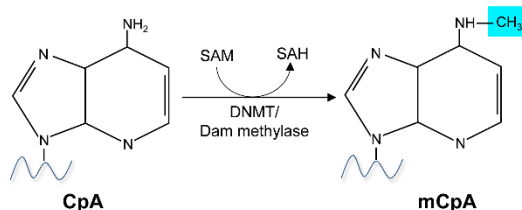
## 1.2 DNA methylation

DNA methylation is one of, if not the most well-studied epigenetic modifications [91]. Initially, DNA methylation was characterized and analyzed solely within the context of CpG dinucleotide methylation, usually referred to as 5-methylcytosine (5mC) [92]. Recent studies however, have revealed a broader variety of methyl marks, including oxidized forms of CpGs [5-hydroxymethylcytosine (5hmC), 5-formylcytosine (5fC) and 5-carboxycytosine (5caC)], and non-CpG methylation/CpH methylation (mHC, in which H = A, C, or T) [24,93] (**Figure 1.1**). The discovery of these base modifications has also led to a better understanding of the overarching influence that DNA methylation has on gene expression. Moreover, the newly discovered variants of methyl marks also provide insights into the intricate mechanisms behind cell type specificity of DNA methylation as well as the significance of their distribution within the genome.



**A CpG Methylation****B Non-CpG (CpH) Methylation (H= A/T/C)**

Example: mCpA

**Figure 1.1 Generation of different types of DNA methylation marks.**

A) CpG methylation. DNA methyltransferase (DNMT) enzymes convert cytosines to 5-methylcytosine (5mC) by transferring a methyl group ( $-\text{CH}_3$ ) from S-adenosyl methionine (SAM). The 5mC is further oxidized into 5-hydroxymethylcytosine (5hmC), 5-formylcytosine (5fC) and 5-carboxycytosine (5caC) through a series of chemical reactions catalyzed by Ten Eleven Translocation (TET) enzymes in a reaction involving *alpha*-ketoglutarate ( $\alpha\text{KG}$ ), oxygen ( $\text{O}_2$ ), adenosine triphosphate (ATP) and  $\text{Fe}^{2+}$ . B) Non-CpG methylation (CpH methylation: H= A/T/C).

*The figure was designed based on [24,93].*

### 1.2.1 CpG methylation

Methylation of DNA within the CpG dinucleotides (mCG) has been implicated in the regulation of multiple biological processes, including X-chromosome inactivation (XCI), genomic imprinting, and chromosome stability [24]. Moreover, CpG methylation has also been identified as a key modulator of thousands of genes in a variety of organisms.

Regarding genomic distribution, repetitive DNA elements and intergenic regions contain higher levels of mCG, whereas active regulatory elements such as promoters and enhancers are mostly devoid of mCG [94,95]. In fact, a large percentage of promoters and enhancers, have been reported to harbor tight clusters of CpG dinucleotides, known as ‘CpG islands’ that are depleted of CpG methylation. Furthermore, methylation patterns have been observed in sequences flanking these CpG islands. These CpG island ‘shores’ are thought to confer tissue specificity to DNA methylation patterns [96,97]. This genomic distribution also appears to be similar in neurons and non-neuronal cell types. Initial studies on the role of mCG in gene regulation strongly pointed towards a predominantly repressive function [98].

In humans, CpG methylation of promoter regions is negatively correlated with gene expression, whereas methylation of gene bodies has been shown to have a positive correlation with gene expression, a notion known as the DNA methylation paradox [99]. However, other studies have indicated a ‘bell-shaped’ correlation between gene-body methylation and gene expression, in which the lowest and highest expressed genes had markedly lower DNA methylation levels, whereas the mid-level expressed genes had the highest DNA methylation levels [100]. The relevance of non-promoter methylation for neurogenic genes was demonstrated by Wu *et al.*, who showed that *Dnmt3a*-dependent methylation of intergenic regions and gene bodies antagonizes Polycomb repression and promotes gene expression in neural stem cells (NSC) [101].

### 1.2.2 Five (5)-Hydroxymethylcytosine

DNA hydroxymethylation occurs when the hydrogen atom at the C5-position of cytosine residues is replaced by a hydroxymethyl group [102]. Hydroxymethylation of DNA (5hmC) was first reported in 1971, in rodent and frog brains [103]. However, at the time this report failed to garner much attention. The 5hmC methyl mark was brought back into the scientific spotlight in 2009 when two independent labs re-discovered this modification [44,104]. In one of these studies, Kriaucionis and Heintz identified an abundance of 5hmC marks in neuronal Purkinje cells, using multiple techniques including mass spectrometry, thin layer chromatography (TLC) and high performance liquid chromatography (HPLC). According to the same study, the estimated abundance of 5hmC in Purkinje cells was approximately 0.6% of all cytosine residues [104]. The other study, reported by Tahiliani *et al.*, identified high levels of 5hmC in mouse embryonic stem cells (ESCs) with an estimated abundance of 4 - 6 % of all CCGGs [44]. In terms of genomic distribution patterns, 5hmC has been shown to be enriched at transcription start sites (TSS) [105]. Furthermore, enrichment of 5hmC has been reported within the intragenic regions of actively transcribed genes and enhancer elements in mouse and human ESCs, respectively [106,107]. The generation of 5hmC marks is catalyzed by the ten-eleven translocation dioxygenase (TET) family which includes TET1, TET2, and TET3 (**Figure 1.1**). The same enzymes are capable of carrying out the oxidation of 5hmC to 5fC and 5caC.

### 1.2.3 Non-CpG methylation

The existence and significance of non-CpG methylation or CpH methylation has only been appreciated recently, mostly due to technical limitations of past studies. In terms of frequency, CpH methylation is found in 20-25% of CpH dinucleotides, compared to the 60-90% observed for

## Chapter 1

CpG dinucleotide methylation in mammalian genomes [108]. CpH methylation has been reported predominantly in ESCs and neurons. However, in human ESCs, CpH methylation occurs predominantly within CAG trinucleotides and in adult mouse dentate neurons, it occurs within the context of CAC trinucleotides [109,110]. The differences in the methylation pattern could enable recruitment of different ‘readers’ of non-CpG methylation and allow cell type-specific gene regulatory mechanisms.

CpH methylation is known to be a repressive epigenetic mark. This concept has been validated by *in vitro* reporter-based assays [109]. In agreement with these findings, the distribution of CpH methylation has been inversely correlated with gene expression in neurons. In contrast, CpH methylation is positively correlated with transcriptional activity in human ESCs [95,108]. Studies in the skeletal muscles of obese individuals have shown that CpH methylation levels of the peroxisome proliferator-activated receptor gamma (PPAR- $\gamma$ ) coactivator-1 alpha (PGC-1 $\alpha$ ) promoter are positively correlated with obesity markers such as body mass index, leptin hormone levels and C-reactive proteins. This was in contrast to CpH methylation observed within the Pyruvate Dehydrogenase Kinase Isozyme 4 (PDK4) promoter, which exhibited a negative correlation with the aforementioned obesity parameters. Importantly, gastric bypass surgery and weight loss reversed the differential methylation patterns observed within these gene promoters to non-obese levels [111]. This study along with other investigations also proves that similar to CpG methylation, CpH methylation is influenced by external/environmental factors [112,113].

## 1.2.4 Writers of DNA methylation

### 1.2.4.1 DNA methyltransferases (DNMTs)

The methylation of cytosine at the C5-position is catalyzed by a group of enzymes known as DNMTs, which mediate the transfer of a methyl group from S-adenosyl methionine (SAM) (**Figure 1.1A**). DNMT3A and DNMT3B, along with DNMT3L (DNA methyltransferase-like protein) constitute the *de novo* DNMTs that methylate DNA during embryogenesis [114]. DNMT3B has been shown to be vital for early embryogenesis, whereas DNMT3A plays a more prominent role in late embryogenesis and is also expressed in differentiated cells. DNMT3L is thought to be a co-factor for methylation due to its lack of a catalytic domain. However DNMT3L has been shown to be vital for the silencing of retrotransposons in male germ cells and the establishment of genomic imprints in oocytes [115]. DNMT1A transfers DNA methyl mark patterns from the parental DNA strand to the daughter strands, thereby mediating the inheritance of epigenetic marks between dividing cells [116]. As such, DNMT1A preferentially binds to hemimethylated DNA.

DNMTs also catalyze CpH methylation. In ESCs, depletion studies of either *Dnmt3a*, *Dnmt3b* or *Dnmt3l*, as well as a combination of *Dnmt3a* and *Dnmt3b* have shown that DNMT3A and DNMT3B, together with DNMT3L mediate CpH methylation. DNMT1, on the other hand, appeared to be dispensable for CpH methylation [117]. These findings were further corroborated by other *in vivo* studies showing altered CpH methylation upon loss of *Dnmt3a/3b* and *Dnmt3l*, but not *Dnmt1* [112,118-120]. The apparent lack of *Dnmt1* involvement suggests that CpH methyl marks might have to be added after each cell division, evidence for which has been observed in non-proliferating mouse germ cells that lose CpH methyl marks upon resumption of proliferation [113,120].

### 1.2.5 DNA methyl-erasers and DNA demethylation

Erasure of DNA methylation can occur through both passive and active mechanisms. Passive DNA demethylation can occur during DNA replication, in the absence of maintenance methyltransferases such as DNMT1 [121]. An excellent example of passive DNA demethylation is the global 5mC depletion that occurs in the maternal genome during preimplantation embryonic development [122]. However, further studies elucidated that passive DNA demethylation could not account for all of the 5mC depletion phenomena observed *in vivo*. Subsequent studies led to the identification of TET proteins, and their role in oxidizing 5mC to 5hmC, turning the spotlight on a novel mechanism by which 5mC DNA methyl marks could be ‘actively’ demethylated [123].

The TET proteins are mammalian homologs of the trypanosome base J-binding proteins, JBP1 and JBP2, which are Fe<sup>2+</sup>- and 2-oxoglutarate (2OG)-dependent dioxygenases that require  $\alpha$ -ketoglutarate ( $\alpha$ KG) as a co-substrate for enzymatic activity [44,124]. The TET1 protein oxidizes the fifth carbon of the cytosine residue to create 5hmC (**Figure 1.1A**). TET proteins are also known to further oxidize 5hmC to 5caC and 5fC in an ATP-dependent manner. All members of the TET protein family harbor a core catalytic domain containing a double-stranded  $\beta$ -helix fold that contains the crucial metal-binding residues found in the family of Fe<sup>2+</sup>/ $\alpha$ -KG-dependent oxygenases. Another common component of all TET proteins is the cysteine-rich domain that precedes the core, which also plays a vital role in their activity. Non-redundant domains of TET family members include the chromatin-associated CXXC domain found in TET1 and TET3 that allow them to interact with CpG sequences. However, the association of TET2 with another protein with CXXC domain (IDAX), also confers it with the same property [125].

Numerous studies have supported the hypothesis that 5hmC is part of an oxidative demethylation mechanism, mediated by TET proteins, by promoting Base Excision Repair (BER)

## Chapter 1

of DNA, resulting in the conversion of the methylated cytosine back to the unmethylated state. The formation of 5fC and 5caC, which are oxidized products of 5hmC, destabilizes the N-glycosidic bond and promotes BER by DNA glycosylase (TDG) and methylated DNA binding domain-containing protein 4 (MBD4). In another instance, deamination of 5hmC by activation-induced cytidine deaminase/apolipoprotein B mRNA-editing, enzyme-catalytic, polypeptide (AID/APOBEC) family of deaminases has been shown to generate 5-hydroxymethyluracil (5hmU). The AID/APOBEC deaminases also cause the formation of apurinic/aprimidinic (AP) sites, which are subsequently cleaved by AP endonuclease 1 (APEX1) and replaced by unmodified cytosine [126,127].

Previous studies have demonstrated that DNMTs could deaminate methylcytosine to thymidine, thereby causing a C/T mismatch, which is subsequently repaired by a mismatch-repair mechanism [128]. Apart from MBD4, MBD3 has also been shown to have demethylase function. Overexpression of MBD3 caused global as well as target-specific demethylation, specifically at promoter regions [129]. Within the brain, growth arrest and DNA-damage-inducible  $\beta$  (GADD45B) has been shown to be critical for neuronal activity-induced DNA demethylation of gene promoters critical for adult neurogenesis [130]. Although a similar DNA demethylation activity has been suggested for GADD45A this activity has been disputed [131-133].

### **1.2.6 Readers of DNA methylation**

The last few decades have witnessed the identification of several families of proteins that are capable of recognizing and binding to methylated DNA, referred to as ‘readers’ of DNA methylation. Three main families of ‘DNA methylation readers’ have been identified so far, the

## Chapter 1

Methyl Binding Domain (MBD) protein family, Kaiso and Kaiso-like proteins, and SRA domain proteins [134].

### *1.2.6.1 MBD Protein Family*

The MBD protein family was the first group of 5mC readers to be identified, with (Methyl CpG Binding Protein 2) MeCP2 being the prototypic family member (**Figure 1.2**) [135]. To date, 11 MBD proteins have been discovered and consist of MBD1, MBD2, MBD3, MBD4, MBD5, MBD6, MeCP2, SETDB1, SETDB2, BAZ2A, and BAZ2B, based on the Conserved Domain Database [CDD, NCBI]. This superfamily can be further categorized as MeCP2\_MBD, KMT\_MBD, and HAT\_MBD [136]. Within this sub-categorization, only MeCP2\_MBD possesses the canonical MBD domain, which has an evolutionarily conserved intron within the MBD coding region [43]. MBD1 is the largest member of the MBD protein family and is known to mediate epigenetic regulation of gene expression and modulating the H3K9me3 histone mark to facilitate heterochromatin formation. Multiple studies have highlighted the role of MBD2 and MeCP2 in gene regulation *via* their interaction with methylated DNA and are known as both transcriptional activators and repressors [137-139]. MBD2 has also been attributed to DNA demethylase activity, further strengthening studies supporting its role as a transcriptional activator [140]. MBD4 has a C-terminal DNA glycosylase domain, apart from its MBD domain, and has been implicated primarily in DNA repair [141]. Intriguingly, even though MBD3, MBD5, and MBD6 also possess the canonical MBD domain, they do not bind to methylated DNA. Nevertheless, they have been shown to be associated with heterochromatin and transcriptional repression [142]. SETDB1 and SETDB2, constituents of the KMT\_MBD family, are both histone methyltransferases (KMTs) which have a SET domain that allows them to transfer a methyl group from SAM to the amino



## Chapter 1

group of a lysine residue on histones or other proteins. BAZ2A is one of the main components of NoRC, which mediates repression of ribosomal RNA (*rRNA*) genes transcription by recruiting histone deacetylases (HDACs), KMTs and DNMTs [143]. Although BAZ2B shares considerable sequence homology with BAZ2A, its functions remain relatively unknown [144].

Apart from MBD proteins, Kaiso proteins are known to bind methylated CGCGs using a three-zinc-finger motif. Similar DNA binding properties have also been identified in Kaiso-related proteins, ZBTB4 and ZBTB3, which can also bind to single methylated CpG dinucleotide [145,146]. The third family of proteins that are capable of binding to methylated DNA is the SRA protein family member, with UHRF1 being the most well-researched protein member. UHRF1 has been primarily characterized as a transcriptional repressor and also interacts with the histone methyltransferase G9a [147].

The structural similarities of proteins with a MBD domain, including MeCP2, are shown below (**Figure 1.2**).

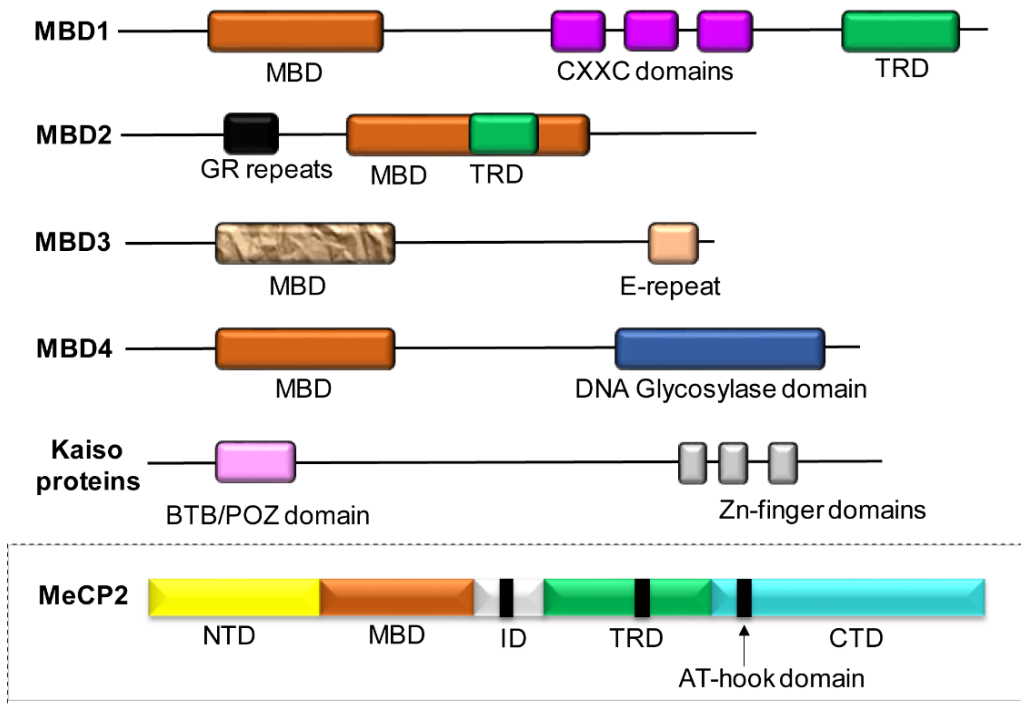


**Figure 1.2 Structural comparison of the members of Methyl CpG Binding Protein (MBP) family.**

Schematic representation of the major functional domains of the MBP family of proteins. The MBP family is mainly characterized by the methyl binding domain (MBD), which facilitates the binding to methylated DNA, except in the case of MBD3. The other major and minor domains found in each MBP are also shown. TRD: transcription repression domain; CXXC: zinc-finger ( $Zn^{2+}$ ) motifs; GR: Glycine and arginine residues; NTD: N-terminal domain; ID: interdomain; CTD: C-terminal domain E-repeats: glutamic acid repeats; BTB/POZ: Broad-Complex, Tramtrack and Bric a brac/ POxvirus and Zinc finger domain.

### 1.3 MeCP2

MeCP2 is a methyl binding protein which belongs to the MBP family. They are characterized by the presence of a MBD domain [24].

#### 1.3.1 *Mecp2/MECP2* gene and MeCP2 protein structure

MeCP2 is encoded by an X-linked gene located within the Xq28 region in humans and XqA7.3 in the mouse (**Figure 1.3**). The human *MECP2* gene is flanked by *IRAK1* and *OPNILW* (also called *RCP*), while the mouse *Mecp2* gene is flanked by *Irak1* and *Opn1mw*. The human *MECP2* gene spans 75925 bp (~76 kb), while the length of mouse *Mecp2* gene is 59099 bp (~59 kb). Both *MECP2* and *Mecp2* genes consist of 4 exons and 3 introns.

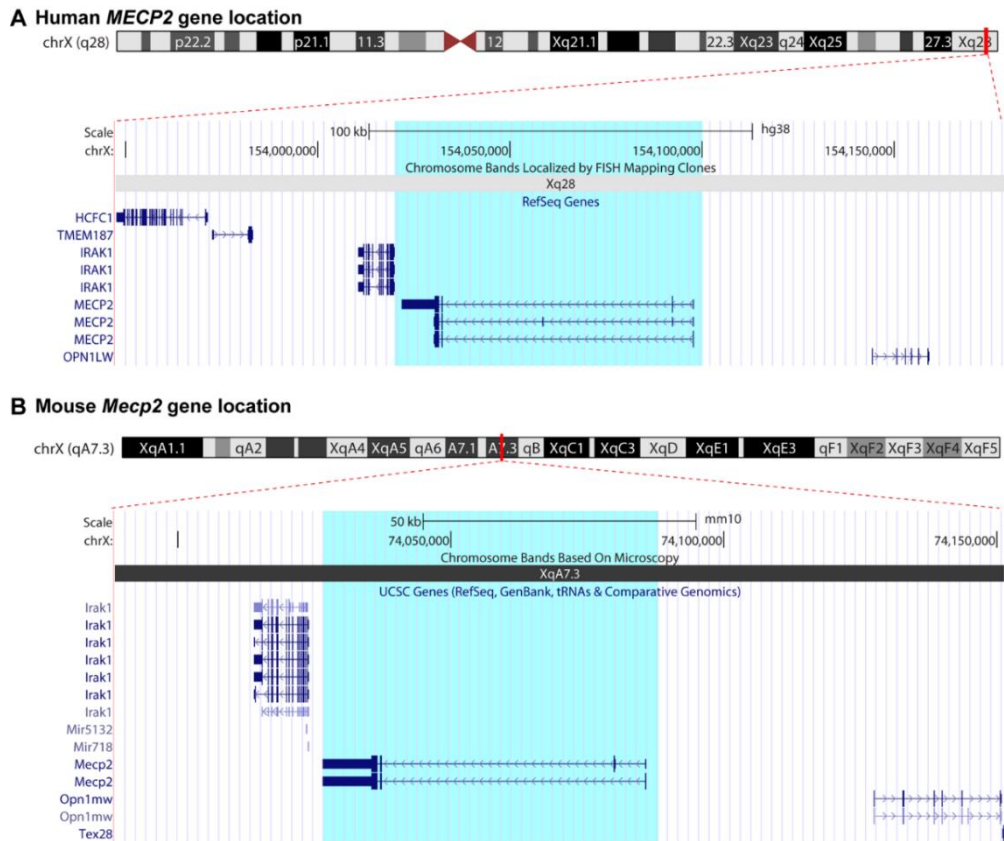


**Figure 1.3 Genome map of the human and mouse *MECP2/Mecp2* genes.**

A) Schematic of the X chromosome marking the Xq28 location in humans. Information was downloaded from the UCSC Genome Browser on the Human Dec. 2013 (GRCh38/hg38) Assembly. B) Schematic of the X chromosome marking the XqA7.3 location in mice. Information was downloaded from the UCSC Genome Browser on the Mouse Dec. 2011 (GRCm38/mm10) Assembly. The *MECP2/Mecp2* gene is highlighted in blue, in both A & B.

## Chapter 1

Three features characterize the *MECP2*: a vast intergenic region (40 kb) separating *MECP2* from the closest upstream gene, the large size of intron 2 (~60 kb) and a highly conserved 8.5 kb 3' untranslated region (3'UTR) with multiple polyadenylation sites [148]. The *Mecp2* promoter resembles that of a housekeeping gene since it does not possess a canonical TATA-box [149]. The core promoter sequence lies between -179 and -309 (relative to the TSS). Several regulatory regions have been identified within the *MECP2* promoter, including two negative regulatory elements [(-309 to -370) and (-553 to -681)] and one positive regulatory element (-847 to -1,071) [148]. Apart from inherent regulatory regions, several transcription factor binding sites have also been identified within the *MECP2* promoter, including those for SP1, TAF1 and CTCF [150]. Interestingly, Adachi *et al.*, identified a minimal segment of the proximal promoter (-677/-56) that is essential to drive *Mecp2* expression in neurons [149]. Moreover, they also demonstrated that the same region is not sufficient to drive *Mecp2* in non-neuronal cells. However, Rastegar *et al.* showed that this promoter is enough to drive *Mecp2* expression in both neurons and glial cells (astrocytes) [151]. Furthermore, *cis*-regulatory G-quadruplexes (nucleic acid secondary structures that form in guanine-rich DNA sequences) have also been identified at the *MECP2* 5'UTR by bioinformatic analyses, which have been proposed to be having significant regulatory functions including the modulation of other *cis*- and *trans*-acting interactions [152].

One of the key defining features of MeCP2 is its ability to recognize and bind to methylated DNA [153]. Interestingly, *MECP2* itself appears to be governed by promoter methylation which was initially discovered by Nagarajan *et al.* [154]. They identified increased methylation within the *MECP2* promoter regions spanning -531 and -243 bp in the cerebral cortex of male autistic patients. Increased methylation correlated with reduced *MECP2* expression, further corroborating the potential involvement of promoter DNA methylation in *MECP2* downregulation [154].

## Chapter 1

Subsequently, our research group demonstrated a correlation between DNA methylation of 6 regulatory elements (three elements within the *Mecp2* promoter and three elements in intron 1), and the expression of *Mecp2* isoforms in NSC and adult mouse brain [2,155,156]. The core promoter of the human and mouse *MECP2/Mecp2* show remarkable similarity [149] and thus might be regulated similarly, which is yet to be confirmed. DNA methylation of the X-chromosome itself has been implicated in the regulation of *Mecp2* expression in neuronal cells since DNA methylation is a major mechanism involved in XCI. Studies in heterozygous MeCP2 mouse models have shown that XCI patterns were unbalanced, favoring the expression of the wild-type allele in most mutant females [157]. However, studies of XCI in Rett Syndrome (RTT) patient brains have indicated balanced XCI, suggesting potential differences of XCI in humans and mouse models of RTT [158].

As mentioned previously, *MECP2* has an unusually long and highly conserved 3'UTR [159]. To date, four mRNA transcripts have been identified which are generated by alternative polyadenylation and producing transcripts with varying lengths (~1.8, ~5.4, ~7.5, and ~10.2 kb) [160]. The precise correlation between the different transcripts and MeCP2 protein expression remains unknown. However, the varying brain developmental expression profiles of the mRNA transcripts suggests an important role for them in the developing brain [161,162]. The significance of the 3'UTR sequence is further corroborated by various reports that have identified multiple mutations within the *MECP2* 3'UTR, the majority been found in autistic patients [163].

### 1.3.2 MeCP2 functional domains

MeCP2 is an intrinsically disordered protein with approximately 60% of the protein being unstructured [164,165]. Five biochemically distinct domains have been identified so far, the N-

## Chapter 1

terminal domain, the MBD domain, the interdomain (ID), the TRD domain and the C-terminal domain (**Figure 1.2 and 1.4**). In RTT patients, mutations in regions coding for all five domains have been identified, highlighting the importance of all five domains for proper MeCP2 function. However, it should be emphasized that the majority of mutations have been localized to the MBD and TRD domains, which are expected considering their central roles in MeCP2 function and interactions.

There are two MeCP2 isoforms named MeCP2E1 and MeCP2E2 [166,167] which differ only at the N-terminal domain (**Figure 1.4**) and has been implicated in MeCP2 isoform-specific functions. For instance, Dastidar *et al.* demonstrated that a unique sequence in the N-terminus of MeCP2E2 allows it to preferentially bind to FOXG1 [168]. MeCP2 has also been shown to be involved in chromocenter (clusters of constitutive heterochromatin) formation during myogenic differentiation and to interact with HP1 *via* its N-terminus [169].

The sequence encoding the MBD domain is a mutational hotspot leading to RTT (approx. 45% of all RTT causal mutations) [170]. The MBD domain allows MeCP2 to recognize and bind to methylated DNA, as well as non-methylated DNA sequences [171,172]. The MBD domain is also known to be involved in MeCP2 protein-protein interactions with mSIN3a, NCoR, and DNMT1 [173]. The ID domain of MeCP2 was initially named solely based on its position between the MBD and TRD domain. However, the ID domain was later found to confer an autonomous methylation-independent DNA-binding activity to MeCP2 as well as promote MBD-dependent interactions [174]. Initially, MeCP2 was characterized as a transcriptional repressor based on its interaction with other transcriptional repressors such as mSIN3A and HDAC [175,176]. These interactions were mostly mediated by the TRD domain [177]. The TRD domain of MeCP2 has

also been shown to allow MeCP2 to interact with YY1, YB1 and c-SKI, highlighting the association of MeCP2 with other transcription factors [178].

### 1.3.3 MeCP2 isoforms: expression and regulation

Alternative splicing of the first two exons of the *MECP2/Mecp2* gene leads to the generation of two splice variants, MeCP2E1 (also known as MeCP2B/α) and MeCP2E2 (also known as MeCP2A/β) (**Figure 1.4**) [166,167]. The inclusion of the TSS from exon 1 codes for MeCP2E1 and comprises exons 1, 3 and 4, whereas the utilization of the TSS from exon 2 translates to MeCP2E2 and comprises exons 2, 3 and 4. In terms of the protein sequence, the two isoforms only differ at their short N-terminal sequences.

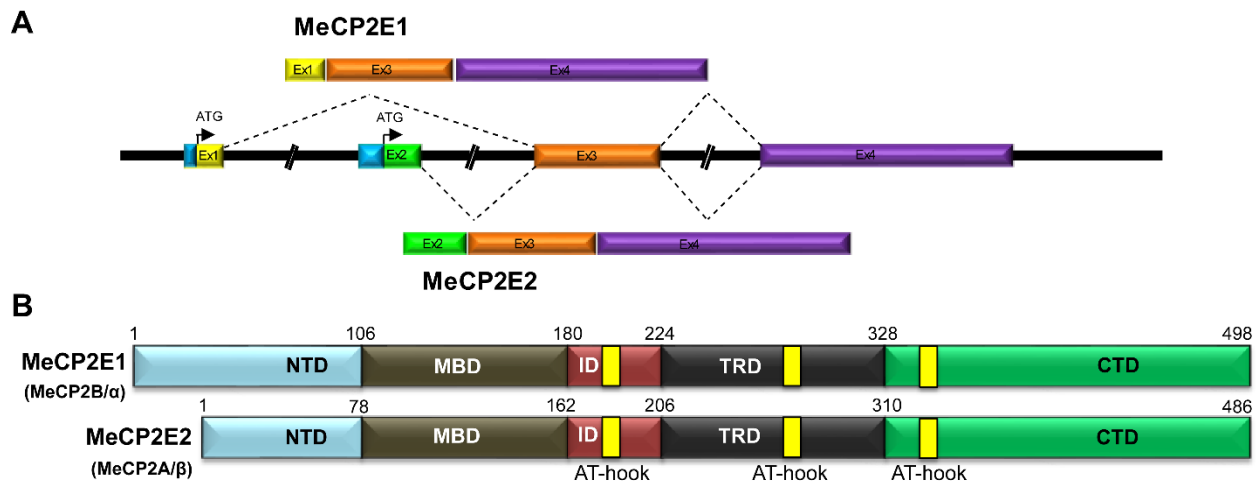


**Figure 1.4** *MECP2/Mecp2* gene and protein isoforms MeCP2E1 and MeCP2E2.

A) Schematic representation of *MECP2/Mecp2* gene structure and the generation of two isoforms, MeCP2E1 and MeCP2E2, by alternative splicing. The MeCP2E1 isoform includes exons 1, 3 and 4, while MeCP2E2 includes exons 2, 3 and 4, arising from the TSS (ATG) found in the exon 1 and exon 2, respectively. B) The major domains of the two MeCP2 isoforms are shown. MeCP2



isoforms differ at their N-termini. The domains are MBD: methyl-CpG-binding domain, ID: Intervening domain, TRD: Transcriptional repression domain, CTD: C-terminal domain and, AT-Hook domains.

---

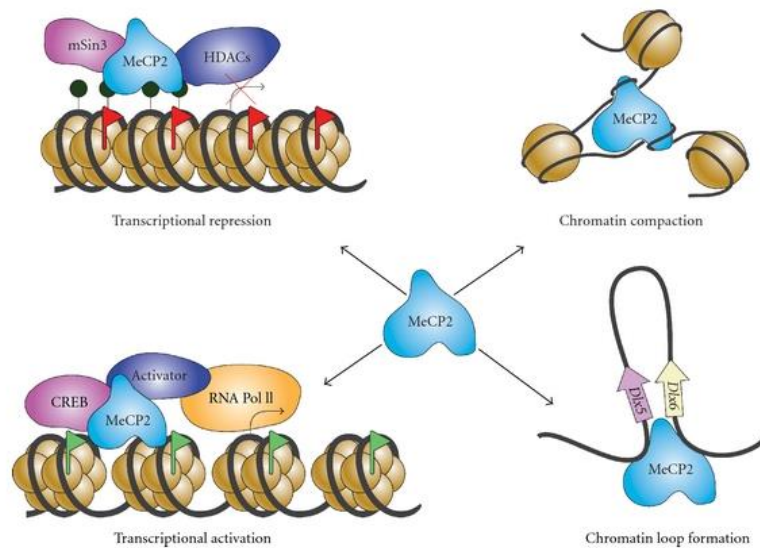
A study from 2004 reported that within the human brain, *MECP2E1* transcript levels are approximately 12-fold greater than *MECP2E2*. In contrast, a relatively higher level of *MECP2E2* expression has been reported in liver, placenta, prostate gland and skeletal muscle [166]. A study of *Mecp2e2* during mouse development revealed a restrictive expression for *Mecp2e2* to the dorsal thalamus and cortical layer V towards P21 and P60, as compared to P1 [179].

An analysis of the expression and distribution patterns of the two MeCP2 isoforms at the protein level were initially hampered by the lack of MeCP2-isoform specific antibodies. In 2012, our lab reported for the first time, the generation of an anti-MeCP2E1-specific antibody and provided evidence for the higher expression of MeCP2E1 in neurons as compared to astrocytes [1]. More recently, we also reported the generation of an anti-MeCP2E2 antibody, which allowed us to perform a direct comparison of the expression patterns of the two isoforms within the murine brain. Our studies revealed temporal as well as brain region specific alterations in the expression levels of MeCP2E1 and MeCP2E2 [2].

### 1.3.4 MeCP2 functions and target genes

Due to its diverse roles in neural cells, MeCP2 is considered to be a ‘master regulator’ of the brain (**Figure 1.5**). As the prototypical member of the MBD protein family, MeCP2 was initially deemed to be a transcriptional repressor. These theories were further strengthened by

studies that demonstrated the recruitment of co-repressor complexes such as Co-REST [180]. However, later studies elucidated that MeCP2 is also involved in transcriptional activation [139]. Subsequent investigations highlighted the significance of MeCP2 PTMs, especially phosphorylation, in MeCP2's role as a transcriptional regulator [181-183]. Additionally, MeCP2 has also been reported to directly interact with chromatin and modulate gene expression *via* chromatin compaction and looping. The latter mechanism has been shown to be critical for the silencing of a particular MeCP2 target, *DLX5* [184].



---

**Figure 1.5 Multiple functions of MeCP2 in the brain.**

MeCP2 is a multifunctional epigenetic and transcriptional regulator. It has known roles in transcriptional activation, transcriptional repression, chromatin compaction and chromatin loop formation.

*Reprinted with permission from [178].*

---

## Chapter 1

Studies analyzing MeCP2 binding patterns have demonstrated that within the neuronal genome, MeCP2 exhibits global binding and tracks methyl-CpG density [185]. In neurons, MeCP2 is as abundant as the histone octamer, and deficiency of *Mecp2* leads to the doubling of histone H1. These observations suggest that MeCP2 could be involved in the DNA methylation-dependent regulation of global transcriptional noise [185].

Hundreds of MeCP2 targets have been identified to date. A partial list of MeCP2-target genes identified till 2012 is shown in **Table 1.2** [178]. Some of these targets, such as Brain-derived neurotrophic factor (*BDNF*) and Insulin-like growth factor-1 (*IGF-1*), have been used as therapeutic options for RTT, with varying degrees of success [186]. However, most of the MeCP2-targets pursued as therapeutic options have a vast array of functions in neurons and other neural cell types. Therefore, the risk of off-target effects is much higher with current therapeutic options, drawing similarities to the ‘grenade effect’ (high risk of collateral damage). Therefore, an active area of research within the field is to identify MeCP2-targets which can be modulated with minimal off-target effects (akin to bullets).

<b>Table 1.2 A list of known MeCP2 target genes (Reprinted with permission from [178])</b>				
<b>Gene target</b>	<b>Function</b>	<b>Cell/tissue type studied</b>	<b>Direct association with MeCP2 (cell line used for ChIP)</b>	<b>Reference</b>
<i>PCDHB1</i>	Cell adhesion	Oral cancer cell lines (ZA, KOSC2, HSC5 and NA)	Yes (SH-SY5Y)	[187]
<i>PCDH7</i>	Cell adhesion		Yes (SH-SY5Y)	
<i>APBP3</i>	Intracellular signal transduction		Yes (SH-SY5Y)	
<i>CLU</i>	Extracellular molecular chaperone		No (SH-SY5Y)	
<i>CRMP1</i>	Component of semaphorin signal transduction pathway		Yes (SH-SY5Y)	
<i>DNMI</i>	Vesicular trafficking, production of microtubule bundles and hydrolyzes GTP		Yes (SH-SY5Y)	[188]

Chapter 1

<i>GNBI</i>	Integrates signals between receptor and effector proteins	RTT patient brain (frontal cortex)	Yes (SH-SY5Y)	
<i>APLP1</i>	Enhancer of neuronal apoptosis		No (SH-SY5Y)	
<i>COI</i>	Mitochondrial respiratory chain		No (SH-SY5Y)	
<i>GDII</i>	Regulates GDP/GTP exchange		No (SH-SY5Y)	
<i>Bdnf</i>	Neuronal plasticity and survival	Mouse E14 cortical culture and rat E18 cortical neurons	Yes (mouse E14 cortical culture and rat E18 cortical neurons)	[189][182]
<i>Fxyd1</i>	Ion transport regulator for Na and K-ATPase	RTT mice cerebellum and RTT patient brain	Yes (adult mouse brain, <i>Mecp2</i> Wild type (WT), and <i>Mecp2</i> null mouse; HEK293T cells)	[190,191]

Chapter 1

		(superior frontal gyrus)		
<i>Reln</i>  <i>Gtl2</i>	Neuronal layer formation and cell-cell interactions  Growth suppressor	RTT mice cerebellum	Yes (adult mouse brain)	[190]
<i>ID1, ID2</i> <i>ID3</i> and <i>ID4</i>	Regulation of neuronal differentiation	SH-SY5Y	Yes (SH-SY5Y)	[192]
<i>IGFBP3</i>	Modulation of IGF functions	RTT mouse model	Yes (HeLa cells; mouse cortex)	[193]
<i>UBE3A</i>  <i>GABRB3</i>	Ubiquitin ligase  GABA-A receptor	Brain cerebral samples of RTT, AS and autism patients	No (adult mouse cerebellum)	[194]
<i>Sst</i>  <i>Oprk1</i>  <i>Gamt</i>  <i>Gprin1</i>	Regulation of cell migration  Signal transduction  Organ	RTT mouse models  ( <i>Mecp2</i> null and <i>MECP2</i> Tg)  and <i>MECP2</i> Tg) and	Yes (RTT mouse models ( <i>Mecp2</i> null and <i>MECP2</i> Tg) and control mice; Hypothalamus)	[139]

Chapter 1

<i>Mef2c</i> <i>A2bp1</i>	morphogenesis Neurite development Neuron development and differentiation RNA splicing and mRNA processing	control mice and Hypothalamus		
<i>xHairy2a</i>	Neuronal differentiation	Xenopus embryos	Yes ( <i>Xenopus</i> neurula stage embryos)	[195]
<i>Sgk1</i> <i>Fkbp5</i>	Cellular stress response Hormone signalling	RTT mouse model	Yes (mouse brain tissue)	[196]
<i>Uqcrc1</i>	Mitochondrial respiratory chain	RTT mouse model	Yes (adult mice; whole brain)	[197]
<i>Crh</i>	Stress response	RTT mouse model	Yes (mouse brain)	[198]
<i>Dlx5</i>	Transcription factor	Not done	Yes (mouse brain)	[184]

## 1.4 Rett Syndrome (RTT)

### 1.4.1 RTT prevalence and phenotypes

RTT is a neurological disorder that predominantly afflicts females. It is a relatively rare disorder, with a prevalence of 1:10,000 live female births [199]. Patients with RTT are asymptomatic for approximately 6-18 months following birth, after which they display regression of learned skills and receding developmental milestones. Prominent RTT phenotypes include mental retardation, stereotypic hand movements, communication deficits and abnormal gait. Other symptoms include seizures, scoliosis, gastrointestinal dysfunction, and respiratory complications [184]. During the initial phase of the disorder, some patients have reduced social interactions. However, this phenotype seems to change as patients mature [200,201]. A broad range of lifespan has been reported for RTT patients, however, most patients require constant medical care [199]. Since *MECP2* is an X-linked gene, XCI greatly influences phenotypic severity in RTT females. Previous reports have suggested that skewing of XCI could correlate with the clinical severity of RTT [202], however, other groups have reported a lack of complete correlation between the two parameters [203,204].

Although considered to be a predominantly female disorder, RTT has also been described in males [205]. However, in males, *MECP2* mutations often cause fatal congenital encephalopathy, and most cases have a shorter lifespan than female RTT patients. Interestingly, a recent review highlighted that in male RTT patients, only 56 % of reported cases have *MECP2* mutations [206]. RTT can be caused by mutations in *MECP2*, other genes such as *CDKL5* and *FOXG1* or multiple genes (reviewed in [207]). Therefore, Reichow *et al.* also found 67% of the patients with other mutations including mutations in *CDKL5* and *FOXG1* [206]. This highlights the possibility that additional genetic factors influencing RTT-like symptoms in males.



### 1.4.2 MeCP2 and Rett Syndrome

Mutations in the *MECP2* gene have been reported in more than 90% of classic RTT patients [208]. Approximately 600 mutations have been identified so far within the *MECP2* gene, with missense and nonsense mutations being the most frequent ones. Even though mutations have been identified across the entire *MECP2* gene, eight recurring mutations account for more than 65% of reported cases. These mutations are clustered within two functional domains of MeCP2, with four mutations located in the MBD domain (R106W, R133C, T158M, and R168X) and four residing within the TRD domain (R255X, R270X, R294X, and R306C) [178,209,210].

As stated earlier, alternative splicing of the first two exons leads to the formation of two MeCP2 isoforms, MeCP2E1 and MeCP2E2. The majority of mutations occur in regions common to both isoforms (80-85%). However, exon one mutations have been identified in approximately 0.03–1 % of RTT patients [208,211,212]. Despite the low-frequency rates of exon one mutations, studies have shown that patients with exon one mutations exhibit greater clinical severity, underscoring its significance [213]. Various groups have reported exon one mutations that either affect or do not alter exon two transcription/translation, suggesting that certain mutations are likely to affect MeCP2 expression/function in an isoform-specific manner [214-216].

### 1.4.3 *Mecp2* mouse models of RTT

Several mouse models have been developed for RTT that recapitulate a broad range of symptoms observed in human patients. The various RTT mouse models can be categorized as either: i) *Mecp2*-deficient mouse models [217-219], ii) *Mecp2* mutant mouse models [220,221], iii) mouse models with brain-region/cell type-specific deletion of *Mecp2* [222-225], and iv) knock-

in mouse models carrying specific *Mecp2* mutations [226,227]. The hemizygous null mice of various models differ in terms of lifespan and range of phenotypes that they exhibit [228]. Of special note, the brain-region/cell type-specific mouse models exhibited both overlapping and non-overlapping phenotypes, implying unique functions of MeCP2 within different parts of the brain. For instance, forebrain neuron-specific conditional *Mecp2* mutant mice displayed several known RTT phenotypes, including increased anxiety, impaired motor coordination, and abnormal social behavior, however, within the same mouse model, locomotor activity remained unaffected [225].

### 1.4.4 Challenges for RTT therapy

The role of MeCP2 as a transcriptional regulator was already recognized before the discovery of *MECP2* mutations as the primary cause of RTT. This link led to a plethora of gene expression studies in a variety of biological samples relevant to RTT. These studies include gene expression profiling of postmortem brain samples from human RTT patients [229] and clonal lymphocyte cell cultures derived from RTT patients [230]. Similar gene expression profiling studies have been conducted in brain samples of RTT mouse models, specifically from brain regions such as cerebellum [231] and striatum [232], or cells isolated from mouse brain [233]. As expected, these studies cumulatively generated a wide list of MeCP2 target genes, partial list of which is shown in **Table 1.2**. However, a distinct shortcoming of these studies was the lack of overlapping targets identified between these studies, as well as the failure to identify a specific cellular or signaling pathway that would connect these targets. A recent study by Li *et al.* has partially addressed this shortcoming by identifying protein synthesis as a major cellular pathway that is hugely influenced by MeCP2-deficiency that, when restored, can also rescue many of the structural and functional deficits observed in neurons lacking MeCP2 [234].

## 1.5 *MECP2* Duplication Syndrome (MDS)

### 1.5.1 Causes of MDS

*MECP2* Duplication Syndrome is caused by overexpression and/or increased copy number of the *MECP2* gene which can occur *de novo* or by maternal inheritance [235]. Synonyms of ‘trisomy Xq28’ and ‘Xq28 Duplication Syndrome’ have also been used to refer to MDS because MDS is caused by duplication of DNA sequences within Xq28, which consist of *MECP2* as well as other genes. The duplicated region within the Xq28 region can range from 200 kb to 2.2 Mb [236], while some reports show that the duplicated region can also exceed 4 Mb [235]. The duplicated regions within Xq28 vary considerably between patients, but in most cases, the minimal duplicated region includes only *MECP2* and the adjacent *IRAK1* gene and seems to be sufficient to cause the major phenotypes of MDS [236-238]. However, the potential contribution of nearby regulatory genes in MDS phenotypes should not be ignored and should be explored further. The MDS discovery represented a paradigm shift in our understanding of MeCP2-associated neurological disorders. Before MDS was established as a neurodevelopmental disorder, *MECP2* mutations were thought to be primarily associated with females, mostly due to its links to RTT. However, the report of a duplication of the entire *MECP2* gene locus in a male patient who presented with similar phenotypes to RTT along with hypotonia and mental retardation [239] suggested that MeCP2 dosage is a critical factor leading to neurological disorders in males and females.

Unlike RTT, MDS has a clear familial disposition, with the majority of cases being reported in males inheriting the duplication from a carrier mother. Many female carriers are asymptomatic due to extreme (>90%) or complete skewing of XCI with the duplication-bearing X chromosome being preferentially inactivated [240]. This is also in agreement with studies that

## Chapter 1

have reported mild learning problems in female carriers with 70% XCI skewing or less [241,242]. Skewing of XCI also confers a longer lifespan for affected females, since 40% of males with MDS tend to die by the age of 25 [243]. However, a rare case of paternal transmission of *MECP2* duplication to an affected daughter who also exhibited similar phenotypes as the father has also been reported [244].

Apart from MDS, there have been reports of patients with *MECP2* triplication [245] and these patients demonstrate much more severe phenotypes compared to MDS patients [236] consistent with MeCP2 dosage effects.

### **1.5.2 Prevalence and phenotypes of MDS**

MDS accounts for approximately 1% of unexplained cases of X-linked mental retardation [238]. As a recently established disorder, MDS prevalence is still unclear. However, according to a previous report, there are approximately 150 MDS patients diagnosed so far, based on information gathered from 14 published studies [236,238-240,242,243,245-253]. A more recent analysis of reports on MDS patients suggests that MDS may represent approximately 1% of X-linked mental retardation cases [235].

MDS is primarily a neurological disorder. The disease is characterized by autistic features, stereotypic behavior, gait abnormalities, infantile hypotonia, recurrent infections and seizures [243,254]. In addition to these phenotypes common to RTT, hyposensitivity to pain and temperature has also been reported [255]. Due to its significant association with immunodeficiency, recurrent infections and allergies, MDS is considered to be a type of 'syndromic immunodeficiency' [235].

Previous studies have also demonstrated that the size of duplication does not correlate with phenotypic severity [256]. As mentioned earlier, the *MECP2* and *IRAK1* minimal duplication are sufficient to cause core MDS phenotypes [236-238]. *IRAK1* is a critical component of several signalling pathways involved in innate immunity [257]. The immunological impairments observed in MDS patients was previously considered to be partly due to *IRAK1* overexpression [248]. However, more recent studies have demonstrated that MeCP2 is also capable of negatively modulating the function of T cells [258], implying that *MECP2* duplication is sufficient to account for most, if not all the phenotypes observed in MDS patients.

### 1.5.3 Mouse models of MDS

Currently, there are two mouse models of MDS, the *MECP2* Tg1 model [259] and the Tau-*Mecp2* model [260]. Interestingly, these mouse models were initially developed to characterize the functional role of MeCP2 in neuronal development and to relate it back to RTT. For the same reason, these models were initially included under animal models of RTT. The two animal models of MDS have contributed significantly in terms of characterizing the functional consequences of *MECP2* overexpression as well as deciphering potential therapeutic strategies for MDS. A comparison of the two MDS mouse models is shown in **Table 1.3**.

<b>Table 1.3 Mouse models of <i>MECP2</i> Duplication Syndrome</b>		
	<b><i>MECP2</i> Tg1 [259]</b>	<b>Tau-<i>Mecp2</i> [260]</b>
<b>Method of <i>MECP2/Mecp2</i> overexpression</b>	PAC clone containing the entire <i>MECP2</i> locus was expressed under human <i>MECP2</i> promoter	<i>Mecp2</i> cDNA was targeted to the endogenous Tau locus which drives neuronal-specific MeCP2 overexpression
<b>Overexpression levels as compared to WT counterpart</b>	Approximately two fold	4-6 fold
<b>Phenotypes</b>	Ataxic gait, stereotypies, spasticity, anxiety, abnormal social behavior, and seizures, reduced fertility	Severe motor dysfunction, tremors, and gait ataxia, growth retardation, cataracts, lesions, reduced fertility
<b>Disease onset in hemizygote mice</b>	10 weeks	Weaning age
<b>Death</b>	1 year/ premature death	No premature death
<b>Sex-specific defects</b>	Severe phenotypes in male mice; female mice were normal or displayed milder phenotypes	Not available

### ***1.5.3.1 MECP2 Tg1 model***

In 2004, Dr. Huda Zoghbi's lab developed the first mouse model for MDS [259]. Overexpression of the *MECP2* gene was achieved by transgenic insertion of a human P1-derived artificial chromosome (PAC) clone that contained the full-length *MECP2*, driven by human *MECP2* promoter. *MECP2* Tg1 transgenic mice developed normally during the first 10-12 weeks with most mice displaying several neurological phenotypes after the 10<sup>th</sup> week. Within the 20-25<sup>th</sup> week, hemizygous mice showed enhanced learning abilities as well as synaptic plasticity. However, this improvement period was followed by a significant decline in physical activity (hypoactivity) and an increase in the frequency of seizures, curvature of the thoracic spine (kyphosis), and loss of control over voluntary muscle movements (ataxia). Approximately 30% of the mice faced premature death. For mice who survived, death occurred within a period of one year. The phenotypic progression of the disease is illustrated in **Figure 1.6**. Many of the phenotypes displayed by these mice are also exhibited in human patients including ataxic gait, stereotypies, spasticity, anxiety, abnormal social behaviors and seizures [254]. For these reasons, we used this model of MDS for some of our studies.

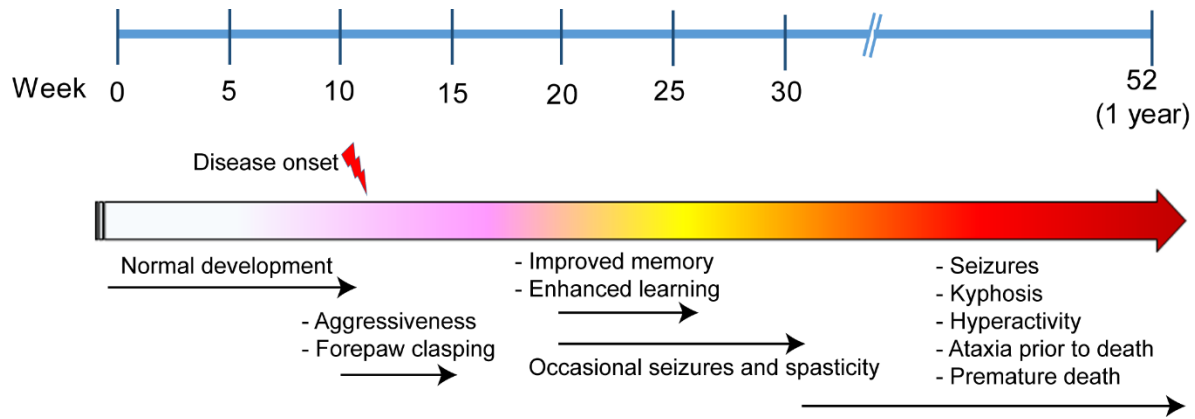


**Figure 1.6 Phenotypic progression of *MECP2* Duplication Syndrome (MDS) in *MECP2* Tg1 mice**

Transgenic mice are born normal and remain relatively normal until 10 weeks of age when phenotypic symptoms appear. The progression of disease varies during the course of the animal's lifetime and improves around 20 weeks of age. This is followed by a severe relapse associated with seizures, kyphosis, hyperactivity, ataxia prior to death or premature death.

*Information extracted from [254].*

Subsequent studies have also identified molecular targets of MeCP2 that have been linked to specific phenotypes observed in the F1 hybrid *MECP2* Tg1 mouse such as corticotropin-releasing hormone (*Crh*) [connected to anxiety] and the opioid receptor mu (*Oprm1*) [connected to abnormal social behavior] [261]. Studies on cellular morphology also revealed alterations in neuron spine turnover and dendritic arborization in *MECP2* Tg1 mice crossed with the *thy1-GFP-M* line [262]. A recent study demonstrated phenotypic rescue of this mouse model using antisense oligonucleotides, opening novel therapeutic avenues [263].



### ***1.5.3.2 Tau-Mecp2 mouse model***

Unlike the *MECP2* Tg1 mice, in the *Tau-Mecp2* mouse model *Mecp2* overexpression was achieved by inserting the *Mecp2* cDNA into the endogenous *Tau* locus which restricts MeCP2 expression within post-mitotic neurons [260]. These mice displayed progressive motor dysfunction characterized by tremors, gait ataxia, and side-to-side swaying. Similar to the *MECP2* Tg1 mice, they were relatively normal at birth. However, they showed ~60% growth retardation at weaning. After nine months, more debilitating phenotypes such as cataracts and lesions caused by scratching developed. In contrast to the *MECP2* Tg1 mice, *Tau-Mecp2* mice did not show premature death.

It should be noted that the two MDS mouse models differ significantly in terms of phenotypes displayed and lifespan. The major differences might arise from the difference in the transgene delivery (human promoter *vs.* endogenous *Tau* promoter) and cell type differences (*Tau* expression is restricted to post-mitotic neurons). A recent study using a similar *MECP2* Tg1 mouse model demonstrated the ability of antisense oligonucleotides to rescue a range of neurological phenotypes caused by *MECP2* duplication [263]. However, the differences in MDS mouse models imply that potential rescue strategies such as the antisense oligonucleotides should be tested in multiple models of MDS to further confirm their efficacy. A comparison of two of the most frequently used mouse models of RTT and MDS has been outlined below (**Table 1.4**).

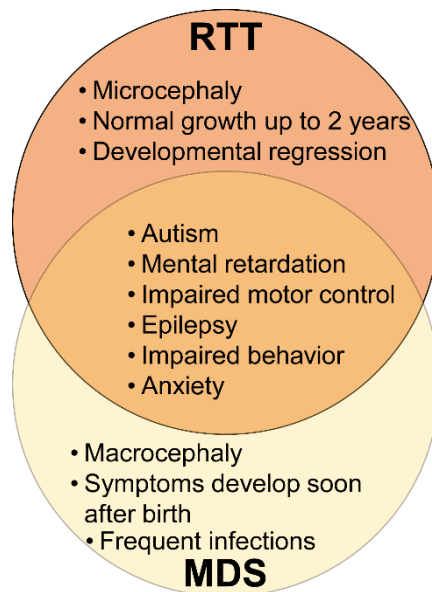
	<b>RTT (<i>Mecp2<sup>tm1.1Bird-/+</sup></i>)</b>	<b>MDS (<i>MECP2 Tg1<sup>-/+</sup></i>)</b>
Changes in MeCP2 expression	Loss of MeCP2 expression	Overexpression of MeCP2 (2-fold)
Differences in phenotypes	Hindlimb grasping, hypoactivity, abnormal gait and breathing, impaired coordination	Increased anxiety, abnormal social behaviors, premature death, seizures, abnormal nervous system phenotypes, increased aggressiveness, abnormal cognitive behaviors
Lifespan	7-8 weeks	~1 year

### 1.6 Phenotypic overlap between RTT and MDS

Interestingly, MDS was first identified and diagnosed in 2004 by Ariani *et al.* in a patient with RTT phenotypes [264]. This study also shows that MDS and RTT share similar phenotypes even though caused by extreme changes in *MECP2* expression and function/expression, respectively. Many of these initial studies mention that the patients diagnosed with MDS also presented RTT phenotypes, further illustrating that the two disorders share a certain set of phenotypes [239,264]. Another point to be noted is that both MDS animal models discussed in Section 1.5 were initially developed to study MeCP2 function in relation to RTT and later established as MDS models.

Studies have demonstrated that loss- and gain-of-function of the same gene can lead to diverse neurological disorders with overlapping phenotypes [265]. A few examples include: 1) Potocki-Lupski and Smith-Magenis syndromes that are caused by duplications and microdeletion of 17p11.2, respectively; 2) Angelman syndrome and 15q11-q13 duplication syndrome, caused by deletion or duplication of 15q11-q13 respectively; 3) RTT and MDS, caused by loss- and gain-of-

MeCP2, respectively [265]. In the case of RTT and MDS, the initial observations suggested RTT and Xq28 duplication had similar overlapping phenotypes, yet within the duplicated genes, dose-dependent *MECP2* expression changes seem to be the primary cause of the core phenotypes [236,248]. The two disorders which are caused by two distinct etiologies, share several key neurological phenotypes including autism, mental retardation, impaired motor control, epilepsy and anxiety (**Figure 1.7**). Similar to RTT, therapeutic strategies are challenged by the lack of knowledge of the molecular pathways affected by *MECP2* overexpression. In this thesis, I am examining if neuronal *rRNA* levels are altered by *MECP2* overexpression.



---

**Figure 1.7 Phenotypic overlap between Rett Syndrome and *MECP2* Duplication Syndrome.**

Rett Syndrome (RTT) is caused by loss-of-function mutations in *MECP2*. In contrast, *MECP2* Duplication Syndrome (MDS) is caused by duplication of the *MECP2* locus, also known as Xq28 duplication. By comparing the major phenotypes seen in human RTT and MDS patients, it was evident that the two disorders share several broad phenotypes.

*Information extracted from [235,265].*

## 1.7 Ribosomal RNA genomic organization, *rDNA* transcription, and processing

### 1.7.1 Ribosomal RNA genomic organization

Ribosomal *rRNA* synthesis which involves *rDNA* transcription and processing occurs within nucleoli. Nucleoli are nuclear subdomains where ribosome biogenesis occurs and therefore is known as the ribosome factory [266] (**Figure 1.8**).

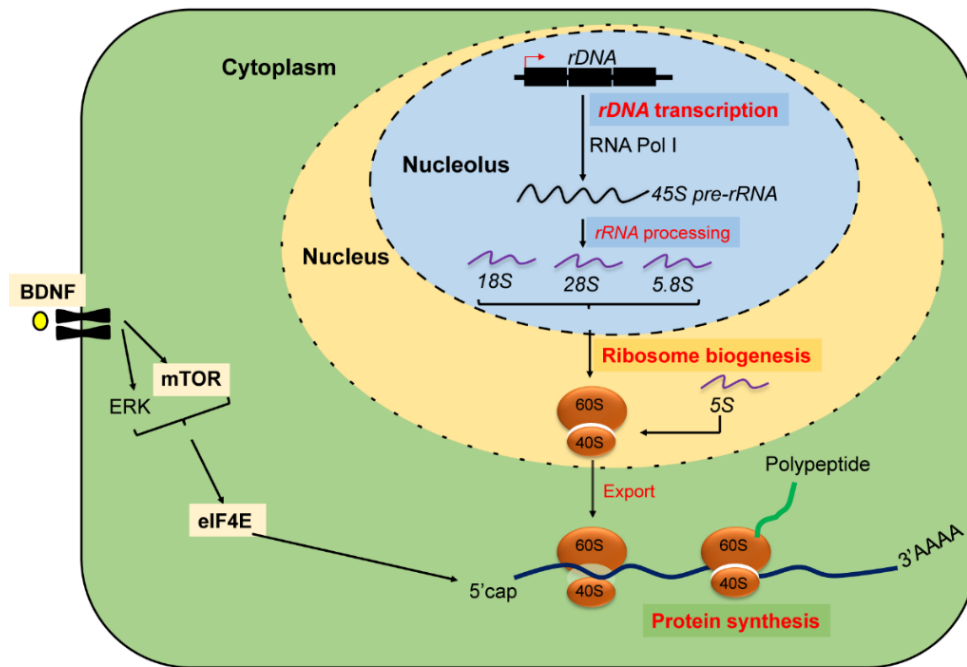


**Figure 1. 8 Ribosome biogenesis and protein synthesis.**

The *rDNA* are transcribed as *45S pre-rRNAs* by RNA polymerase I (PolI). The *45S pre-rRNA* is processed to mature *rRNA* including *18S*, *5.8S* and *28S*, which in combination with ribosomal proteins form the *40S* and *60S* ribosomal subunits. The two subunits are then transported outside of the nucleolus to the nucleus to generate the mature ribosomes. BDNF and mTOR are major regulators of protein synthesis.

## Chapter 1

In mammalian cells, *rDNAs* exist as tandem repeats of 100 or more genes within each genome. Apart from occurring as clusters known as nucleolar organizer regions (NORs), *rDNAs* are also distributed between multiple chromosomes. In humans, *rDNA* repeats are found in five acrocentric chromosomes, namely chromosomes 13, 14, 15, 21 and 22, whereas in mouse, they are located on chromosomes 12, 15, 16, 17, 18, and 19 [267,268]. Individual *rDNA* transcription units are quite large, with sizes of approximately 43 kb and 45 kb in humans and mouse, respectively [269,270]. The majority of this vast region is covered by the intergenic spacers (IGSs), which covers approximately 30 kb and consists of simple sequence repeats, transposable element spacer promoters, repetitive enhancer elements, gene promoters and transcription terminators (reviewed in [271]). The *rDNA* promoter possesses a bipartite structure, with a core promoter and upstream control element (UCE) [272,273]. Sequences coding for *45S pre-rRNA* account for the remaining ~13-15 kb of the *rDNA* transcription units. As part of an epigenetic regulatory mechanism, terminator sequences are found flanking each *rDNA* transcription unit which facilitate the release of PolII, thereby promoting further *rRNA* synthesis by increasing the pool of transcription-competent PolII units [274].

### 1.7.2 RNA polymerase I-mediated *rDNA* transcription

Optimal ribosome biogenesis rates in mammalian cells require the synthesis of approximately 8-10 million *rRNA* transcripts every 24 hours [275]. Transcription of *rRNA* is mediated by PolII, along with a multitude of accessory factors, and involves various steps including polymerase recruitment, initiation, promoter escape, elongation, termination and re-initiation all of which occurs within the nucleolus (reviewed in [274]) (**Figure 1.8**).

## Chapter 1

The initial step in *rDNA* transcription is the formation of pre-initiation complex (PIC) at the core promoter. The PIC complex consists mainly of PolII and SL1 [(TIF)-IB in mouse]. The SL1 itself is a complex of the TATA-box binding protein (TBP) and other TBP-associated factors (TAF) consisting of TAFI110, TAFI63, and TAFI48 [276,277]. SL1 confers selectivity and specificity for PolII recruitment and PIC formation since PolII itself does not possess sequence-specific DNA-binding activity [277]. SL1 recruits PolII to the *rDNA* promoters by the interaction of TAFI63 and TAFI110 subunits with RRN3, a factor associated with PolII. In addition to SL1, PIC formation and recruitment of PolII also requires Upstream Binding Factor (UBF). The exact role of UBF in this process remains unclear, however, conditional deletion of UBF leads to dissociation of both PolII and SL1 from the *rDNA* promoter, highlighting its significance [278]. Human PolII units consist of PolII $\alpha$  and PolII $\beta$ . Even though PolII $\alpha$  comprises 90% of this pool and is catalytically active, it is incapable of initiating *rDNA* transcription. Instead, PolII $\beta$  is the polymerase that can initiate *rDNA* transcription accurately [279].

Successful PIC formation and initiation is followed by promoter escape, wherein PolII leaves the *rDNA* promoter and proceeds to the transcription elongation phase. During, PolII-promoter escape, RRN3 dissociates from PolII $\beta$  and becomes inactivated [280]. Termination of PolII transcription elongation requires two separate factors, transcription termination factor for PolII (TTF1), which bends the 3' end of the transcribed region thereby pausing PolII and transcript release factor (PTRF), that mediates the dissociation of TTF1-paused ternary transcription complex [281]. Previous studies have also suggested that transcription termination facilitates reinitiation of PolII transcription through PTRF by recycling PolII released from termination sites back to the initial promoter, where UBF and SL1 remain bound, even after PolII promoter escape [277,281].

### 1.7.3 Epigenetic regulation of ribosome biogenesis

The *rDNAs* are the most abundant genes within the eukaryotic genome [282]. However, only a fraction of the *rDNAs* are transcriptionally active, with the remaining subpopulation existing as transcriptionally inactive genes. The active/inactive fractions of *rDNA* possess distinct epigenetic signatures as well as different nucleosome positioning [283]. A major decider of the active/inactive fraction of *rDNA* is TTF1. Apart from mediating transcriptional termination, TTF1 also binds to the 5' end of individual *rDNA* units at the T<sub>0</sub> termination site (promoter-proximal terminator) and recruits chromatin remodeling complexes that determine the transcriptional activity of the corresponding *rDNA* units [284]. In the active *rDNAs*, TTF1 recruits Cockayne syndrome protein B (CSB), a DNA-dependent ATPase remodeler, as well as G9a, a histone methyltransferase that is responsible for mono- and dimethylation of H3K9. G9a, in turn, facilitates the association of heterochromatin protein1 $\gamma$  (HP1 $\gamma$ ) capable of recognizing H3K9 methylation, to the *rDNA* [285]. Despite the common association of H3K9 methylation and HP1 $\gamma$ -binding with transcriptional repression, the aforementioned studies confirmed that within the context of *rDNA* transcription, these marks correlate with transcriptional activation.

TTF1-mediated inactivation of *rDNAs* occurs through a temporally regulated and sequential process involving significant crosstalk between multiple epigenetic mechanisms [286]. In inactive *rDNAs*, TTF1 recruits the nucleolar remodeling complex (NoRC), an ISWI/SNF2-containing ATP-dependent chromatin remodeler. NoRC is comprised of two individual subunits, ATPase SNF2h and TIP5 (TTF-I-interacting protein 5). Initially, NoRC is recruited to the *rDNA* promoter by the interaction between TIP5 and TTF1 bound to the promoter-proximal terminator T<sub>0</sub>. Subsequently, NoRC recruits histone methyltransferases and histone deacetylases, causing methylation of H3K9, H3K20, as well as H3K27 and H4 deacetylation, respectively. These histone

## Chapter 1

modifications are followed by recruitment of DNMTs leading to methylation of CpG dinucleotides within the *rDNA* promoter [284].

The murine *rDNA* has four CpG dinucleotides within its regulatory region at positions -167, -143, -133, and +8. However, studies have shown that methylation of CpG -133 is sufficient to impair *rDNA* transcription [287]. Methylation of CpG-133 has been demonstrated to inhibit the binding of UBF to the UCE region, which prevents initiation complex formation and thereby, transcription [287]. The correlation between DNA methylation and *rDNA* transcription is a bit more complex in humans, with 25 CpGs in the *rDNA* promoter. Human *rDNAs* often exhibit a mosaic methylation pattern wherein they are neither completely methylated nor unmethylated [288]. However, the correlation between decreased *rRNA* expression and significant hypermethylation in the promoter and 5' regulatory region observed in suicide patients suggest that DNA methylation has a repressive role in the regulation of human *rDNA* transcription, similar to mice [289].

The role of ncRNAs in the regulation of *rDNA* expression represents an additional layer of epigenetic complexity. In mouse cells, transcripts from promoters residing within the IGS regions [promoter-associated RNA (*pRNA*)] are known to bind to the NoRC complex [290]. Studies have demonstrated that knockdown of *pRNA* leads to displacement of NoRC from the nucleoli as well as alterations of histone modifications, decreased *rDNA* DNA methylation, and enhanced *45S pre-rRNA* synthesis [290]. Subsequent studies have linked the function of *pRNA* to its RNA structure (reviewed in [291]). The recognition of TIP5 towards *pRNA* is based on its phylogenetically conserved secondary structure. Mutations that alter the secondary stem-loop structure of *pRNA* impair binding of the TIP5 subunit of NoRC to *pRNA*, thereby compromising the nucleolar localization of NoRC and consequently its repressive functions [292]. In addition to highlighting



the critical role of *ncRNA* in *rRNA* transcription, these studies also provide evidence for an RNA-dependent association of NoRC with *rDNA* promoters.

Aside from epigenetic marks that mediate various layers of repression, inactive *rDNAs* are also characterized by a change in nucleosome positions with respect to their coverage of the promoter and TSS [293]. In mouse cells, within the active *rDNAs*, nucleosomes span the region covering -157 to the TSS, whereas in inactive *rDNAs*, nucleosomes shift by approximately 25 nucleotides, from -132 to +22, implying a strong correlation between active/inactive *rDNA* ratio and nucleosome positioning. This shift in nucleosome positioning is mediated by NoRC, specifically the ATPase SNF2h subunit. In the repressive state, the nucleosome position, the UCE region harboring the CpG-133 and the UBF binding site are shifted to the nucleosomal linker region, whereas the core promoter is displaced to the inside of the nucleosome. Thus, in silent *rDNAs*, the nucleosome separates the UCE and core promoter, hindering the binding of the UBF/SL1 complex, thereby preventing PIC formation.

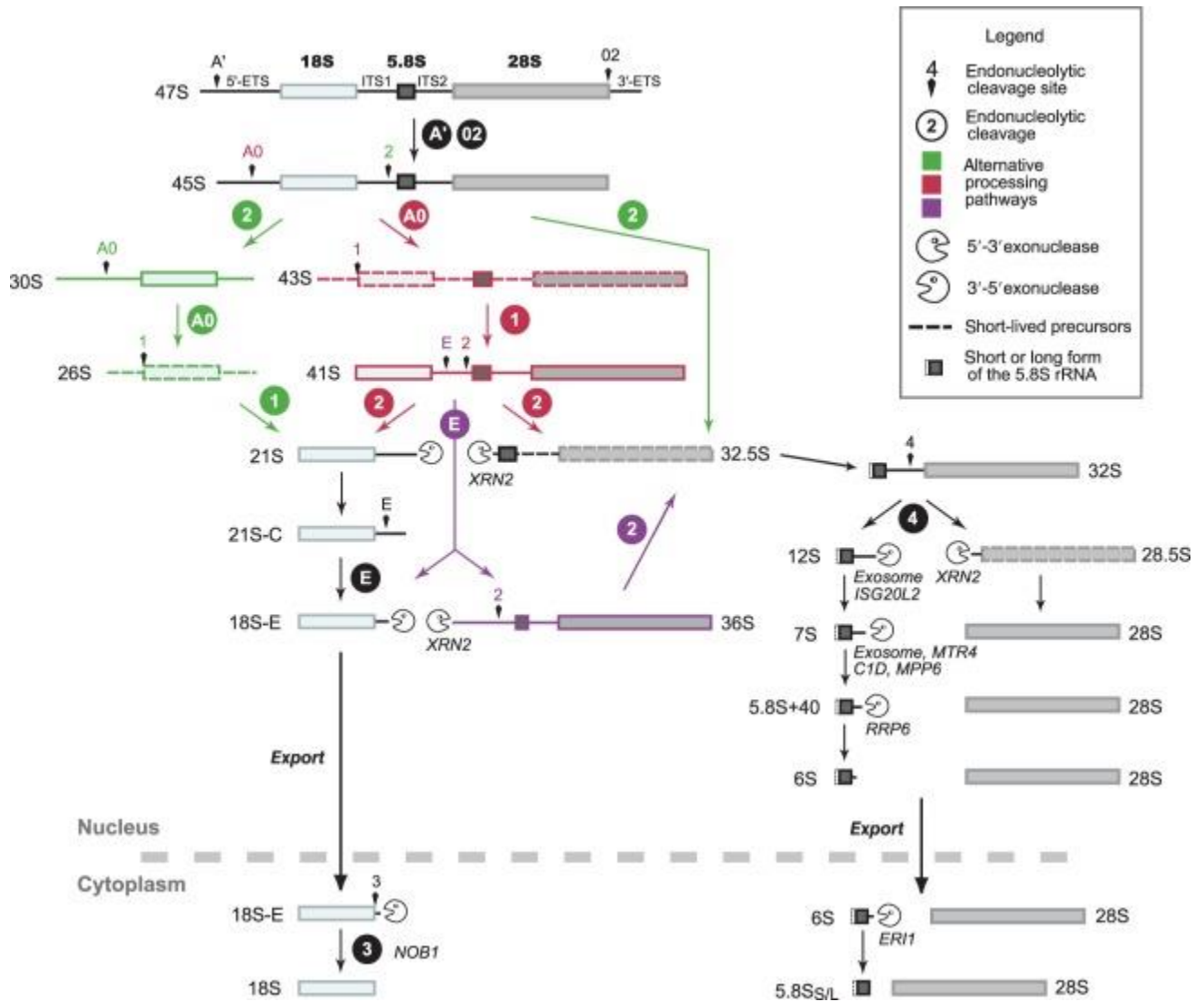
In summary, the interplay of different epigenetic mechanisms leads to the formation of active and inactive *rDNA* fractions. TTF1 has been proven to be the master regulator of this process, based on its recruitment of CSB/G9a or NoRC.

### 1.7.4 Ribosomal RNA processing

PollI-mediated transcription of *rDNAs* leads to the generation of a polycistronic primary transcript, named *45S pre-rRNA* (reviewed in [271]). This primary transcript then undergoes a series of both endonucleolytic as well as exonucleolytic cleavages to yield the mature forms of *rRNAs* namely, *18S*, *28S*, and *5.8S rRNA* (**Figure 1.9**). The *18S*, *28S*, and *5.8S rRNAs* are flanked

# Chapter 1

by the 5' and 3' external transcribed sequences (ETS) in the primary transcript and are also separated from each other by two internal transcribed sequences (ITS). Co-transcriptional association of the newly transcribed 45S pre-rRNA with ribosomal proteins (RPs), pre-ribosomal factors (PRFs), and small nucleolar ribonucleoprotein particles (snoRNPs) leads to the formation of ribonucleoprotein complexes, which become the focal point of 45S pre-rRNA folding, rRNA modifications and the initial stages of ribosome assembly .



---

**Figure 1.9 Ribosomal RNA (*rRNA*) processing in mammalian cells.** “Pre-ribosomal RNA (*rRNA*) processing in mammalian cells. The *pre-rRNA* processing presented here combines data from studies in human and murine cells. Alternative cleavage sequences are depicted in different colors. Short-lived precursors are represented with dotted lines. Cleavage of the *45S pre-rRNA* can either start in the 5'-ETS (red) or in the ITS1 (green), which defines two pathways. If cleavage of the 5'-ETS occurs first (*41S pre-rRNA*), subsequent cleavage in the ITS1 takes place either at site 2 or at site E (purple). Initial cleavage at site 2 is the major pathway in HeLa cells, considering the abundance of the *30S pre-rRNA* relative to the *41S*. In mouse cell lines, the *36S pre-rRNA* is readily detected. The endonuclease NOB1 is necessary for maturation of the 3' end of the *18S-E pre-rRNA* in the cytoplasm. Formation of the long and short 5' ends of the *5.8S rRNA* is not fully documented in mammalian cells. The *5.8S rRNA* 3'-end maturation pathway primarily involves exonucleases, but the *7S pre-rRNA* was also proposed to result from endonucleolytic cleavage of the *12S pre-rRNA*. It has not been formally demonstrated that final maturation of the *6S pre-rRNA* takes place in the cytoplasm in mammalian cells, but this was shown in *Xenopus laevis* and *Saccharomyces cerevisiae*.”

*Reprinted with permission from [294]*

---

#### **1.7.4.1 5'ETS processing**

The initial stage of *rRNA* processing involves the endonucleolytic processing of the 5'ETS and cleavage within the ITS1. An early event in this step involves the cleavage of the two sites A' or A0 within the 5'ETS. Efficient cleavage of A' has been shown to be dependent on U3, U14, E1, and E3 snoRNPs [295]. However, in human cells, the recruitment of the U Three Protein (UTP-A) complex upstream of U3 snoRNAs has been shown to be critical for this step, as well as 5'→3'

## Chapter 1

exoribonuclease-2 (XRN2) [296]. This cleavage step appears to promote access to the processing machinery for further processing of the primary transcript. The temporal sequence of 5'ETS removal relative to ITS1 cleavage varies greatly between species. For instance, in humans, the generation of the *30S pre-rRNA* indicates that ITS cleavage preceded 5'ETS cleavage. Moreover, in mouse, ITS1 cleavage at site E before cleavage at site two leads to the generation of *36S rRNA* [297,298].

In mammalian cells, two alternate pathways exist for 5'ETS cleavage, endonucleolytic cleavage at sites A0 and A1, which leads to the formation of the *43S* and *30S rRNA* precursors, both reactions being mediated by endoribonucleases. The U3 snoRNA is critical for 5'ETS processing as it hybridizes with distant segments of the *pre-rRNA* and chaperones of RNA folding. A multitude of factors are also involved besides U3 snoRNA, including snR30/U17, U14 snoRNAs, the SSU processome and a host of ribosomal proteins [299,300].

### ***1.7.4.2 18S rRNA maturation***

Excision of nucleotides from the 3' end of the *21S pre-rRNA* leads to the formation of the *21S-C* intermediate. This trimming of the *21S pre-rRNA* has been proposed to be mediated by the exosome and does not proceed further than the boundary of domain C within ITS1 in mammals [301]. In mammalian cells, the formation of the 3' end of the *18S rRNA* requires both endonucleases and exonucleases. Cleavage within the endonucleolytic site two and site E leads to the formation of *18S-E pre-rRNA*. Subsequently, these *pre-rRNA* undergo 3'→5' exonucleolytic trimming. This shortening of the 3' end of the *18S-E* precursor occurs within the nucleus and the cytoplasm. Following nuclear export, processing of the *18S-E pre-rRNA* is likely mediated by NIN1/PSMD8 binding protein 1 homolog (NOB1), *via* cleavage at site three, leading to the

formation of mature *18S rRNA* [301,302]. The oligouridylation of *18S-E pre-rRNA*, which occurs in the cytoplasm, is thought to promote the recruitment of an exonuclease. Cytoplasmic processing of *18S-E pre-rRNA* by exonucleolytic trimming could facilitate NOB1 access to site 3 [301].

#### ***1.7.4.3 Maturation of 5.8S rRNA and 28S rRNA***

The initial processing of the 5' end of *32S rRNA* is mediated by the exonuclease XRN2 [303]. Subsequent endonucleolytic cleavage of *32S rRNA*, within the ITS2 (site 4b in mouse), leads to the formation of *12S* and *28.5S rRNAs*. The transition from *28.5S rRNA* to *28S rRNA* is relatively quick, with one intermediary step involving trimming of the 5' end of the *28.5S rRNA*, which is mediated by XRN2 [303]. Processing of *5.8S rRNA* however, is a multi-step process. Endonucleolytic cleavage of site 4a within ITS2 leads to the formation of *7S rRNA* [304,305]. Further maturation of *7S rRNA* involves the function of several exosome components and exosome-associated factors such as MTR4, MPP6, and CD1 [306,307]. The resultant *rRNA*, termed *6S rRNA*, undergoes a final processing step mediated by 3'→5' exoribonuclease ERI1 to form *5.8S rRNA* [308].

### **1.8 Role of epigenetics in neural differentiation and neuronal disorders**

Brain development is an extremely complicated biological process with intertwined influences of genetics, epigenetics, and environmental cues. These factors fine tune the development of interconnections between brain cell types during brain development. Epigenetic mechanisms are involved in numerous processes during brain development which include cellular

differentiation [309], experience-dependent cellular adaptations that modulate neuronal plasticity [310], and finally maintaining proper brain functions throughout life [24].

### **1.8.1 The role of epigenetics in neurogenesis and neural cell function**

Different epigenetic mechanisms such as DNA methylation, hPTMs, and miRNAs are known to be involved in the development, differentiation and function of various brain cell types. The role of DNA methylation in neurogenesis has been primarily studied by deletion studies of DNMTs and MBD proteins. In the case of DNMT1, specific deletion in embryonic neural progenitor cells leads to hypomethylation and subsequent derepression of glial differentiation-related genes and premature astroglial differentiation [311]. *Dnmt3a*-null mice exhibit impaired neurogenesis and have approximately 10-fold fewer neurons [312]. Deficiency of *DNMT3B* specifically within the neuroepithelium (cells generate neurons and astrocytes at specific stages of development) leads to premature neuronal differentiation [84]. Moreover, hypomorphic germline mutations of *DNMT3B* are associated with immunodeficiency, centromere instability, facial anomalies (ICF) syndrome, a disorder which also leads to mental retardation [313]. In terms of MBD proteins, MBD1-deficiency is known to impair adult hippocampal neurogenesis [314]. *Mbd2* depletion leads to decreased lifespan of olfactory receptor neurons [315]. Depletion of MBD3, on the other hand, leads to altered neural cell fate determination in the cerebral cortex [316].

MeCP2 has been shown to promote neuronal differentiation in neural precursor cells [317]. However, another study demonstrated that MeCP2 is involved in the maturation of neurons rather than regulating cell fate decisions during neurodifferentiation [318]. Apart from being a central player of gene regulation and a chromatin structural protein, MeCP2 also regulates neuronal morphology and maintenance of neural connections. MeCP2 expression peaks around the time of

## Chapter 1

synaptogenesis (formation of synapses, which are points of communication between two neurons) during mouse brain development suggesting its involvement in synaptic plasticity as well [207].

Several histone modifiers have been identified as regulators of adult neurogenesis. The histone acetyltransferase Querkopf is known to regulate adult neurogenesis *in vivo* [319,320]. NSC/neural progenitor cells derived from Querkopf mutant mice display reduced self-renewal and differentiation capacity [319]. Apart from histone acetyltransferases, histone deacetylases like HDAC2 are also known to regulate adult neurogenesis [321]. Both HDAC1 and HDAC2 are known to regulate the differentiation of oligodendrocytes [322].

Another intriguing involvement of histones is the utilization of histone variants for specific neuronal functions such as activity-dependent gene regulation [323]. Histone variants are non-allelic histone proteins capable of replacing their canonical counterparts within nucleosomes. For instance, following neuronal depolarization, the histone chaperone DAXX facilitates the incorporation of the H3.3 variant into chromatin associated with several activity-dependent gene loci, leading to their transcriptional activation [324]. A recent study has shown that the incorporation of canonical histones of H3 family such as H3.1 and H3.2 versus the variant H3.3 could be developmentally regulated in neurons. In embryonic neurons, H3.1 and H3.2 constitute the majority of H3. However, as neurons mature, H3.3 accumulates to become the predominant H3 in adult neurons. Moreover, the expression and turnover of H3.3 was sensitive to environmental influences, in contrast to the canonical H3 [325]. These observations suggest that the incorporation of histone variants is an epigenetic mechanism that allows experience-mediated regulation in neurons.

Neuron-specific isoforms of histone modifiers also play a major role in regulating neuronal activity-dependent functions. For example, Lysine-specific demethylase 1 (LSD1/KDM1A) is a

transcriptional co-repressor that demethylates H3K4 [326]. The mammalian *LSD1* gene has 21 exons and alternative splicing of the *LSD1* gene which includes exon E8a leads to the generation of two isoforms restricted to the nervous system. These two isoforms, LSD1-8a and LSD1-2a/8a, are collectively known as neuroLSD1 and co-exist with LSD1 in neurons [327]. Toffolo *et al.* showed that LSD1-8a is capable of promoting neurite growth, upon phosphorylation of the Thr369b residue encoded by exon E8a, suggesting a unique function that is carried out by the neuro-specific isoform [328]. Subsequent studies by the same group demonstrated that neuroLSD1 levels are regulated by neuronal activity and control neuronal excitation in the mammalian brain [329].

Approximately 40% of highly expressed lncRNAs exhibit brain-specific expression [330,331]. A prominent example of regulatory RNAs within the brain is Natural antisense transcripts (NATs), a relatively novel epigenetic mechanism with significant implications in brain function [332,333]. Studies have shown that *BDNF*, which encodes a growth factor critical for numerous aspects of neuronal growth and function as well as a target of MeCP2, exhibits active transcription from both strands, leading to the transcription of a noncoding natural antisense transcript, *BDNF-AS*. Knockdown of *BDNF-AS* leads to an increase in BDNF levels *in vitro*, suggesting that the antisense transcript negatively regulates *BDNF* itself. The increased levels of BDNF led to induced neuronal outgrowth, suggesting that pharmacological inhibition of *BDNF-AS* could be a significant tool for locus-specific upregulation of *BDNF* [334].

### **1.8.2 Epigenetics and neurodevelopment (neurogenesis and brain development)**

Several studies have demonstrated the general importance of miRNAs in brain development by conditional Dicer knockout studies, which in most cases leads to neuronal



## Chapter 1

apoptosis [335-337]. The *miR-17-92* cluster has been shown to play a vital role in neuronal generation during corticogenesis by regulating neural stem cell expansion [338]. *miR-124* is a neural-specific miRNA that acts as a neuronal fate determinant in the subventricular zone, and thus plays a significant role in brain development [339]. *miR-124-1* knockout mice exhibit decreased brain size, as well as cell death in the hippocampus and cortex. The extent of neuronal damage was also evident by the front and hind limb clasping response in *miR-124-1* knockout mice, a phenotype observed in many neurodegenerative disorders [340]. Altogether, these studies demonstrate the critical role of miRNAs in mammalian brain development.

Histone modifying enzymes are also known to affect brain development [341]. For instance, HDAC1 and HDAC2 are known to have critical roles in regulating the progression of neuronal precursors to mature neurons *in vivo*. Simultaneous deletion of HDAC1 and HDAC2 leads to hippocampal abnormalities and death within seven days following birth, highlighting the essential role of the two HDACs in brain development [342]. Mice lacking HDAC3 die within 24 hours of birth, and have altered proportions of oligodendrocytes and astrocytes [343].

Intergenerational as well as transgenerational epigenetic effects influence brain development [344]. Transgenerational epigenetic effects include epigenetic memory of exposure to environmental insults such as alcohol, drugs, smoking, nutritional changes and parental stress at the pre-conception stage or even before that. These environmental insults can change epigenetic mechanisms in the germ-line and thereby transmit epigenetic memory [345]. For example, pre-conception paternal alcohol consumption has been shown to change DNA methylation profiles of the sperm and somatic cells of the offspring. As these DNA methylation patterns are associated with imprinting and chromatin remodeling [346], they have been postulated to be linked to the

severe spectrum of neurodevelopmental disorders referred to as Fetal Alcohol Spectrum Disorders, in which brain development is severely affected [347].

### 1.8.3 Epigenetic modifiers involved in neuronal disorders

Many CNS disorders have direct links to alterations in epigenetic mechanisms. One of the most well-studied neuronal disorders directly linked to epigenetics is RTT, caused by mutations on *MECP2* [178,207]. Alpha-thalassemia X-linked (ATR-X) syndrome, characterized by profound mental retardation, is caused by changes in the methylation of *rDNAs*, Y-specific repeats, and subtelomeric repeats [348]. Methylation-coupled silencing of the *FMRI* gene following an expansion of its 5'UTR leads to Fragile X syndrome, the most prevalent cause of heritable mental retardation [349]. Rubinstein-Taybi syndrome is an example of a CNS disorder caused by mutations in a histone acetyltransferase coding gene (*CREBBP*) and is characterized by impaired long-term memory [350].

Several epigenetic mechanisms have also been linked to disorders with genetic causal factors. In many human postmortem Parkinson's disorder (PD) brains, DNMT1 has been observed to relocate from the nucleus to the cytoplasm. This translocation has led to hypomethylation of many genes associated with PD, including *SCNA* (which encodes  $\alpha$ -synuclein) [351]. Higher levels of  $\alpha$ -synuclein are associated with defects in the dendritic development of newly generated neurons in the adult mouse hippocampus [352]. *LRRK2*, which encodes a Leucine-rich repeat kinase 2, is another gene that is significantly associated with PD [353]. Mutations in *LRRK2*, such as *LRRK2* G2019S, result in impaired survival of newly generated neurons in the olfactory bulb and mouse dentate gyrus [354]. Recent studies have shown that *miR-205* post-transcriptionally regulates *LRRK2*. Intriguingly, the expression of *miR-205* itself is downregulated in patients with sporadic

PD, suggesting that alterations of epigenetic regulators could be a causal factor of PD [355]. Reduction in the levels of *miR-133b* and *miR-34b/34c* have also been reported in PD patients [356].

Alzheimer's disease (AD) is another epigenetics-associated disorder [357]. Both genome-wide and gene-specific DNA methylation changes have been reported in AD patients [358]. Genome-wide decrease in both 5mC and 5hmC levels have been observed in the hippocampus of AD patients [359]. Moreover, the expression of *Psen1* and *Psen2*, mutations of which is known to be associated with early-onset AD, is regulated by both DNA methylation as well as H3K9/14 acetylation in the mouse cerebral cortex during development [360].

Overall, epigenetic mechanisms and its associated factors, specifically MeCP2, play a critical role in brain and nervous system development. Alternations in these fine-tuned epigenetic mechanisms lead to neurodevelopmental disorders such as RTT and MDS. Understanding the role of epigenetic mechanisms in brain cell types as well as models of neurological disorders should lead to the development of better rescue and treatment strategies for these disorders.

### **1.9 MeCP2 and *rRNA* synthesis**

A direct role for MeCP2 in regulating *rRNA* biogenesis has not been investigated before. However, previous studies on the effects of *Mecp2/MECP2* deficiency has often reported observations that suggest a potential role of MeCP2 in regulating neuronal *rRNA* biogenesis. One of the first observations were reported by Singleton et al., (2011), by demonstrating that *Mecp2* deficient neurons had significantly smaller number of nucleoli [361]. Within the same study, the authors hypothesized that the smaller neurons could be indicative of *rDNA* silencing by *Mecp2* deficiency, but the hypothesis was never tested nor proven by future studies. In a separate study, Gabel *et al.*, demonstrated decreased levels of *18S* and *28S rRNA* in mouse primary neurons in

## Chapter 1

which *Mecp2* was depleted by shRNA knockdown [362]. These observations were part of a study in which the primary objective was to investigate the repression of long genes (>100kb) by MeCP2 in a DNA methylation-dependent manner [362]. In a separate study, aimed to analyze the globally compromised transcription and protein translation in *MECP2*-deficient neurons, Li *et al.*, demonstrated that 5.8S *rRNA* was also decreased. These studies used a human *in vitro* experimental model in which neuronal cells derived from human embryonic stem cells with a loss-of-function *MECP2* allele [234]. Collectively, these studies hint towards *rRNA* regulation by MeCP2.

### 1.10 Summary

MeCP2 is a multifunctional transcriptional regulator that is highly expressed in neurons and is capable of recognizing and binding to methylated DNA [80]. Alternate splicing of the first two exons of *Mecp2/MECP2* leads to the generation of two isoforms, MeCP2E1 and MeCP2E2 [166,167]. Since the discovery of the two MeCP2 isoforms, further characterization of their expression in the central nervous system and their functions had been hindered by the lack of specific antibodies that can differentiate the isoforms. For the same reason, little is known about the expression and localization within different neural cell types of the brain. In order to understand the significance of MeCP2 functions and neurological disorders caused by loss or overexpression of MeCP2, characterization of MeCP2 isoform-specific expression and localization patterns is essential.

Loss-of-function/expression mutations in the *MECP2* gene are the primary cause of RTT, while increased expression (overexpression) of *MECP2* through gene duplication leads to MDS. Both diseases are neurological disorders which have no cure [178,207]. RTT is a

## Chapter 1

neurodevelopmental disorder affecting mostly young females. MDS, on the other hand, occurs almost exclusively in males [243]. Surprisingly, even with extremely different etiologies, the two disorders exhibit many overlapping phenotypes [265]. This observation suggests that at least for a subset of cellular processes, the net outcome of *MECP2*-deficiency and *MECP2* overexpression could be the same. However, such a central cellular process that is common to the two disorders has not been identified to date.

Ribosomal RNA synthesis is a critical cellular process, essential for proper survival and function of all cells, including neurons. The synthesis of *rRNA* occurs within the nucleoli which are sites of active *rDNA* transcription and *rRNA* processing. The *45S pre-rRNAs* generated by *rDNA* transcription are processed to generate mature *rRNAs* (*28S*, *18S*, and *5.8S*), which are then assembled into ribosomes along with ribosomal proteins. Regulation of *rRNA* synthesis occurs at two stages, at the *rDNA* transcription and *rRNA* processing. Multiple epigenetic mechanisms modulate *rRNA* synthesis, which is a tightly regulated process, controlled at multiple steps.. However, the role of MeCP2 in regulating neuronal *rRNA* synthesis and its relevance to MeCP2-associated disorders is not yet fully investigated.

### **1.11 Rationale, Hypotheses, and Research Aims**

#### **1.11.1 Rationale**

Despite the discovery of the second isoform of MeCP2 in 2004, endogenous protein expression levels of MeCP2E1 and MeCP2E2 remained unexplored due to the absence of reagents that could specifically detect the individual isoforms. Even though other groups had studied the two MeCP2 isoforms at the transcript level, the question remained whether transcript levels accurately reflect expression levels of the proteins. Furthermore, regulatory mechanisms that could

## Chapter 1

affect individual MeCP2 isoforms at the protein level were also unexplored due to a lack of MeCP2 isoform-specific antibodies. Therefore, the development of MeCP2 isoform-specific antibodies was a critical step in the advancement of MeCP2 research. Nonetheless, at the transcript level, *Mecp2e1/MECP2E1* was shown to be expressed at much higher levels than *Mecp2e2/MECP2E2* in mouse and human brain samples [167]. Moreover, deletion of *Mecp2* specifically in mice neurons was shown to be sufficient for the occurrence of RTT-like phenotypes [220]. Collectively, these studies suggested that MeCP2 expression, presumably MeCP2E1, was critical for neuronal function. However, abnormalities in astrocytes deficient of *Mecp2* were also reported, and was implicated in the etiology of RTT [363]. The individual contributions of neurons and glia towards MDS are still unknown. As a primary step towards understanding the contribution of MeCP2 isoforms in the function of neurons and astrocytes, the development of MeCP2 isoform-specific antibodies and subsequent expression studies in both cell types was essential.

MDS is one of the primary disorders associated with MeCP2 dysfunction. Behavioral impairments caused by *MECP2* duplication have been extensively characterized in human patients, as well as primate and rodent animal models [364-366]. However, the molecular mechanism underlying the MDS phenotype is poorly understood. MDS and RTT share many phenotypes including mental retardation and autistic features which implies that there might be cellular processes that are similarly affected in both disorders. Previous research studies have reported that *Mecp2/MECP2*-deficient neurons have lower levels of mature *rRNAs*, in addition to decreased protein synthesis [234]. Perturbations in *rRNA* biogenesis are increasingly being associated with neurological disorders [367]. However, potential alterations in *rRNA* levels by MeCP2 overexpression have not been investigated to date. In the current study, I examined the

## Chapter 1

effect of MeCP2 overexpression on neuronal *rRNA* levels *in vitro*, as well as *in vivo* in a mouse model of MDS.

### 1.11.2 Hypotheses

- The MeCP2E1 isoform exhibits differential expression patterns and/or levels in neurons, as compared to astrocytes.
- Overexpression of *MECP2* changes the levels of precursor and mature *rRNA* levels in primary neurons.

### 1.11.3 Research aims

Specific Aim 1. Analysis of MeCP2 isoform-specific expression in murine neural cells using custom-made antibodies

Specific Aim 2. Determine the effects of *MECP2* overexpression on *rRNA* levels in neurons

## **Chapter 2: Materials and Methods**

### **2.1 Ethics statement**

Experiments were conducted in accordance with the standards of the Canadian Council on Animal Care with the approval of the Office of Research Ethics at the University of Manitoba. All experiments were conducted in accordance with animal experimentation guidelines (University of Manitoba). All experimental procedures outlined here were reviewed and approved (protocol numbers: 09-020/1, 09-020/1/2, 12-031, 12-031/1/2, 12-031/1/2/3) by the University of Manitoba Bannatyne Campus Protocol Management and Review Committee.

### **2.2 MeCP2 isoform-specific antibody production**

#### **2.2.1 Peptide selection for antibody synthesis**

Peptide selection was performed by Dr. Rastegar and her team, in consultation with commercial companies. As the ultimate purpose of the MeCP2 antibodies generated was to study expression and functions of human MeCP2, the human MeCP2 amino acid sequence was used to identify a suitable peptide. Moreover, the human MeCP2E1 and MeCP2E2 amino acid sequences are 94% and 95.3% similar to that of the mouse sequence, respectively, as determined by Pairwise Sequence Alignment (PROTEIN) in EMBOSS Needle (**Figure 2.1**). This high percentage of sequence similarity implicated its suitability in using the generated antibody in mouse model systems as well.



## Chapter 2

### A) MeCP2E1

H-MeCP2E1	1	-----MAAAAAAAPS GGGGGGEEERLEEKSE DQDLQGLKDKPLKFKKVKK	45
M-MeCP2E1	1	MAAAAATAAAAAAPS GGGGGGEEERLEEKSE DQDLQGLRDKPLKFKKAKK	50
H-MeCP2E1	46	DKKEEKEGKHEPVQPSAHHSAEPAEAGKAETSESGSAPAVPEASASPKQ	95
M-MeCP2E1	51	DKKEDKEGKHEPLQPSAHHSAEPAEAGKAETSESSGSAPAVPEASASPKQ	100
H-MeCP2E1	96	RRSIIRDGRPMYDDPTLPEGWTRKLRKQRKSGRSAGKYDVYLINPQGKAFR	145
M-MeCP2E1	101	RRSIIRDGRPMYDDPTLPEGWTRKLRKQRKSGRSAGKYDVYLINPQGKAFR	150
H-MeCP2E1	146	SKVELIAYFEKVGDTSLDPNDFDFTVTGRGSPSRREQPKPKPKSPKAPG	195
M-MeCP2E1	151	SKVELIAYFEKVGDTSLDPNDFDFTVTGRGSPSRREQPKPKPKSPKAPG	200
H-MeCP2E1	196	TGRGRGRPKGSGTTRPKAATSEGVQVKRVLEKSPGKLLVKMPFQTSPPGK	245
M-MeCP2E1	201	TGRGRGRPKGSGTGRPKAAASEGVQVKRVLEKSPGKLVVKMPFQASPPGK	250
H-MeCP2E1	246	AEGGGATTSTQVMVIKRPGRKRKAEADPQAI PPKRGRKPGSVVAAAAAEA	295
M-MeCP2E1	251	GEGGGATTSAQVMVIKRPGRKRKAEADPQAI PPKRGRKPGSVVAAAAAEA	300
H-MeCP2E1	296	KKKAVKESSIRSVQETVLP I KKRKTRETVSI EVKEVVKPLL VSTLGEKSG	345
M-MeCP2E1	301	KKKAVKESSIRSVHETVLP I KKRKTRETVSI EVKEVVKPLL VSTLGEKSG	350
H-MeCP2E1	346	KGLKTCKSPGRKSKESSPKGRSSASSPPKKEHHHHHHHSESPKAPVPLL	395
M-MeCP2E1	351	KGLKTCKSPGRKSKESSPKGRSSASSPPKKEHHHHHHHSESTKAPMPLL	400
H-MeCP2E1	396	PPLPPPPPEPESEDPTSPPEPQDLSSSVCKEEKMPRGGSLSDGCPKEP	445
M-MeCP2E1	401	P--SPPPPPEPESEDPI SPPEPQDLSSSICKEEKMPRGGSLSDGCPKEP	448
H-MeCP2E1	446	AKTQPAVATAATAAEKYKHRGEGERKDIVSSMPRPNREEPVDSRTPVTE	495
M-MeCP2E1	449	AKTQPMVATTTTVAEKYKHRGEGERKDIVSSMPRPNREEPVDSRTPVTE	498
H-MeCP2E1	496	RVS 498	
M-MeCP2E1	499	RVS 501	

### B) MeCP2E2

H-MeCP2E2	1	MVAGMLGLREEKSE DQDLQGLKDKPLKFKKVKKDKKEEKEGKHEPVQPSA	50
M-MeCP2E2	1	MVAGMLGLREEKSE DQDLQGLRDKPLKFKKAKKDKKEDKEGKHEPLQPSA	50
H-MeCP2E2	51	HHSAEPAEAGKAETSESGSAPAVPEASASPKQRRSIIRDGRPMYDDPTL	100
M-MeCP2E2	51	HHSAEPAEAGKAETSESSGSAPAVPEASASPKQRRSIIRDGRPMYDDPTL	100
H-MeCP2E2	101	PEGWTRKLRKQRKSGRSAGKYDVYLINPQGKAFRSKVELIAYFEKVGDTSL	150
M-MeCP2E2	101	PEGWTRKLRKQRKSGRSAGKYDVYLINPQGKAFRSKVELIAYFEKVGDTSL	150

## Chapter 2

H-MeCP2E2	151	DPNDFDFTVTGRGSPSRREQPKPKKPKSPKAPGTGRGRGRPKGSGTTRPK	200
M-MeCP2E2	151	DPNDFDFTVTGRGSPSRREQPKPKKPKSPKAPGTGRGRGRPKGSGTGRPK	200
H-MeCP2E2	201	AATSEGVQVKRVLEKSPGKLLVKMPFQTSPPGGKAEGGGATTSTQVMVIKR	250
		.     :     .     .     .	
M-MeCP2E2	201	AAASEGVQVKRVLEKSPGKLVVKMPFQASPPGGKGEAGGGATTSAQVMVIKR	250
H-MeCP2E2	251	PGRKRKAEADPQAI PKKRGRKPGSVVAAAAAEAKKKAVKESSIRSVQETV	300
M-MeCP2E2	251	PGRKRKAEADPQAI PKKRGRKPGSVVAAAAAEAKKKAVKESSIRSVHETV	300
H-MeCP2E2	301	LPIKKRKTRETIVSIEVKEVVKPLL VSTLGEKSGKGLKTCKSPGRKSKESS	350
M-MeCP2E2	301	LPIKKRKTRETIVSIEVKEVVKPLL VSTLGEKSGKGLKTCKSPGRKSKESS	350
H-MeCP2E2	351	PKGRSSSASSPPKKEHHHHHHHSESPKAPVPLLPPLPPPPPEPESSEDPT	400
		:     .     .     .	
M-MeCP2E2	351	PKGRSSSASSPPKKEHHHHHHHSESTKAPMPLLP--SPPPEPESSEDPTI	398
H-MeCP2E2	401	SPPEPQDLSSSVCKEEKMPRGGSLSDGCPKEPAKTQPAVATAATAAEKY	450
		:	
M-MeCP2E2	399	SPPEPQDLSSSICKEEKMPRGGSLSDGCPKEPAKTQPMVATTTTVAEKY	448
H-MeCP2E2	451	KHRGEGERKDIVSSSMRPNREEPVDSRTPVTERVS	486
M-MeCP2E2	449	KHRGEGERKDIVSSSMRPNREEPVDSRTPVTERVS	484

**Figure 2.1 Amino acid sequence alignments of human and mouse MeCP2 isoforms.**

A) Alignment of human (H-MeCP2E1) and mouse MeCP2E1 (M-MeCP2E1). B) Alignment of human (H-MeCP2E2) and mouse MeCP2E2 (M-MeCP2E2). Pairwise sequence alignment was done by EMBOSS Needle in which Matrix: EBLOSUM62, Gap-penalty: 10.0, Extend-penalty: 0.5 were used.

In order to identify an epitope that was specific for MeCP2E1, we aligned the amino acid sequences of the two isoforms using Pairwise Sequence Alignment (PROTEIN) in EMBOSS Needle (**Figure 2.2**). There was a 96% similarity between the sequences. The two isoforms differ by 21 unique N-terminal amino acids in MeCP2E1 and 9 unique N-terminal amino acids in MeCP2E2. Therefore, in order to generate an antibody that was specific for MeCP2E1, the 21 amino acids MAAAAAAAPSGGGGGGEEERL was used for further analysis.

## Chapter 2

H-MeCP2E1	1	MAAAAAAAPS GGGGGGEEERL	E EKSE DQDLQGLKDKPLKFKKVKKDKKKEE	50
		..... .....		
H-MeCP2E2	1	-----MVAGMLGLR	E EKSE DQDLQGLKDKPLKFKKVKKDKKKEE	38
H-MeCP2E1	51	KEGKHEPVQPSAHHSAEPAEAGKAETSEGGSGSAPAVPEASASPQRRSII		100
H-MeCP2E2	39	KEGKHEPVQPSAHHSAEPAEAGKAETSEGGSGSAPAVPEASASPQRRSII		88
H-MeCP2E1	101	RDRGPMYDDPTLPEGWTRKLRKQKSGRSAGKYDVYLINPQGKAFRSKVEL		150
H-MeCP2E2	89	RDRGPMYDDPTLPEGWTRKLRKQKSGRSAGKYDVYLINPQGKAFRSKVEL		138
H-MeCP2E1	151	IAYFEKVGDTSLDPNDFDFTVTGRGSPSRREQPKPKPKSPKAPGTGRGR		200
H-MeCP2E2	139	IAYFEKVGDTSLDPNDFDFTVTGRGSPSRREQPKPKPKSPKAPGTGRGR		188
H-MeCP2E1	201	GRPKGSGTTRPKAATSEGVQVKRVLEKSPGKLLVKMPFQTS PGGAEGGG		250
H-MeCP2E2	189	GRPKGSGTTRPKAATSEGVQVKRVLEKSPGKLLVKMPFQTS PGGAEGGG		238
H-MeCP2E1	251	ATTSTQVMVIKRPGRKRKAEDPQAI PPKRGRKPGSVVAAAAAEAKKAV		300
H-MeCP2E2	239	ATTSTQVMVIKRPGRKRKAEDPQAI PPKRGRKPGSVVAAAAAEAKKAV		288
H-MeCP2E1	301	KESSIRSVQETVLP I KKRKTRETVSIEVKEVVKPLLVSTLGEKSGKGLKT		350
H-MeCP2E2	289	KESSIRSVQETVLP I KKRKTRETVSIEVKEVVKPLLVSTLGEKSGKGLKT		338
H-MeCP2E1	351	CKSPGRKSKESSPKGRSSSASSPPKKEHHHHHHHSESPKAPVLLPPLPP		400
H-MeCP2E2	339	CKSPGRKSKESSPKGRSSSASSPPKKEHHHHHHHSESPKAPVLLPPLPP		388
H-MeCP2E1	401	PPPEPESSEDPTSPPEPQDLSSSVCKEEKMPRGGSLSDGCPKEPAKTQP		450
H-MeCP2E2	389	PPPEPESSEDPTSPPEPQDLSSSVCKEEKMPRGGSLSDGCPKEPAKTQP		438
H-MeCP2E1	451	AVATAATAAEKYKHRGEGERKDIVSSSMRPNRNREEPVDSRTPVTERVS		498
H-MeCP2E2	439	AVATAATAAEKYKHRGEGERKDIVSSSMRPNRNREEPVDSRTPVTERVS		486

**Figure 2.2 Selection of peptide sequence for anti-MeCP2E1 and anti-MeCP2E2 antibodies.**

Amino acid sequence alignment of human MeCP2E1 (H-MeCP2E1) and MeCP2E2 (H-MeCP2E2). Pairwise sequence alignment was done by EMBOSS Needle in which Matrix: EBLOSUM62, Gap-penalty: 10.0, Extend-penalty: 0.5 were used.

Once the amino acids that determine the specificity of MeCP2E1 were identified, the peptide sequence was selected by our lab. ThermoFisher Antigen Profiler Peptide Tool (ThermoFisher Scientific) was used to determine which regions of the two MeCP2 isoforms could be used to generate a potent antigen. The antigenicity of the sequences, based on scores displayed by the antigen profiler peptide tool were determined using sequence length (10-20 amino acids), amino acid composition (at least 4 distinct residues, even proportion of hydrophilic and hydrophobic amino acids) (**Table 2.1**). Ultimately, the peptide sequences were chosen based on their antigenicity score as well as their sequence conservation between humans and mice.

<b>Table 2.1 Identification of peptide sequence for MeCP2 isoform-specific antibodies using Antigen Profiler Peptide Tool</b>		
	<b>Peptide Sequence</b>	<b>Antigen Profiler Score</b>
<b>MeCP2E1</b>	MAAAAAAPS	0.2
	AAAPSGGGGGGEEEE	1.4
	PSGGGGGGGEEERL	1.9
	PSGGGGGGGEEERLEEK	2.2
	GGGEEERLEEK	4.6
<b>MeCP2E2</b>	MVAGMLGLR	1.7
	MVAGMLGLRE	2.0
	VAGMLGLREE	2.5
	VAGMLGLREEKS	2.6

< 1.0
1.0-1.9
2.0-2.6
2.7-3.5
3.6-5.0  
 poor antigen ← → excellent antigen

### **2.2.2 Chicken anti-MeCP2E1 antibody generation**

A peptide sequence from the N-terminus of the MeCP2E1 isoform (GGGEEERLEEK) that is conserved in mouse and human MeCP2 protein was selected as the antigen for polyclonal antibody production in chicken. Peptide conjugation (KLH), antibody synthesis in chicken, and affinity purification of the antibodies were done as a commercial service. Sera from chicken were sent periodically to our lab to test for the presence of antibodies, which we tested using Western Blots (WB), Immunocytochemistry (ICC) and using Immunohistochemistry (IHC) by another member of our lab (Carl Olson). IgY molecules were purified from chicken egg yolks and anti-MeCP2E1-specific immunoglobulins were isolated by peptide affinity purification by a company as a paid service.

### **2.2.3 Rabbit anti-MeCP2E1 antibody generation**

A peptide sequence from the N-terminus of MeCP2E1 isoform (GGGEEERLEEK) that is conserved in mouse and human MeCP2 protein was selected as the antigen for polyclonal antibody production in rabbit. Peptide conjugation, antibody synthesis in rabbit, and affinity purification of the antibodies were done as a commercial service. Sera from rabbit were sent periodically to our lab to test for the presence of antibodies, which we tested using WB and ICC and using Immunohistochemistry (IHC) by another member of our lab (Carl Olson)

### **2.2.4 Chicken anti-MeCP2E2 antibody development**

Conserved sequences between human and mouse MeCP2 protein, in the N-termini of MeCP2E2 (VAGMLGLREEKS) was selected as peptide antigen for polyclonal antibody

## Chapter 2

production in chicken. The anti-MeCP2 isoform-specific immunoglobulins were isolated by peptide affinity purification. Sera from chicken were sent periodically to test for antibody generation to our lab, where we tested the antibody specificity using WB and ICC and using IHC by another member of the Rastegar lab (Carl Olson). The IgY molecules were purified from chicken egg yolks and anti-MeCP2E1-specific immunoglobulins were isolated by peptide affinity purification by a company as a paid service.

### **2.3 Cell Culture**

#### **2.3.1 Culture and maintenance of cell lines**

NIH3T3, HEK293T and Phoenix cells were maintained in Dulbecco's modified Eagle's medium (DMEM) Supplemented with 10% FBS (Fetal Bovine Serum) and 1% of an antibiotic mixture containing 10,000 units of penicillin, 10,000 µg of streptomycin, and 29.2 mg/ml of L-glutamine in a 10 mM citrate buffer (for pH stability). All cells were maintained in a humidified chamber at 37°C in 5% CO<sub>2</sub>.

For passaging NIH3T3 and Phoenix cells, confluent cultures were washed once with phosphate buffered saline (PBS), and incubated with 0.25% trypsin at 37°C for 1-2 minutes or until the cells were visibly detached from the plate. The detached cells were centrifuged, and the media was replaced with fresh media. Cells were then seeded onto new plates at 20-30% confluence.

#### **2.3.2 Primary cortical neuron isolation**

The reagents used in this protocol are listed in **Appendix A**.

## Chapter 2

Section 2.3.2.1 and 2.3.2.2 were performed by Mr. Carl Olson.

### ***2.3.2.1 Embryo harvest and preparation***

For dissection of mouse embryos (CD-1 strain), embryonic day (E) 18.5 pregnant females were anesthetized by CO<sub>2</sub> and wiped with 70% ethanol to clear loose hair and dander. The pregnant mice were then decapitated and the embryo sacs removed and placed in a 50ml conical tube containing ice-cold PBS [Gibco]. The embryo sacs were then transferred to a sterile petri dish, and individual embryos were separated. The embryos were subsequently decapitated and the separated embryos were placed in a clean sterile petri dish containing ice-cold PBS.

### ***2.3.2.2 Embryonic Forebrain dissection***

The severed embryo heads were transferred to a sterile petri dish containing artificial cerebrospinal fluid (ACSF) [2M NaCl, 1M KCl, 1M MgCl<sub>2</sub>, 155mM NaHCO<sub>3</sub>, 1M Glucose, 108mM CaCl<sub>2</sub> and 1X antibiotic/antimycotic]. The heads were oriented in an upright position secured firmly by piercing the eyes and clasping the snout with one forcep. The scalp of the head was then peeled back from the snout to the back of the head. Subsequently, a lateral cut was made at the base of the skull and the skull was snipped along the midline from the back, cut to the snout, and removed. The brain was then gently removed from the skull cavity, and securely held by the hind brain. Subsequently, the olfactory bulb, hippocampal formation, and meninges were excised, and the cortices were separated and transferred to a conical tube containing fresh ACSF.

### ***2.3.2.3 Coating plates for neuron seeding***

For coating the plates, 1% v/v of Poly-D-Lysine (dissolved in water) [BD Biosciences] was added to each well (500µl per 24 well and 1ml per 6 well), and incubated for 1-2 hours (h) in a

## Chapter 2

sterile cell/tissue culture hood. Afterwards, the coating solution was aspirated, the plates washed once with sterile water and left for drying.

### ***2.3.2.4 Dissociation, plating and initial culturing of the cortices***

The ACSF from the dissected cortices were aspirated and 3 ml of heat-activated papain [Worthington] solution was added to the cells, along with 400  $\mu$ l of 0.1% Deoxyribonuclease (DNase) solution [Sigma], for tissue digestion. The cortices were incubated with papain-DNase solution for 20 minutes (min) at 37°C, with periodic mixing. After 20 min, the papain action was halted with 300 $\mu$ l of 10/10 solution [a mixture of ovomucoid and Bovine Serum Albumin (BSA)], and centrifuged (1000 rpm) for 3 min. The supernatant was aspirated gently with a glass pipette. Subsequently, three ml of 1/10 solution (1/10<sup>th</sup> of the 10/10 solution of ovomucoid and BSA) and 600-800 $\mu$ l of DNase was added to the digested tissue and cells were dissociated mechanically, first with a 1000 $\mu$ l filter-tip pipette and then with a glass Pasteur pipette, till no cell clumps could be seen. The dissociated cells were then overlaid above an equal volume of 10/10 solution and centrifuged (1000 rpm) for 5 min. The supernatant was aspirated gently with a P1000 pipette and resuspended in Neurobasal media [Gibco] containing B27 supplement [Gibco] as described previously [151]. The cells were counted using a hemocytometer and seeded at specific densities onto appropriate cell-culture compatible dishes, coated as described in in 2.3.3.3. The seeding densities for a 10 cm<sup>2</sup> plate was  $12 \times 10^6$  cells and scaled according to the plate size. Cells were also seeded on coverslips in 24-well plates for ICC.

### ***2.3.2.5 Maintenance of primary neuron culture***

The seeded cells were left in the original plating media for the first 72 h. On the fourth day, 50% of the media was removed and replaced with neuronal selection media which is the plating media supplemented with Cytosine Arabinoside (CA) (0.07% final CA concentration). CA is used



to inhibit the growth of proliferating cells such as glia and thereby select for a neuronal population [368]. After 48h, the media was replaced to CA-free plating media. Cells were harvested 7 days after the initial isolation [151].

### **2.3.3 Primary cortical astrocytes isolation and culture**

Embryo harvest and preparation, forebrain dissection (under cold light dissecting microscope) were performed using identical steps as outlined in Section 2.3.2.1 and 2.3.2.2 by Mr. Carl Olson. Coating of plates before cell seeding was also performed as described in section 2.3.2.3.

#### ***2.3.3.1 Dissociation, plating and initial culturing of the cortices***

The dissected cortices were transferred to a tube containing 1ml papain and 1ml DNase, and incubated at 37°C for 10 min followed by centrifugation (1000 rpm) for 5 min. The supernatant was aspirated gently with a pipette and the digested tissue was resuspended in 2 ml of media, which consisted of Minimum Essential Medium (MEM) with 10% FBS. The cells were then dissociated mechanically with a 1ml pipette tip and subsequently with a Pasteur pipette, till no cell clumps could be seen. The dissociated cells were then further resuspended in 15-25 ml of media before being counted using a hemocytometer. Cells were subsequently seeded onto Poly-D-lysine coated plates at a density of  $2.4 \times 10^6$  cells in 10 cm<sup>2</sup> plates and scaled appropriately for other dishes. Cells were also cultured on coverslips in 24-well plates for ICC.

### **2.3.3.2 Maintenance of primary astrocyte culture**

Culture media (MEM with 10% FBS) was replaced every 72 h. Five days after isolation, the dishes were agitated manually for 20 seconds to mechanically detach the microglia population. After agitation, the media containing microglia was aspirated and replaced with fresh culture media. Astrocyte cultures were harvested 14 days after isolation [369].

## **2.4 Lentiviral Transduction**

### **2.4.1 Plasmid amplification and purification**

Vectors for lentiviral packaging proteins *rev*, *tat*, *gag/pol* and *vsv-g* were a gift from Dr. James Ellis (University of Toronto), reported by Rastegar *et al.*, (2009) [151]. For plasmid amplification, the vectors were transformed into competent DH5 $\alpha$  bacterial cells [ThermoFisher]. One microliter of plasmid was incubated with 30 $\mu$ l of DH5 $\alpha$  competent cells on ice for 10 min. Afterwards, the cells were exposed to a heatshock by incubation at 42°C for 45 seconds, followed by incubation on ice for 10 min. Subsequently, 250 $\mu$ l of Super Optimal broth with Catabolite repression (SOC) media was added to the plasmid-DH5 $\alpha$  mix and incubated for 1 hour at 37°C. The cells were then plated onto agar plates containing selective antibiotic (Ampicillin at 100 $\mu$ g/ml) and incubated overnight at 37°C, along with a negative control plate with mock-transformed DH5 $\alpha$  cells. After overnight incubation, individual colonies were isolated and subcultured into 3-6 ml Luria-Bertani (LB) broth containing the appropriate antibiotic and incubated with shaking at 37°C for 6-8 h. These subcultures were used to prepare glycerol stocks for long-term plasmid storage or to inoculate larger cultures for plasmid isolation.

Plasmid isolations were performed using Qiagen MIDI prep kits (Qiagen, 12143), according to manufacturer's instructions [370]. Purified plasmids were quantified using a

## Chapter 2

Nanodrop spectrophotometer. The identity of the plasmids were confirmed after the purification process using diagnostic digests with specific restriction enzymes.

### 2.4.2 Generation of lentiviral particles

HEK293T cells were cultured in T-75 plates at a seeding density of  $7.5 \times 10^6$  cells in DMEM medium containing 10% FBS one day before the transfection of viral vectors. Plasmids encoding *rev*, *tat*, *gag/pol* and *vsv-g* along with individual overexpression complementary DNA (cDNA) encoding vectors were transfected into HEK293T cells in T-75 plates for the generation of lentiviral particles. After 24h, cells were transfected using Lipofectamine 2000 (Life Technologies) with 10  $\mu\text{g}$  of *rev*, *tat*, *gag/pol* and 5  $\mu\text{g}$  of *vsv-g* along with 15  $\mu\text{g}$  of the respective cDNA encoding vectors used for overexpression (*MECP2E1*, *MECP2E2*, *EGFP*). Culture media was changed 16h after initial transfection and replaced with Neurobasal media containing B27 supplement. Viruses were collected 48h later. The viruses were filtered through 0.45  $\mu\text{m}$  pore filters to exclude cell debris before addition to neurons. Polybrene (Sigma) was added to the virus at a concentration of 0.6  $\mu\text{g}/\text{ml}$  to enhance transduction efficiency.

### 2.4.3 Transduction of primary neurons

Primary neurons were cultured as described in section 2.3.4. Three days after isolation of neurons, neurons were transduced with lentiviral particles. The viral particles are incubated with the cells for 12h before media replacement (ratio of virus to fresh media was 1:7). Transduced cells were harvested 96h after transduction for downstream analysis.

## **2.5 Retroviral Transduction**

### **2.5.1 Plasmid amplification and purification**

Retroviral vectors [Retro-EF1 $\alpha$ -E1 (expressing *MECP2E1*) and Retro-EF1 $\alpha$ -E2 (expressing *MECP2E2*)] vectors were a kind gift from Ellis Lab, University of Toronto. The retroviral plasmids were amplified and purified using the same protocol as detailed in section 2.4.1

### **2.5.2 Generation of retroviral particles**

Retroviral vectors were transfected into Phoenix retroviral packaging cells using Lipofectamine 2000 (Invitrogen) and 8  $\mu$ g of retroviral DNA for the generation of retroviral particles.

### **2.5.3 Transduction of NIH3T3 cells**

Phoenix cell culture supernatants containing retroviral particles were harvested at 48 hours (h) post-transfections. The Phoenix cell culture supernatant containing the virus was centrifuged, and the supernatant was filtered with 0.45 $\mu$ m filter to remove cell debris. NIH3T3 cells were infected overnight with freshly made virus (1:1 virus: media fresh media) in the presence of 6  $\mu$ g/ml Polybrene (Sigma). The virus was removed the next day and the cells were plated in fresh media. NIH3T3 cells were harvested 72 hours after initial transduction.

## **2.6 Immunocytochemistry (ICC)**

### **2.6.1 Fixation of cells**

Cells were cultured on coverslips in 24-well plates as described in sections 2.3.1, 2.3.4 and 2.3.5. Cells were washed twice with PBS to remove debris and remnant media. Cells were then

## Chapter 2

fixed with 4% paraformaldehyde [PFA (Electron Microscopy Sciences)], for 10 min, on ice. Subsequently, cells were washed three times with PBS, at intervals of 5 min. After the final wash step, cells were stored in PBS at 4°C.

### **2.6.2 Primary/Secondary antibody addition**

Fixed cells were permeabilized with 2% NP-40 in PBS for 10 min, followed by preblocking with 10% (v/v) Normal Goat Serum (NGS, Jackson ImmunoResearch Laboratories Inc., 005-000-121) in PBS for 1 h. Primary antibodies were diluted in PBS with 10% NGS as specified in Table 2.2. Cells were then incubated with primary antibodies overnight at 4°C followed by three washes with PBS. Secondary antibodies diluted in 10% NGS were added to the cells for 1 h, followed by three washes with PBS, five minutes each. Coverslips were mounted on glass slides with Prolong Gold antifade (Molecular Probes, P36930) containing 2 µg/ml 4',6-diamidino-2-phenylindole (DAPI) (Calbiochem, EMD Millipore, 268298) counter-stain. The primary and secondary antibodies used in this study are shown in **Table 2.2 and Table 2.3**.

**Table 2.2 Primary antibodies used in ICC, WB and ChIP**

<b>Primary Antibody</b>	<b>Application/Dilution</b>	<b>Description</b>	<b>Source</b>
MeCP2 (C-terminal)	WB - 1:1000 ICC - 1:200	Rabbit polyclonal	Millipore, 07-013
Beta ( $\beta$ ) ACTIN	WB - 1:2500	Mouse monoclonal	Sigma, A2228
GAPDH	WB - 1:500	Rabbit polyclonal	Santa Cruz, Sc-25778
GFAP	ICC - 1:200	Mouse monoclonal	Invitrogen, 421262
Beta ( $\beta$ ) TUBULIN III (TUB III)	ICC - 1:200	Mouse monoclonal	Chemicon, MAB1637
Beta ( $\beta$ ) TUBULIN III (TUB III)	ICC - 1:200	Chicken polyclonal	Millipore, AB9354
UBF	WB - 1:500 ICC - 1:200 ChIP - 5 $\mu$ g	Mouse monoclonal	Santa Cruz, SC-13125
MeCP2E1	WB - 2 $\mu$ g/ml ICC - 1:100	Chicken polyclonal	Custom-made [1]
MeCP2E1	WB - 1:1000 ICC - 1:200	Rabbit polyclonal	Custom-made[2]
MeCP2E2	WB - 3 $\mu$ g/ml ICC - 1:200	Chicken polyclonal	Custom-made [2]
5mC	ICC - 1:100	Mouse monoclonal	Abcam, ab10805
EGFP	ICC - 1:200	Mouse monoclonal	Millipore, MAB3580
MeCP2	ChIP - 5 $\mu$ g	Rabbit polyclonal	Abcam, ab2828

Nucleolin	ICC – 1:200	Rabbit polyclonal	Abcam, ab22758
H3K9me2	ICC - 1:200	Mouse monoclonal	Abcam, ab1298
H3K9me	ICC - 1:200	Rabbit polyclonal	Abcam, ab9045
H3K27me3	ICC - 1:200	Mouse monoclonal	Abcam, ab6002
H4K20me3	ICC - 1:200	Rabbit polyclonal	Abcam, ab9053

**Table 2.3 Secondary antibodies used in ICC and WB**

<b>Secondary Antibody</b>	<b>Application/Dilution</b>	<b>Source</b>
Rhodamine Red-X conjugated goat anti-mouse IgG	ICC - 1:400	Jackson Immunoresearch, 115- 259-146
Alexa Fluor 594 conjugated donkey anti-mouse IgG	ICC - 1:2000	Invitrogen, 987237
Alexa Fluor 448 conjugated donkey anti-rabbit IgG	ICC - 1:2000	Invitrogen, 913921
Peroxidase-AffiniPure goat anti- mouse IgG	WB 1:7500	Jackson ImmunoResearch 115- 035-174
Peroxidase-AffiniPure donkey anti-rabbit IgG	WB 1:7500	Jackson ImmunoResearch 711- 035-152
Dylight 649 conjugated goat anti- chicken IgY	ICC - 1:400	Jackson Immunoresearch, 103- 485-155
Rhodamine Red-X conjugated goat anti-chicken IgY	ICC – 1:400	Jackson Immunoresearch, 103- 295-155

Peroxidase-AffiniPure goat anti-chicken IgY	WB 1:5000	Jackson ImmunoResearch 103-035-155
Rhodamine Red-X goat anti-rabbit IgG	ICC – 1:400	Jackson ImmunoResearch 111-295-144
Alexa 488 goat anti mouse IgG	ICC - 1:400	Invitrogen, A11017
Alexa 488 goat anti rabbit IgG	ICC - 1:400	Invitrogen, A11034

For visualization of 5mC signals, cells were exposed to 4N HCl for 10 min, neutralized with 100 mM Tris-HCl (pH 8.5) for 15 minutes and washed three times with PBS before addition of primary antibodies, based on previous reports [371]. The cells were further treated with 100mM Tris-HCl for 10 min before resuming the blocking step of the aforementioned protocol.

### 2.6.3 Imaging

Fluorescence-based images were collected using an Axio Observer Z1 inverted microscope equipped with an Axiocam MRm camera and LSM710 confocal microscope (Carl Zeiss Canada Ltd.). All images were collected using a 10X lens [Numerical Aperture (NA) =0.3], 40X lens (NA = 0.95) or 63X oil-immersion lens (NA=1.4). Images were captured using Zen Blue 2011, 2012 and Zen Black 2011 (Carl Zeiss Canada Ltd.) software. Data compilation from the images were done using Adobe Photoshop C5 and Adobe Illustrator C5.

### 2.6.4 Quantification of nuclear and nucleolar size

At least 30 cells per biological replicate were imaged for a total of three biological replicates (processed at the same time). The images were converted to TIFF files and opened in



## Chapter 2

Image J for analysis. For image scaling in ImageJ program, 0.102  $\mu\text{m}$  was set equal to one pixel. The image color was adjusted to pick up accurate size of either the nucleus or the nucleoli stained with DAPI and anti-Nucleolin, respectively. The tracing tool (wand) was used to select the margins of each nucleus and nucleolus and then using ROI manager of the ImageJ software, areas of each nucleus and nucleolus were captured. Once the sizes were obtained, the average size, nucleolar size/nuclear size, nucleoli number per cell (nucleolar coefficient) were calculated using Microsoft Excel. GraphPad Prism was used to draw frequency distribution histograms using different bin sizes (categories).

## 2.7 Western blot

### 2.7.1 Extraction and quantification of total cell lysates and nuclear fractions

Total cell lysates were prepared for the comparison of MeCP2E1 levels between primary neurons and astrocytes and antibody validation experiments used Phoenix cells [1], as described previously [151,372]. The salt shock total cell extraction buffer was utilized in this protocol (**Appendix A3**) [464]. Briefly, cell pellets were washed in PBS. Then, lysis buffer was added to the cell pellet and vortexed until homogenized. The cell lysate was kept in ice for 20-30 mins. The cell lysate was then centrifuged (13,000 rpm) for 2 mins at 4°C and the supernatant was transferred to pre-chilled Eppendorf tubes for storage at -80°C and subsequent use.

The nuclear protein fraction was isolated using the NE-PER Nuclear and Cytoplasmic Extraction Kit [Thermo Scientific, Cat. No. 78833], following the manufacturer's instructions [373]. Briefly, frozen cell pellets were initially lysed in ice-cold Cytoplasmic Extraction Reagent I, by vigorously vortexing the pellet for 15 seconds followed by incubation for 10 min on ice. Ice-cold Cytoplasmic Extraction Reagent II was added and the cells were further incubated for 1 minute before centrifugation at 16,000g for 5 min. At this stage, the supernatant containing the

## Chapter 2

cytoplasmic fraction was transferred to another tube. The pellet, in turn was resuspended in ice-cold Nuclear Extraction Reagent II containing protease inhibitors (Roche), and vortexed for 15 seconds, every 10 min, for four rounds. Subsequently, the suspension was centrifuged at 16,000g for 10 min. The supernatant, containing the nuclear extract, was aliquoted and stored at -80°C until further use. Nucleolar protein extracts were isolated using a previously reported protocol [374].

Protein samples were quantified by Bradford assay using Bio-Rad Protein Assay Dye Reagent [Bio-Rad #5000006] using the manufacturer's instructions [375]. Briefly, diluted or undiluted samples were mixed with recommended amount of dye reagent and the absorbance values were captured using a spectrophotometer [SpectraMax M2e, Molecular Devices]. The absorbance values of the samples were compared against a standard curve generated by assaying five known concentrations of BSA using the same dye reagent. Final protein concentrations were calculated using Softmax Pro 5.3.

### **2.7.2 Sodium dodecyl sulfate polyacrylamide gel electrophoresis (SDS-PAGE) and WB**

Proteins were separated based on their molecular weight by SDS-PAGE. Electrophoresis was performed under denaturing conditions, using a 10% polyacrylamide resolving gel (0.375M Tris-HCL (pH 8.8), 0.1% SDS, 0.1% ammonium-persulfate, 0.0004% TEMED) and a 4% stacking gel (0.125M Tris-HCl (pH 6.8), 0.1% SDS, 0.05% ammonium-persulfate, 0.001% TEMED) in a Bio-rad Mini protean 3 apparatus. Samples were mixed with loading buffer (50 mM Tris-HCL pH 8.0, 2%SDS, 10% glycerol, 1%  $\beta$ -Mercaptoethanol, 12.5 mM EDTA and 0.02% bromophenol blue) and kept at 100°C for 5 min before loading. SDS-PAGE was performed at 100V at 4°C for 5 h in running buffer (25 mM Tris, 192 mM glycine, 0.1% SDS, pH 8.3). The separated proteins were subsequently transferred to a nitrocellulose membrane in transfer buffer (192 mM glycine, 25 mM Tris, 0.05% SDS, 20% methanol), at 100V in a 4°C cold room. Membranes were blocked

## Chapter 2

for 1-3 h at room temperature with non-fat skim milk (3%) dissolved in tris-buffered saline (TBS) solution with the 0.2% detergent Tween 20 (TBST) and incubated with primary antibodies overnight at 4°C.

### **2.7.3 Development of blots and quantification of signal intensity**

After primary incubation, membranes were rinsed twice with 0.2% TBST and subsequently washed with 0.2% TBST three times, for 20 min intervals. At this stage, membranes were incubated with appropriate secondary antibodies for 1 h at room temperature. Once again, membranes were rinsed twice with 0.2% TBST and subsequently washed with 0.2% TBST three times, for 20 min intervals. After the final wash, membranes were exposed to Chemiluminescent HRP Substrate (ECL) [Millipore] and the signals were captured using a Biorad Universal Hood III Chemidoc imaging system. Signal intensity quantifications were performed using Image Lab Software. Primary and secondary antibodies used for WB are listed in the **Table 2.2** and **Table 2.3**, respectively.

Quantification of detected bands was done with Adobe Photoshop CS5 software. The signals for test MeCP2 were normalized to ACTIN signals. Student's *t*-test was used to analyze the significance of MeCP2 protein levels between samples.

### **2.8 Quantitative reverse transcription real-time PCR (qRT-PCR)**

Total RNA were extracted using RNeasy Mini Kit (Qiagen Canada Inc., 74134) and converted to cDNA using Superscript III Reverse Transcriptase (Life Technologies Inc., 18080-044), as reported previously [3-5]. Quantitative RT-PCR was carried out as described previously using

## Chapter 2

SYBR Green-based RT<sup>2</sup> qPCR Master Mix (Applied Biosystems, 4367659) in a Fast 7500 Real-Time PCR machine (Applied Biosystems). Transcript levels of all genes were examined using the gene specific primers listed in **Table 2.4**.

The threshold cycle value (Ct) for each gene was normalized against the housekeeping gene *Gapdh* to obtain  $\Delta Ct$  values for each sample. Relative quantification of gene expression was carried out by calculating  $2^{-\Delta Ct}$  of each sample as outlined below. Fold changes with respect to control were calculated as outlined below. Analysis was performed using Microsoft Excel 2010 and GraphPad Prism 6.0.

Calculation of  $\Delta Ct$

$$\Delta Ct = Ct_{(Gene\ of\ Interest)} - Ct_{(Gapdh)}$$

Calculation of relative expression

$$Relative\ expression = 2^{-\Delta Ct}$$

Calculation of fold change for *MECP2* overexpression

$$Fold\ change = \frac{[2^{-\Delta Ct}]_{Test}}{[2^{-\Delta Ct}]_{Control}}$$

Calculation of fold change for *MDS* mice brain

$$Fold\ change = \frac{[2^{-\Delta Ct}]_{Tg1}}{[2^{-\Delta Ct}]_{WT}}$$

<b>Table 2.4 Primers used for qRT-PCR experiments</b>			
<b>Gene/Locus</b>	<b>Primer Sequence (5' - 3')</b>		<b>Reference</b>
<i>Mouse (Ms)</i>	Forward primer	AGGAGAGACTGGAGGAAAAGTC	[166]

<i>Mecp2e1</i>	Reverse primer	AATACAGGATCCTCAGCTAACTC	
<i>Ms Mecp2e2</i>	Forward primer	CTCACCAGTTCCTGCTTTGATGT	[166]
	Reverse primer	AATACAGGATCCTCAGCTAACTC	
<i>Human (Hu) MECP2E1</i>	Forward primer	AGGAGAGACTGGAAGAAAAGTC	[376]
	Reverse primer	CTTGAGGGGTTTGTCTTGA	
<i>Hu MECP2E2</i>	Forward primer	CTCACCAGTTCCTGCTTTGATGT	[376]
	Reverse primer	CTTGAGGGGTTTGTCTTGA	
<i>Ms 45S pre-rRNA</i>	Forward primer	GAGAGTCCCGAGTACTTCAC	[377]
	Reverse primer	GGAGAAACAAGCGAGATAGG	
<i>Ms 28S rRNA</i>	Forward primer	AGAGGTAAACGGGTGGGGTC	[378]
	Reverse primer	GGGTCTGGGAGGAACGG	
<i>Ms 18S rRNA</i>	Forward primer	GATGGTAGTCGCCGTGCC	[378]
	Reverse primer	GCCTGCTGCCTTCCTTGG	
<i>cMYC</i>	Forward primer	CGCCGCAGAAAAGTACAAAC	[379]
	Reverse primer	CAGATCCTCTTCTGAGATGAG	
<i>Gapdh</i>	Forward primer	AACGACCCCTTCATTGAC	[380]
	Reverse primer	TCCACGACATACTCAGCAC	

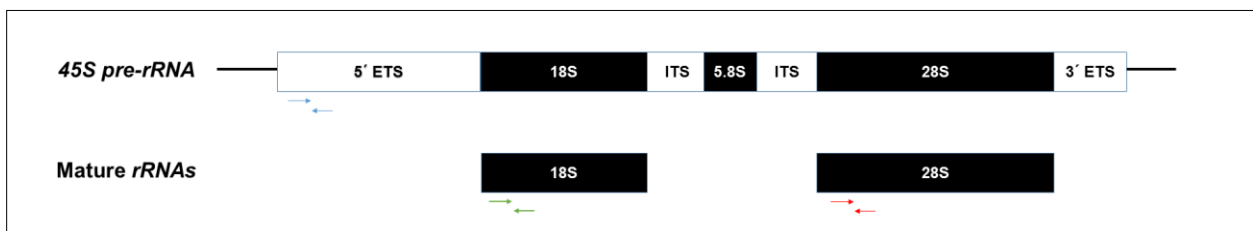


**Figure 2.3** Primer locations for *45S pre-rRNA*, *18S rRNA* and *28S rRNA*. Schematic not to scale.

## **2.9 Chromatin immunoprecipitation (ChIP) and quantitative real-time PCR (qPCR)**

ChIP experiments were performed using the EZ-ChIP kit from Millipore with minor modifications based on our previous studies [6-9]. All reagents for the protocol were provided and used from the kit, unless otherwise specified. Briefly,  $0.5 \times 10^6$  neurons cultured for 7 days were crosslinked by addition of 1% formaldehyde [EMD] for 10 minutes. At the end of 10 minutes, unreacted formaldehyde was quenched by addition of 1X Glycine for 5 min. The fixed cells were then washed twice with 10 ml of ice-cold PBS. Cells were scraped in 1 ml of PBS and centrifuged at  $700 \times g$  at  $4^\circ\text{C}$  for 2-5 min to pellet the cells. The pelleted cells were subsequently lysed by the addition of SDS Lysis Buffer (1% SDS, 10mM EDTA and 50mM Tris, pH 8.1) containing a protease inhibitor cocktail. Lysed cells were subsequently sonicated using a Sonics Vibracell sonicator with a 3mm probe [10 x 15 sec pulses at 30% amplitude] to produce fragments between 200 and 600bp. The sonicated cells were centrifuged at  $12,000 \times g$  at  $4^\circ\text{C}$  for 10 minutes to remove insoluble material. The supernatants were transferred to fresh tubes in a volume equivalent to  $0.5 \times 10^6$  cells. Subsequently, dilution buffer (0.01% SDS, 1.1% Triton X- 100, 1.2mM EDTA, 16.7mM Tris-HCl, pH 8.1, 167mM NaCl) containing a protease inhibitor cocktail was added to the sonicated cells. Chromatin was precleared (removal of DNA or proteins that may bind non-specifically to the Protein G agarose) by addition of 60  $\mu\text{L}$  of Protein G Agarose and incubation at  $4^\circ\text{C}$  for 1 hour. After preclearing, the agarose was removed by centrifugation at  $3000\text{-}5000 \times g$  for 1 minute and removal of supernatant to a fresh tube. 10  $\mu\text{l}$  (1%) of the supernatant was removed and kept at  $4^\circ\text{C}$  as input. The remaining chromatin was incubated overnight at  $4^\circ\text{C}$  with 5 $\mu\text{g}$  of antibodies against either MeCP2 (Ab2828, Abcam), UBF (SC-13125, Santa Cruz) or isotype-specific IgG (negative control antibody).

## Chapter 2

The antibody/antigen/DNA complex was collected by addition of Protein G Agarose and incubation at 4°C for one hour and removal of the supernatant by centrifugation at 3000-5000 x g for 1 minute. The Protein G Agarose-antibody/chromatin complex were then washed in 4 different buffers, a) Low Salt Immune Complex Wash Buffer [0.1% SDS, 1% Triton X-100, 2mM EDTA, 20mM Tris-HCl, pH 8.1, 150mM NaCl], b) High Salt Immune Complex Wash Buffer [0.1% SDS, 1% Triton X-100, 2mM EDTA, 20mM Tris-HCl, pH 8.1, 500mM NaCl.], c) LiCl Immune Complex Wash Buffer [0.25M LiCl, 1% IGEPAL CA630, 1% deoxycholic acid (sodium salt), 1mM EDTA, 10mM Tris, pH 8.1.], and d) TE Buffer [10mM Tris-HCl, pH 8.0, 1mM EDTA]. The washes were done by suspending the Protein G Agarose-antibody/chromatin complex in individual buffers, incubating for 3-5 minutes on a rotating platform followed by centrifugation at 3000-5000 x g for 1 minute and careful removal of the supernatant fraction. Protein/DNA complexes from immunoprecipitated samples and input samples were eluted twice by the addition of elution buffer (20% SDS and 1 M NaHCO<sub>3</sub>) and incubation at room temperature for 15 minutes. The Protein G Agarose samples were removed by centrifugation at 3000-5000 x g for 1 minute and supernatant collected to fresh chilled tubes. The crosslinks of protein/DNA complexes were reversed to free DNA by three sequential steps: a) addition of 8 µl 5 M NaCl and incubation at 65°C for 4-5 hours, b) addition of 1 µl RNase A and incubation at 37°C for 30 minutes, and c) addition of 4 µl 0.5M EDTA, 8 µl 1M Tris-HCl and 1 µl Proteinase K to each tube and incubate at 45°C for 1-2 hours.

DNA was purified using spin columns and assayed by qPCR using primers for the promoter sequences [Upstream Control Element (UCE)] of *rDNA*. As positive controls for ChIP experiments with MeCP2, PCR of the Major satellite markers (*MSP*) was included while for ChIP experiments with UBF, PCR of the same *rDNA* UCE region was used. The primers used in ChIP-qPCR experiments are shown in **Table 2.5**.

Table 2.5 Primers used for ChIP-qPCR experiments			
Gene/Locus	Primer Sequence (5' - 3')		Ref.
<i>rDNA UCE</i>	Forward primer	AGTTGTTTCCTTTGAGGTCCGGT	[381]
	Reverse primer	AGGAAAGTGACAGGCCACAGAG	
<i>Major Satellite Marker (MSP)</i>	Forward primer	GGCGAGAAAACCTGAAAATCACG	[382]
	Reverse primer	AGGTCCTTCAGTGTGCATTTC	
<i>Beta-Actin (Promoter)</i>	Forward primer	AAAATGCTGCACTGTGCGGCGA	[383]
	Reverse primer	GGACGCGACTCGACAGTGGCTG	
<i>Beta-Actin (Coding Region)</i>	Forward primer	AGAGGGAAATCGTGCGTGAC	[384]
	Reverse primer	CAATAGTGATGACCTGGCCGT	
<i>Gapdh (Coding Region)</i>	Forward primer	AACGACCCCTTCATTGAC	[380]
	Reverse primer	TCCACGACATACTCAGCAC	

### 2.9.1 Calculation of ChIP percentage input.

The calculations of percentage input were adapted from the guidelines detailed in the ThermoFisher website [342]. Briefly, the Ct values of the Input was initially adjusted to 100% by subtracting the dilution factor [1000 or 9.965784 cycles (i.e., log<sub>2</sub> of 1000)] from the raw input Ct. The percentage input values were subsequently calculated based on the equations shown below.

$$\Delta Ct = Ct_{(Adjusted\ input)} - Ct_{(IP)}$$

$$\text{Percentage input} = 2^{\Delta Ct} \times 100$$



### 2.10 ChIP-CHOP Assay

The ChIP-CHOP assay was done to determine the percentage DNA methylation of the *rDNA* promoter DNA bound by MeCP2. It was performed as described elsewhere with modifications [385]. Briefly, ChIP experiments of control neurons were carried out with either MeCP2 or UBF. Genomic DNA bound to either MeCP2 or UBF was collected and 1µg of DNA digested with *HpaII* enzyme. As a control, undigested samples were used. The undigested (UD) and digested (D) DNA were subsequently subjected to qRT-PCR with primers encompassing the CpG-143 of the *rDNA* promoter. DNA methylation was assessed based on *HpaII* resistance, which allows for amplification of the targeted region. CpG methylation levels are measured by qRT-PCR, using a sets of primers that encompasses the CpG-143, with *HpaII* restriction site (-165 to -1). The primer sequences are listed in **Table 2.6**. The methylation of the CpG site was calculated as resistance to *HpaII* (percentage input) as shown in the equation below.

Difference between undigested sample (UD) and digested with *HpaII* sample (D)

$$\Delta Ct = Ct_{(UD)} - Ct_{(D)}$$

$$\text{Resistance to } HpaII \text{ (Percentage input)} = 2^{\Delta Ct} \times 100$$

<b>Table 2.6 Primers used for ChIP-CHOP experiments</b>		
<b>Gene/Locus</b>	<b>Primer Sequence (5' - 3')</b>	<b>Reference</b>
Forward primer	GACCAGTTGTTTCCTTTGAGG	[385]
Reverse primer	ACCTATCTCCAGGTCCAATA	

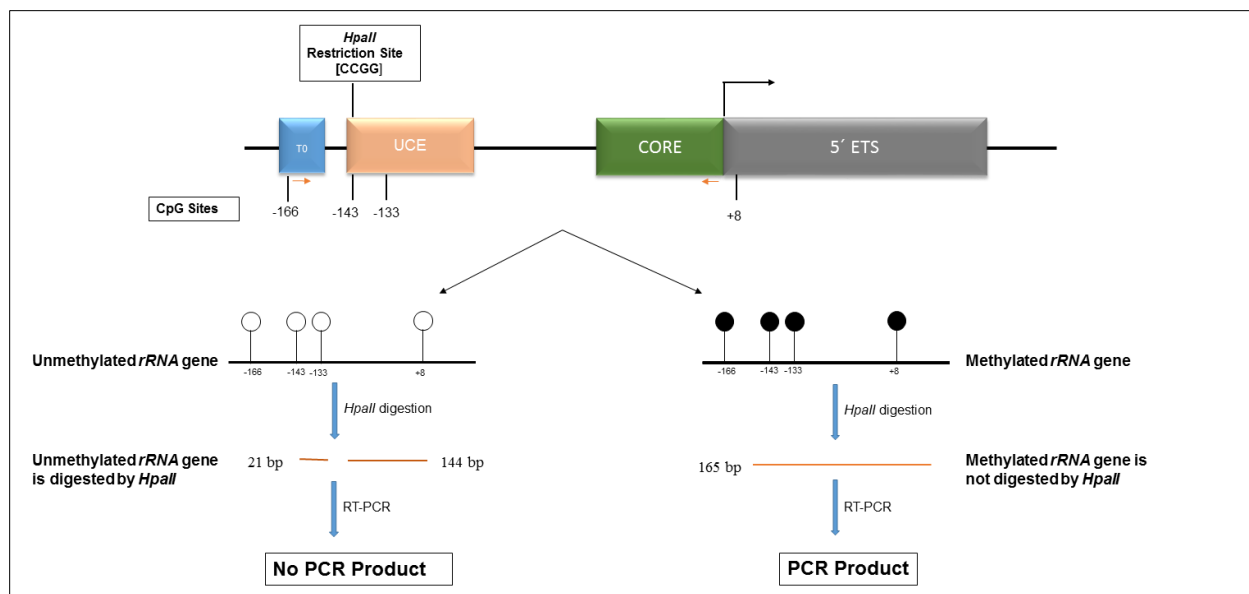


**Figure 2.3 Schematic representation of CHIP-ChOP Assay**

### 2.11 CHOP assay

The CHOP assay was done to determine the percentage DNA methylation of the *rDNA* promoter as described in section 2.9, but excluding the CHIP step. Briefly, genomic DNA was extracted from transduced neurons and 1  $\mu$ g of DNA was digested with *HpaII* enzyme. Undigested samples were used as a control. The undigested (UD) and digested (D) DNA were subsequently subjected to qRT-PCR with primers encompassing the CpG-143. DNA methylation was assessed based on *HpaII* resistance, which allows for amplification of the targeted region. CpG methylation levels are measured by qRT-PCR, using a sets of primers that encompasses the CpG-143, with *HpaII* restriction site (-165 to -1). (**Table 2.6**). The resistance to *HpaII* was calculated as shown in the equation in section 2.9.

## 2.12 MeCP2 ChIPseq data mining using CistromeDB

CistromeDB dataset browser (<http://cistrome.org/db/#/>) was used to access the publicly available ChIPseq data for MeCP2. MeCP2 ChIPseq datasets utilized and the references are shown in Table 2.7.

<b>ChIPseq antibody</b>	<b>Cell/tissue type</b>	<b>Accession number</b>	<b>Reference</b>
5hmC	ESC	53977	[386]
MeCP2	Neurons	53892	[387]
	ESC	58774	[387]
	Cerebellum	3611	[185]

The ChIPseq data accessed from each dataset was then opened in UCSC Genome Browser on Mouse Dec. 2011 (GRCm38/mm10) Assembly (<http://genome.ucsc.edu/>). The binding of MeCP2 to *rDNA* was detected using the link for the UCSC gene *Mus musculus 45S pre-ribosomal RNA* (Rn45s), *ribosomal RNA* [Rn45s (uc012ath.2)] at chr17:39842997-39848829. All ChIPseq data were assembled and labelled in Adobe Illustrator.

## 2.13 Statistical analysis

The statistical analysis for all the studies outlined here were done as reported previously [1,2,151,155,156,380]. GraphPad Prism software was used to generate all graphs and perform statistical analyses. All the graphs represent the average of either N= 3 or 4 unless otherwise specified. Error bars indicate standard error of the mean (SEM). For *MECP2* overexpression

## Chapter 2

studies, one-way ANOVA was performed. For the mouse model of MDS, Student's *t*-test performed for each brain region. Statistical significance was determined using  $p < 0.05^*$ ,  $p < 0.01^{**}$ ,  $p < 0.001^{***}$ , and  $p < 0.0001^{****}$ . Differences showing  $p < 0.05$  were considered statistically significant.

## **Chapter 3: Analysis of Mecp2 Isoform-Specific Expression in Murine Neural Cells Using Custom-Made Antibodies**

### **3.1 Background**

In the present chapter, I have detailed the validation of custom-made antibodies that were generated to detect MeCP2E1 and MeCP2E2 separately. Until 2004, only one MeCP2 isoform (MeCP2E2) was known [166,167]. The second isoform (MeCP2E1) was discovered primarily through bioinformatic analysis of expressed sequence tags (EST), and transcript level studies [166,167]. The localization patterns of the two isoforms were determined by overexpression in a mouse fibroblast cell line [167]. Subsequent studies also focused on the characterization of the two *MECP2/Mecp2* isoforms only at the transcript levels [179]. A major obstacle towards the investigation of MeCP2E1 and MeCP2E2 at the protein level was the lack of antibodies that could distinguish between the two isoforms. Commercial anti-MeCP2 antibodies that were available at that time were generated against the C-terminal end of the protein and thus would recognize both isoforms. These limitations hindered the analysis of the endogenous expression patterns of the two MeCP2 isoforms. In an attempt to address this caveat, we generated and validated MeCP2 isoform-specific antibodies. I also utilized these antibodies to investigate the expression patterns of the two isoforms in primary neural cells isolated from of the embryonic mouse brain. These antibodies were utilized for *in vivo* studies in the developing and adult mouse brain and in an *in vitro* model of neural stem cell differentiation by members of the Rastegar Lab [1,2,156,388] .

### 3.2 General model for testing antibody specificity

The peptides for the generation of the custom-made antibodies were designed within the Rastegar lab. Specific peptides were synthesized and used to generate rabbit and chicken MeCP2 isoform-specific antibodies commercially. At various stages of antibody production, sera from the animals were sent to our lab to verify the presence of antibodies by WB, ICC, and IHC techniques. In order to minimize data redundancy, only the experiments validating the specificity of the final purified antibodies have been included in the thesis.

For the analysis of purified antibodies by WB, Phoenix cells transfected with retroviral vectors containing individual MeCP2 isoforms were utilized. Phoenix cells are retroviral packaging cell lines used for the synthesis of retroviral vectors. Importantly, Phoenix cells lack endogenous MeCP2 expression (based on our own observations). The retroviral vectors (Retro-EF1 $\alpha$ -*MECP2E1*, and Retro-EF1 $\alpha$ -*MECP2E2*) and Phoenix cells reported by Rastegar *et al.* [151], were made available by Dr. James Ellis, University of Toronto. Sera obtained during antibody production were tested on western blot membranes containing Phoenix cell protein lysates overexpressing *MECP2E1* or *MECP2E2*. Both *MECP2* vectors had a C-MYC tag at the C-terminal end of the overexpressed protein, therefore detection of C-MYC was performed to confirm the presence of the transgene in transfected cells. Anti-MeCP2 isoform specificity was validated by WB based on three criteria:

1. Absence of MeCP2 in the negative controls (Protein extracts prepared from non-transfected Phoenix cells, Phoenix cells transfected with the alternate *MECP2* isoform, or Phoenix cells transfected with the test MeCP2 isoform pre-incubated with the corresponding antigenic peptide before blotting).

## Chapter 3

2. Presence of MeCP2 in the positive control (Protein extracts prepared from Phoenix cells overexpressing the test *MECP2* isoform against which the antibody was synthesized).
3. Cells transfected with both MeCP2 isoforms were confirmed by blotting the membranes with an anti-C-MYC antibody.

For the analysis of the purified antibodies by IF, NIH3T3 cells transduced with retroviral vectors containing individual MeCP2 isoforms were utilized. The retroviral vectors (Retro-EF1 $\alpha$ -*MECP2E1*, and Retro-EF1 $\alpha$ -*MECP2E2*) and NIH3T3 cells were a gift from Dr. James Ellis, University of Toronto. MeCP2 isoform specificity was established based on these three criteria:

1. Absence of MeCP2 protein detection in the negative controls (Paraformaldehyde fixed NIH3T3 cells overexpressing the alternate *MECP2* isoform, non-transduced NIH3T3 cells and NIH3T3 cells incubated only with secondary antibodies [primary antibody omission control]).
2. Presence of MeCP2 in the positive control (Paraformaldehyde fixed NIH3T3 cells overexpressing the test *MECP2* isoform against which the antibody was synthesized).
3. Cells transduced with the MeCP2 isoforms were confirmed by immunolabelling with an anti-C-MYC antibody.

### **3.3 Validation of anti-MeCP2E1 antibodies**

As part of my initial studies, I participated in the validation of anti-MeCP2E1 antibodies that could be used in the subsequent analysis of MeCP2E1 expression in neural cells. In order to do this, I contributed to the validation of two custom anti-MeCP2E1 antibodies created in chicken

and rabbit. Antibodies targeting the same isoforms in different species are often useful in double-labeling experiments when colocalization of MeCP2E1 with other proteins is required. This analysis was performed during the greater part of the initial three years of my PhD studies.

### **3.3.1 Peptide selection for the MeCP2E1 antibodies**

The peptide used for MeCP2E1 antibody production was selected and synthesized as described in the material and methods section 2.2.1. Since the two MeCP2 isoforms only differ at their N-terminus, this region was targeted for the generation of MeCP2E1 isoform-specific antibodies. This region is conserved between human and mouse. The MeCP2E1-specific peptide was analyzed using the ThermoFisher Antigen Profiler Peptide Tool, which calculates the antigenicity of the sequence based on sequence length and amino acid composition. Peptides should be between 10-20 amino acids in length, have at least 4 distinct residues, and an equal proportion of hydrophilic and hydrophobic amino acids.

Peptide and antibody generation for anti-MeCP2E1 antibody were done commercially as a paid service through Dr. Rastegar's grants and funding support.

### **3.3.2 Validation of the Chicken anti-MeCP2E1 antibody**

The polyclonal chicken anti-MeCP2E1 antibody was generated commercially as a paid service using a synthetic peptide spanning the N-terminal region of MeCP2E1. Specificity of the MeCP2E1 antibody was validated by western blot (WB) and immunofluorescent (IF) experiments throughout the course of antibody production and after IgY purification. For WB application, the purified antibody was tested using cell extracts from Phoenix cells transfected with either Retro-



EF1 $\alpha$ -E1 or Retro-EF1 $\alpha$ -E2 (**Figure 3.1C**), in parallel with non-transfected cells. As expected, WB analysis with the MeCP2E1 antibody yielded a specific band at the expected molecular weight of approximately 75kDa in *MECP2E1*-transfected cells (**Figure 3.1C, lane 2**). In contrast, MeCP2E1 was not detected in non-transfected cells (**Figure 3.1C, lane 1**), nor in cells transfected with Retro-EF1 $\alpha$ -E2 (**Figure 3.1C, lane 3**). Importantly, pre-incubation of the MeCP2E1 antibody with the antigenic peptide used to generate the antibody (peptide competition) eliminated the detection of MeCP2E1 in Retro-EF1 $\alpha$ -E1 transfected cells, which was dose-dependent on the concentration of peptide used to compete out the MeCP2E1 antibody (**Figure 3.1C, lane 7; 3.1D**). The presence of exogenous MeCP2 in cells transduced with either Retro-EF1 $\alpha$ -E1 or Retro-EF1 $\alpha$ -E2 was confirmed by WB using an anti-C-MYC antibody (**Figure 3.1C, lane 5-6**). No C-MYC signal was detected in non-transfected cells (**Figure 3.1C, lane 4**).

IF staining with the anti-MeCP2E1 antibody revealed the presence of MeCP2 in the DAPI-rich heterochromatic foci in NIH3T3 cells transduced with *MECP2E1*, but no signal was detected in *MECP2E2* transduced cells (**Figure 3.1E**). This indicates that our newly developed antibody does not cross-react with the overexpressed MeCP2E2. In both MeCP2E1 and MeCP2E2 overexpressed cells, incubation with an anti-C-MYC antibody resulted in detectable signals indicating that the protein is properly expressed in both cases. The absence of endogenous MeCP2E1 expression was confirmed in the non-transduced NIH3T3 cells using the anti-MeCP2E1 antibody (**Figure 3.2A**). We did not detect any signal in primary antibody omission experiments in which Retro-EF1 $\alpha$ -E1 transduced cells were labelled with secondary antibodies only (**Figure 3.2B**). Parallel studies (by Carl Olson) in our lab by challenging MeCP2E1 antibody with a MeCP2E2-specific peptide or a C-terminal peptide further confirmed the specificity of the MeCP2E1 antibody endogenously [2].

These results demonstrate that the newly generated anti-MeCP2E1 antibody specifically detects MeCP2E1 protein, and shows no cross-reactivity with MeCP2E2.

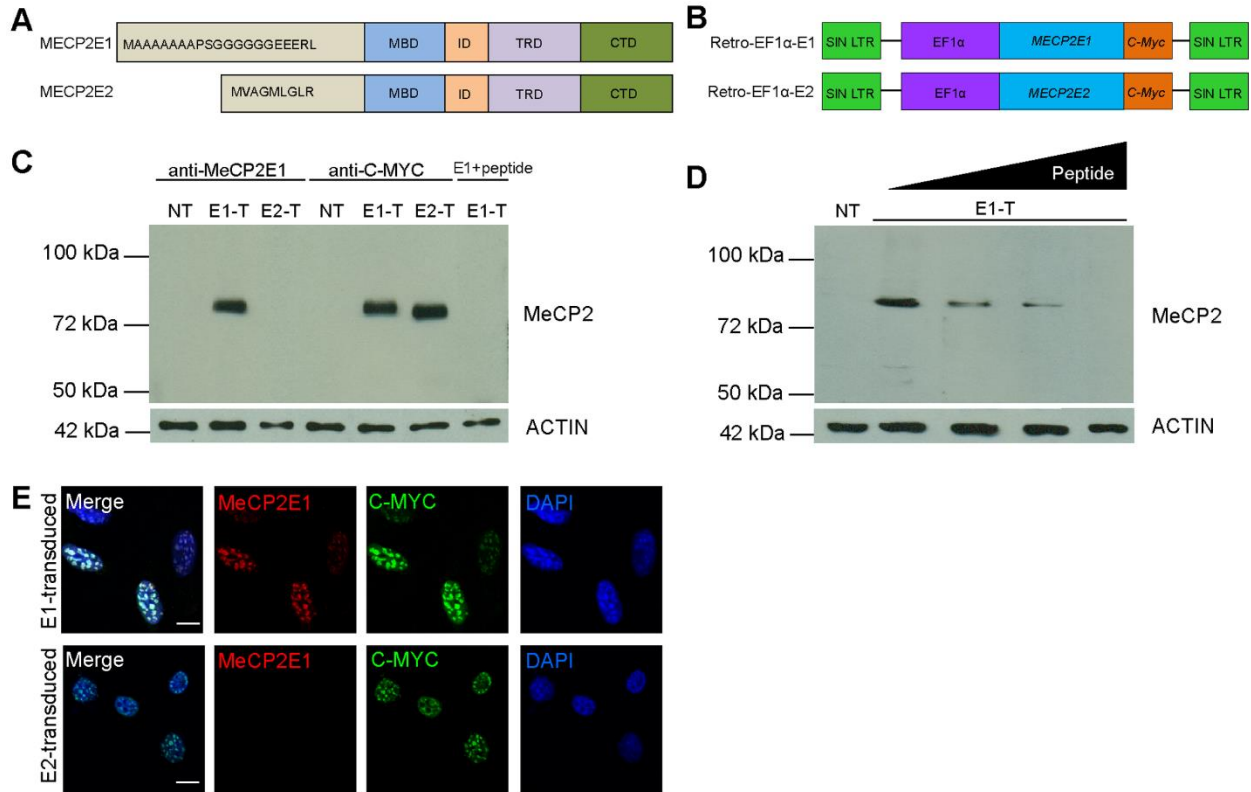


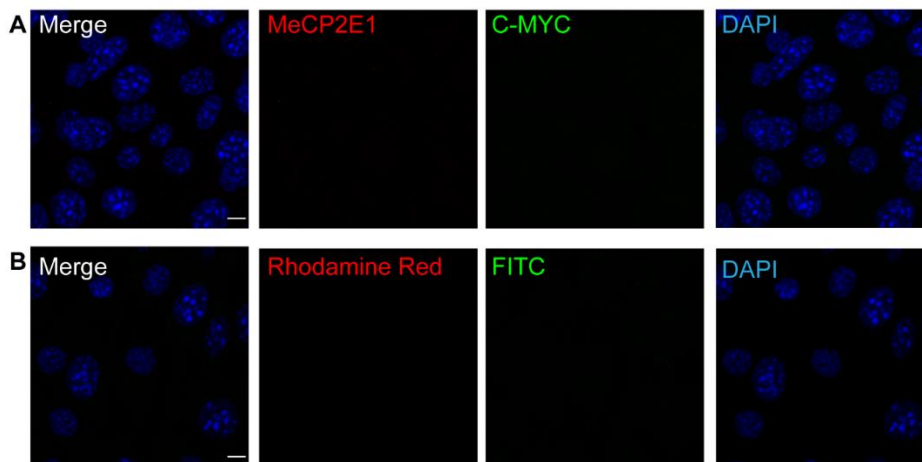
**Figure 3.1 Validation of the newly developed chicken anti-MeCP2E1 antibody.**

A) Schematics of MeCP2 isoforms with known functional domains. The difference in the initial amino acids of the N-terminus is highlighted. B) Schematics of the previously reported [151] *MECP2E1* (Retro-EF1 $\alpha$ -E1) and *MECP2E2* (Retro-EF1 $\alpha$ -E2) retroviral vectors that were used for transfections (C-D) and transductions (E). C) Western blot experiments with Phoenix cell extracts from non-transfected (NT), *MECP2E1* transfected (E1-T), *MECP2E2* transfected (E2-T) cells, and *MECP2E1* transfected cells with peptide competition. Anti-MYC labelling was used as a positive control for transfection and ACTIN was used as a loading control. Peroxidase- AffiniPure goat anti-chicken IgY (for chicken anti-MeCP2E1 antibody) and Peroxidase-AffiniPure goat anti-

## Chapter 3

mouse IgG (for mouse anti-C-MYC antibody) were used as secondary antibodies. D) Western blot experiments with Phoenix cell extracts from non-transfected cells (NT), and *MECP2E1* transfected cells (E1-T), blotted with the anti-MeCP2E1 antibody after pre-incubation with increasing concentrations of peptide used to generate the antibody (0%, 0.1%, 1%, and 5%, of peptide as compared to the amount of antibody used). Peroxidase- AffiniPure goat anti-chicken IgY was used for chicken anti-MeCP2E1 antibody as a secondary antibody. E) Immunofluorescence labelling of NIH3T3 cells transduced with *MECP2E1* (top row) or *MECP2E2* (bottom row), with the anti-MeCP2E1 and an anti-C-MYC antibody are shown. DAPI signals are shown in blue. The secondary antibodies used were Rhodamine Red-X conjugated goat anti-chicken IgY (for chicken anti-MeCP2E1 antibody) and Alexa 488 goat anti mouse IgG (for mouse anti-C-MYC antibody). Note that the signals in both transduced cells are detectable with anti-C-MYC, but only transduced cells with *MECP2E1* show positive signals when incubated with the anti-MeCP2E1 antibody. Scale bars represent 10  $\mu\text{m}$ . MBD: methyl binding domain, ID: intervening domain, TRD: transcriptional repression domain, CTD: C-terminal domain.”

Figure taken and legend adapted from [1].



---

**Figure 3.2 Controls for MeCP2 overexpression in NIH3T3 cells.**

---

A) Absence of MeCP2 and C-MYC signals in non-transfected NIH3T3 cells. B) Absence of signals in primary antibody omission controls with Rhodamine Red-X conjugated goat anti-chicken IgY (for chicken anti-MeCP2E1 antibody) and Alexa 488 goat anti mouse IgG (for mouse anti-C-MYC antibody) in *MECP2E1* transfected NIH3T3 cells. Images are taken at the same exposure time as in **Figure 3.1E**. Scale bars represent 10  $\mu\text{m}$ .

Figure taken and legend adapted from [1].

---

### 3.3.3 Validation of the Rabbit anti-MeCP2E1 antibody

The selection of the peptide for anti-MeCP2E1 antibody production was performed as described in the materials and methods section 2.2.1.

For double-labelling of MeCP2E1 and MeCP2E2, we required an isoform-specific antibody that was generated in a different species. Therefore, we applied the same strategy as reported for developing the chicken anti-MeCP2E1 [1], but this anti-MeCP2E1 was created as a rabbit polyclonal antibody. The specificity and sensitivity of this newly developed anti-MeCP2E1 antibody was initially verified by WB. Blotting protein extracts from non-transfected, MeCP2E1-transfected and MeCP2E2-transfected Phoenix cells, and the affinity purified anti-MeCP2E1 detected specific bands at ~75 kDa in MeCP2E1-transfected extracts (**Figure 3.3A, lane 2**). No signal was detected in non-transfected cells (**Figure 3.3A, lane 1**), nor in cells transfected with *MECP2E2* (**Figure 3.3A, lane 3**). As done previously, the presence of exogenous MeCP2 in the transfected cells with either Retro-EF1 $\alpha$ -E1 or Retro-EF1 $\alpha$ -E2 was verified by immunoblotting with an anti-C-MYC antibody (**Figure 3.3A, lanes 5-6**). No C-MYC signal was detected in non-transfected cells (**Figure 3.3A, lane 4**). Furthermore, pre-incubation of the anti-MeCP2E1 antibody with the antigenic peptide used to create the antibody before blotting the membranes

(**Figure 3.3A, lane 7**) completely abrogated the detection of exogenous MeCP2E1. IF staining with the anti-MeCP2E1 antibody revealed the presence of MeCP2 in the DAPI-rich heterochromatic foci within the NIH3T3 cells transduced with *MECP2E1*, but no signal was detected in the *MECP2E2* transduced cells (**Figure 3.3B: a-b**). This indicates that our newly developed anti-MeCP2E1 antibody does not cross-react with the overexpressed *MECP2E2*. In both *MECP2E1* and *MECP2E2* overexpressed cells, incubation with an anti-C-MYC antibody resulted in detectable signals indicating that the transduced protein is properly expressed in both cases. As expected, we did not detect any signal in primary antibody omission experiments using Retro-EF1 $\alpha$ -E1 transduced cells with the same secondary antibody (**Figure 3.3B: c**). The absence of endogenous *MECP2E1* expression was confirmed in the non-transduced NIH3T3 cells by using the chicken anti-MeCP2E1 antibody (**Figure 3.3B: d**). Adapted from [2].

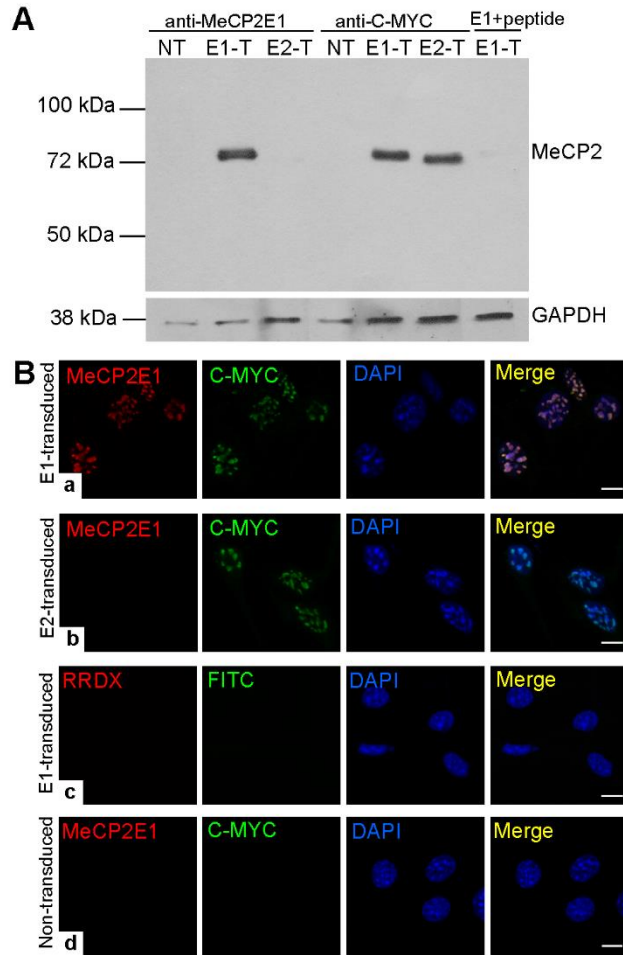


**Figure 3.3 Validation of the custom-made rabbit MeCP2E1 antibody.**

A) Western blot experiment to detect MeCP2E1 expression in control non-transfected (NT), *MECP2E1* transfected (E1-T), and *MECP2E2* transfected (E2-T) cells, or *MECP2E1* transfected cells but with antibody pre-incubated with the antigenic peptide. Anti-MYC labelling was used as a positive control. GAPDH labelling was used as a loading control. Peroxidase-AffiniPure donkey anti-rabbit IgG (for rabbit anti-MeCP2E1 antibody) and Peroxidase-AffiniPure goat anti-mouse IgG (for mouse anti-C-MYC antibody) were used as secondary antibodies B) Detection of MeCP2E1 by immunofluorescence in NIH3T3 cells transduced with a) *MECP2E1*, or b) *MECP2E2*; c) Absence of signal in primary antibody omission controls labelled with Rhodamine

Red-X conjugated goat anti-mouse IgG (for mouse anti-C-MYC antibody) and Alexa Fluor 488 conjugated donkey anti-rabbit IgG (for rabbit anti-MeCP2E1 antibody) in *MECP2E1* transfected NIH3T3 cells; d) Absence of MeCP2 and C-MYC signals in non-transfected NIH3T3 cells. Scale bars represent 10  $\mu\text{m}$ .

Figure taken and legend adapted from [2].

---

### **3.4 Analysis of MeCP2 expression and localization in embryonic primary cortical neurons and astrocytes**

#### **3.4.1 Characterization of total MeCP2 localization within the nucleus of primary embryonic cortical neurons**

Previous studies suggested that MeCP2 expression in primary neurons might vary from diffuse to punctate staining within the nucleus based on culture conditions [149,189]. Therefore, we examined nuclear MeCP2 expression in primary embryonic cortical neurons by confocal co-localization studies compared to constitutive and facultative heterochromatin marks (**Figure 3.4**). As shown in **Figure 3.4**, MeCP2 is primarily co-localized with the two constitutive heterochromatin marks (H3K9me3, H4K20me3), but showed minimal overlap with the facultative heterochromatin marks (H3K27me3, H3K9me2) interrogated.

Since  $\beta$ -Tubulin III is not expressed in the nucleus of neurons, only baseline readings were observed (dark-blue lines).

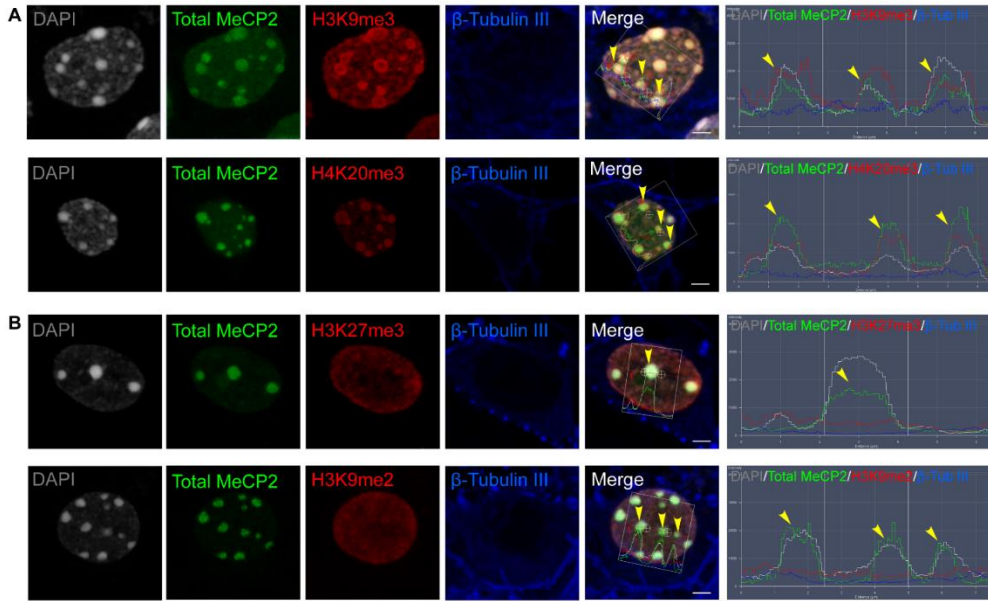


**Figure 3.4 Nuclear localization of total MeCP2 and heterochromatin marks in primary neurons.** A) Total MeCP2 signals in embryonic primary cortical neurons overlapped with signals corresponding to constitutive heterochromatin marks; H3K9me3 and H4K20me3. B) MeCP2 displays minimal overlap with facultative heterochromatin marks; H3K27me3 and H3K9me2. Scale bars represent 2  $\mu$ m. Total MeCP2 was immunolabelled with a C-terminal antibody (Millipore). Secondary antibodies used were Alexa 488 goat anti rabbit (for rabbit anti-MeCP2 antibody) and Rhodamine Red-X conjugated goat anti-mouse IgG (for mouse anti-H3K9me3, anti-H4K20me3, anti-H3K27me3, and anti-H3K9me2 antibodies).

Figure taken and legend adapted from [1].



### 3.4.2 Determination of MeCP2E1 expression patterns in embryonic primary cortical neurons and astrocytes

The expression of MeCP2 in astrocytes has been a relatively recent discovery, which has led to a significant paradigm shift regarding the contribution of glial cells in RTT pathophysiology [363,389,390]. Previous studies have shown that mutant astrocytes from a RTT mouse model (*Mecp2*<sup>-/-</sup>) failed to support normal dendritic morphology of neurons under *in vitro* co-culture experiments [390]. Re-expression of MeCP2 in astrocytes of a RTT mouse model mitigates many RTT phenotypes and also restores impaired dendritic morphology and decreased neuronal VGLUT1 levels [389]. These observations suggest that MeCP2 expression and function within astrocytes are essential for optimal neuronal function within the brain. However, the expression of MeCP2 isoforms and their potential role in astrocyte function remain to be determined. Additionally, the expression pattern of MeCP2 isoforms in neurons, at the protein level, is still unknown. Therefore, we next used our newly developed anti-MeCP2E1 antibody and examined the expression of MeCP2E1 in embryonic primary cortical neurons and astrocytes. As expected, we detected endogenous expression of total MeCP2 in both primary cortical neurons and astrocytes using a C-terminal antibody (mainly at the chromocenters) (**Figure 3.5A**). Immunofluorescence experiments with our chicken MeCP2E1-specific antibody detected endogenous MeCP2E1 expression in both primary neurons and astrocytes which displayed a nuclear heterochromatic expression pattern overlapping with DAPI signals. MeCP2E1 signals were also detected throughout the nucleus, especially in the astrocytes (**Figure 3.5B**). Although this indicates that MeCP2E1 has a similar nuclear localization profile compared to the total MeCP2 in both embryonic primary neurons and astrocytes, it does not inform regarding the protein levels in these two cell types. As a quantitative approach, we examined the total amount of MeCP2E1 in primary

neurons and astrocytes by WB analysis and compared it to the loading control Actin levels. We found that that the level of MeCP2E1 protein is five times higher in primary neurons compared to primary astrocytes (**Figure 3.5C**). This is not surprising, as primary astrocytes are reported to express approximately 25% of the MeCP2 levels observed in primary neurons [390].

Taken together, these results indicate that while MeCP2E1 is expressed in both primary cortical neurons and astrocytes, its level of expression is much higher in neurons. The regulatory mechanisms dictating the higher expression of neuronal MeCP2 is not fully clear. Also, the exact functions of MeCP2 in astrocytes remains to be elucidated. Recent studies have shown that depressed hypercapnic ventilatory response (HCVR) observed in RTT mouse models are caused by the loss of MeCP2 within astrocytes [391]. However, reports on astrocytic links to cognitive defects observed in RTT and MDS are still lacking. Our data further indicate that MeCP2E1 signals highly overlap with DAPI-rich heterochromatin in the nucleus in both primary neurons and astrocytes. Additionally, we show that punctate MeCP2 heterochromatic localization in neurons shows significant overlap with constitutive heterochromatin marks, but has little or no overlap with the facultative heterochromatin marks.

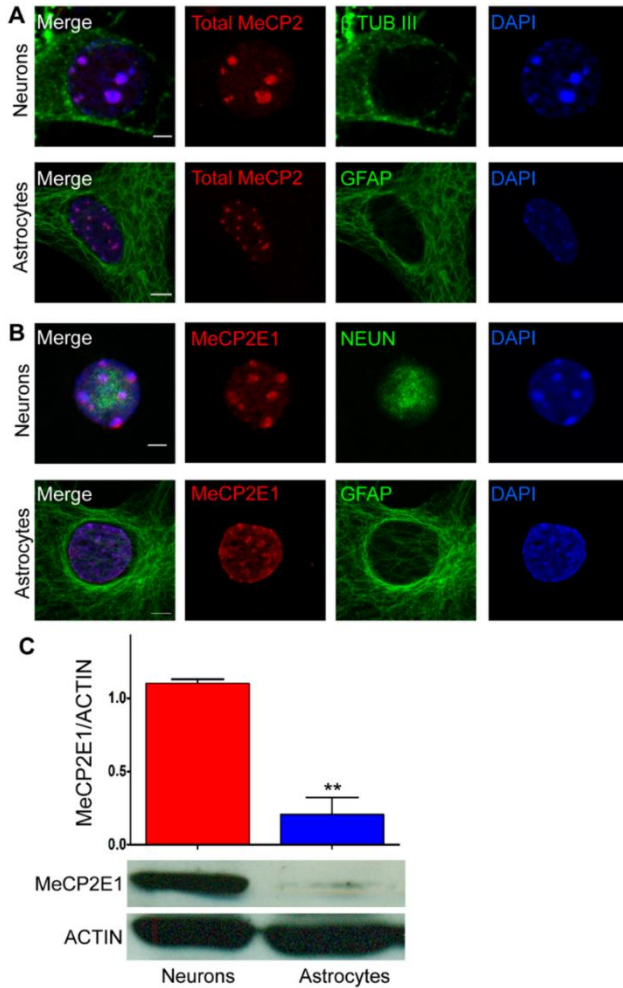


**Figure 3.5 Expression of total MeCP2 and MeCP2E1 in primary neurons and astrocytes.**

A) Expression of total MeCP2 in embryonic primary cortical neurons and astrocytes as detected by immunofluorescence labelling. Cells were labelled with  $\beta$ -III tubulin ( $\beta$  TUB III) and GFAP to mark neurons and astrocytes, respectively. B) Expression of MeCP2E1 in embryonic primary cortical neurons and astrocytes. Cells were labelled with NEUN and GFAP to mark neurons and astrocytes, respectively. Scale bars represent 5  $\mu$ m. Total MeCP2 was immunolabelled with a C-terminal antibody (Millipore). MeCP2E1 was immunolabelled using custom-made chicken anti-

MeCP2E1. Secondary antibodies used were Rhodamine Red-X conjugated goat anti-chicken IgY, Rhodamine Red-X goat anti-rabbit IgG and Alexa 488 goat anti mouse IgG. C) Western blot analysis of MeCP2E1 levels in embryonic primary cortical neurons and astrocytes. The graph depicts the relative quantification of MeCP2E1 in neurons and astrocytes relative to actin,  $p < 0.01$  ( $N = 2 \pm \text{SEM}$ ).

Figure taken and legend adapted from [1].

---

### **3.5 Validation of the Chicken anti-MeCP2E2 antibody**

#### **3.5.1 Identification of a peptide to generate an anti-Chicken MeCP2E2 antibody**

Previously, I described the procedure for the identification of a suitable peptide to generate a MeCP2E1 antibody. A similar procedure was followed to identify a suitable peptide for MeCP2E2. The identification of the peptide for the MeCP2E2 antibody was performed as described in the materials and methods section 2.2.1. The generation of the peptide was done commercially as a paid service.

Peptide and antibody generation for anti-MeCP2E2 antibody were done commercially as a paid service through Dr. Rastegar's grants and funding support.

#### **3.5.2 Validation of Chicken anti-MeCP2E2 antibody**

A sequential antibody validation process was followed for the anti-MeCP2E2 antibody, similar to the protocol described in section 3.3.2 for the MeCP2E1 antibody.

As there was no commercially available MeCP2E2-specific antibody, we validated a novel chicken polyclonal MeCP2E2 antibody using an antigenic peptide corresponding to the N-

terminus of MeCP2E2, using a similar approach to one we previously reported for MeCP2E1 [21]. We validated the specificity of this novel anti-MeCP2E2 antibody by multiple techniques including WB and immunofluorescence in transfected Phoenix cells (for WB) and transduced NIH3T3 cells (for IF) with either Retro-EF1 $\alpha$ -E1 or Retro-EF1 $\alpha$ -E2, [151] (**Figure 3.6B**).

To investigate the endogenous expression pattern of MeCP2E2, we initially developed a MeCP2E2 isoform-specific antibody using an antigenic peptide unique to the MeCP2E2 N-terminus. We validated the specificity of the MeCP2E2 antibody by techniques including Western blot and immunofluorescence experiments at various stages of the antibody production and after IgY purification. For validations by WB, the affinity purified antibody was tested using protein extracts from Phoenix cells transfected with either Retro-EF1 $\alpha$ -E1 or Retro-EF1 $\alpha$ -E2 [151] in parallel with non-transfected control cells, as previously described [1]. Western blot analysis with the anti-MeCP2E2 antibody yielded a specific band at the expected molecular weight (approximately 75 kDa) in *MECP2E2*-transfected cells (**Figure 3.6C, lane 3**). In contrast, no signal was detected in non-transfected cells (**Figure 3.6C, lane 1**), nor in cells transfected with *MECP2E1* (**Figure 3.6C, lane 2**). Importantly, pre-incubation of the anti-MeCP2E2 antibody with the antigenic peptide used to generate the antibody (peptide competition) eliminated the detection of the signal in the *MECP2E2* transfected cells (**Figure 3.6C, lane 7**). The specificity and sensitivity of this newly developed anti-MeCP2E2 antibody was further verified by pre-incubation of the antibody with increasing concentrations of the antigenic peptide before blotting the membranes (**Figure 3.7A, lanes 2–4**). The presence of exogenous MeCP2 in the cells transfected with either Retro-EF1 $\alpha$ -E1 or Retro-EF1 $\alpha$ -E2 was verified by immunoblotting with an anti-C-MYC antibody (**Figure 3.6C, lanes 5–6**). No C-MYC signal was detected in non-transfected cells (**Figure 3.6C, lane 4**).

Further verification of the specificity of the custom-made anti-MeCP2E2 antibody using IF, revealed the localization of MeCP2E2 in the DAPI-rich heterochromatic foci within the nuclei of NIH3T3 cells transduced with *MECP2E2*. No signal was detected in the *MECP2E1* transduced cells (**Figure 3.6D; a-b**). C-MYC labelling confirmed successful transduction of both MeCP2E1 and MeCP2E2 vectors (**Figure 3.6D: a-b**). The absence of endogenous *MECP2E2* expression was evident in non-transduced NIH3T3 cells probed with the anti-MeCP2E2 antibody (**Figure 3.7B: a**). No signal was observed in primary omission experiments using Retro-EF1 $\alpha$ -E1 transduced cells labelled with secondary antibodies alone (**Figure 3.7B: b**).

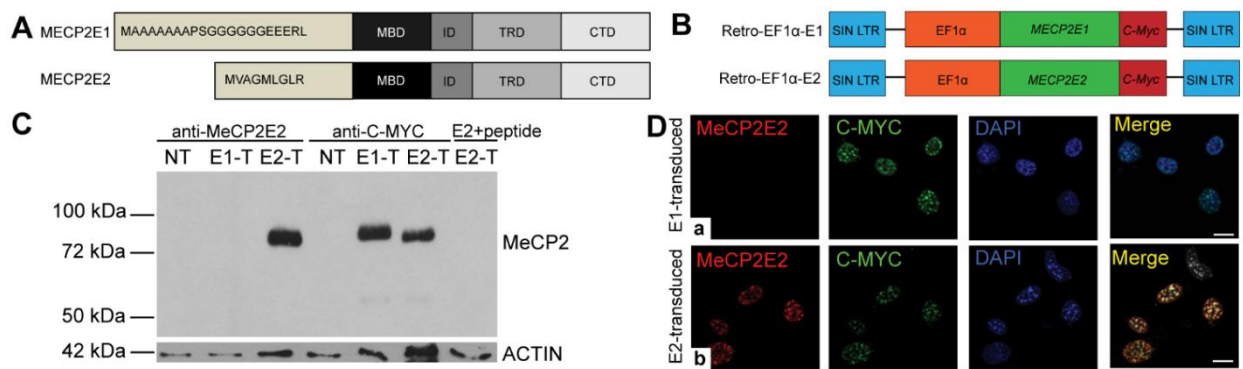


**Figure 3.6 Validation of the Chicken anti-MeCP2E2 antibody.**

A) Schematic representation of the domain organization of MeCP2E1 and MeCP2E2 protein, which differ only in their N-terminal sequences. MBD: methyl binding domain, ID: intervening domain, TRD: transcriptional repression domain, CTD: C-terminal domain (adapted from [1]). B) Schematic of C-MYC tagged *MECP2E1* (Retro-EF1 $\alpha$ -E1) and *MECP2E2* (Retro-EF1 $\alpha$ -E2) retroviral vectors that were used for the transfection of Phoenix cells (in C) and transduction of NIH3T3 cells (in D) (adapted from [151]). C) Western blot experiment to detect MeCP2E2 expression in non-transfected (NT), *MECP2E1* transfected (E1-T), *MECP2E2* transfected (E2-T) cells, and *MECP2E2* transfected cells probed with the MeCP2E2 antibody pre-incubated with the E2 antigenic peptide. Anti-MYC labelling was used as a positive control of

transfection/transduction. Peroxidase- AffiniPure goat anti-chicken IgY (for chicken anti-MeCP2E2 antibody) and Peroxidase-AffiniPure goat anti-mouse IgG (for mouse anti-C-MYC antibody) were used as secondary antibodies. D) MeCP2E2 detection by immunofluorescence staining in transduced NIH3T3 cells with either a) *MECP2E1*, or b) *MECP2E2* retroviral vectors. The secondary antibodies used were Rhodamine Red-X conjugated goat anti-chicken IgY (for chicken anti-MeCP2E2 antibody) and Alexa 488 goat anti mouse IgG (for mouse anti-C-MYC antibody).

Figure taken and legend adapted from [3].

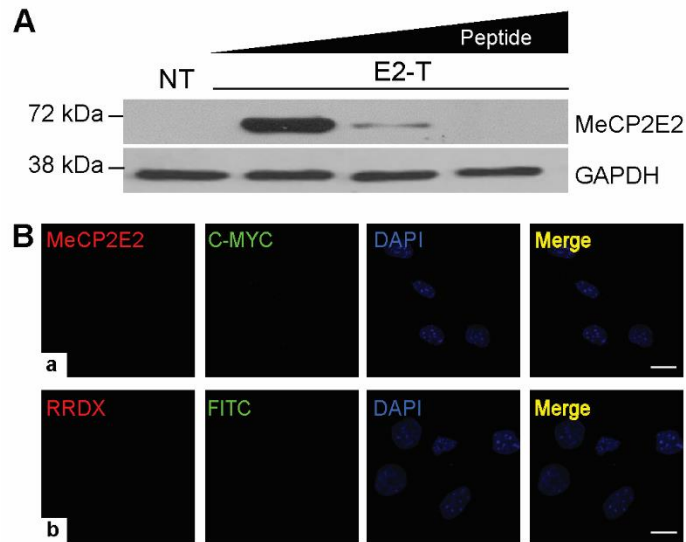


**Figure 3.7 Additional controls for chicken anti-MeCP2E2 antibody validation.**

A) Western blot experiments with Phoenix cell extracts from non-transfected cells (NT), and *MECP2E2* transfected cells (E2-T), probed with the MeCP2E2 antibody after pre-incubation with increasing concentrations of the E2 antigenic peptide (0%, 0.1%, 1%, and 5%, of peptide as compared to the amount of antibody used). Peroxidase- AffiniPure goat anti-chicken IgY was

## Chapter 3

used as the secondary antibody (for chicken anti-MeCP2E2 antibody). B) Negative controls for immunofluorescence detection of; a) MeCP2E2 and C-MYC in non-transduced NIH3T3 cells, and b) primary antibody omission controls with Rhodamine Red-X conjugated goat anti-chicken IgY (for chicken anti-MeCP2E2 antibody) and Alexa 488 goat anti mouse IgG (for mouse anti-C-MYC antibody) in *MECP2E2* transduced NIH3T3 cells. Scale bars represent 10  $\mu\text{m}$ .

Figure taken and legend adapted from [2].

---

In parallel to our WB and ICC studies, the specificity of MeCP2E1 and MeCPE2 custom-made antibodies were also validated by IHC experiments using tissue samples by another member of our lab (Carl Olson). As part of the negative controls for IHC experiments in the mouse brain, the custom-made antibodies were pre-incubated with peptides against the alternate isoform and a C-terminal peptide before labelling tissue samples. These experimental conditions did not result in the detection of MeCP2 (data not shown) which further demonstrated the specificity of these antibodies

The development of the chicken anti-MeCP2E2 antibody (Section 3.5.2) along with the rabbit anti-MeCP2E1 antibody (Section 3.3.3) and the previously reported chicken anti-MeCP2E1 (Section 3.3.2) antibody allowed the investigation of the endogenous expression profiles of the two isoforms in various brain regions, as well as during mouse brain development in our lab through research conducted by other lab members [2,388]. The chicken anti-MeCP2E1 antibody was also used to detect the expression of MeCP2E1 during differentiation of neural stem cells



isolated from E14.5 forebrain and the effect of Decitabine, a DNA demethylating agent and a potential drug for autism, on MeCP2E1 expression [156].

### 3.6 Discussion

For nearly two decades, *Mecp2/MECP2* was thought to encode a single protein. Thus, many of the studies conducted prior to 2004 that investigated MeCP2 expression were blind to the existence of the two protein variants. The isoform that was discovered in 2004, *Mecp2e1*, had its own unique N-terminus, and was more abundant than *Mecp2e2* in most mouse tissues at the mRNA level [167]. Subsequent studies on *Mecp2e1* and *Mecp2e2* transcript levels demonstrated differential expression patterns of the two isoforms in postnatal mouse brain [179]. However, a lack of correlation between MeCP2 mRNA and protein levels had also been reported [392], which warranted further investigations on the differential distribution of the two MeCP2 isoforms at the protein level. In order to study MeCP2 isoform-specific functions, overexpression of the two MeCP2 isoforms with a tag such as C-MYC or EGFP had to be done [156]. However, MeCP2 isoform-specific antibodies were necessary for *in vivo* expression and localization studies. The generation and validation of the MeCP2E1 antibody was an essential step towards addressing this caveat that existed in the field prior to 2012.

My immunofluorescent colocalization studies of total MeCP2 with euchromatic and heterochromatic markers are in agreement with previous studies that have shown punctate localization of MeCP2. Even though diffuse nuclear staining has been reported for MeCP2 previously [318], it has been shown that changes from diffuse to punctate MeCP2 localization occur as neurons mature [393]. Whether this change in localization also signifies a change in MeCP2 function at different developmental stages remains to be established. Similar to the

## Chapter 3

localization of total MeCP2 in the chromocenters of primary embryonic neurons, we detected total MeCP2 being localized to the DAPI-rich chromocenters in hippocampal nuclei of the adult mouse brain [2]. MeCP2E1 being the major MeCP2 isoform found in neurons, it followed a similar localization pattern within the nucleus of neurons. MeCP2 localization to heterochromatic regions of the nucleus is more congruent with its known functions as a transcriptional repressor and a chromatin architectural protein [70]. As a chromatin architectural protein, MeCP2 has been shown to be involved in the clustering of chromocenters during myogenic differentiation [394]. Even though the majority of studies, including ours, have shown chromocenter localization of MeCP2 and MeCP2E1, there have been reports which show otherwise. For example, in a joint-publication with our lab, Yasui *et al.*, demonstrated that MeCP2E1 can be detected in the nuclear matrix in association with Splicing factor, proline- and glutamine-rich (SFPQ) and Y-box-binding protein 1 (YB-1) in human neuronal cell line SH-SY5Y. These results were significant since the study was the first to report the association of MeCP2 with the nuclear matrix factor (SFPQ), and provided further evidence for its association with YB-1, a splicing factor [395].

For many years, MeCP2 expression within the brain was thought to be confined to neurons, and absent in astrocytes as well as other glial cells [220,318,396]. However in 2009, three independent groups reported that MeCP2 is expressed in glial cells [151,363]. In 2013, in a report from our lab, we showed the detection of MeCP2 in neurons (TUB III<sup>+</sup>), astrocytes (GFAP<sup>+</sup> and S100B<sup>+</sup>), oligodendrocytes (CNPase<sup>+</sup>, BMP<sup>+</sup>, and OLIG2<sup>+</sup>) and ki67<sup>+</sup> proliferating cells in a population of differentiating neural stem cells (Liyanage, Zachariah, and Rastegar, 2013) [156]. Subsequently, glial cells have been shown to play a significant role in the pathogenesis of RTT [363,397,398]. However, expression levels of MeCP2E1 or MeCP2E2 protein in these cell types was unknown. My studies presented in this chapter provide evidence that MeCP2E1 is expressed

## Chapter 3

in primary embryonic neurons and astrocytes, with significantly higher expression in neurons. This higher neuronal MeCP2E1 expression was congruent with the previously-reported total MeCP2 expression differences between neurons and glia [390]. With the generation and validation of the anti-MeCP2E2 antibody, we were able to show the comparative detection of MeCP2E1 and MeCP2E2 in neurons (NEUN<sup>+</sup>), astrocytes (GFAP<sup>+</sup>) and oligodendrocytes (CNPase<sup>+</sup>) in the hippocampus of male and female adult mouse brain [2]. As expected, MeCP2E1 and MeCP2E2 in the adult hippocampal neurons, astrocytes and oligodendrocytes were majorly localized to the chromocenters.

The cell-type specific levels of MeCP2 expression could be a critical factor in the functional significance of MeCP2. For instance, in neurons, MeCP2 is known to almost ‘coat’ the genome and have genome-wide effects in terms of transcriptional and translational control [185,234]. Whether the same MeCP2 functions exists in cells with lower levels of MeCP2 remains to be investigated. Also, the dynamics of MeCP2E1 and MeCP2E2 expression, and their redundant and/or non-redundant roles in the functions attributed to MeCP2 to date are still a subject of inquiry.

The development of a MeCP2E1-specific antibody allowed us to examine and explore the expression patterns of MeCP2E1 endogenously both *in vitro* and *in vivo* [1]. However, the possibility of non-redundancy between the two MeCP2 isoforms in terms of expression could not be investigated. This caveat was addressed with the development of the MeCP2E2-specific antibody. Using this antibody, our lab has shown that MeCP2E1 and MeCP2E2 display different expression levels in adult mouse brain which correlated with DNA methylation patterns at the *Mecp2* regulatory regions found within the *Mecp2* promoter and intron 1 [2]. Therefore, these antibodies aided in studying MeCP2 isoform-specific expression and regulation within the adult

## Chapter 3

mouse brain. Moreover, these antibodies were used to show the dynamics of MeCP2 isoform-specific expression during mouse brain development by another lab member [2,388].

In my studies, I mainly focused on MeCP2E1 expression as it is shown to be the major neuronal isoform. Therefore, exploration of MeCP2E2 expression patterns in neurons and astrocytes will be a future direction. The expression patterns of MeCP2E1 and MeCP2E2 in the hippocampus of the adult mouse brain, as published by Olson *et al.*, [2], suggests that the two MeCP2 isoforms may have similar localization patterns in neurons but are expressed at different levels. In a collaborative study within our lab, we showed the induction of MeCP2E1 by Decitabine during neural stem cell differentiation while reporting the impact of DNA methylation on *Mecp2* isoform regulation [156]. These antibodies were further used to detect increased hippocampal expression of MeCP2E2 levels in a mouse model lacking MeCP2E1 isoform [395].

In summary, the development of the MeCP2 isoform-specific antibodies enabled studies that filled several knowledge gaps that existed in the field. Further validation of these antibodies for other applications such as ChIP experiments could allow even further in-depth studies on potential functions of MeCP2 isoforms (discussed in Chapter 6).

## Chapter 4: Analyzing the Effect of Neuronal *MECP2E1* and *MECP2E2*

### Overexpression on *rRNA* Biogenesis

#### 4.1 Background

The results presented in Chapter 3, along with subsequent publications from our laboratory, provided significant insights into MeCP2 isoform-specific expression patterns within the murine brain and specific neural cells [1,2].

The effect of MeCP2 on *rRNA* levels has been studied mainly within the context of MeCP2-deficiency, as published by Li *et al.*, (2013) and Gabel *et al.* (2015) [234,362]. Using human embryonic stem cell-derived neurons lacking MeCP2, Li *et al.*, (2013) demonstrated global repression of neuronal transcription and translation [234]. Li *et al.*, (2013) used human ESCs with a loss-of-function *MECP2* allele, generated by TALEN-mediated gene editing, to generate differentiated neurons. The gene editing strategy employed targeted the third exon of the *MECP2* gene, and therefore affected both MeCP2 isoforms. Gene editing was performed in both male and female ESC lines to generate *MECP2* hemizygous and heterozygous mutant male and female clones, respectively. The control and mutant ESCs were initially differentiated into neural precursors and subsequently into neurons. WB and qRT-PCR were used to confirm the presence and absence of MeCP2 in control and mutant cells respectively. As part of their studies Li *et al.*, (2013) reported decreased levels of total RNA and 5.8S *rRNA* in MeCP2-deficient neurons. The levels of 5.8S *rRNA* was analyzed by loading total RNA extracted from equal numbers of control and *MECP2* mutant cells. These results implied that mature *rRNA* levels were decreased by the loss of MeCP2.

Gabel *et al.*, (2015) knocked down MeCP2 in E16.5 mouse cortical neurons using shRNA that targeted both MeCP2 isoforms and observed decreased levels of 28S and 18S *rRNA*. Together with the decrease in 5.8S *rRNA* reported by Li *et al.*, (2013) the two studies suggested that mature *rRNA* levels are affected by the loss of MeCP2. The results from the two studies also suggested that the decrease in mature *rRNA* levels is observed in both mouse and human experimental models.

Since a decrease in mature *rRNA* levels following MeCP2-deficiency had been reported [234,362], we focussed our studies on the effect of MeCP2 overexpression on mature and precursor *rRNA*. This strategy is relevant because overexpression of *MECP2* due to gene duplication has been identified as the primary cause of a neuronal disorder known as *MECP2* Duplication Syndrome that was initially reported in 2005 [239,240]. MDS is characterized by severe motor dysfunction, cognitive and social disabilities, seizures, and recurrent infections. A transgenic mouse model of MDS, *MECP2* Tg1, shows severe progressive neurological symptoms such as seizures, anxiety, learning and memory impairments, behavioural deficits, and premature death [259,261,366]. These observations indicate that even mild (~2-fold) overexpression of MeCP2 can have detrimental effects on the brain.

The molecular mechanisms leading to MDS remains unknown. Therefore, the discovery of potential targets that are altered by MeCP2E1 or MeCP2E2 overexpression could provide insights into MDS pathogenesis. In the current chapter, I am investigating whether MeCP2 overexpression deregulates *rRNA* levels. For this purpose, I have used an *in vitro* model of primary neurons, as well as the examination of brain regions *in vivo* using a transgenic mouse model of MDS.

## 4.2 Overexpression of *MECP2* isoforms in primary neurons

To elucidate the effects of MeCP2 overexpression on *rRNA* synthesis, primary cortical neurons transduced with lentiviral vectors containing either *MECP2E1* or *MECP2E2* were used as an experimental model. The lentiviral vectors, Lenti-*EF1 $\alpha$ -MECP2E1* and Lenti-*EF1 $\alpha$ -MECP2E2* (both of which had a C-terminal *cMYC* tag) were a generous gift from the Ellis Lab, University of Toronto. [151] reported by Rastegar *et al.*, 2009 [151] (**Figure 4.1**). The presence of a *cMYC* tag allowed easy monitoring of expression levels arising from the lentiviral vectors in contrast to the endogenous *MeCP2E1* and *MECP2E2* in neurons. As a control for the lentiviral transduction experiments, I also included an *EGFP* (Lenti-*EF1 $\alpha$ -EGFP*) vector with the same lentiviral backbone as the *MECP2E1/E2* vectors. For simplicity, the vectors will be described as *EF1 $\alpha$ -MECP2E1*, *EF1 $\alpha$ -MECP2E2* and *EF1 $\alpha$ -EGFP*.

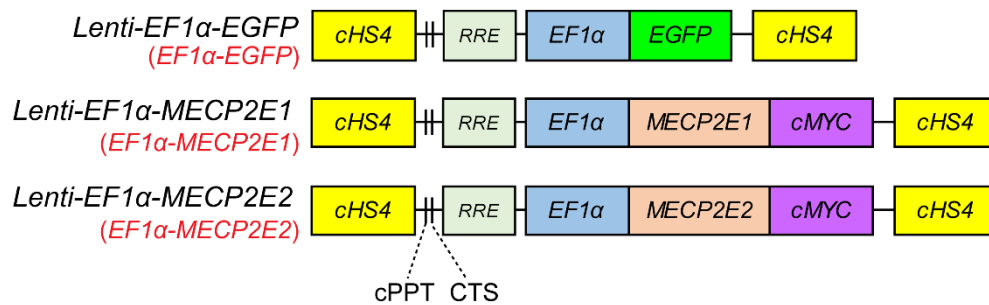


**Figure 4.1** Lentiviral *MECP2E1*, *MECP2E2* overexpression vectors and *EGFP* control vector.

Lenti-*EF1 $\alpha$ -EGFP* vector was used as a control. Lenti-*EF1 $\alpha$ -MECP2E1* and Lenti-*EF1 $\alpha$ -MECP2E2* vectors have a C-terminal *cMYC* tag. cHS4: chicken  $\beta$ -globin locus Hypersensitive Site 4, cPPT: central Poly Purine Tract, CTS: Central Terminal Sequence, RRE: Rev-Responsive Element.

*Adapted from [151].*

Validation of *MECP2E1* and *MECP2E2* overexpression in neurons was performed by qRT-PCR (to monitor transcript levels), and immunofluorescence experiments (to confirm overexpression at the protein level). Quantitative RT-PCR analysis of *cMYC* levels revealed *cMYC* expression in both *MECP2E1* and *MECP2E2* transduced neurons, but not in the *EGFP* overexpressing neurons, as expected (**Figure 4.2A**). In immunofluorescence experiments, transduced neurons could be detected by an anti-EGFP antibody in the *EGFP*-transduced neurons. Similarly, an anti-*cMYC* antibody detected *MECP2E1*- and *MECP2E2*-transduced neurons (**Figure 4.2B**). Importantly, the overexpressed MeCP2E1 and MeCP2E2 localized to the chromocenter of the neurons, in a pattern identical to endogenous MeCP2E1 and MeCP2E2. *EGFP* expression in transduced neurons, however, exhibited a diffuse nuclear expression pattern (**Figure 4.2B**), as reported previously [151].

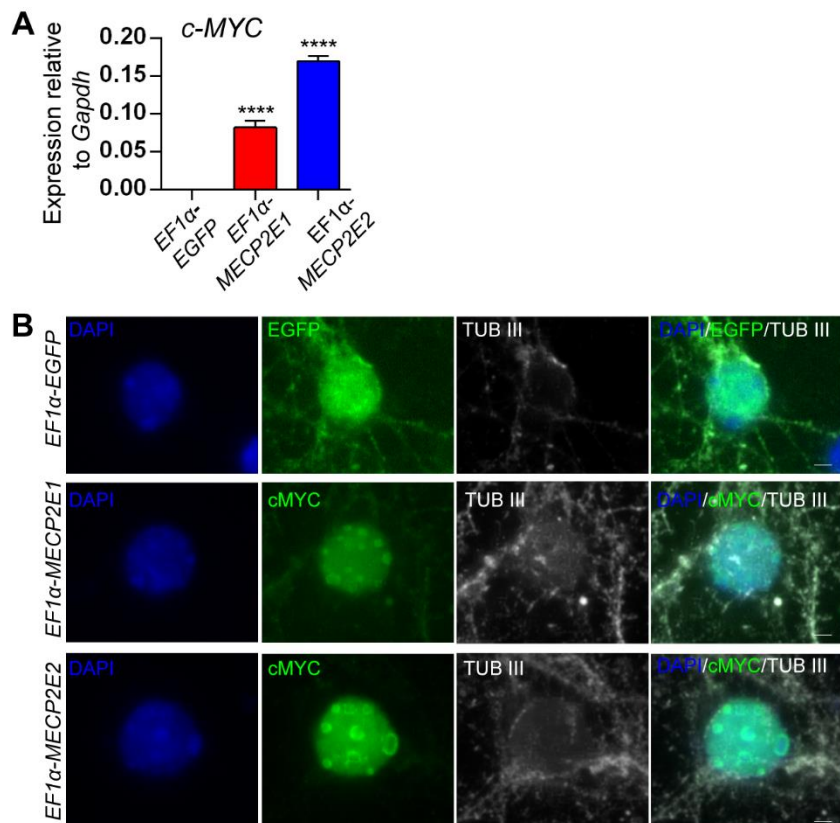


**Figure 4.2 Confirmation of neuronal overexpression of *MECP2* isoforms.**



A) Transcript level detection of *cMYC* in *MECP2*-transduced neurons. The c-MYC expression is normalized to the endogenous *Gapdh* levels. N=7 (primary neurons isolated from 7 independent mice). B) Immunofluorescent labelling of neurons transduced with Lenti-*EF1 $\alpha$ -EGFP* control, cMYC-tagged Lenti-*EF1 $\alpha$ -MECP2E1* and Lenti-*EF1 $\alpha$ -MECP2E2*. Note that EGFP labels the whole neuron while cMYC-tagged MeCP2 isoforms are localized to the neuronal chromocenters. Scale bars represent 10  $\mu$ m. Dylight 649 conjugated goat anti- chicken IgY (for  $\beta$ -Tubulin III) and Alexa 488 goat anti mouse IgG (for mouse anti-EGFP and anti-C-MYC antibody) were used as secondary antibodies.

---

### 4.3 Analysis of *45S pre-rRNA* levels in *MECP2E1*- and *MECP2E2*-overexpressing neurons

Previous studies have shown decreased *rRNA* synthesis in RTT-neurons [234]. In order to gain further insight into the regulation of *rDNA* expression by MeCP2 isoforms and to gain insight on the potential involvement of *rRNA* synthesis in MDS, I analyzed *rDNA* transcripts in neurons overexpressing *MECP2* isoforms.

When I performed qRT-PCR analysis of the *45S pre-rRNA* in *MECP2E1* or *MECP2E2* overexpressing neurons, I observed that overexpression of *MECP2E1* led to 1.68-fold reduction of *45S pre-rRNA* levels. Correspondingly, *MECP2E2* overexpression also led to 1.55-fold reduction of *45S pre-rRNA* levels (**Figure 4.3**). As both overexpression of *MECP2E1* and *MECP2E2* led to significantly reduced *45S pre-rRNA* levels, it is possible that *MECP2*-deficiency results in reduced *rDNA* transcription, directly or indirectly. Whether the decrease in *45S pre-rRNA* levels is reflective of changes in *rDNA* transcription needs to be determined in future studies, using assays that measure nascent *rRNA* production such as metabolic labelling studies.

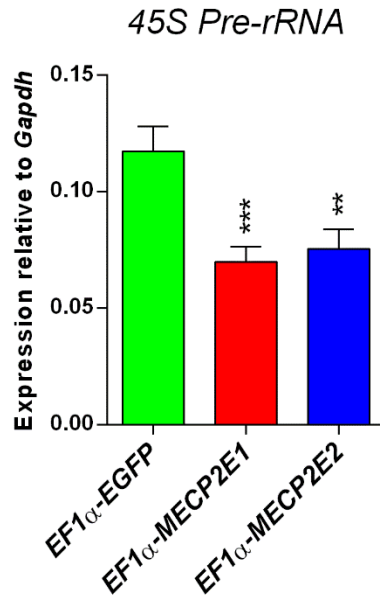


**Figure 4.3** Effect of *MECP2* overexpression on *45S pre-rRNA* levels.

Transcript detection of *45S pre-rRNA* in *MECP2E1* and *MECP2E2* overexpressing neurons. *45S pre-rRNA* expression is normalized against endogenous *Gapdh*. Error bars represent SEM, N=8 primary neurons isolated from 8 independent mice. Statistical significance from *EGFP* control is represented by  $p < 0.05^*$ ,  $p < 0.01^{**}$ ,  $p < 0.001^{***}$ .

#### 4.4 Analysis of mature *rRNA* levels in *MECP2E1* and *MECP2E2* overexpressing neurons

In order to test whether the reduction in *45S pre-rRNA* would lead to reduced levels of mature *rRNA*, I performed qRT-PCR analysis of mature *rRNAs*. Overexpression of *MECP2E1* in neurons caused *28S rRNA* levels to be reduced by 1.34-fold, however, this change was not statistically significant ( $p = 0.4074$ ) (**Figure 4.4A**). The lack of statistical significance may have been an experimental limitation, since there was considerable variation *28S rRNA* levels in *MECP2E1*-overexpressing neurons, based on the SEM values. Analysis of *18S rRNA* in *MECP2E1*-overexpressing neurons revealed that it is repressed by 1.30-fold ( $p < 0.05$ ) (**Figure**

**4.4B).** Collectively, *MECP2E1* overexpression led to statistically significant reduction only in *18S rRNA*.

*MECP2E2* overexpression on the other hand, caused a reduction in *28S rRNA* (2.96-fold,  $p < 0.05$ ) (**Figure 4.4A**). The *18S rRNA* levels in the *MECP2E2* overexpressing cells dropped by 1.38-fold ( $p < 0.05$ ) (**Figure 4.4B**). Hence, *MECP2E2* overexpression significantly reduced levels of both *28S rRNA* and *18S rRNA*.

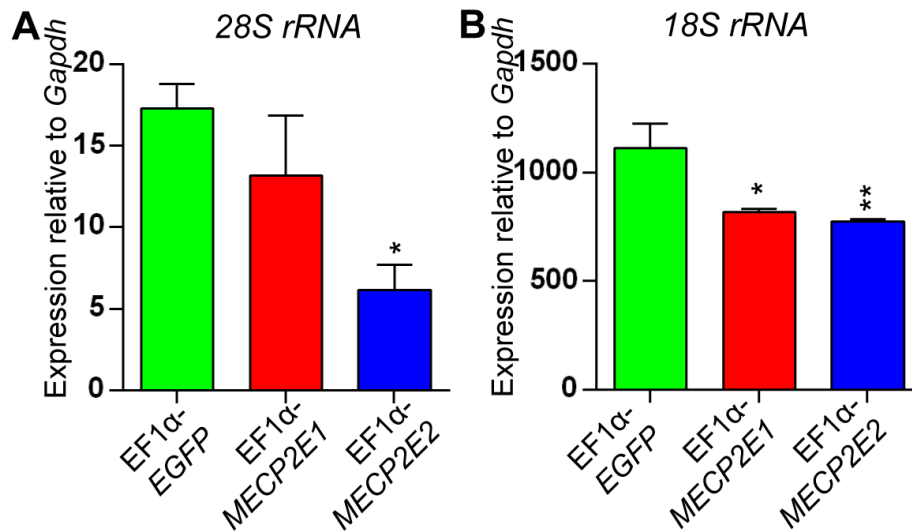
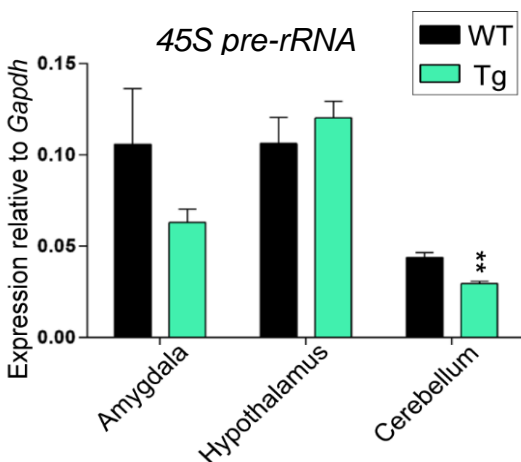


**Figure 4.4** Effect of *MECP2* overexpression on mature *rRNA* levels.

Transcript detection of mature *rRNAs* in neurons overexpressing *MECP2E1* and *MECP2E2*. A) *28S rRNA*, and B) *18S rRNA*. Transcript expression is normalized to the endogenous control *Gapdh*. Error bars represent SEM, N=3. Primary neurons isolated from 3 independent mice. Statistical significance compared to the *EGFP* control is represented by  $p < 0.05^*$ ,  $p < 0.01^{**}$ .

#### 4.5 Deregulation of *rRNA* synthesis in *MECP2* Tg1 mice

As the *in vitro* overexpression of *MECP2* isoforms led to decreased levels of *rRNA* transcripts, the next step was to validate this observation *in vivo*. To this end, we obtained RNA samples of *MECP2* Tg1 mice (expressing ~2-fold increase in *MECP2* levels) brain regions from Dr. Huda Zoghbi's lab [259]. I analyzed three brain regions namely, amygdala, hypothalamus and cerebellum for *MECP2* Tg1 and its WT counterpart. The three regions were chosen based on previous reports on their relevance to MeCP2-related disorders as well as sample availability. Both increased and decreased MeCP2 expression levels have been associated with heightened anxiety, linked to gene expression changes in amygdala and hypothalamus [198,261]. Alterations in MeCP2 dosage has also been linked to changes in a large cohort of genes in the mouse cerebellum [231]. The levels of *45S pre-rRNA* in all three brain regions were analyzed by qRT-PCR. There was a 1.68-fold reduction of *45S pre-rRNA* in the Tg1 amygdala, which was not statistically significant when compared to amygdala samples from WT mice. The lack of statistical significance may have been an experimental limitation, since there was considerable variation between amygdala samples from WT animals, based on the SEM values. The *45S pre-rRNA* levels were increased by 1.13-fold in the hypothalamus of Tg1 mice, which was not statistically significant. In the cerebellum of Tg1, however, I observed a 1.49-fold reduction in *45S pre-rRNA* levels. Collectively, *45S pre-rRNA* levels was significantly decreased in cerebellum, a trend towards reduction in amygdala, but was not changed in the hypothalamus (**Figure 4.5**).



---

**Figure 4.5 Analysis of 45S pre-rRNA levels in brain regions of MECP2 Tg1 mice (Tg).**

Quantitative RT-PCR analysis of 45S pre-rRNA in three brain regions in MECP2 Tg1 mice and its wildtype (WT) counterpart. Error bars represents the standard error of the mean (SEM), N=4 independent mice. Significant differences from WT controls are indicated with  $p < 0.01^{**}$ .

---

Unlike the case for 45S pre-rRNA levels, where only cerebellum showed a molecular phenotype, all three brain regions showed statistically significant changes in 28S rRNA levels (**Figure. 4.6A**). In the amygdala of MECP2 Tg1 mice, 28S rRNA showed a decrease of 1.86-fold ( $p < 0.01$ ). In the hypothalamus there was a 1.41-fold reduction ( $p < 0.001$ ). The reduction of 28S rRNA in cerebellum was 2.11-fold ( $p < 0.0001$ ). Similar qRT-PCR analyses were done for 18S rRNA. Changes in 18S rRNA levels in amygdala (-1.13-fold), hypothalamus (1.12-fold) and cerebellum (-1.16-fold) were not statistically significant (**Figure. 4.6B**). Therefore, collectively, the decrease in steady-state levels of mature rRNAs was limited to 28S rRNA since 18S rRNA levels remained relatively unchanged in all three regions. These results suggests that rRNA processing might be affected by MeCP2 overexpression. As described in detail in Section 1.7.4, the precursors for 18S rRNA and 28S rRNA are processed separately to form their mature rRNA products. The factors involved in 18S rRNA and 28S rRNA processing are also different. It is possible that MeCP2 overexpression can result in distinct specific alterations in the rRNA processing pathway; however, further experiments, such as metabolic labelling of nascent RNA would be required to verify this possibility.

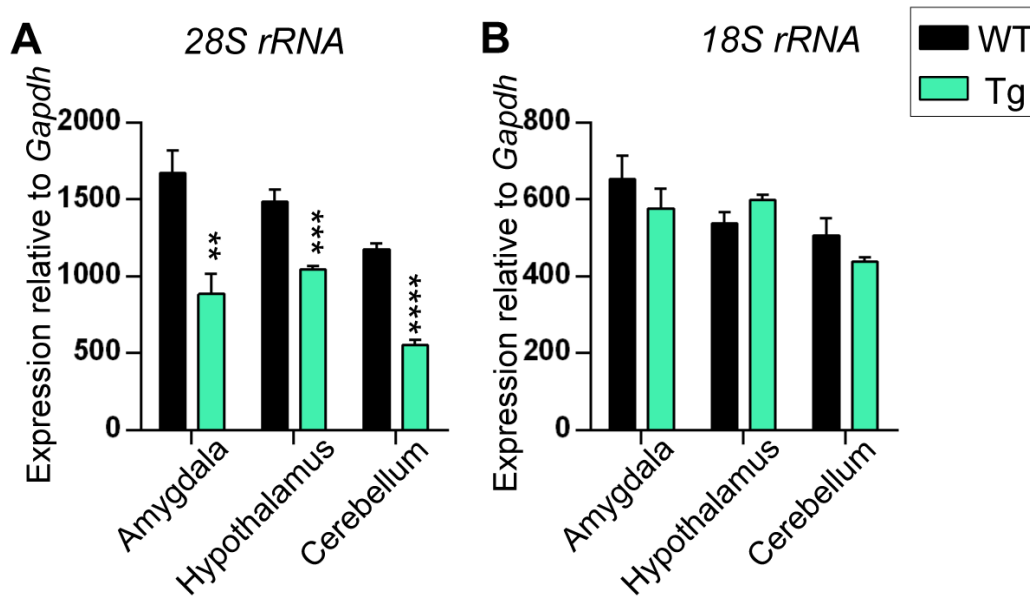


**Figure 4.6** Analysis of processed *rRNA* in brain regions of the *MECP2* Tg1 mouse model (Tg).

Quantitative RT-PCR showing A) 28S *rRNA*, and B) 18S *rRNA* levels in *MECP2* Tg1 and WT mouse brain regions. Error bars represent the standard error of means (SEM) for 4 independent mice. Significant differences from controls are indicated with  $p < 0.01^{**}$ ,  $p < 0.001^{***}$  or  $p < 0.0001^{****}$ .

#### 4.6 Summary of findings

In summary, my studies indicate that *in vitro* overexpression of *MECP2* isoforms is associated with alterations in *rRNA* levels in primary neurons overexpressing MeCP2 isoforms as well, as in the amygdala, hypothalamus and cerebellum of *MECP2* Tg1 mice. *MECP2E1* and *MECP2E2* overexpression affects the levels of not only the mature *rRNA* transcripts but also the precursor transcript. The effects of *MECP2* overexpression in *MECP2* Tg1 mice leads to reduced *rRNA* levels in a brain region-specific manner.

<b>Table 4.1 Summary of findings of the <i>MECP2</i> overexpression and <i>MECP2</i> duplication mice studies</b>					
<b>Experimental Model</b>		<b>Description</b>	<b><i>45S pre-rRNA</i></b>	<b><i>28S rRNA</i></b>	<b><i>18S rRNA</i></b>
<b><i>In vitro</i></b>	<i>MECP2</i> overexpression	<i>MECP2E1</i> overexpression	↓	No Change	↓
		<i>MECP2E2</i> overexpression	↓	↓	↓
<b><i>In vivo</i></b>	<i>MECP2</i> Tg1 mice	Amygdala	No Change	↓	No Change
		Hypothalamus	No Change	↓	No Change
		Cerebellum	↓	↓	No Change

↓ downregulation

#### 4.7 Discussion

In the current chapter, I have provided evidence for compromised *rRNA* levels due to *MECP2* overexpression. Using an *in vitro* experimental model, I have shown that the overexpression of either MeCP2 isoform in primary neurons led to decreased *45S* and *18S rRNA*, whereas only MeCP2E2 overexpression led to decreased *28S rRNA*. Within the three MDS mouse brain regions studied, only cerebellum had lower *45S pre-rRNA* levels. More significantly, in all three brain regions studied, only *28S rRNA* was altered.

The use of primary neurons as an *in vitro* experimental model has advantages and disadvantages. Many studies have shown that *rRNA* biogenesis varies between dividing and non-dividing cells, in terms of *rRNA* levels and active/inactive *rDNA* ratios [399-401]. Therefore, the

## Chapter 4

use of post-mitotic primary neurons is a more accurate model to study potential changes in *rRNA* levels, in comparison to cell lines. However *in vitro* overexpression studies have certain inherent caveats such as off-target effects caused by a) expression of proteins considerably above physiological levels, b) cellular stress due to experimental conditions such as viral transduction and c) the presence of non-neuronal cell types.

In my *in vitro* model, I attempted to analyze the level of *MECP2E1/E2* overexpression in comparison to the endogenous *Mecp2e1/e2* levels. The expression of *MECP2E1* could be confirmed using primers specific for human *MECP2E1* (data not shown) using previously reported human *MECP2E1*-specific primers [376]. However, due to the lack of sequence variation between mouse and human *Mecp2e2/MECP2E2*, I was unable to confirm *MECP2E2* overexpression, using the same technique. In order to assess the overexpression of both isoforms using a common methodology, I analyzed the levels of *C-MYC*, which was fused to the C-terminal end of both transgenes, and demonstrated successful overexpression of both isoforms.

When comparing the effects of two proteins on the same target by overexpression studies, any dissimilarity between the levels of overexpression of the two proteins can confound the experimental results and analysis. In my studies, the level of *MECP2E1* overexpression was approximately two-fold higher than *MECP2E2*. The effects of this disparity on *rRNA* levels is currently unknown. Since the lower amount of *MECP2E2* was still sufficient for decreasing *45S pre-rRNA* and *18S rRNA* to the same extent as *MECP2E1* overexpression, it can be hypothesized that under experimental conditions where both MeCP2 isoforms are overexpressed to the same level, *MECP2E2* overexpression might have a more pronounced effect on *rRNA* levels.

For my *in vitro* studies I used *EGFP* transduced neurons as a control since it would adjust for any variations in gene expression caused by culture conditions and/or viral transduction. However,



## Chapter 4

in order to truly evaluate the results of the *in vitro* model compared to the *in vivo* results, it would be essential to examine the potential effects of culture conditions and viral transduction on *rRNA* levels, which can be assessed by comparing *rRNA* levels between non-transduced and *EGFP* transduced neurons.

MeCP2 is capable of modulating large-scale chromatin organization [394,402,403]. Therefore, one potential caveat of this study is that the effect of MeCP2 overexpression on *rRNA* levels could be an indirect result of the over-abundance of a chromatin-modulating protein within neurons. A potential method to examine this would be to investigate the effects of MeCP2 overexpression using vectors with the endogenous MeCP2 promoter (MeP) [151], which is less robust than the EF1 $\alpha$ -promoter employed in the current experiments. Comparing the effects of the overexpression of another known global repressor such as histone H1, with the effects of MeCP2 would also be an excellent experimental model to study the specific and off-target influences of MeCP2 overexpression.

One potential drawback for the *in vitro* system employed in my studies is the possibility that the presence of non-neuronal cells such as astrocytes in the primary neuronal culture could have influenced the experimental results. Even though the neuronal cultures used for the *in vitro* studies have a purity of 80 - 90% (data not shown), the possibility that the presence of mitotic glial cells in the culture could confound the postulated effects of MeCP2 on neuronal *rRNA* levels should be considered. An alternate technique to circumvent this problem would be to sort the neuronal cells before experimentation, a technique that has been previously employed to study MeCP2 functions [185].

My studies have shown that overexpression of *MECP2* isoforms in neurons leads to reduced *45S pre-rRNA* levels. This is in complete agreement with a study reported in hepatocellular

## Chapter 4

carcinoma cell line which demonstrated that overexpression of MeCP2E2 led to repressed PolII activity, a molecular indicator of reduced *rDNA* transcription [288]. My experiments also demonstrated that *MECP2E1* and *MECP2E2* overexpression in primary neurons is associated with decreased *45S pre-rRNA* levels, suggesting that the potential effect of either MeCP2 isoform on *rRNA* levels could be a redundant function.

The results from my *in vivo* studies revealed a more complex association between MeCP2 and *rRNA* levels. Analysis of *45S pre-rRNA* levels in *MECP2* Tg1 mice revealed that the *45S pre-rRNA* levels are decreased only in the cerebellum, suggesting that the effects of MeCP2 overexpression on MeCP2 could be brain region-specific. In contrast, *28S rRNA* levels were decreased in all three brain regions studied, suggesting that *rRNA* processing might be affected by overexpression of MeCP2. The specific downregulation of *28S rRNA* but not *18S rRNA* indicates that a particular segment of the *rRNA* processing pathway might be differentially affected in brain regions of MDS mice. Such differential effects on *18S rRNA*, but not *28S rRNA* levels was seen in *MECP2E1* overexpressing neurons. Therefore, it is possible that the mature *rRNA* processing pathway might be affected.

In my studies, the *in vitro* data did not fully correlate with my *in vivo* results, especially regarding the effect of MeCP2 isoform's overexpression on *45S pre-rRNA* levels. The *45S pre-rRNA* levels were decreased in the *in vitro* experiments but not in the specific brain tissues from *MECP2* Tg1 mice, except for the cerebellum. One explanation could be that the effects of MeCP2 on *45S pre-rRNA* levels could be specific for neurons. This could also explain the specific downregulation of *rRNA* levels (both pre- and mature) in cerebellum, since the cerebellum has the highest number of neurons compared to other regions of the mammalian central nervous system [404].

One of the distinct observations made during the current set of studies was the relative level of *rRNAs* in comparison to *Gapdh*. The relative levels of mature *rRNA* were much higher than *45S* pre-*rRNA* levels. One potential explanation for this difference is the relative half-lives of the transcripts being analyzed. Mouse *Gapdh* mRNA has been shown to have a half-life of more than 6 hours [405]. In comparison, the half-lives of mouse *45S* pre-*rRNA*, *28S rRNA* and *18S rRNA* are  $1.29 \pm 0.19$  min, 50 hours and 72 hours, respectively [406,407]. Therefore, when comparing the steady state levels, pre-*rRNA* levels will be lower than *Gapdh*, whereas mature *rRNA* would be considerable higher than *Gapdh*. The reason for differences observed between the relative values of mature *rRNAs* detected between the *in vitro* and *in vivo* samples is currently unknown.

Even though the present study reports decreased levels of *45S pre-rRNA* and mature *rRNA*, the specific effects of MeCP2 on *rDNA* transcription or *rRNA* processing have not been elucidated. This is mainly due to the fact that the methodology used in my study (RNA extraction from cells followed by qRT-PCR) only measures the steady-state level of *rRNA*. The assessment of steady-state level of *rRNA* does not reveal the specific stage of *rRNA* transcription or processing that is potentially affected by MeCP2 overexpression. Complementary experiments such as nuclear run-on assays and other metabolic assays that measure nascent *rRNA* transcripts would be required to decipher the more intricate details of these mechanisms (further discussed in Chapter 6). Future studies would determine if the potential regulation of *rRNA* processing by MeCP2 is mediated by direct binding of MeCP2 to *rRNA* transcripts, since MeCP2 has the ability to bind to RNA molecules [408].

## **Chapter 5: Exploring the Potential Binding of MeCP2 to *rDNA***

### **5.1 Introduction**

In Chapter 4, I have provided evidence for a potential link between altered neuronal *rRNA* levels and MeCP2 overexpression. Many regulators of *rDNA* expression are known to localize within the nucleolus. However, the evidence for nucleolar localization of MeCP2 is scarce and controversial (discussed in section 5.6) [288,409,410]. Therefore in this chapter, I have investigated the potential nucleolar localization of MeCP2 in E18 primary mouse neurons, and shown that MeCP2 does not localize within the nucleolus in my experimental model. However, in support of my observations linking altered neuronal *rRNA* levels and MeCP2, I have provided evidence for the direct binding of MeCP2 to the methylated *rDNA* promoter. Deficiency of *Mecp2* has been previously shown to affect the size and number of nucleoli (sites of *rRNA* biogenesis), as well as nuclear size in neurons [361]. In this chapter, I investigate if MeCP2 overexpression also affects the size and size/number of neuronal nuclei and nucleoli, respectively.

### **5.2 Potential localization of MeCP2 within the neuronal nucleolus**

The observations made in Chapter 4 suggested that MeCP2 alters *45S pre-rRNA* and mature *rRNA* levels. Since, the nucleolus is the site for both *rDNA* transcription and *rRNA* processing, we initially aimed to determine if MeCP2 is localized within the nucleolus of primary neurons.

#### **5.2.1 Localization of MeCP2 to the neuronal perinucleolar chromocenters**

Many chromocenters are localized proximal to nucleoli in regions referred to as ‘*perinucleolar chromocenters*’ [411]. My confocal microscopic analysis of endogenous MeCP2E1

## Chapter 5

in primary neurons using the previously described custom-made rabbit MeCP2E1-specific antibody, along with a known nucleolar protein Upstream Binding Factor (UBF), illustrated that MeCP2E1 is localized within chromocenters in primary neurons (red arrows) and that some MeCP2E1 was incorporated into the perinucleolar chromocenters (white arrows) forming a partial circle around the nucleoli marked by UBF staining (yellow arrows) (**Figure 5.1A**). Similarly, total MeCP2 was detected in the chromocenters (white arrow), adjacent to DNA-free regions (yellow arrow) (**Figure 5.1B**). Since a nucleolar marker was not used in the ICC experiment testing for MeCP2 localization in neurons (**Figure 5.1B**), it is not possible to definitively characterize the DNA-free region as nucleoli. However, the exclusion of MeCP2 from DNA-free region was indicative of a non-nucleolar expression pattern.

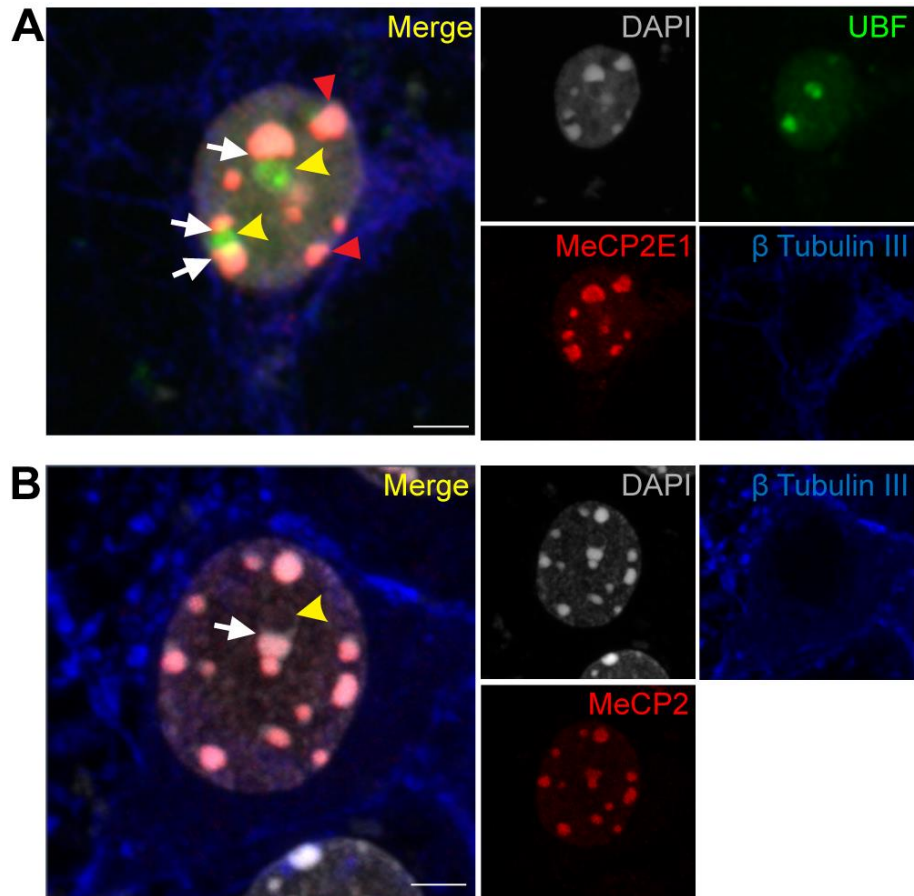
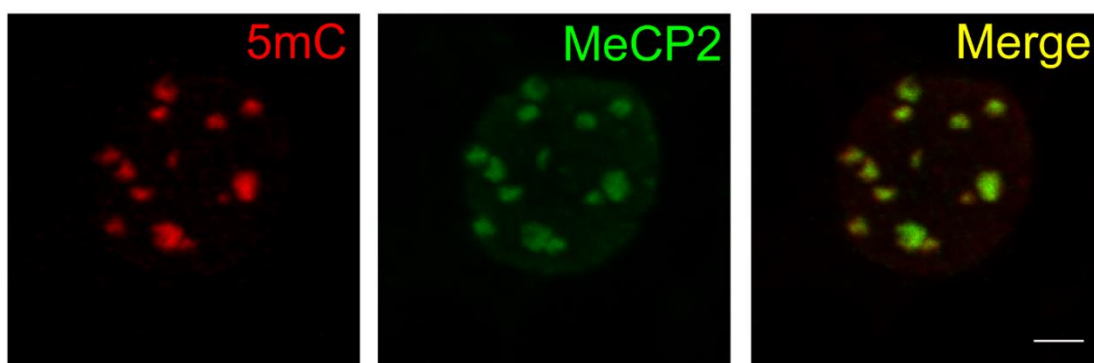


**Figure 5.1 Localization of MeCP2 to perinucleolar chromocenters in primary neurons.**

A) Immunocytochemical detection of MeCP2E1 in chromocenters (red arrows) and perinucleolar chromocenters (white arrows) forming a partial circle around nucleoli marked by UBF staining (yellow arrows). B) Immunocytochemical detection of total MeCP2 in perinucleolar chromocenters (white arrow) next to a suspected nucleolus situated with the yellow arrow. Scale bars represent 2  $\mu\text{m}$ . MeCP2E1 was immunolabelled using custom-made rabbit anti-MeCP2E1 antibody. Total MeCP2 was immunolabelled using a C-terminal anti-MeCP2 antibody (Millipore). Rhodamine Red-X goat anti-rabbit IgG, Alexa 488 goat anti mouse IgG and Dylight 649 conjugated goat anti- chicken IgY were used as secondary antibodies.

MeCP2, as a transcriptional repressor and a major chromatin architectural protein, is involved in heterochromatin formation, and binds to 5mC-enriched chromatin [24]. The 5mC methyl modification is largely associated with heterochromatin. To further characterize the nuclear localization of MeCP2 in neurons, I performed immunocytochemistry with MeCP2 and 5mC antibody. Co-localization confocal imaging analysis showed that in these neurons, MeCP2 is highly co-localized with 5mC-enriched heterochromatin (**Figure 5.2**).



---

**Figure 5.2 Co-localization of MeCP2 and 5mC in the nucleus of primary neurons.**

Immunocytochemical and confocal microscopic analysis showing the co-localization of MeCP2 and 5mC in neurons. Scale bars represent 2  $\mu\text{m}$ . Total MeCP2 was immunolabelled using a C-terminal anti-MeCP2 antibody (Millipore). Rhodamine Red-X conjugated goat anti-mouse IgG and Alexa Fluor 488 conjugated donkey anti-rabbit IgG were used as secondary antibodies.

---

Taken together, my immunocytochemical analyses consistently suggested that MeCP2 is localized outside the neuronal nucleolus and colocalizes with the methylated, heterochromatin containing chromocenters.

### 5.3 Direct binding of MeCP2 to *rDNA*

My experiments to determine the potential nucleolar localization of MeCP2 consistently demonstrated that MeCP2 is localized in the extranucleolar regions, predominantly in the heterochromatic chromocenters, including perinucleolar heterochromatin, which are known to be associated with the transcriptionally inactive *rDNA* fraction [410]. These observations indicated that MeCP2 could be directly associated with the inactive *rDNA* fraction, which is characterized by DNA methylation and repressive histone marks. Previous reports have shown that methylation of the upstream control element (UCE) of the *rDNA* promoter leads to transcriptional silencing in murine cells [286]. In chapter 4, I have provided evidence for the association between overexpression of MeCP2 isoforms and altered *rRNA* levels. In this section, I examine if MeCP2 is associated with the methylated *rDNAs*.

#### 5.3.1 Analyzing direct binding of MeCP2 to the *rDNA* promoter

In order to study the potential binding of MeCP2 directly to *rDNA* promoter, I performed ChIP analysis using primary cortical neurons. The immunoprecipitated DNA was analyzed by qPCR using primers encompassing the UCE of the *rDNA* promoter (**Figure 5.5A**). ChIP experiments demonstrated direct binding of MeCP2 to the *rDNA* promoter's UCE (**Figure 5.5B**). MeCP2 binding to Major satellite regions (*MSP*) was demonstrated as a positive control for MeCP2 ChIP (**Figure 5.5C**). Additionally, ChIP with UBF, followed by qPCR with primers specific for UCE was used as another positive control for regulatory protein binding to UCE region of the *rDNA* promoters (**Figure 5.5D**). As the percentage input values represented the percent binding of a particular protein to its target, I compared the percent input values for MeCP2 and UBF binding to the UCE of the *rDNA* promoters. For MeCP2, a percentage input of  $0.18 \pm 0.01$



was observed compared to  $0.12 \pm 0.02$  for UBF binding to the same UCE region. Provided that the two antibodies had the same binding efficiencies, MeCP2 binding to the *rDNA* appeared to be as strong as UBF, a known activator of *rDNA* transcription. Therefore, this data clearly confirms and provides evidence of MeCP2 binding to *rDNA* promoters in neurons.

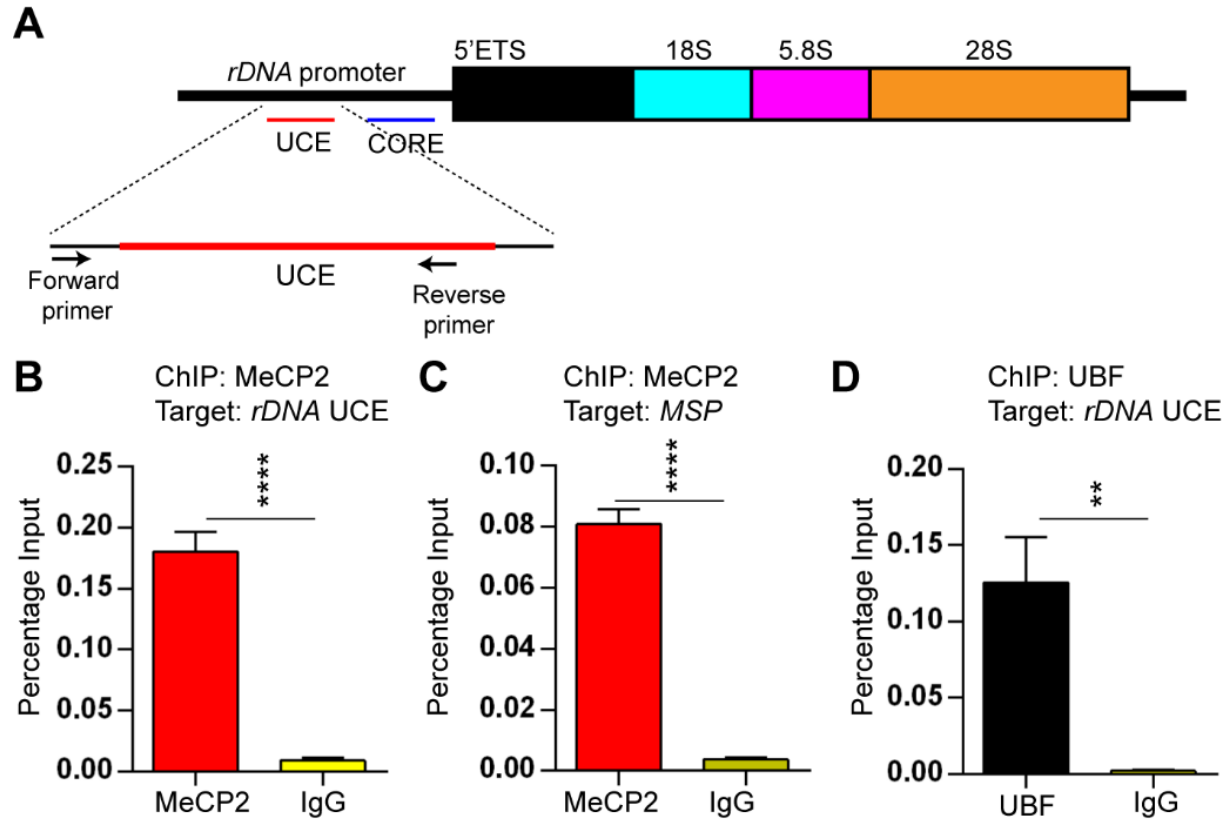


**Figure 5.3 MeCP2 binding to the promoter of the *rDNA*.**

A) Schematic representation of the mouse *rDNA* and the relative position of the upstream control element (UCE) with respect to the other regulatory elements and coding regions. Chromatin immunoprecipitation (ChIP) analysis of MeCP2 binding to B) UCE of the *rDNA* and C) *MSP* (known MeCP2 target gene), and D) binding of UBF to the UCE of the *rDNA*.  $N=2 \pm \text{SEM}$ , for each biological replicate, two qPCR experiments were performed. Both biological replicates were

## Chapter 5

processed at the same time. Significant differences from IgG controls are indicated with  $p < 0.0001$ \*\*\*\* or  $p < 0.01$ \*\*.

---

To further validate the binding of MeCP2 to *rDNA*, I performed data mining of published ChIPseq data. Based on the ChIPseq data from Baubec *at al* [387], MeCP2 binding to the *rDNA* promoter region was evident in mouse ESC and ESC-derived post-mitotic neurons (**Figure 5.4**).

## Chapter 5

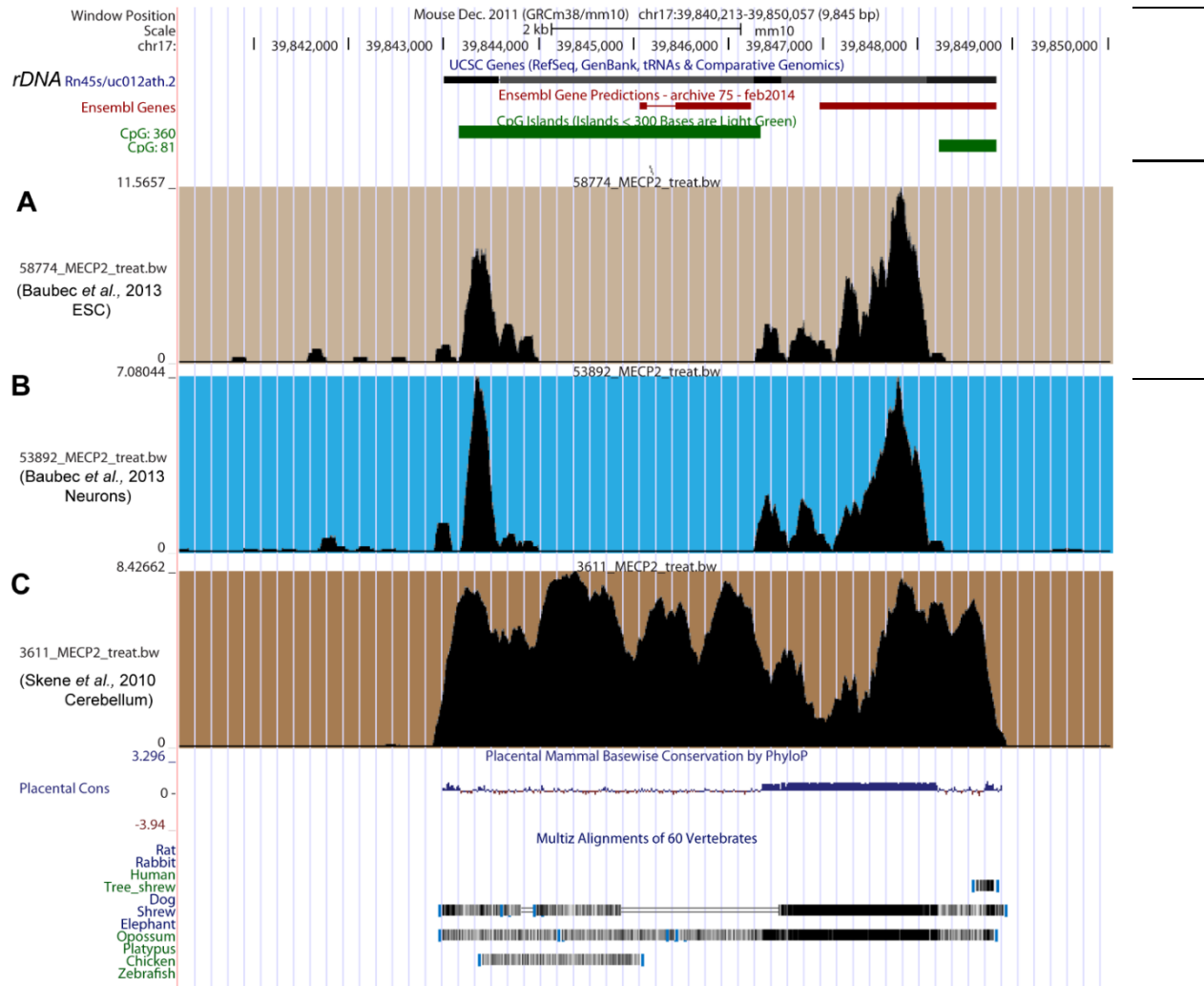


**Figure 5.4 Enrichment of MeCP2 at the *rDNA* in mouse embryonic stem cells, neurons and cerebellum.**

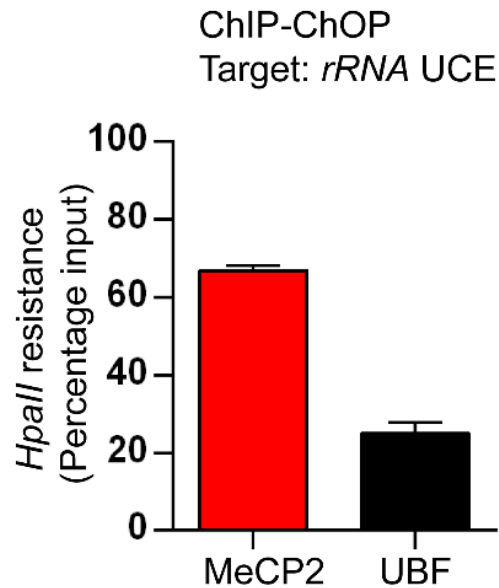
The Cistrome Finder System (<http://cistrome.org/finder>) was used to extract ChIPseq data for MeCP2 binding to the *rDNA* [185,387]. A) MeCP2 enrichment at the *rDNA* in ESCs. B) MeCP2 enrichment at the *rDNA* in mouse ESC-derived post-mitotic neurons. ChIPseq data depicted in A and B was extracted from Baubec *et al.*, [387]. C) MeCP2 enrichment at the *rDNA* in the adult mouse brain cerebellum. ChIPseq data was extracted from Skene *et al* [185].

In contrast, ChIPseq data from Skene *et al* [185] provided evidence for MeCP2 binding throughout the *rDNA* present in the mouse cerebellum (**Figure 5.4**).

### 5.3.2 Analyzing direct binding of MeCP2 to the methylated/unmethylated fraction of *rDNAs*

Tandem repeats of *rDNAs* are arranged as actively transcribed (unmethylated) and inactive (methylated) fractions. This distinct epigenetic signature of transcriptionally active and inactive *rDNAs* prompted us to investigate MeCP2 binding to the methylated or unmethylated *rDNA* copies. We assessed MeCP2 association with the methylated/unmethylated *rDNA* fractions by a standard assay known as ‘ChIP-CHOP’. In the ChIP-CHOP assay, the precipitated DNA is followed by a simple methylation analysis of specific sequences with a methylation-sensitive enzyme called *HpaII*. The methylation of target sequences would lead to resistance of *HpaII* enzymatic digestion that can be analyzed by qRT-PCR (**Figure 2.3**) [385].

To this end, I performed a ChIP-CHOP analysis of DNA precipitated with anti-MeCP2 in neurons. Our analysis of the *rDNA* sequences showed that 66% of bound MeCP2 is detected in methylated *rDNAs* (**Figure 5.5**). As a positive control, I also performed ChIP with a UBF antibody, a major transcriptional activator of the *rDNA*. This experiment indicated that only ~25% (lower, as compare to MeCP2) of UBF association was with the methylated *rRNA* fraction (**Figure 5.5**). Taken together, these results suggested that MeCP2 directly binds to *rDNA* promoters, and is mainly (66%) associated with the methylated *rDNA* fraction.




---

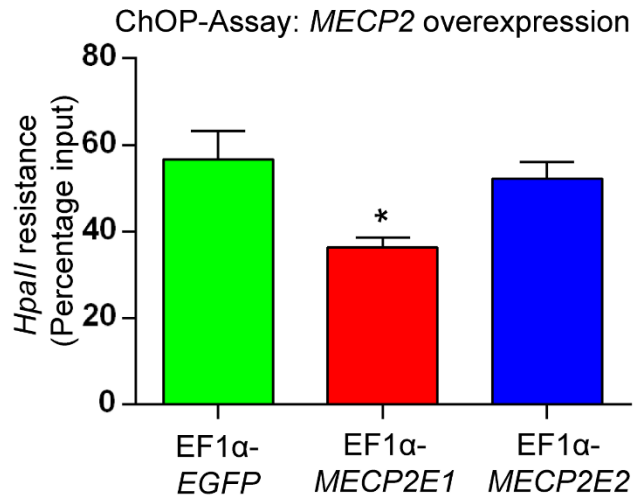
**Figure 5.5 Determination of MeCP2 binding to the methylated *rDNA* fraction in primary cortical neurons.**

ChIP-CHOP analysis to show the extent of the binding of endogenous MeCP2 and UBF to the methylated fraction of *rDNAs*, N=2±SEM. Both biological replicates were processed simultaneously. Methylation of *rDNAs* was determined by *HpaII* resistance.

---

#### 5.4 Analysis of DNA methylation at the *rDNA* promoters

Next, in order to analyze if *MECP2* overexpression leads to changes in the methylation of *rDNA* promoters, I performed *HpaII* digestion analysis on genomic DNA isolated from *MECP2*-overexpressing neurons (**Figure 5.6**). CHOP-assay analysis in *MECP2E1/E2* overexpressing neurons revealed that *MECP2E1* overexpression leads to reduced *HpaII* resistance, while this is not observed with *MECP2E2* overexpression (**Figure 5.6**). This observation suggested that overexpression of *MECP2E1* reduced the methylation of *rDNA* promoters.




---

**Figure 5.6 CHOP assay for *rDNA* promoters in neurons overexpressing *MECP2*.**

CHOP assay under conditions of *MECP2* overexpression. The table below shows the changes to *45S pre-rRNA* in neurons transduced with vectors expressing *MECP2E1* and *MECP2E2*, as analyzed by qRT-PCR. Note that the reduced *HpaII* resistance indicates reduced methylation status of the *rDNA* promoters,  $N=3\pm\text{SEM}$ . All biological replicates were processed simultaneously. Significant differences from *EGFP* control are indicated with or  $p<0.05^*$ .

---

### **5.5 Alterations in nucleolar and nuclear parameters by *MECP2E1* and *MECP2E2* overexpressing neurons**

In my DNA methylation analysis of the *rDNA* after *MECP2E1* overexpression, I observed a reduction in DNA methylation, suggesting a potential change in the ratio of transcriptionally active to inactive *rDNAs*. As nucleoli are formed around active regions of *rRNA* transcription; I therefore asked the question whether *MECP2* overexpression affects the formation of nucleoli or if it changes the number and/or size of nucleoli in primary neurons.

Previous studies have shown that the size of nuclei are decreased and nucleolar size and numbers are increased and decreased respectively, in the absence of *Mecp2* [361]. However, the effects of overexpression of the *MECP2* isoforms on these nuclear and nucleolar parameters are unknown. In this section, I will determine the effects of overexpression of *MECP2* isoforms on nuclear and nucleolar parameters using a series of immunocytochemical analysis.

### 5.5.1 Number of nucleoli (nucleolar coefficient)

First, I aimed to determine if *MECP2E1* and *MECP2E2* overexpression lead to alterations in nucleolar formation. Thus, I performed immunocytochemical labelling of *EGFP*-transduced control neurons and *MECP2E1*-, *MECP2E2*-overexpressing neurons with *EGFP*- and cMYC-specific antibodies, respectively. Additionally, I used an anti-Nucleolin (NCL) antibody (**Figure 5.7A**) because NCL is an established marker for nucleoli [412]. Specifically, I quantified the number of nucleoli found within each nucleus in primary neurons, referred to as the ‘nucleolar coefficient’ [413]. The average number of nucleoli per neuronal nuclei in the *EGFP* control and in *MECP2E1*- and *MECP2E2*-overexpressing cells was 2.90, 3.01 and 2.89, respectively (**Figure 5.7B**). These nucleoli coefficients were not significantly different between the *EGFP* control, *MECP2E1* and *MECP2E2*-overexpressing neurons. Next, in order to determine whether there is a difference in the frequency distribution of the nucleoli coefficients in the three test conditions, I performed a frequency distribution analysis using a nucleolar coefficient of 1 as the bin number (range of values). This analysis also did not reveal alterations at specific nucleolar sizes in between the *EGFP* control and *MECP2E1*- and *MECP2E2*-overexpressing neurons (**Figure 5.7C**). Collectively, these data show that the overexpression of MeCP2 isoforms does not lead to a change in the nucleolar coefficient.

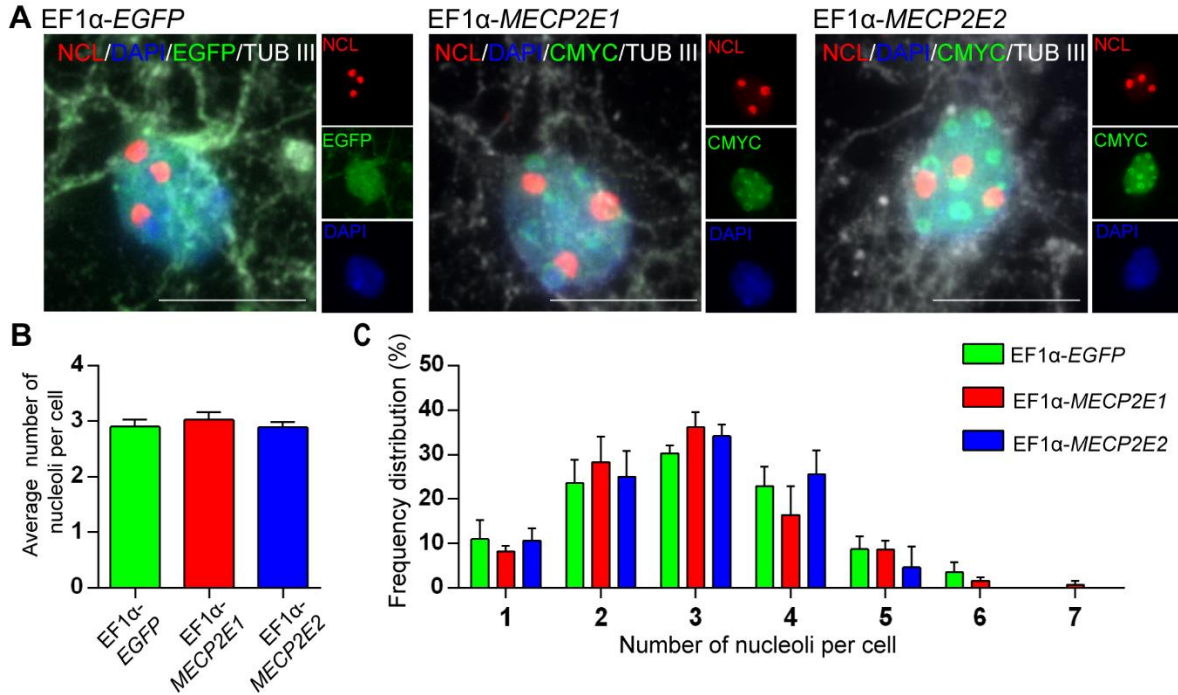


**Figure 5.7** Analysis of the nucleolar coefficient in neurons overexpressing *MECP2* isoforms.

A) Representative images of nuclei from *EGFP* control and neurons with each *MECP2* isoform being overexpressed showing the average number and size of nucleoli. A minimum of 30 cells from three biological replicates (processed at the same time) were included for each quantification, for a total minimum of 90 cells. Scale bars represent 10  $\mu$ m. B) The average nucleolar number per cell (nucleolar coefficient) in *MECP2*-overexpressing neurons in contrast to the *EGFP* control. C) Histogram showing the frequency distribution of the nucleolar coefficient, represented as percentages,  $N=3\pm$ SEM. Significant differences from *EGFP* control were considered at  $p<0.05$ . Rhodamine Red-X goat anti-rabbit IgG (for rabbit anti-Nucleolin antibody), Dylight 649 conjugated goat anti chicken IgY (for chicken anti- $\beta$ -Tubulin III antibody) and Alexa 488 goat anti mouse IgG (for mouse anti-EGFP and anti-C-MYC antibodies) were used as secondary antibodies.



### 5.5.2 Size of nucleoli

In order to determine the effects of overexpression of the *MECP2* isoforms on nucleolar size, I performed high resolution microscopy to quantify the size of nucleoli in all three experimental groups. The sizes of nucleoli were then categorized into bin size increments of 1  $\mu\text{m}^2$ . This analysis showed that MeCP2E1 overexpression caused a reduction of nucleolar size in 7.3% of nucleoli within the bin category of 0-0.5  $\mu\text{m}^2$  (**Figure 5.8**). Similarly, in the same bin category, MeCP2E2 overexpression caused a reduction of nucleolar size in 8.7% of nucleoli (**Figure 5.8**). Overall, these results suggested that overexpression of MeCP2 isoforms does not lead to reduction in the size of neuronal nucleoli, except for nucleoli within the range of 0-0.5 $\mu\text{m}^2$ .

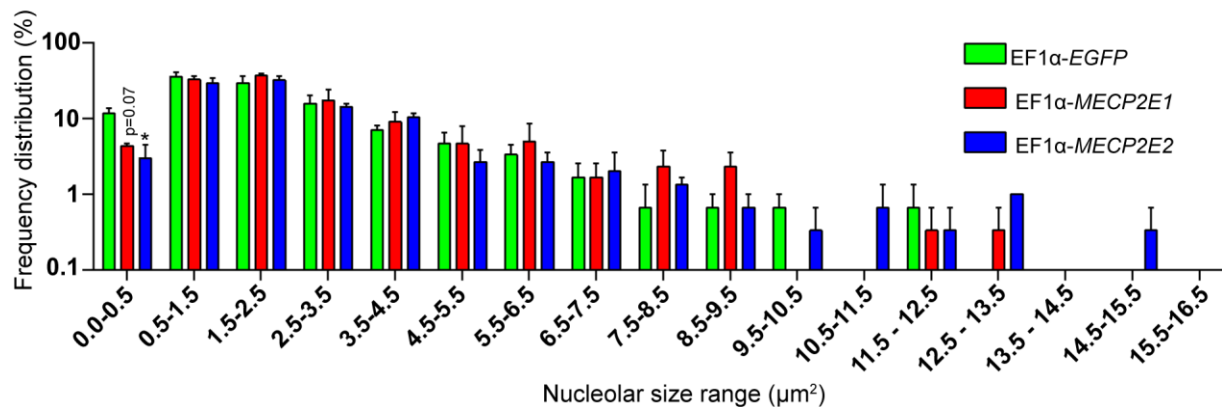


**Figure 5.8 Analysis of the nucleolar size in *MECP2*-overexpressing neurons.**

Histogram showing the frequency distribution of different ranges (bins) of nucleolar size, represented as percentages. A minimum of 30 cells from three biological replicates (processed at the same time) were included for each quantification, for a total minimum of 90 cells. Frequency distribution is represented as a log scale. Bin size is 1  $\mu\text{m}^2$ ,  $N=3\pm\text{SEM}$ . Significant differences from *EGFP* control were considered at  $p<0.05^*$ .

### 5.5.3 Size of nuclei in primary neurons

The next parameter that I analysed in *MECP2E1*- and *MECP2E2*-overexpressing neurons was the size of nuclei which has been reported to be altered by MeCP2. To this end, I performed quantitative analyses of nuclear size in *EGFP* control, *MECP2E1*- and *MECP2E2*-overexpressing neurons. First, calculations of the average nuclear size indicated that *MECP2E1*-overexpressing neurons have  $8.35 \mu\text{m}^2$  larger nuclei compared to the *EGFP* control ( $p < 0.0001$ ) (**Figure 5.9A**). Similarly, *MECP2E2*-overexpressing neurons contained  $5.238 \mu\text{m}^2$  larger nuclei compared to control neurons. The *MECP2E1*-overexpressing nuclei were  $3.11 \mu\text{m}^2$  larger than *MECP2E2*-overexpressing neurons (**Figure 5.9A**). Frequency distribution analyses based on nuclear size revealed that *MECP2E1* had effects in the  $37.5\text{-}42.5$  and  $52.5\text{-}57.5 \mu\text{m}^2$  sized bins; however, they were opposite to each other. *MECP2E1*-overexpression caused a reduction in the number of nuclei within the size range of  $37.5\text{-}42.5 \mu\text{m}^2$  whereas *MECP2E1*-overexpression resulted in an increased number of nuclei within the  $52.5\text{-}57.5 \mu\text{m}^2$  size range. *MECP2E2*-overexpression only had effects on nuclei of  $57.5\text{-}62.5 \mu\text{m}^2$  in size (**Figure 5.9B**). These data collectively show that overexpression of *MECP2* isoforms are generally associated with increased average nuclear size in neurons while their effect on various sizes of nuclei are different.

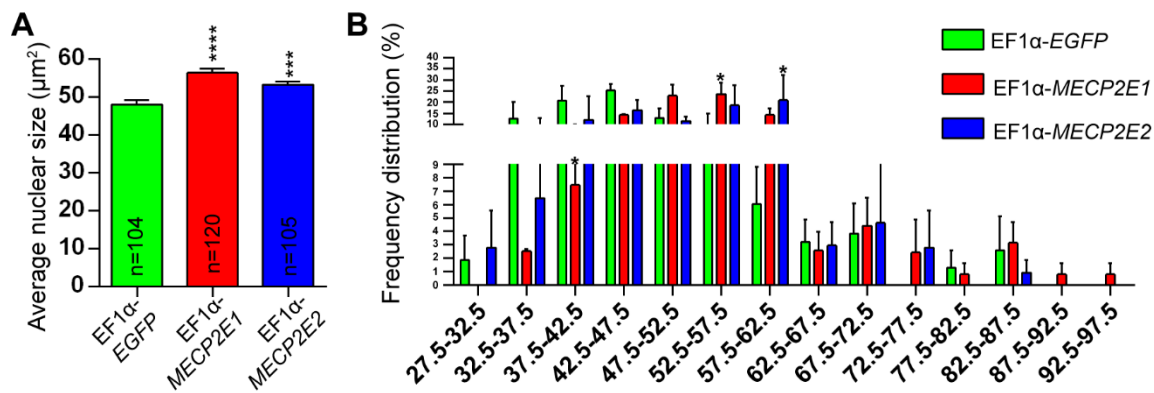


**Figure 5.9** Analysis of nuclear size in *MECP2*-overexpressing neurons.

A) The average neuronal nuclear size ( $\mu\text{m}^2$ ),  $N=3$ . The total number of nuclei counted are indicated within each column. A minimum of 30 cells from three biological replicates (processed at the same time) were included for each quantification, for a total minimum of 90 cells. B) Histogram showing the frequency distribution of different bins of nuclear size, represented as percentages. Bin size are shown as increments of  $5\mu\text{m}^2$ ,  $N=3\pm\text{SEM}$ . Significant differences from the *EGFP* control were considered at  $p<0.0001$ \*\*\*\*,  $p<0.001$ \*\*\* or  $p<0.05$ .\*.

### 5.5.4 Nucleolar size normalized to nuclear size

For the next analysis, I normalized the nucleolar size reported in 4.3.2 to the nuclear size reported in 4.3.3; the results are summarized in **Figure 5.10**. Based on this analysis, it was shown that the number of nucleoli in the size range of  $0.025\text{-}0.075\ \mu\text{m}^2$ , was increased by both MeCP2E1- and MeCP2E2-overexpression by 34.97% and 33.63%, respectively.

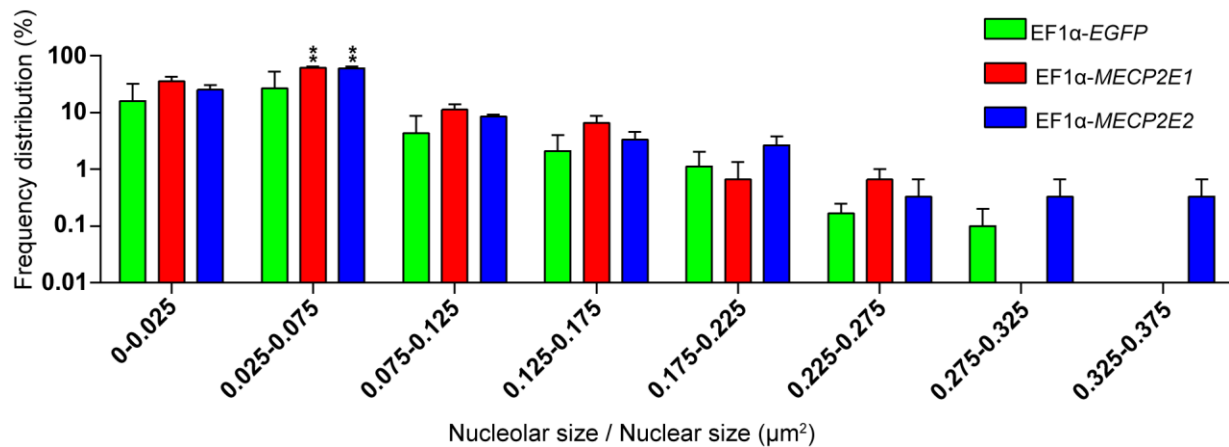


**Figure 5.10 Nucleolar size normalized against nuclear size in *MECP2*-overexpressing neurons.**

Histogram showing the frequency distribution of different bins of ratio of nucleolar size to nuclear size, represented as percentages. Frequency distribution is represented as log scale. A minimum of

## Chapter 5

30 cells from three biological replicates (processed at the same time) were included for each quantification, for a total minimum of 90 cells. Bin sizes are in  $0.05 \mu\text{m}^2$  increments,  $N=3$ . Error bars represent the SEM. Significant differences from the *EGFP* control are indicated with  $p<0.01^{**}$ .

---

Taken together, reduction in the number of micronucleoli and induction in the number of medium range nucleoli appears to be a cellular phenotype in MeCP2E1 and MeCP2E2-overexpressing neurons. Whether these morphological changes are caused by or a consequence of altered *rRNA* synthesis remains to be determined.

### 5.6 Discussion

In Chapter 4, I had provided evidence for decreased *45S pre-rRNA* and mature *rRNA* levels upon MeCP2E1 and MeCP2E2 overexpression in primary embryonic neurons. In the present chapter, I demonstrate that in neurons, MeCP2 is not localized within the nucleolus (site of active *rRNA* transcription), and is associated with methylated *rDNA* promoters (previously characterized as a mark of inactive *rDNAs* [271]). Collectively, the data I have presented in Chapters 4 and 5 suggests that MeCP2 could be a repressor of neuronal *rRNA* biogenesis. Additionally, I also demonstrate that neuronal nuclear size increases upon overexpression of both MeCP2E1 and MeCP2E2, whereas number of nucleoli is unaffected. These results, along with previous reports, suggests that both loss- and gain-of-function of MeCP2 can affect nuclear size in neurons [361,409].

Previous reports investigating the nucleolar localization of MeCP2 have provided conflicting evidence. Ghoshal *et al.*, (2004) reported nucleolar localization of MeCP2 in the human liver carcinoma cell line, HepG2 [288]. In contrast, two independent reports have demonstrated

that in mouse neurons, MeCP2 is localized to the heterochromatic region outside the nucleolus, which is in agreement with my own observations [410,414]. One explanation for this discrepancy could be that the nucleolar localization of MeCP2 is species-dependent. Such species-specific nucleolar localization have been reported for TATA-binding protein (TBP)-related factor 2 (TRF2) [415]. However, the molecular mechanisms that determine species-specific nucleolar localization remains unknown. Cell-type specific nucleolar expression of MeCP2 is also a distinct possibility since proteomic analysis of the nucleolus in other human cell lines such as HeLa and Jurkat cell lines by multiple groups did not detect MeCP2 within the nucleolus [374,416-421].

The results of my ChIP experiments suggest that endogenous MeCP2 directly binds to the *rDNA* promoter. My results are in agreement with previous ChIP-seq reports on MeCP2 binding at the *rDNA* promoter [185,387]. The validation of MeCP2 binding to the *rDNA* promoter was based on an increased percentage input of MeCP2 binding as compared to IgG controls, similar to previous studies [190]. One potential caveat of the experiment is the lack of an internal control, namely, the inclusion of a gene target which is not bound by MeCP2. Several attempts were made by myself to identify such a target but those experiments were unsuccessful (analyzed targets include *Gapdh*, *beta-actin* and *Bdnf*). Previous studies have demonstrated that MeCP2 ‘coats’ the neuronal genome [185], a factor which impedes the selection of an appropriate internal control. Alternate negative controls would include parallel ChIP experiments performed with a) an antibody pre-incubated with the peptide antigen against which it was generated, b) chromatin isolated from *Mecp2*-null mice which would reveal any non-specific binding by the test antibody and, c) neurons in which *Mecp2* has been knocked down by RNA interference.

Methylation of the mouse *rRNA* promoter at CpG -133 has been identified as one of the key features of inactive *rDNAs* [422]. My ChIP-ChOP analysis suggests that MeCP2 is associated

with the methylated pool of *rDNAs*, further suggesting a potential role of MeCP2 in regulating *rDNA* expression. *HpaII* resistance is a widely used technique for analyzing the methylation status of mouse *rRNA* promoters [381,401,423-425]. However, an often overlooked caveat for the technique is that the *HpaII* digestion site is present at CpG (-143), ten bases apart from CpG -133 [425,426]. Despite this caveat, *HpaII* resistance is still considered a valid technique to measure *rDNA* promoter methylation since previous reports have demonstrated that within the methylated pool of *rDNAs*, all CpG sites of the *rDNA* promoter are methylated [427]. In order to examine the functional significance of the MeCP2-*rDNA* promoter association, it would be essential to confirm the specific methylation of CpG -133 within the *rRNA* promoters associated with MeCP2, which can be addressed by Bisulfite sequencing analysis, which allows the analysis of individual CpG methylation [428].

The results from the CHOP analysis suggested that the overexpression of MeCP2E1, but not MeCP2E2 leads to a decrease in methylation of *rDNA* promoter. Previous studies that compared gene expression changes in *MECP2* Tg1 mice and *Mecp2<sup>tm1.1Bird</sup>* have shown that a subset of genes are specifically altered by MeCP2 overexpression [139]. Such dosage-specific targets could provide an explanation for MeCP2E1 overexpression affecting *rDNA* methylation. Furthermore, overexpression of individual MeCP2 isoforms have been shown to affect targets with distinct functions [429]. Whether an unidentified MeCP2E1-specific target is responsible for the changes in *rDNA* promoter methylation remains to be determined. However, as mentioned previously, it would be essential to determine if CpG -133 is being demethylated to formulate a functional link between promoter methylation and *rDNA* expression. As a positive control for the ChOP assay, future studies could include genomic DNA from cells overexpressing Myb-binding protein 1a (*Mybbp1a*), which is known to associate with methylated *rDNAs* [430].

At first glance, my observations suggesting that MeCP2 binds to the methylated *rDNA* promoter (section 5.3) and that MeCP2E1 overexpression decreases the methylation of *rDNA* promoter (section 5.4) might appear contradictory. The ChIP-ChOP data was based on the methylation analysis of the *rDNA* promoters specifically bound by MeCP2, whereas the ChOP data was collected from genomic data directly derived from neurons overexpressing *MECP2E1* and *MECP2E2*, without a preceding ChIP step. The analysis of MeCP2-bound *rDNA* promoters following MeCP2E1 and MeCP2E2 overexpression would be necessary to link these two observations. Another caveat is that the ChOP analysis was not performed as part of the experiments that analyzed the *rRNA* levels following MeCP2 overexpression. The combined analysis of *rRNA* following MeCP2 overexpression by qRT-PCR, ChIP, ChIP-ChOP and ChOP assay from the same biological replicates would be required to form more definitive conclusions.

The analysis of potential alterations in nuclei and nucleoli in neurons overexpressing MeCP2 isoforms revealed that overexpression of both MeCP2E1 and MeCP2E2 lead to a modest but statistically significant increase in nuclear size in primary neurons. This change is expected since *Mecp2*-deficiency has been previously report to result in reduced nuclear size [409]. Changes in nucleoli by *MECP2E1* or *MECP2E2* overexpression were limited to a decrease in nucleoli within the 0 - 0.5  $\mu\text{m}^2$  size range. This category of nucleoli is referred to as the ‘*micronucleoli*’, which have been previously reported to occur predominantly in terminally differentiated cell types [431]. Collectively, overexpression of both MeCP2E1 and MeCP2E2 in neurons caused a reduction in the number of micronucleoli (**Fig. 5.11**). Whether the reduction of micronucleoli itself could result in changes in *rRNA* synthesis remains to be determined.

## Chapter 6: Conclusion and Future Directions

### 6.1 Development of MeCP2 isoform-specific antibodies allowed the investigation of cell-type specific, spatial, and temporal expression patterns of MeCP2E1 and MeCP2E2

The generation of the MeCP2 isoform-specific antibodies was a critical step towards the study of the endogenous expression patterns of MeCP2E1 and MeCP2E2. In my own studies, I have utilized one of the custom-made antibodies to demonstrate the expression of MeCP2E1 in primary astrocytes, as well as to quantify its level of expression relative to primary neurons. The role of astrocytes in MeCP2-mediated functions was underappreciated for a long time, primarily due to many early studies reporting the lack of MeCP2 expression in astrocytes. However, subsequent studies demonstrated that MeCP2 is indeed expressed in astrocytes and plays a critical role in regulating many genes crucial for astrocytic function [151,317,390,432]. Moreover, *Mecp2/MECP2*-deficient astrocytes have been shown to negatively influence the growth and function of normal neurons in both mouse and human experimental models [363,433]. More importantly, re-expression of *Mecp2* specifically in astrocytes improved many RTT-like phenotypes such as respiratory abnormalities, anxiety levels, and defects in locomotion in a RTT mouse model [389]. However, the exact role of astrocytes in the exacerbation of cognitive defects, epilepsy and learning in RTT or MDS patients are currently unknown. A study by Ballas *et al.*, (2009) showed that expression of the branched-chain aminotransferase (*BCAT*) mRNA was up-regulated by 3-fold in *Mecp2*-deficient astrocytes relative to wild-type astrocytes (*in vitro* cultures). *BCAT* can modulate the supply of glutamate, a neurotransmitter essential for neuronal function. Increased levels of glutamates have been linked to epilepsy and cognitive defects, both of which are observed in RTT mouse models [434,435]. However, the exact link between *Mecp2*-



## Chapter 6

mutant astrocytes and brain-specific phenotypes observed in RTT and MDS mouse models are yet to be elucidated. Together, these studies highlight the significance of normal MeCP2 expression and function in astrocytes. My studies were the first to investigate MeCP2E1-specific expression patterns and levels in primary astrocytes [1]. My studies demonstrated that the majority of MeCP2E1 in astrocytes is localized at the nuclear chromocenters, similar to that observed in primary embryonic neurons. However, the level of MeCP2 in astrocytes is lower, as compared to neurons, suggesting neural cell type-specific regulation of MeCP2 expression levels.

Using MeCP2 isoform-specific antibodies, our laboratory has reported the localization pattern of MeCP2E1 in astrocytic cells of the adult mouse brain, which is similar to the pattern I observed in primary embryonic astrocytes. These antibodies have also been used to study the localization of MeCP2 isoforms in neurons and oligodendrocytes of the adult mouse brain. The development of MeCP2 isoform-specific antibodies has also enabled our laboratory to investigate the spatial and temporal localization patterns of MeCP2E1 and MeCP2E2 during mouse brain development [1,2]. These studies have revealed that the expression of MeCP2 isoforms are different across various developmental time points as well as different brain regions of adult mice [1,2]. In a joint publication with our lab, these MeCP2 isoform-specific antibodies have also been used by Yasui *et al.*, (2014) to characterize the first *Mecp2e1*-deficient mice, studies which implicated MeCP2E1 as the sole contributor to RTT phenotypes [395]. In summary, the development of MeCP2 isoform-specific antibodies has contributed to significant advances in MeCP2 isoform-specific research.

To date, the use of our custom-made MeCP2 isoform-specific antibodies have been limited to WB, ICC, and IHC experiments. Future endeavours should investigate the applicability of these antibodies for additional assays such as ChIP and Co-Immunoprecipitation (Co-IP) experiments.

Specifically, experiments that examine the ability of the custom-made MeCP2 isoform-specific antibodies to bind known target genomic regions (eg: *Bdnf* promoter) and interacting proteins (eg: c-SKI) would enable us to determine the applicability of these antibodies for ChIP and Co-IP. Such experiments would allow further investigation of novel MeCP2 isoform-specific targets and protein partners.

The ultimate goal of the generation of MeCP2 isoform-specific antibodies was to explore the endogenous expression patterns of the two MeCP2 isoforms in human patients of MeCP2-associated disorders. Analyzing the detection capabilities of our custom antibodies in human tissues and optimizing the experimental conditions would be a significant step towards this goal. Moreover, a comprehensive spatial and temporal analysis of MeCP2E1 and MeCP2E2 expression could be compared to our previous data on the mouse brain and would provide essential data to determine if our observations are comparable to human MeCP2 expression patterns. Preliminary data from the Rastegar lab indicates that our custom-made antibodies can detect MeCP2E1 and MeCP2E2 in human brain samples (Olson *et al.*, unpublished).

### **6.2 Overexpression of MeCP2 isoforms is associated with downregulation of neuronal *rRNA* levels**

The results documented in this thesis provided evidence for alterations in *rRNA* levels by overexpression of MeCP2 isoforms. To my knowledge, these results are the first study to elucidate the effect of MeCP2 on neuronal *rDNA* transcripts, since previous studies in neural cells have only reported on the mature *rRNA* levels, bypassing an important regulatory step in *rRNA* biogenesis [234,362]. Furthermore, the observation of altered *rRNA* levels in brain regions of MDS mice suggest that these changes may be part of the MDS phenotype as well, albeit in a brain-region

## Chapter 6

specific manner. Based on the evidence gathered, a potential model is proposed that includes the results obtained from my studies and incorporates testable hypotheses as future directions.

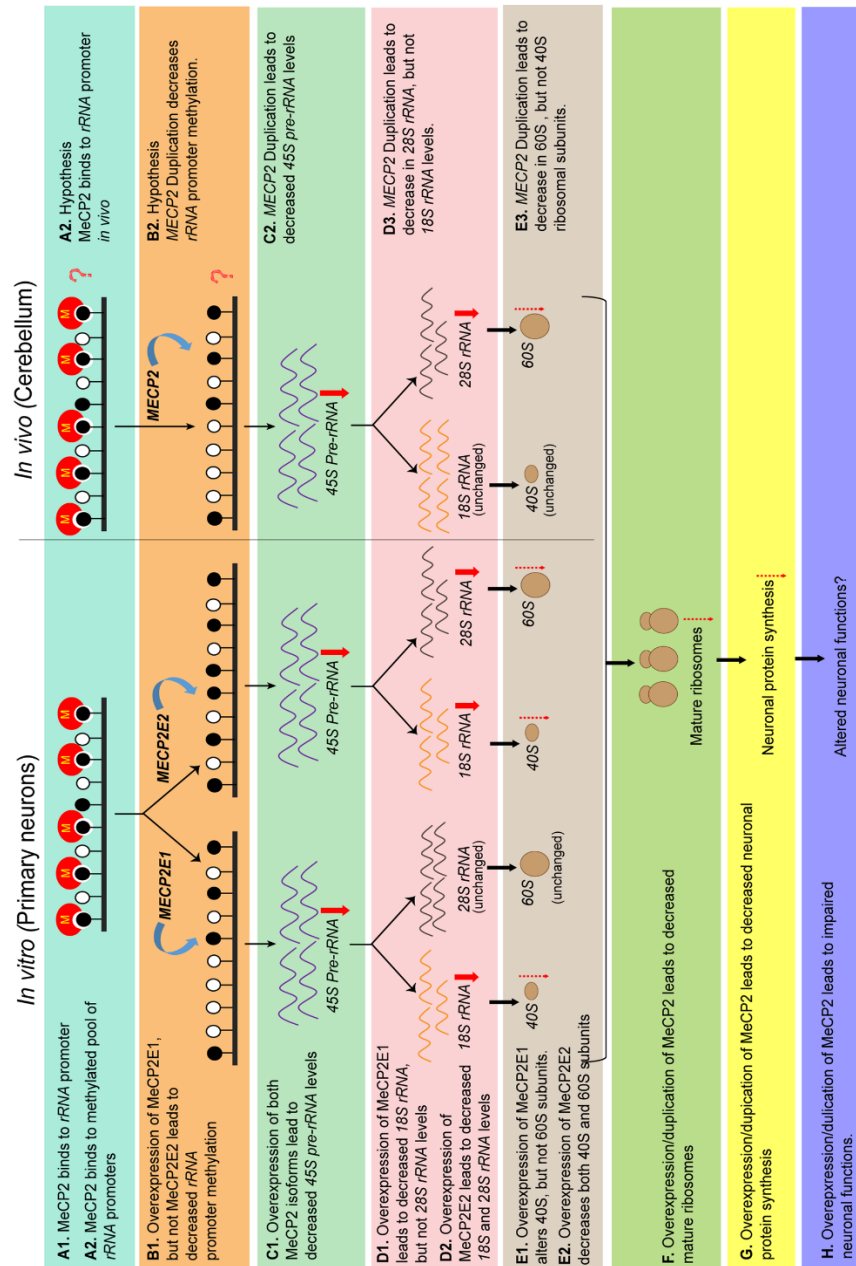


**Figure 6.1 Proposed model for MeCP2's effect on neuronal rRNA levels and its potential downstream role.**

This hypothetical model was proposed based on the data generated in primary neurons *in vitro* and adult mouse cerebellum *in vivo*.

A thorough validation of the present data as well as follow-up studies would be necessary to tease out the cellular mechanisms involved in the potential regulation of *rRNA* by MeCP2. In the next few sections I outline the methods by which the continuation of my findings can be carried out. For the sake of simplicity, the sections have been categorized based on the various steps of the model proposed in **Figure 6.1**.

### **6.3 MeCP2 binds to the methylated promoter of the *rDNA***

#### **6.3.1 Does MeCP2 bind to methylated *rDNA* promoter *in vivo*?**

The results of my *in vitro* studies provide evidence for the direct binding of MeCP2 to the methylated fraction of *rDNA* genes (Figure 6.1, Sections A1 and A2). Based on these results, it is likely that MeCP2 binding to the methylated *rDNA* promoter can also be detected *in vivo* in mice brain (Figure 6.1, Section A3). Previous studies have indicated that the binding profiles of transcription factors can vary between tissue samples and in *in vitro* culture models [436,437]. Therefore, one of the primary steps towards establishing a functional significance for MeCP2 binding to the methylated *rDNA* promoter would be to validate its binding profile in mouse brain samples.

For *in vivo* analysis, neurons sorted from mouse brain regions or mouse cerebellum could be utilized as a sample source. Sorting of neurons from mouse brain regions has previously been performed to study MeCP2 binding, and can be adapted for the proposed ChIP experiment [185]. An additional negative control for the *in vivo* ChIP analysis would be neurons isolated from *Mecp2*-null mice, provided that they are from the same genetic background, and are matched in terms of age and sex. ChIP experiments using neurons isolated from *Mecp2*-null mice would

ideally result in a complete absence of MeCP2 binding signals or reveal potential non-specific background signals.

The association of MeCP2 with the methylated pool of *rDNA* promoters can be verified by

- a) Bisulfite sequencing of *rRNA* promoter fragments immunoprecipitated by a MeCP2 antibody,
- b) Sequential ChIP analysis of *rRNA* promoter fragments immunoprecipitated from MeCP2 with histone marks associated with the methylated pool of *rDNA* promoters such as H3K9me3 or H4K20me3, and
- c) Psoralen crosslinking.

In a sequential ChIP experiment, the DNA-protein complexes are subjected to sequential immunoprecipitations with antibodies targeting different proteins [438]. Methylated *rDNA* promoters have been shown to be associated with repressive histone marks such as H3K9me3 and H4K20me3 [401]. Therefore, examining the association of MeCP2 with H3K9me3 and H4K20me3 would provide indirect evidence for MeCP2 binding to the methylated *rDNA* promoter. Previous reports have demonstrated that the open chromatin structure of unmethylated *rDNAs* make them accessible to psoralen (a DNA cross-linking reagent), whereas silent genes are inaccessible. The active and inactive genes can be identified following psoralen-crosslinking using southern blotting since the psoralen-crosslinked active fraction and the unbound inactive fraction will have different rates of migration [439].

Based on the similarities observed between the downstream effects of MeCP2 on *rRNA* levels both *in vitro* and *in vivo* (cerebellum) in my studies, I expect to observe MeCP2 binding to the methylated *rRNA* promoters *in vivo* as well. Whether the observed MeCP2 binding to the methylated *rRNA* promoters would be brain-region specific can also be determined using the proposed study.

### **6.3.2 Does MeCP2 bind to the methylated CpG -133 of the *rDNA* promoter?**

In mouse, the methylation of a specific CpG at the *rDNA* promoter (CpG -133), is reported to determine the transcriptional status of the adjoined *rDNA* units [286]. Whether the effect of MeCP2 on *45S pre-rRNA* levels are dependent on its association with the *rDNA* promoter can be examined by investigating the binding of MeCP2 to CpG -133 of the *rDNA* promoter.

The functional significance of the association of MeCP2 with the *rDNA* promoter can be further deciphered using *in vitro* reporter assays and *in vivo* mouse models. The characteristics of MeCP2's association with the *rDNA* promoter, including its binding to CpG-133, the role of methylated CpG-133 in mediating MeCP2 binding, the effect of MeCP2 binding on *rRNA* promoter activity can be tested with *rRNA* reporter constructs with site-specific mutations and methylations, both of which have been previously reported [286]. As an *in vivo* experimental model, a previously developed conditional knockdown model of MeCP2 can be used [440]. The *rRNA* levels before and after reactivation of MeCP2 could be correlated with potential binding of MeCP2 to the *rDNA* promoter to determine if this binding is correlated with *45S pre-rRNA* levels.

The results of these experiments might provide evidence for a mechanism wherein MeCP2 binds to methylated CpG -133 of the *rDNA* promoter and represses *rDNA* expression.

### **6.3.3 Does MeCP2 bind to 5mC, 5hmC or both modifications at the *rDNA* promoters?**

Analysis of DNA methylation using *HpaII* digestion does not distinguish between 5mC and 5hmC methyl modifications [441]. However the highest levels of 5hmC has been reported in the brain and in neurons, with MeCP2 being identified as the major 5hmC-binding protein in the brain [442]. Based on these observations, a part of the methylated *rDNA* promoters in neurons could contain 5hmC modifications, and could be bound by MeCP2. Immunoprecipitation

experiments of neuronal genomic DNA with 5hmC antibody followed by PCR amplification (hMeDIP), could be used to test the presence of 5hmC at the neuronal *rDNA* promoters. ChIP experiments with MeCP2 followed by hMeDIP experiments would be an ideal assay to test the association of MeCP2 with *rRNA* promoters that contain 5hmC methylation. The functional significance of 5hmC in a potential role of MeCP2 on *rRNA* synthesis can be investigated by analysis of neuronal *rRNA* levels and MeCP2-*rDNA* promoter binding profiles in a previously reported RTT mouse model. This mouse model has a particular *Mecp2* mutation (R133C) that disrupts its binding to 5hmC [443,444]. Therefore, examination of *rRNA* levels and MeCP2-*rRNA* promoter binding profiles in R133C mouse model would provide new insights on the potential occurrence and significance of 5hmC on neuronal *rRNA* promoters.

The physiological significance of 5hmC modification on *rRNA* promoter is currently unknown. However, since both the active and poised pool of *rDNAs* are known to have unmethylated promoters [271], it is tempting to speculate that the 5hmC bound *rRNA* promoters represent a hitherto uncharacterised fraction of inactive *rDNA*. This would be in agreement with previous observations of 5hmC modifications on promoters of inactive genes [445].

#### **6.3.4 Do both MeCP2 isoforms bind to the *rRNA* promoter?**

The ChIP experiments in the present study did not investigate the binding of individual MeCP2 isoforms to the *rRNA* promoter. Subsequent ChIP experiments with our custom-made MeCP2E1 and MeCP2E2 antibodies might reveal specific binding patterns for individual MeCP2 isoforms at the *rRNA* promoters.



The observation that MeCP2 is associated with the methylated *rRNA* promoter implies that MeCP2 association might be mediated through its MBD domain, which is common for both MeCP2 isoforms. Therefore, both isoforms are likely to have the same potential to bind at the *rDNA* promoter. However, the precise ratio with which MeCP2 isoforms are associated with the *rDNA* promoter as well as potential binding preferences to the promoters carrying 5mC/5hmC modifications will have to be addressed in future studies.

## **6.4 Overexpression of MeCP2E1, but not MeCP2E2 leads to decreased methylation of the *rDNA* promoter**

### **6.4.1 Can the decrease in *rDNA* promoter methylation by MeCP2E1 be replicated?**

Based on my lentiviral *MECP2* overexpression studies in primary cortical neurons, overexpression of MeCP2E1 leads to demethylation of *rDNA* promoter, whereas overexpression of MeCP2E2 does not affect the methylation status of the *rDNA* promoter (Figure 6.1, Sections B1 and B2). Since MeCP2E1 is the major isoform within brain [1,2], it is likely that duplication of *Mecp2/MECP2* also leads to decreased methylation of the *rDNA* promoter (Figure 6.1, Section B3). The potential demethylation of the *rDNA* promoter by MeCP2E1 suggests a MeCP2 isoform-specific ability to alter *rDNA* promoter methylation upon overexpression. However, due to the inherent caveats of an *in vitro* overexpression study (significantly higher levels of test protein compared to physiological levels, off-target effects on gene expression changes), it would be essential to replicate the observation of the increase in methylation caused by MeCP2E1 overexpression both *in vitro* (using additional controls) and *in vivo*.

The effects of MeCP2E1 on *rDNA* promoter methylation can be indirectly assessed by analysing *rDNA* promoter methylation in the cerebellum of a previously developed MeCP2E1

isoform-specific knockdown mouse model [395]. An increase in *rDNA* promoter methylation in the knockdown mouse model would strengthen the data from my *in vitro* overexpression studies. However, this method of verification will have to be done under the assumption that the effect of MeCP2E1 on *rDNA* promoter methylation is dose-dependent and bidirectional.

To date, there have been no reports that would suggest an isoform-specific demethylation function for MeCP2E1. However, if the findings of my *in vitro* overexpression studies can be corroborated with the proposed *in vivo* study, it would reveal a novel isoform-specific role for MeCP2E1. A potential mechanism for MeCP2E1-specific demethylation could be mediated by a preferential/exclusive binding to TET proteins and/or Gadd45b, both of which have been linked to DNA demethylation in neurons [446,447].

#### **6.4.2 What could be the potential mechanism/s for MeCP2 mediated demethylation?**

Active DNA methylation in post-mitotic neurons, once considered a rare phenomenon, is increasingly being identified as an integral part of cellular mechanisms underlying memory, behaviour and brain development [448-452]. However, the mechanism for active DNA demethylation itself is still a subject of debate. A cellular process that leads to the direct removal of the methyl group from a methylated cytosine has not been identified to date [121]. Instead, active DNA demethylation is thought to occur in a multistep process by sequential chemical modifications. Two main sites within 5mC are amenable to chemical modification, the amine group and methyl group. Deamination of the amine group by AID/APOBEC to a carbonyl group converts 5mC to thymine, which creates a G/T mismatch and is subsequently converted to unmodified cytosine by the BER pathway. Consequent oxidation reactions catalyzed by TET proteins can convert 5mC to 5hmC, 5fC and 5caC, which in turn, can be converted to unmodified cytosine by the BER pathway [453]. Interestingly, two members of the MBD family (MBD4 and

MBD2) and DNMT family of proteins (DNMT3A and DNMT3B) have also been shown to be involved in active DNA demethylation [451,453].

MeCP2 can mediate DNA demethylation by associating with TET1 or members of the MBD family capable of demethylating DNA. Previous reports have demonstrated that MeCP2 can bind to MBD2 and TET1 both *in vitro* and *in vivo* [454,455]. Based on these reports, it can be hypothesized that overexpression of MeCP2E1 leads to recruitment of MBD2 or TET1 to *rDNA* promoter, initiating active DNA demethylation at the recruited sites. This hypothesis does assume the preferential binding of MBD2 or TET1 to MeCP2E1 which has to be tested as well.

#### **6.4.3 Does overexpression of MeCP2 in MDS mice cerebellum lead to changes in *rDNA* methylation?**

The methylation status of the mouse cerebellar *rRNA* promoter following *MECP2* duplication is unknown. An initial step towards understanding the effects of *MECP2* duplication in the mouse would be to determine the levels of MeCP2 isoforms in the mouse cerebellum and the role of individual isoforms in regulating *rDNA* promoter methylation. Subsequent analysis of the methylation status of the MDS mouse cerebellum compared to its genotypic control would be necessary to determine potential alterations in methylation levels.

## **6.5 Overexpression of MeCP2 leads to a decrease in 45S pre-rRNA levels**

### **6.5.1 Does the decrease in 45S pre-rRNA levels following the overexpression of MeCP2 isoforms correlate with alterations in rDNA transcription?**

In the present study, I have provided evidence for a decrease in 45S pre-rRNA levels in neurons following MeCP2 overexpression. Overexpression of MeCP2 isoforms in primary cortical neurons as well as duplication of *Mecp2/MECP2* in a *MECP2* Tg1 mouse model resulted in decreased 45S pre-rRNA levels (Figure 6.1, Section C1 and C2). To further link the reduced 45S pre-rRNA levels to rRNA transcription, metabolic labelling of nascent RNA using <sup>3</sup>H-Uridine labelling and nuclear run-off analysis of newly labelled 45S pre-rRNA can be performed in both primary neurons and mouse cerebellum based on previous protocols [456,457].

As part of future directions, it would also be essential to determine if MeCP2 overexpression leads to downregulation of rRNA in humans. Li *et al.*, (2013) observed a decrease in 5.8S rRNA levels in *MECP2*-deficient neurons [234]. However, a concurrent decrease in other mature rRNAs were not determined. Ghoshal *et al.*, (2004) also reported that overexpression of *MECP2* downregulates PolII activity [288]. These studies suggest that MeCP2 overexpression could lead to decreased levels of human rRNA as well. However, the potential mechanism by which MeCP2 could regulate human rDNA transcripts could be different, due to the variation in promoter sequences of mouse and human rDNA. The human rDNA has 25 CpG sites within its promoter. In contrast to the mouse rDNA promoter, CpGs at the human rDNA promoter do not exhibit complete methylation or non-methylation status. Instead, human rDNA promoter CpG sites have a mosaic methylation pattern wherein few CpGs are methylated and few are unmethylated [271]. Collectively, these observations highlight the importance of verifying the potential role of MeCP2 in regulating human rRNA synthesis.

## **6.6 Overexpression of MeCP2 leads to altered levels of mature *rRNAs***

### **6.6.1 Does the alteration in mature *rRNA* levels following the overexpression of MeCP2 isoforms correlate with alterations in *rRNA* processing?**

In the present study, I have provided evidence for a decrease in 28S and 18S *rRNA* levels in neurons following MeCP2 overexpression. Based on my MeCP2 overexpression analysis in primary neurons, overexpression of *MECP2E1* leads to decrease in 18S *rRNA* alone, whereas overexpression of *MECP2E2* decreases both 28S and 18S *rRNA* levels (Figure 6.1, Sections D1 and D2). Within the *MECP2* Tg1 mice cerebellum, 28S *rRNA*, not 18S *rRNA* were decreased by *Mecp2/MECP2* duplication, suggesting a potential *rRNA* processing defect (Figure 6.1, Section D3). To link the altered mature *rRNA* levels to *rRNA* processing defects, metabolic labelling of nascent RNA using <sup>3</sup>H-Uridine labelling and northern blot analysis of newly labelled 18S and 28S *rRNA* can be performed in both primary neurons and mouse cerebellum based on previous protocols [456,457].

### **6.7 Does the alterations in mature *rRNA* levels following the overexpression of MeCP2 lead to decreased ribosome biogenesis?**

Since *rRNA* synthesis is a rate-limiting step in ribosome biogenesis, the most likely consequence of reduced mature *rRNA* levels following MeCP2 overexpression is a reduction in the formation of ribosome subunits and mature assembled ribosomes (Figure 6.1, Sections E1-E3 and F). This hypothesis can be tested by polysome profiling. In polysome profiling, dissociated ribosomes (40S, 60S) as well as mature ribosomes (80S) and polysomes (ribosomes attached to mRNAs) can be separated by running cell extracts through a sucrose gradient. The dissociated and mature ribosomes are subsequently identified by measuring their absorbance at 254 nm, which generates a ‘polysome profile’ with distinct peaks for ribosomal subunits, mature ribosomes and

polysomes [458]. A comparison of the polysome profile generated by neurons overexpressing MeCP2 isoforms and the corresponding controls would reveal potential defects in mature ribosome formation.

### **6.8 Does MeCP2 overexpression lead to reduced protein synthesis?**

The reduction in ribosome biogenesis could lead to translation initiation defects, which could affect global protein synthesis (Figure 6.1, Section G). However, defects in *rRNA* synthesis are also associated with translational defects in specific mRNA populations, even though the precise mechanism behind this effect is unknown [459]. Therefore, it is important to examine alterations in both global protein synthesis as well as changes in translation of specific mRNA populations in neurons under resting and active states.

Global changes in nascent protein synthesis rates in both isolated neurons and mouse brain regions can be assessed by the incorporation of <sup>35</sup>S methionine into total cellular proteins for a specific interval of time. This method provides a gross estimate of global changes in protein synthesis rates in experimental models. Alternatively, global protein synthesis can be measured by mass spectrometry-based techniques such as pulsed stable isotope labeling by amino acids in cell culture (pSILAC) [460].

Changes in translation of specific mRNA populations can be examined by ribosome profiling, in which polysomes from cellular extracts are separated by sucrose gradient – fractionation and subsequently subjected to deep sequencing to determine ribosome occupancy and rates of translation. A comparison of ribosome profiling data along with mRNA abundance assessed by RNA-seq will determine two parameters: mRNA abundance and relative amount of ribosomes involved in translating mRNAs. The comparison of these parameters would enable us to determine if a) a specific populations of mRNA are affected by MeCP2 overexpression, and b)

if the alterations in mRNA are due to changes in ribosome occupancy on the affected transcripts. These assays in turn, would provide insights to the possibility that specific proteins could be affected due to potential defects in ribosome biogenesis.

### **6.9 Can change in mature *rRNA* levels by MeCP2 overexpression lead to compromised neuronal functions?**

A potential effect of reduced protein synthesis in neurons would be an inability to respond to signalling cues, which is often mediated by active protein synthesis, and could potentially lead to impaired neuronal functions (Figure 6.1, Section H). The occurrence of such a functional deficit could be addressed through <sup>35</sup>S metabolic labelling studies following neuronal activity. Previous studies have shown that neuronal activity induced by BDNF is associated with increased protein synthesis, as measured by <sup>35</sup>S metabolic labelling [461]. An experimental model in which neuronal activity is induced by BDNF in neurons overexpressing MeCP2 isoforms and subjected to <sup>35</sup>S metabolic labelling of nascent proteins could be utilized to determine if the widespread increase in protein synthesis caused by neuronal activity is compromised.

Neuronal activity-dependent protein synthesis is mainly carried out within the axons and dendrites of neurons, which have their own ribosomal populations. One potential consequence of reduced ribosome biogenesis could be an alteration in the distribution of ribosomes within the neuron, leading to altered protein synthesis capacity. The distribution of ribosomes could be verified by *in situ* hybridization techniques, or immunolabelling experiments with Y10b antibody, which is known to label ribosomes specifically.

Dendritic protein synthesis can be analyzed by reporter assays using a previously reported, well-defined approach to specifically detect protein synthesis in dendrites [462]. This method involves the usage of a neuronal activity reporter construct in which the region encoding a

## Chapter 6

myristoylated green fluorescent protein (GFP) is flanked by the 3' - and 5' UTRs of CAMKII $\alpha$  to encode sequences that direct protein translocation to the dendrite and prevent translation unless the neuron is active [462]. The myristoylation tag ensures that the GFP protein being synthesized remains attached to the neuronal membrane adjacent to where it is translated. Previous studies have demonstrated increased dendritic protein synthesis by neuronal activity induced by various signalling cues, including exposure to neurotransmitters like glutamate or growth factors like BDNF [463]. We will analyze if such neuronal activity-dependent dendritic protein synthesis is compromised in neurons with MeCP2 overexpression by transducing *MECP2E1* or *MECP2E2* with the reporter construct. After transduction with the reporter construct, neurons will be exposed to BDNF and protein synthesis will be assessed by analysis of EGFP expression. Based on the hypothesis that MeCP2 overexpression reduces ribosome synthesis in neurons, I expect to observe a reduction in dendritic protein synthesis as well.

### 6.10 Summary

Ribosome biogenesis is a critical cellular process that is essential for normal cell survival and function. In the current study, I have provided evidence for alterations in neuronal *rRNA* levels following MeCP2 overexpression. Understanding the functional significance of my observations through the proposed studies would provide critical insights into the various mechanisms by which overexpression of MeCP2 leads to MDS.



## Chapter 7: References

1. Zachariah RM, Olson CO, Ezeonwuka C, Rastegar M (2012) Novel MeCP2 isoform-specific antibody reveals the endogenous MeCP2E1 expression in murine brain, primary neurons and astrocytes. PLoS One 7: e49763.
2. Olson CO, Zachariah RM, Ezeonwuka CD, Liyanage VR, Rastegar M (2014) Brain region-specific expression of MeCP2 isoforms correlates with DNA methylation within Mecp2 regulatory elements. PLoS One 9: e90645.
3. The PONES (2014) Correction: Brain Region-Specific Expression of MeCP2 Isoforms Correlates with DNA Methylation within Mecp2 Regulatory Elements. PLoS One 9: e101030.
4. Portugal FH, Cohen JS (1977) A Century of DNA: A History of the Discovery of the Structure and Function of the Genetic Substance.
5. Waddington CH (1968) Towards a theoretical biology. Nature 218: 525-527.
6. White CL, Suto RK, Luger K (2001) Structure of the yeast nucleosome core particle reveals fundamental changes in internucleosome interactions. EMBO J 20: 5207-5218.
7. Luger K, Mader AW, Richmond RK, Sargent DF, Richmond TJ (1997) Crystal structure of the nucleosome core particle at 2.8 Å resolution. Nature 389: 251-260.

## Chapter 7

8. Arents G, Burlingame RW, Wang BC, Love WE, Moudrianakis EN (1991) The nucleosomal core histone octamer at 3.1 Å resolution: a tripartite protein assembly and a left-handed superhelix. *Proc Natl Acad Sci U S A* 88: 10148-10152.
9. Arents G, Moudrianakis EN (1993) Topography of the histone octamer surface: repeating structural motifs utilized in the docking of nucleosomal DNA. *Proc Natl Acad Sci U S A* 90: 10489-10493.
10. Cutter AR, Hayes JJ (2015) A brief review of nucleosome structure. *FEBS Lett* 589: 2914-2922.
11. Bohm L, Crane-Robinson C (1984) Proteases as structural probes for chromatin: the domain structure of histones. *Biosci Rep* 4: 365-386.
12. Hansen JC, Lu X, Ross ED, Woody RW (2006) Intrinsic protein disorder, amino acid composition, and histone terminal domains. *J Biol Chem* 281: 1853-1856.
13. Lee KM, Hayes JJ (1997) The N-terminal tail of histone H2A binds to two distinct sites within the nucleosome core. *Proc Natl Acad Sci U S A* 94: 8959-8964.
14. Lee KM, Hayes JJ (1998) Linker DNA and H1-dependent reorganization of histone-DNA interactions within the nucleosome. *Biochemistry* 37: 8622-8628.
15. Simpson RT (1978) Structure of the chromatosome, a chromatin particle containing 160 base pairs of DNA and all the histones. *Biochemistry* 17: 5524-5531.
16. Allan J, Hartman PG, Crane-Robinson C, Aviles FX (1980) The structure of histone H1 and its location in chromatin. *Nature* 288: 675-679.

## Chapter 7

17. Blank TA, Becker PB (1995) Electrostatic mechanism of nucleosome spacing. *J Mol Biol* 252: 305-313.
18. Vyas P, Brown DT (2012) N- and C-terminal domains determine differential nucleosomal binding geometry and affinity of linker histone isoforms H1(0) and H1c. *J Biol Chem* 287: 11778-11787.
19. Allan J, Mitchell T, Harborne N, Bohm L, Crane-Robinson C (1986) Roles of H1 domains in determining higher order chromatin structure and H1 location. *J Mol Biol* 187: 591-601.
20. Clark DJ, Kimura T (1990) Electrostatic mechanism of chromatin folding. *J Mol Biol* 211: 883-896.
21. Carruthers LM, Bednar J, Woodcock CL, Hansen JC (1998) Linker histones stabilize the intrinsic salt-dependent folding of nucleosomal arrays: mechanistic ramifications for higher-order chromatin folding. *Biochemistry* 37: 14776-14787.
22. Hendzel MJ, Lever MA, Crawford E, Th'ng JP (2004) The C-terminal domain is the primary determinant of histone H1 binding to chromatin in vivo. *J Biol Chem* 279: 20028-20034.
23. Maeshima K, Imai R, Tamura S, Nozaki T (2014) Chromatin as dynamic 10-nm fibers. *Chromosoma* 123: 225-237.
24. Liyanage VR, Jarmasz JS, Murugesan N, Del Bigio MR, Rastegar M, Davie JR (2014) DNA modifications: function and applications in normal and disease States. *Biology (Basel)* 3: 670-723 <https://www.ncbi.nlm.nih.gov/pmc/articles/PMC4280507/>.

## Chapter 7

25. Liyanage VRB, Zachariah RM, Delcuve GP, Davie JR, Rastegar M (2015) Chromatin Structure and Epigenetics. In: Urbano KV, editor. *Advances in Genetics Research*: Nova Science Publishers. pp. 57-88.
26. Miescher F (1871) Ueber die chemische Zusammensetzung der Eiterzellen. *Hoppe-Seyler, med chem Unters* 4: 441–460.
27. Kossel A (1911) Ueber die chemische Beschaffenheit des Zellkerns. *Munchen Med Wochenschrift* 58: 65–69.
28. Watson JD, Crick FH (1953) Molecular structure of nucleic acids; a structure for deoxyribose nucleic acid. *Nature* 171: 737-738.
29. Johns EW (2008) The Histones, their Interactions with DNA, and Some Aspects of Gene Control. *Ciba Foundation Symposium - Homeostatic Regulators*: John Wiley & Sons, Ltd. pp. 128-143.
30. Kornberg RD (1974) Chromatin structure: a repeating unit of histones and DNA. *Science* 184: 868-871.
31. Kornberg RD, Thomas JO (1974) Chromatin structure; oligomers of the histones. *Science* 184: 865-868.
32. Richmond TJ, Finch JT, Rushton B, Rhodes D, Klug A (1984) Structure of the nucleosome core particle at 7 Å resolution. *Nature* 311: 532-537.
33. Allfrey VG, Faulkner R, Mirsky AE (1964) Acetylation and Methylation of Histones and Their Possible Role in the Regulation of Rna Synthesis. *Proc Natl Acad Sci U S A* 51: 786-794.

## Chapter 7

34. Cano A, Pestana A (1979) Purification and properties of a histone acetyltransferase from *Artemia salina*, highly efficient with H1 histone. *Eur J Biochem* 97: 65-72.
35. Mizzen CA, Yang XJ, Kokubo T, Brownell JE, Bannister AJ, Owen-Hughes T, Workman J, Wang L, Berger SL, Kouzarides T, Nakatani Y, Allis CD (1996) The TAF(II)250 subunit of TFIID has histone acetyltransferase activity. *Cell* 87: 1261-1270.
36. Taunton J, Hassig CA, Schreiber SL (1996) A mammalian histone deacetylase related to the yeast transcriptional regulator Rpd3p. *Science* 272: 408-411.
37. Chen D, Ma H, Hong H, Koh SS, Huang SM, Schurter BT, Aswad DW, Stallcup MR (1999) Regulation of transcription by a protein methyltransferase. *Science* 284: 2174-2177.
38. Jenuwein T, Allis CD (2001) Translating the histone code. *Science* 293: 1074-1080.
39. Lyon MF (1961) Gene action in the X-chromosome of the mouse (*Mus musculus* L.). *Nature* 190: 372-373.
40. Holliday R, Pugh JE (1975) DNA modification mechanisms and gene activity during development. *Science* 187: 226-232.
41. Dosekocil J, Sorm F (1962) Distribution of 5-methylcytosine in pyrimidine sequences of deoxyribonucleic acids. *Biochim Biophys Acta* 55: 953-959.
42. Bird AP (1978) Use of restriction enzymes to study eukaryotic DNA methylation: II. The symmetry of methylated sites supports semi-conservative copying of the methylation pattern. *J Mol Biol* 118: 49-60.

## Chapter 7

43. Hendrich B, Bird A (1998) Identification and characterization of a family of mammalian methyl-CpG binding proteins. *Mol Cell Biol* 18: 6538-6547.
44. Tahiliani M, Koh KP, Shen Y, Pastor WA, Bandukwala H, Brudno Y, Agarwal S, Iyer LM, Liu DR, Aravind L, Rao A (2009) Conversion of 5-methylcytosine to 5-hydroxymethylcytosine in mammalian DNA by MLL partner TET1. *Science* 324: 930-935.
45. Warner JR, Soeiro R, Birnboim HC, Girard M, Darnell JE (1966) Rapidly labeled HeLa cell nuclear RNA. I. Identification by zone sedimentation of a heterogeneous fraction separate from ribosomal precursor RNA. *J Mol Biol* 19: 349-361.
46. Berget SM, Moore C, Sharp PA (1977) Spliced segments at the 5' terminus of adenovirus 2 late mRNA. *Proc Natl Acad Sci U S A* 74: 3171-3175.
47. Chow LT, Gelinis RE, Broker TR, Roberts RJ (1977) An amazing sequence arrangement at the 5' ends of adenovirus 2 messenger RNA. *Cell* 12: 1-8.
48. Kruger K, Grabowski PJ, Zaug AJ, Sands J, Gottschling DE, Cech TR (1982) Self-splicing RNA: autoexcision and autocyclization of the ribosomal RNA intervening sequence of *Tetrahymena*. *Cell* 31: 147-157.
49. Guerrier-Takada C, Gardiner K, Marsh T, Pace N, Altman S (1983) The RNA moiety of ribonuclease P is the catalytic subunit of the enzyme. *Cell* 35: 849-857.
50. Lee RC, Feinbaum RL, Ambros V (1993) The *C. elegans* heterochronic gene *lin-4* encodes small RNAs with antisense complementarity to *lin-14*. *Cell* 75: 843-854.

## Chapter 7

51. Brown CJ, Hendrich BD, Rupert JL, Lafreniere RG, Xing Y, Lawrence J, Willard HF (1992) The human XIST gene: analysis of a 17 kb inactive X-specific RNA that contains conserved repeats and is highly localized within the nucleus. *Cell* 71: 527-542.
52. Brockdorff N, Ashworth A, Kay GF, McCabe VM, Norris DP, Cooper PJ, Swift S, Rastan S (1992) The product of the mouse Xist gene is a 15 kb inactive X-specific transcript containing no conserved ORF and located in the nucleus. *Cell* 71: 515-526.
53. Brannan CI, Dees EC, Ingram RS, Tilghman SM (1990) The product of the H19 gene may function as an RNA. *Mol Cell Biol* 10: 28-36.
54. Waterhouse PM, Graham MW, Wang MB (1998) Virus resistance and gene silencing in plants can be induced by simultaneous expression of sense and antisense RNA. *Proc Natl Acad Sci U S A* 95: 13959-13964.
55. Fire A, Xu S, Montgomery MK, Kostas SA, Driver SE, Mello CC (1998) Potent and specific genetic interference by double-stranded RNA in *Caenorhabditis elegans*. *Nature* 391: 806-811.
56. Li W, Notani D, Ma Q, Tanasa B, Nunez E, Chen AY, Merkurjev D, Zhang J, Ohgi K, Song X, Oh S, Kim HS, Glass CK, Rosenfeld MG (2013) Functional roles of enhancer RNAs for oestrogen-dependent transcriptional activation. *Nature* 498: 516-520.
57. Kim JK, Gabel HW, Kamath RS, Tewari M, Pasquinelli A, Rual JF, Kennedy S, Dybbs M, Bertin N, Kaplan JM, Vidal M, Ruvkun G (2005) Functional genomic analysis of RNA interference in *C. elegans*. *Science* 308: 1164-1167.

## Chapter 7

58. Lee Y, Ahn C, Han J, Choi H, Kim J, Yim J, Lee J, Provost P, Radmark O, Kim S, Kim VN (2003) The nuclear RNase III Drosha initiates microRNA processing. *Nature* 425: 415-419.
59. Bernstein E, Caudy AA, Hammond SM, Hannon GJ (2001) Role for a bidentate ribonuclease in the initiation step of RNA interference. *Nature* 409: 363-366.
60. Langst G, Manelyte L (2015) Chromatin Remodelers: From Function to Dysfunction. *Genes (Basel)* 6: 299-324.
61. Clapier CR, Cairns BR (2009) The biology of chromatin remodeling complexes. *Annu Rev Biochem* 78: 273-304.
62. Davie JR, Moniwa M (2000) Control of Chromatin Remodeling. *10*: 24.
63. Filippakopoulos P, Knapp S (2012) The bromodomain interaction module. *FEBS Lett* 586: 2692-2704.
64. Watson AA, Mahajan P, Mertens HD, Deery MJ, Zhang W, Pham P, Du X, Bartke T, Edlich C, Berridge G, Chen Y, Burgess-Brown NA, Kouzarides T, Wiechens N, Owen-Hughes T, Svergun DI, Gileadi O, Laue ED (2012) The PHD and chromo domains regulate the ATPase activity of the human chromatin remodeler CHD4. *J Mol Biol* 422: 3-17.
65. Shen X, Mizuguchi G, Hamiche A, Wu C (2000) A chromatin remodelling complex involved in transcription and DNA processing. *Nature* 406: 541-544.



## Chapter 7

66. Wu S, Shi Y, Mulligan P, Gay F, Landry J, Liu H, Lu J, Qi HH, Wang W, Nickoloff JA, Wu C (2007) A YY1-INO80 complex regulates genomic stability through homologous recombination-based repair. *Nat Struct Mol Biol* 14: 1165-1172.
67. Tjeertes JV, Miller KM, Jackson SP (2009) Screen for DNA-damage-responsive histone modifications identifies H3K9Ac and H3K56Ac in human cells. *EMBO J* 28: 1878-1889.
68. Dawson MA, Bannister AJ, Gottgens B, Foster SD, Bartke T, Green AR, Kouzarides T (2009) JAK2 phosphorylates histone H3Y41 and excludes HP1 alpha from chromatin. *Nature* 461: 819-822.
69. Chatterjee C, Muir TW (2010) Chemical approaches for studying histone modifications. *J Biol Chem* 285: 11045-11050.
70. Liyanage VRB, Zachariah RM, Delcuve GP, Davie JR, Rastegar M (2012) New Developments in Chromatin Research: An Epigenetic Perspective. In: Simpson NM, Stewart VJ, editors. *New Developments in Chromatin Research*: Nova Science Publishers pp. 29-58.
71. Kouzarides T (2007) Chromatin modifications and their function. *Cell* 128: 693-705.
72. Patel DJ, Wang Z (2013) Readout of epigenetic modifications. *Annu Rev Biochem* 82: 81-118.
73. Thompson LL, Guppy BJ, Sawchuk L, Davie JR, McManus KJ (2013) Regulation of chromatin structure via histone post-translational modification and the link to carcinogenesis. *Cancer Metastasis Rev* 32: 363-376.

## Chapter 7

74. DesJarlais R, Tummino PJ (2016) Role of Histone-Modifying Enzymes and Their Complexes in Regulation of Chromatin Biology. *Biochemistry* 55: 1584-1599.
75. Turner BM (2005) Reading signals on the nucleosome with a new nomenclature for modified histones. *Nat Struct Mol Biol* 12: 110-112.
76. Shimko JC, North JA, Bruns AN, Poirier MG, Ottesen JJ (2011) Preparation of fully synthetic histone H3 reveals that acetyl-lysine 56 facilitates protein binding within nucleosomes. *J Mol Biol* 408: 187-204.
77. Simon M, North JA, Shimko JC, Forties RA, Ferdinand MB, Manohar M, Zhang M, Fishel R, Ottesen JJ, Poirier MG (2011) Histone fold modifications control nucleosome unwrapping and disassembly. *Proc Natl Acad Sci U S A* 108: 12711-12716.
78. North JA, Javaid S, Ferdinand MB, Chatterjee N, Picking JW, Shoffner M, Nakkula RJ, Bartholomew B, Ottesen JJ, Fishel R, Poirier MG (2011) Phosphorylation of histone H3(T118) alters nucleosome dynamics and remodeling. *Nucleic Acids Res* 39: 6465-6474.
79. North JA, Simon M, Ferdinand MB, Shoffner MA, Picking JW, Howard CJ, Mooney AM, van Noort J, Poirier MG, Ottesen JJ (2014) Histone H3 phosphorylation near the nucleosome dyad alters chromatin structure. *Nucleic Acids Res* 42: 4922-4933.
80. Ye J, Ai X, Eugeni EE, Zhang L, Carpenter LR, Jelinek MA, Freitas MA, Parthun MR (2005) Histone H4 lysine 91 acetylation a core domain modification associated with chromatin assembly. *Mol Cell* 18: 123-130.

## Chapter 7

81. Yang X, Yu W, Shi L, Sun L, Liang J, Yi X, Li Q, Zhang Y, Yang F, Han X, Zhang D, Yang J, Yao Z, Shang Y (2011) HAT4, a Golgi apparatus-anchored B-type histone acetyltransferase, acetylates free histone H4 and facilitates chromatin assembly. *Mol Cell* 44: 39-50.
82. Swygert SG, Peterson CL (2014) Chromatin dynamics: interplay between remodeling enzymes and histone modifications. *Biochim Biophys Acta* 1839: 728-736.
83. Costa FF (2010) Non-coding RNAs: Meet thy masters. *Bioessays* 32: 599-608.
84. Martins-Taylor K, Schroeder DI, LaSalle JM, Lalande M, Xu RH (2012) Role of DNMT3B in the regulation of early neural and neural crest specifiers. *Epigenetics* 7: 71-82.
85. Wilson RC, Doudna JA (2013) Molecular mechanisms of RNA interference. *Annu Rev Biophys* 42: 217-239.
86. Rinn JL, Chang HY (2012) Genome regulation by long noncoding RNAs. *Annu Rev Biochem* 81: 145-166.
87. Kaikkonen MU, Lam MT, Glass CK (2011) Non-coding RNAs as regulators of gene expression and epigenetics. *Cardiovasc Res* 90: 430-440.
88. van Wolfswinkel JC, Ketting RF (2010) The role of small non-coding RNAs in genome stability and chromatin organization. *J Cell Sci* 123: 1825-1839.
89. Prensner JR, Iyer MK, Sahu A, Asangani IA, Cao Q, Patel L, Vergara IA, Davicioni E, Erho N, Ghadessi M, Jenkins RB, Triche TJ, Malik R, Bedenis R, McGregor N, Ma T, Chen W, Han S, Jing X, Cao X, Wang X, Chandler B, Yan W, Siddiqui J, Kunju LP, Dhanasekaran

## Chapter 7

- SM, Pienta KJ, Feng FY, Chinnaiyan AM (2013) The long noncoding RNA SChLAP1 promotes aggressive prostate cancer and antagonizes the SWI/SNF complex. *Nat Genet* 45: 1392-1398.
90. Wade SL, Langer LF, Ward JM, Archer TK (2015) MiRNA-Mediated Regulation of the SWI/SNF Chromatin Remodeling Complex Controls Pluripotency and Endodermal Differentiation in Human ESCs. *Stem Cells* 33: 2925-2935.
91. Kundu TK (2012) *Epigenetics: Development and Disease*: Springer Netherlands.
92. Jones PA (2012) Functions of DNA methylation: islands, start sites, gene bodies and beyond. *Nat Rev Genet* 13: 484-492.
93. G.P. Delcuve, D.H. Khan, V.R.B. Liyanage, S.Jahan, M. Rastegar, and LAK, Davie JR (2015) Chromatin Organization and functions. *Epigenetics in Cardiac Disease*.
94. Ziller MJ, Gu H, Muller F, Donaghey J, Tsai LT, Kohlbacher O, De Jager PL, Rosen ED, Bennett DA, Bernstein BE, Gnirke A, Meissner A (2013) Charting a dynamic DNA methylation landscape of the human genome. *Nature* 500: 477-481.
95. Lister R, Pelizzola M, Dowen RH, Hawkins RD, Hon G, Tonti-Filippini J, Nery JR, Lee L, Ye Z, Ngo QM, Edsall L, Antosiewicz-Bourget J, Stewart R, Ruotti V, Millar AH, Thomson JA, Ren B, Ecker JR (2009) Human DNA methylomes at base resolution show widespread epigenomic differences. *Nature* 462: 315-322.
96. Irizarry RA, Ladd-Acosta C, Wen B, Wu Z, Montano C, Onyango P, Cui H, Gabo K, Rongione M, Webster M, Ji H, Potash JB, Sabunciyan S, Feinberg AP (2009) The human colon

## Chapter 7

- cancer methylome shows similar hypo- and hypermethylation at conserved tissue-specific CpG island shores. *Nat Genet* 41: 178-186.
97. Illingworth RS, Bird AP (2009) CpG islands--'a rough guide'. *FEBS Lett* 583: 1713-1720.
98. Miranda TB, Jones PA (2007) DNA methylation: the nuts and bolts of repression. *J Cell Physiol* 213: 384-390.
99. Bird A, Tate P, Nan X, Campoy J, Meehan R, Cross S, Tweedie S, Charlton J, Macleod D (1995) Studies of DNA methylation in animals. *J Cell Sci Suppl* 19: 37-39.
100. Jjingo D, Conley AB, Yi SV, Lunyak VV, Jordan IK (2012) On the presence and role of human gene-body DNA methylation. *Oncotarget* 3: 462-474.
101. Wu H, Coskun V, Tao J, Xie W, Ge W, Yoshikawa K, Li E, Zhang Y, Sun YE (2010) Dnmt3a-dependent nonpromoter DNA methylation facilitates transcription of neurogenic genes. *Science* 329: 444-448.
102. Richa R, Sinha RP (2014) Hydroxymethylation of DNA: an epigenetic marker. *EXCLI J* 13: 592-610.
103. Penn NW, Suwalski R, O'Riley C, Bojanowski K, Yura R (1972) The presence of 5-hydroxymethylcytosine in animal deoxyribonucleic acid. *Biochem J* 126: 781-790.
104. Kriaucionis S, Heintz N (2009) The nuclear DNA base 5-hydroxymethylcytosine is present in Purkinje neurons and the brain. *Science* 324: 929-930.
105. Song CX, Szulwach KE, Fu Y, Dai Q, Yi C, Li X, Li Y, Chen CH, Zhang W, Jian X, Wang J, Zhang L, Looney TJ, Zhang B, Godley LA, Hicks LM, Lahn BT, Jin P, He C (2011)

## Chapter 7

- Selective chemical labeling reveals the genome-wide distribution of 5-hydroxymethylcytosine. *Nat Biotechnol* 29: 68-72.
106. Wu H, D'Alessio AC, Ito S, Wang Z, Cui K, Zhao K, Sun YE, Zhang Y (2011) Genome-wide analysis of 5-hydroxymethylcytosine distribution reveals its dual function in transcriptional regulation in mouse embryonic stem cells. *Genes Dev* 25: 679-684.
107. Stroud H, Feng S, Morey Kinney S, Pradhan S, Jacobsen SE (2011) 5-Hydroxymethylcytosine is associated with enhancers and gene bodies in human embryonic stem cells. *Genome Biol* 12: R54.
108. Kinde B, Gabel HW, Gilbert CS, Griffith EC, Greenberg ME (2015) Reading the unique DNA methylation landscape of the brain: Non-CpG methylation, hydroxymethylation, and MeCP2. *Proc Natl Acad Sci U S A* 112: 6800-6806.
109. Guo JU, Su Y, Shin JH, Shin J, Li H, Xie B, Zhong C, Hu S, Le T, Fan G, Zhu H, Chang Q, Gao Y, Ming GL, Song H (2014) Distribution, recognition and regulation of non-CpG methylation in the adult mammalian brain. *Nat Neurosci* 17: 215-222.
110. Chen PY, Feng S, Joo JW, Jacobsen SE, Pellegrini M (2011) A comparative analysis of DNA methylation across human embryonic stem cell lines. *Genome Biol* 12: R62.
111. Barres R, Kirchner H, Rasmussen M, Yan J, Kantor FR, Krook A, Naslund E, Zierath JR (2013) Weight loss after gastric bypass surgery in human obesity remodels promoter methylation. *Cell Rep* 3: 1020-1027.

## Chapter 7

112. Barres R, Osler ME, Yan J, Rune A, Fritz T, Caidahl K, Krook A, Zierath JR (2009) Non-CpG methylation of the PGC-1alpha promoter through DNMT3B controls mitochondrial density. *Cell Metab* 10: 189-198.
113. Patil V, Ward RL, Hesson LB (2014) The evidence for functional non-CpG methylation in mammalian cells. *Epigenetics* 9: 823-828.
114. Turek-Plewa J, Jagodzinski PP (2005) The role of mammalian DNA methyltransferases in the regulation of gene expression. *Cell Mol Biol Lett* 10: 631-647.
115. Jurkowska RZ, Jurkowski TP, Jeltsch A (2011) Structure and function of mammalian DNA methyltransferases. *Chembiochem* 12: 206-222.
116. Kar S, Deb M, Sengupta D, Shilpi A, Parbin S, Torrisani J, Pradhan S, Patra S (2012) An insight into the various regulatory mechanisms modulating human DNA methyltransferase 1 stability and function. *Epigenetics* 7: 994-1007.
117. Arand J, Spieler D, Karius T, Branco MR, Meilinger D, Meissner A, Jenuwein T, Xu G, Leonhardt H, Wolf V, Walter J (2012) In vivo control of CpG and non-CpG DNA methylation by DNA methyltransferases. *PLoS Genet* 8: e1002750.
118. Shirane K, Toh H, Kobayashi H, Miura F, Chiba H, Ito T, Kono T, Sasaki H (2013) Mouse oocyte methylomes at base resolution reveal genome-wide accumulation of non-CpG methylation and role of DNA methyltransferases. *PLoS Genet* 9: e1003439.

## Chapter 7

119. Ramsahoye BH, Biniszkiwicz D, Lyko F, Clark V, Bird AP, Jaenisch R (2000) Non-CpG methylation is prevalent in embryonic stem cells and may be mediated by DNA methyltransferase 3a. *Proc Natl Acad Sci U S A* 97: 5237-5242.
120. Ichiyanagi T, Ichiyanagi K, Miyake M, Sasaki H (2013) Accumulation and loss of asymmetric non-CpG methylation during male germ-cell development. *Nucleic Acids Res* 41: 738-745.
121. Moore LD, Le T, Fan G (2013) DNA methylation and its basic function. *Neuropsychopharmacology* 38: 23-38.
122. Wu H, Zhang Y (2014) Reversing DNA methylation: mechanisms, genomics, and biological functions. *Cell* 156: 45-68.
123. Tan AY, Manley JL (2009) The TET family of proteins: functions and roles in disease. *J Mol Cell Biol* 1: 82-92.
124. Iyer LM, Tahiliani M, Rao A, Aravind L (2009) Prediction of novel families of enzymes involved in oxidative and other complex modifications of bases in nucleic acids. *Cell Cycle* 8: 1698-1710.
125. Kohli RM, Zhang Y (2013) TET enzymes, TDG and the dynamics of DNA demethylation. *Nature* 502: 472-479.
126. Okashita N, Kumaki Y, Ebi K, Nishi M, Okamoto Y, Nakayama M, Hashimoto S, Nakamura T, Sugawara K, Kojima N, Takada T, Okano M, Seki Y (2014) PRDM14 promotes active



## Chapter 7

- DNA demethylation through the ten-eleven translocation (TET)-mediated base excision repair pathway in embryonic stem cells. *Development* 141: 269-280.
127. Moore SP, Toomire KJ, Strauss PR (2013) DNA modifications repaired by base excision repair are epigenetic. *DNA Repair (Amst)* 12: 1152-1158.
128. Kangaspekka S, Stride B, Metivier R, Polycarpou-Schwarz M, Ibberson D, Carmouche RP, Benes V, Gannon F, Reid G (2008) Transient cyclical methylation of promoter DNA. *Nature* 452: 112-115.
129. Brown SE, Suderman MJ, Hallett M, Szyf M (2008) DNA demethylation induced by the methyl-CpG-binding domain protein MBD3. *Gene* 420: 99-106.
130. Ma DK, Jang MH, Guo JU, Kitabatake Y, Chang ML, Pow-Anpongkul N, Flavell RA, Lu B, Ming GL, Song H (2009) Neuronal activity-induced Gadd45b promotes epigenetic DNA demethylation and adult neurogenesis. *Science* 323: 1074-1077.
131. Barreto G, Schafer A, Marhold J, Stach D, Swaminathan SK, Handa V, Doderlein G, Maltry N, Wu W, Lyko F, Niehrs C (2007) Gadd45a promotes epigenetic gene activation by repair-mediated DNA demethylation. *Nature* 445: 671-675.
132. Jin SG, Guo C, Pfeifer GP (2008) GADD45A does not promote DNA demethylation. *PLoS Genet* 4: e1000013.
133. Szyf M (2011) The early life social environment and DNA methylation: DNA methylation mediating the long-term impact of social environments early in life. *Epigenetics* 6: 971-978.

## Chapter 7

134. Defossez PA, Stancheva I (2011) Biological functions of methyl-CpG-binding proteins. *Prog Mol Biol Transl Sci* 101: 377-398.
135. Meehan RR, Lewis JD, Bird AP (1992) Characterization of MeCP2, a vertebrate DNA binding protein with affinity for methylated DNA. *Nucleic Acids Res* 20: 5085-5092.
136. Li L, Chen BF, Chan WY (2015) An epigenetic regulator: methyl-CpG-binding domain protein 1 (MBD1). *Int J Mol Sci* 16: 5125-5140.
137. Weaver IC, Hellstrom IC, Brown SE, Andrews SD, Dymov S, Diorio J, Zhang TY, Szyf M, Meaney MJ (2014) The methylated-DNA binding protein MBD2 enhances NGFI-A (egr-1)-mediated transcriptional activation of the glucocorticoid receptor. *Philos Trans R Soc Lond B Biol Sci* 369.
138. Ng HH, Zhang Y, Hendrich B, Johnson CA, Turner BM, Erdjument-Bromage H, Tempst P, Reinberg D, Bird A (1999) MBD2 is a transcriptional repressor belonging to the MeCP1 histone deacetylase complex. *Nat Genet* 23: 58-61.
139. Chahrour M, Jung SY, Shaw C, Zhou X, Wong ST, Qin J, Zoghbi HY (2008) MeCP2, a key contributor to neurological disease, activates and represses transcription. *Science* 320: 1224-1229.
140. Detich N, Theberge J, Szyf M (2002) Promoter-specific activation and demethylation by MBD2/demethylase. *J Biol Chem* 277: 35791-35794.
141. Hendrich B, Hardeland U, Ng HH, Jiricny J, Bird A (1999) The thymine glycosylase MBD4 can bind to the product of deamination at methylated CpG sites. *Nature* 401: 301-304.

## Chapter 7

142. Laget S, Joulie M, Le Masson F, Sasai N, Christians E, Pradhan S, Roberts RJ, Defossez PA (2010) The human proteins MBD5 and MBD6 associate with heterochromatin but they do not bind methylated DNA. *PLoS One* 5: e11982.
143. Tallant C, Valentini E, Fedorov O, Overvoorde L, Ferguson FM, Filippakopoulos P, Svergun DI, Knapp S, Ciulli A (2015) Molecular basis of histone tail recognition by human TIP5 PHD finger and bromodomain of the chromatin remodeling complex NoRC. *Structure* 23: 80-92.
144. Ferguson FM, Dias DM, Rodrigues JP, Wienk H, Boelens R, Bonvin AM, Abell C, Ciulli A (2014) Binding hotspots of BAZ2B bromodomain: Histone interaction revealed by solution NMR driven docking. *Biochemistry* 53: 6706-6716.
145. Prokhortchouk A, Hendrich B, Jorgensen H, Ruzov A, Wilm M, Georgiev G, Bird A, Prokhortchouk E (2001) The p120 catenin partner Kaiso is a DNA methylation-dependent transcriptional repressor. *Genes Dev* 15: 1613-1618.
146. Fillion GJ, Zhenilo S, Salozhin S, Yamada D, Prokhortchouk E, Defossez PA (2006) A family of human zinc finger proteins that bind methylated DNA and repress transcription. *Mol Cell Biol* 26: 169-181.
147. Kim JK, Esteve PO, Jacobsen SE, Pradhan S (2009) UHRF1 binds G9a and participates in p21 transcriptional regulation in mammalian cells. *Nucleic Acids Res* 37: 493-505.
148. Liu J, Francke U (2006) Identification of cis-regulatory elements for MECP2 expression. *Hum Mol Genet* 15: 1769-1782.

## Chapter 7

149. Adachi M, Keefer EW, Jones FS (2005) A segment of the *Mecp2* promoter is sufficient to drive expression in neurons. *Hum Mol Genet* 14: 3709-3722.
150. Singh J, Saxena A, Christodoulou J, Ravine D (2008) MECP2 genomic structure and function: insights from ENCODE. *Nucleic Acids Res* 36: 6035-6047.
151. Rastegar M, Hotta A, Pasceri P, Makarem M, Cheung AY, Elliott S, Park KJ, Adachi M, Jones FS, Clarke ID, Dirks P, Ellis J (2009) MECP2 isoform-specific vectors with regulated expression for Rett syndrome gene therapy. *PLoS One* 4: e6810.
152. Bagga JS, D'Antonio LA (2013) Role of conserved cis-regulatory elements in the post-transcriptional regulation of the human MECP2 gene involved in autism. *Hum Genomics* 7: 19.
153. Ho KL, McNae IW, Schmiedeberg L, Klose RJ, Bird AP, Walkinshaw MD (2008) MeCP2 binding to DNA depends upon hydration at methyl-CpG. *Mol Cell* 29: 525-531.
154. Nagarajan RP, Hogart AR, Gwye Y, Martin MR, LaSalle JM (2006) Reduced MeCP2 expression is frequent in autism frontal cortex and correlates with aberrant MECP2 promoter methylation. *Epigenetics* 1: e1-11.
155. Liyanage VR, Zachariah RM, Davie JR, Rastegar M (2015) Ethanol deregulates *Mecp2*/MeCP2 in differentiating neural stem cells via interplay between 5-methylcytosine and 5-hydroxymethylcytosine at the *Mecp2* regulatory elements. *Exp Neurol* 265: 102-117.

## Chapter 7

156. Liyanage VR, Zachariah RM, Rastegar M (2013) Decitabine alters the expression of Mecp2 isoforms via dynamic DNA methylation at the Mecp2 regulatory elements in neural stem cells. *Mol Autism* 4: 46.
157. Young JI, Zoghbi HY (2004) X-chromosome inactivation patterns are unbalanced and affect the phenotypic outcome in a mouse model of rett syndrome. *Am J Hum Genet* 74: 511-520.
158. Shahbazian MD, Sun Y, Zoghbi HY (2002) Balanced X chromosome inactivation patterns in the Rett syndrome brain. *Am J Med Genet* 111: 164-168.
159. Coy JF, Sedlacek Z, Bächner D, Delius H, Poustka A (1999) A complex pattern of evolutionary conservation and alternative polyadenylation within the long 3'-untranslated region of the methyl-CpG-binding protein 2 gene (MeCP2) suggests a regulatory role in gene expression. *Hum Mol Genet* 8: 1253-1262.
160. Pelka GJ, Watson CM, Christodoulou J, Tam PP (2005) Distinct expression profiles of Mecp2 transcripts with different lengths of 3'UTR in the brain and visceral organs during mouse development. *Genomics* 85: 441-452.
161. Balmer D, Goldstine J, Rao YM, LaSalle JM (2003) Elevated methyl-CpG-binding protein 2 expression is acquired during postnatal human brain development and is correlated with alternative polyadenylation. *J Mol Med (Berl)* 81: 61-68.
162. Samaco RC, Nagarajan RP, Braunschweig D, LaSalle JM (2004) Multiple pathways regulate MeCP2 expression in normal brain development and exhibit defects in autism-spectrum disorders. *Hum Mol Genet* 13: 629-639.

## Chapter 7

163. McGowan H, Pang ZP (2015) Regulatory functions and pathological relevance of the MECP2 3'UTR in the central nervous system. *Cell Regen (Lond)* 4: 9.
164. Adams VH, McBryant SJ, Wade PA, Woodcock CL, Hansen JC (2007) Intrinsic disorder and autonomous domain function in the multifunctional nuclear protein, MeCP2. *J Biol Chem* 282: 15057-15064.
165. Ausio J, Martinez de Paz A, Esteller M (2014) MeCP2: the long trip from a chromatin protein to neurological disorders. *Trends Mol Med* 20: 487-498.
166. Mnatzakanian GN, Lohi H, Munteanu I, Alfred SE, Yamada T, MacLeod PJ, Jones JR, Scherer SW, Schanen NC, Friez MJ, Vincent JB, Minassian BA (2004) A previously unidentified MECP2 open reading frame defines a new protein isoform relevant to Rett syndrome. *Nat Genet* 36: 339-341.
167. Kriaucionis S, Bird A (2004) The major form of MeCP2 has a novel N-terminus generated by alternative splicing. *Nucleic Acids Res* 32: 1818-1823.
168. Dastidar SG, Bardai FH, Ma C, Price V, Rawat V, Verma P, Narayanan V, D'Mello SR (2012) Isoform-specific toxicity of Mecp2 in postmitotic neurons: suppression of neurotoxicity by FoxG1. *J Neurosci* 32: 2846-2855.
169. Agarwal N, Hardt T, Brero A, Nowak D, Rothbauer U, Becker A, Leonhardt H, Cardoso MC (2007) MeCP2 interacts with HP1 and modulates its heterochromatin association during myogenic differentiation. *Nucleic Acids Res* 35: 5402-5408.

## Chapter 7

170. Ghosh RP, Horowitz-Scherer RA, Nikitina T, Gierasch LM, Woodcock CL (2008) Rett syndrome-causing mutations in human MeCP2 result in diverse structural changes that impact folding and DNA interactions. *J Biol Chem* 283: 20523-20534.
171. Free A, Wakefield RI, Smith BO, Dryden DT, Barlow PN, Bird AP (2001) DNA recognition by the methyl-CpG binding domain of MeCP2. *Journal of Biological Chemistry* 276: 3353-3360.
172. Galvão TC, Thomas JO (2005) Structure-specific binding of MeCP2 to four-way junction DNA through its methyl CpG-binding domain. *Nucleic Acids Res* 33: 6603-6609.
173. Guy J, Cheval H, Selfridge J, Bird A (2011) The role of MeCP2 in the brain. *Annu Rev Cell Dev Biol* 27: 631-652.
174. Ghosh RP, Nikitina T, Horowitz-Scherer RA, Gierasch LM, Uversky VN, Hite K, Hansen JC, Woodcock CL (2010) Unique physical properties and interactions of the domains of methylated DNA binding protein 2. *Biochemistry* 49: 4395-4410.
175. Jones PL, Veenstra GCJ, Wade PA, Vermaak D, Kass SU, Landsberger N, Strouboulis J, Wolffe AP (1998) Methylated DNA and MeCP2 recruit histone deacetylase to repress transcription. *Nat Genet* 19: 187-191.
176. Nan X, Ng H-H, Johnson CA, Laherty CD, Turner BM, Eisenman RN, Bird A (1998) Transcriptional repression by the methyl-CpG-binding protein MeCP2 involves a histone deacetylase complex. *Nature* 393: 386-389.

## Chapter 7

177. Nan X, Campoy FJ, Bird A (1997) MeCP2 is a transcriptional repressor with abundant binding sites in genomic chromatin. *Cell* 88: 471-481.
178. Zachariah RM, Rastegar M (2012) Linking epigenetics to human disease and Rett syndrome: the emerging novel and challenging concepts in MeCP2 research. *Neural Plast* 2012: 415825.
179. Dragich JM, Kim YH, Arnold AP, Schanen NC (2007) Differential distribution of the MeCP2 splice variants in the postnatal mouse brain. *J Comp Neurol* 501: 526-542.
180. Ballas N, Grunseich C, Lu DD, Speh JC, Mandel G (2005) REST and its corepressors mediate plasticity of neuronal gene chromatin throughout neurogenesis. *Cell* 121: 645-657.
181. Chen WG, Chang Q, Lin Y, Meissner A, West AE, Griffith EC, Jaenisch R, Greenberg ME (2003) Derepression of BDNF transcription involves calcium-dependent phosphorylation of MeCP2. *Science* 302: 885-889.
182. Zhou Z, Hong EJ, Cohen S, Zhao WN, Ho HY, Schmidt L, Chen WG, Lin Y, Savner E, Griffith EC, Hu L, Steen JA, Weitz CJ, Greenberg ME (2006) Brain-specific phosphorylation of MeCP2 regulates activity-dependent Bdnf transcription, dendritic growth, and spine maturation. *Neuron* 52: 255-269.
183. Tao J, Hu K, Chang Q, Wu H, Sherman NE, Martinowich K, Klose RJ, Schanen C, Jaenisch R, Wang W, Sun YE (2009) Phosphorylation of MeCP2 at Serine 80 regulates its chromatin association and neurological function. *Proc Natl Acad Sci U S A* 106: 4882-4887.



## Chapter 7

184. Horike S, Cai S, Miyano M, Cheng JF, Kohwi-Shigematsu T (2005) Loss of silent-chromatin looping and impaired imprinting of DLX5 in Rett syndrome. *Nat Genet* 37: 31-40.
185. Skene PJ, Illingworth RS, Webb S, Kerr AR, James KD, Turner DJ, Andrews R, Bird AP (2010) Neuronal MeCP2 is expressed at near histone-octamer levels and globally alters the chromatin state. *Mol Cell* 37: 457-468.
186. Gadalla KK, Bailey ME, Cobb SR (2011) MeCP2 and Rett syndrome: reversibility and potential avenues for therapy. *Biochem J* 439: 1-14.
187. Miyake K, Hirasawa T, Soutome M, Itoh M, Goto Y, Endoh K, Takahashi K, Kudo S, Nakagawa T, Yokoi S, Taira T, Inazawa J, Kubota T (2011) The protocadherins, PCDHB1 and PCDH7, are regulated by MeCP2 in neuronal cells and brain tissues: implication for pathogenesis of Rett syndrome. *BMC Neurosci* 12: 81.
188. Gibson JH, Slobedman B, K NH, Williamson SL, Minchenko D, El-Osta A, Stern JL, Christodoulou J (2010) Downstream targets of methyl CpG binding protein 2 and their abnormal expression in the frontal cortex of the human Rett syndrome brain. *BMC Neurosci* 11: 53.
189. Martinowich K, Hattori D, Wu H, Fouse S, He F, Hu Y, Fan G, Sun YE (2003) DNA methylation-related chromatin remodeling in activity-dependent BDNF gene regulation. *Science* 302: 890-893.
190. Jordan C, Li HH, Kwan HC, Francke U (2007) Cerebellar gene expression profiles of mouse models for Rett syndrome reveal novel MeCP2 targets. *BMC medical genetics* 8: 1.

## Chapter 7

191. Deng V, Matagne V, Banine F, Frerking M, Ohliger P, Budden S, Pevsner J, Dissen GA, Sherman LS, Ojeda SR (2007) FXYD1 is an MeCP2 target gene overexpressed in the brains of Rett syndrome patients and Mecp2-null mice. *Hum Mol Genet* 16: 640-650.
192. Peddada S, Yasui DH, LaSalle JM (2006) Inhibitors of differentiation (ID1, ID2, ID3 and ID4) genes are neuronal targets of MeCP2 that are elevated in Rett syndrome. *Hum Mol Genet* 15: 2003-2014.
193. Itoh M, Ide S, Takashima S, Kudo S, Nomura Y, Segawa M, Kubota T, Mori H, Tanaka S, Horie H (2007) Methyl CpG-binding protein 2 (a mutation of which causes Rett syndrome) directly regulates insulin-like growth factor binding protein 3 in mouse and human brains. *Journal of Neuropathology & Experimental Neurology* 66: 117-123.
194. Samaco RC, Hogart A, LaSalle JM (2005) Epigenetic overlap in autism-spectrum neurodevelopmental disorders: MECP2 deficiency causes reduced expression of UBE3A and GABRB3. *Hum Mol Genet* 14: 483-492.
195. Stancheva I, Collins AL, Van den Veyver IB, Zoghbi H, Meehan RR (2003) A mutant form of MeCP2 protein associated with human Rett syndrome cannot be displaced from methylated DNA by notch in *Xenopus* embryos. *Mol Cell* 12: 425-435.
196. Nuber UA, Kriaucionis S, Roloff TC, Guy J, Selfridge J, Steinhoff C, Schulz R, Lipkowitz B, Ropers HH, Holmes MC (2005) Up-regulation of glucocorticoid-regulated genes in a mouse model of Rett syndrome. *Hum Mol Genet* 14: 2247-2256.

## Chapter 7

197. Kriaucionis S, Paterson A, Curtis J, Guy J, MacLeod N, Bird A (2006) Gene expression analysis exposes mitochondrial abnormalities in a mouse model of Rett syndrome. *Mol Cell Biol* 26: 5033-5042.
198. McGill BE, Bundle SF, Yaylaoglu MB, Carson JP, Thaller C, Zoghbi HY (2006) Enhanced anxiety and stress-induced corticosterone release are associated with increased *Crh* expression in a mouse model of Rett syndrome. *Proceedings of the National Academy of Sciences* 103: 18267-18272.
199. Chahrour M, Zoghbi HY (2007) The story of Rett syndrome: from clinic to neurobiology. *Neuron* 56: 422-437.
200. Neul JL (2012) The relationship of Rett syndrome and MECP2 disorders to autism. *Dialogues Clin Neurosci* 14: 253-262.
201. Rett A (1966) [On a unusual brain atrophy syndrome in hyperammonemia in childhood]. *Wien Med Wochenschr* 116: 723-726.
202. Archer H, Evans J, Leonard H, Colvin L, Ravine D, Christodoulou J, Williamson S, Charman T, Bailey ME, Sampson J, de Klerk N, Clarke A (2007) Correlation between clinical severity in patients with Rett syndrome with a p.R168X or p.T158M MECP2 mutation, and the direction and degree of skewing of X-chromosome inactivation. *J Med Genet* 44: 148-152.
203. Takahashi S, Ohinata J, Makita Y, Suzuki N, Araki A, Sasaki A, Murono K, Tanaka H, Fujieda K (2008) Skewed X chromosome inactivation failed to explain the normal

## Chapter 7

- phenotype of a carrier female with MECP2 mutation resulting in Rett syndrome. *Clin Genet* 73: 257-261.
204. Xinhua B, Shengling J, Fuying S, Hong P, Meirong L, Wu XR (2008) X chromosome inactivation in Rett Syndrome and its correlations with MECP2 mutations and phenotype. *J Child Neurol* 23: 22-25.
205. Hagberg B, Aicardi J, Dias K, Ramos O (1983) A progressive syndrome of autism, dementia, ataxia, and loss of purposeful hand use in girls: Rett's syndrome: report of 35 cases. *Ann Neurol* 14: 471-479.
206. Reichow B, George-Puskar A, Lutz T, Smith IC, Volkmar FR (2015) Brief report: systematic review of Rett syndrome in males. *J Autism Dev Disord* 45: 3377-3383.
207. Liyanage VR, Rastegar M (2014) Rett syndrome and MeCP2. *Neuromolecular Med* 16: 231-264.
208. Amir RE, Fang P, Yu Z, Glaze DG, Percy AK, Zoghbi HY, Roa BB, Van den Veyver IB (2005) Mutations in exon 1 of MECP2 are a rare cause of Rett syndrome. *J Med Genet* 42: e15.
209. Bienvenu T, Carrie A, de Roux N, Vinet MC, Jonveaux P, Couvert P, Villard L, Arzimanoglou A, Beldjord C, Fontes M, Tardieu M, Chelly J (2000) MECP2 mutations account for most cases of typical forms of Rett syndrome. *Hum Mol Genet* 9: 1377-1384.

## Chapter 7

210. Schanen C, Houwink EJ, Dorrani N, Lane J, Everett R, Feng A, Cantor RM, Percy A (2004) Phenotypic manifestations of MECP2 mutations in classical and atypical Rett syndrome. *Am J Med Genet A* 126A: 129-140.
211. Evans JC, Archer HL, Whatley SD, Kerr A, Clarke A, Butler R (2005) Variation in exon 1 coding region and promoter of MECP2 in Rett syndrome and controls. *Eur J Hum Genet* 13: 124-126.
212. Quenard A, Yilmaz S, Fontaine H, Bienvenu T, Moncla A, des Portes V, Rivier F, Mathieu M, Raux G, Jonveaux P, Philippe C (2006) Deleterious mutations in exon 1 of MECP2 in Rett syndrome. *Eur J Med Genet* 49: 313-322.
213. Bartholdi D, Klein A, Weissert M, Koenig N, Baumer A, Boltshauser E, Schinzel A, Berger W, Matyas G (2006) Clinical profiles of four patients with Rett syndrome carrying a novel exon 1 mutation or genomic rearrangement in the MECP2 gene. *Clin Genet* 69: 319-326.
214. Fichou Y, Nectoux J, Bahi-Buisson N, Rosas-Vargas H, Girard B, Chelly J, Bienvenu T (2009) The first missense mutation causing Rett syndrome specifically affecting the MeCP2\_e1 isoform. *Neurogenetics* 10: 127-133.
215. Ravn K, Nielsen JB, Schwartz M (2005) Mutations found within exon 1 of MECP2 in Danish patients with Rett syndrome. *Clin Genet* 67: 532-533.
216. Saxena A, de Lagarde D, Leonard H, Williamson SL, Vasudevan V, Christodoulou J, Thompson E, MacLeod P, Ravine D (2006) Lost in translation: translational interference from a recurrent mutation in exon 1 of MECP2. *J Med Genet* 43: 470-477.

## Chapter 7

217. Guy J, Hendrich B, Holmes M, Martin JE, Bird A (2001) A mouse *Mecp2*-null mutation causes neurological symptoms that mimic Rett syndrome. *Nat Genet* 27: 322-326.
218. Pelka GJ, Watson CM, Radziewicz T, Hayward M, Lahooti H, Christodoulou J, Tam PP (2006) *Mecp2* deficiency is associated with learning and cognitive deficits and altered gene activity in the hippocampal region of mice. *Brain* 129: 887-898.
219. Ezeonwuka C, Rastegar M (2014) MeCP2-Related Diseases and Animal Models. *Diseases* 2: 45.
220. Chen RZ, Akbarian S, Tudor M, Jaenisch R (2001) Deficiency of methyl-CpG binding protein-2 in CNS neurons results in a Rett-like phenotype in mice. *Nat Genet* 27: 327-331.
221. Shahbazian M, Young J, Yuva-Paylor L, Spencer C, Antalffy B, Noebels J, Armstrong D, Paylor R, Zoghbi H (2002) Mice with truncated MeCP2 recapitulate many Rett syndrome features and display hyperacetylation of histone H3. *Neuron* 35: 243-254.
222. Fyffe SL, Neul JL, Samaco RC, Chao HT, Ben-Shachar S, Moretti P, McGill BE, Goulding EH, Sullivan E, Tecott LH, Zoghbi HY (2008) Deletion of *Mecp2* in *Sim1*-expressing neurons reveals a critical role for MeCP2 in feeding behavior, aggression, and the response to stress. *Neuron* 59: 947-958.
223. Samaco RC, Mandel-Brehm C, Chao HT, Ward CS, Fyffe-Maricich SL, Ren J, Hyland K, Thaller C, Maricich SM, Humphreys P, Greer JJ, Percy A, Glaze DG, Zoghbi HY, Neul JL (2009) Loss of MeCP2 in aminergic neurons causes cell-autonomous defects in neurotransmitter synthesis and specific behavioral abnormalities. *Proc Natl Acad Sci U S A* 106: 21966-21971.

## Chapter 7

224. Adachi M, Autry AE, Covington HE, 3rd, Monteggia LM (2009) MeCP2-mediated transcription repression in the basolateral amygdala may underlie heightened anxiety in a mouse model of Rett syndrome. *J Neurosci* 29: 4218-4227.
225. Gemelli T, Berton O, Nelson ED, Perrotti LI, Jaenisch R, Monteggia LM (2006) Postnatal loss of methyl-CpG binding protein 2 in the forebrain is sufficient to mediate behavioral aspects of Rett syndrome in mice. *Biol Psychiatry* 59: 468-476.
226. Lawson-Yuen A, Liu D, Han L, Jiang ZI, Tsai GE, Basu AC, Picker J, Feng J, Coyle JT (2007) Ube3a mRNA and protein expression are not decreased in Mecp2R168X mutant mice. *Brain Res* 1180: 1-6.
227. Jentarra GM, Olfers SL, Rice SG, Srivastava N, Homanics GE, Blue M, Naidu S, Narayanan V (2010) Abnormalities of cell packing density and dendritic complexity in the MeCP2 A140V mouse model of Rett syndrome/X-linked mental retardation. *BMC Neurosci* 11: 19.
228. Calfa G, Percy AK, Pozzo-Miller L (2011) Experimental models of Rett syndrome based on Mecp2 dysfunction. *Exp Biol Med (Maywood)* 236: 3-19.
229. Colantuoni C, Jeon O-H, Hyder K, Chenchik A, Khimani AH, Narayanan V, Hoffman EP, Kaufmann WE, Naidu S, Pevsner J (2001) Gene expression profiling in postmortem Rett Syndrome brain: differential gene expression and patient classification. *Neurobiology of disease* 8: 847-865.

## Chapter 7

230. Delgado IJ, Kim DS, Thatcher KN, LaSalle JM, Van den Veyver IB (2006) Expression profiling of clonal lymphocyte cell cultures from Rett syndrome patients. *BMC medical genetics* 7: 1.
231. Ben-Shachar S, Chahrour M, Thaller C, Shaw CA, Zoghbi HY (2009) Mouse models of MeCP2 disorders share gene expression changes in the cerebellum and hypothalamus. *Hum Mol Genet* 18: 2431-2442.
232. Zhao Y-T, Goffin D, Johnson B, Zhou Z (2013) Loss of MeCP2 function is associated with distinct gene expression changes in the striatum. *Neurobiology of disease* 59: 257-266.
233. Vacca M, Tripathi KP, Speranza L, Cigliano RA, Scalabrì F, Marracino F, Madonna M, Sanseverino W, Perrone-Capano C, Guarracino MR (2016) Effects of Mecp2 loss of function in embryonic cortical neurons: a bioinformatics strategy to sort out non-neuronal cells variability from transcriptome profiling. *BMC bioinformatics* 17: 189.
234. Li Y, Wang H, Muffat J, Cheng AW, Orlando DA, Loven J, Kwok SM, Feldman DA, Bateup HS, Gao Q, Hockemeyer D, Mitalipova M, Lewis CA, Vander Heiden MG, Sur M, Young RA, Jaenisch R (2013) Global transcriptional and translational repression in human-embryonic-stem-cell-derived Rett syndrome neurons. *Cell Stem Cell* 13: 446-458.
235. Ramocki MB, Tavyev YJ, Peters SU (2010) The MECP2 duplication syndrome. *Am J Med Genet A* 152A: 1079-1088.
236. del Gaudio D, Fang P, Scaglia F, Ward PA, Craigen WJ, Glaze DG, Neul JL, Patel A, Lee JA, Irons M, Berry SA, Pursley AA, Grebe TA, Freedenberg D, Martin RA, Hsich GE, Khera JR, Friedman NR, Zoghbi HY, Eng CM, Lupski JR, Beaudet AL, Cheung SW, Roa



## Chapter 7

- BB (2006) Increased MECP2 gene copy number as the result of genomic duplication in neurodevelopmentally delayed males. *Genet Med* 8: 784-792.
237. Carvalho CM, Zhang F, Liu P, Patel A, Sahoo T, Bacino CA, Shaw C, Peacock S, Pursley A, Tavyev YJ, Ramocki MB, Nawara M, Obersztyn E, Vianna-Morgante AM, Stankiewicz P, Zoghbi HY, Cheung SW, Lupski JR (2009) Complex rearrangements in patients with duplications of MECP2 can occur by fork stalling and template switching. *Hum Mol Genet* 18: 2188-2203.
238. Lugtenberg D, Kleefstra T, Oudakker AR, Nillesen WM, Yntema HG, Tzschach A, Raynaud M, Rating D, Journel H, Chelly J, Goizet C, Lacombe D, Pedespan JM, Echenne B, Tariverdian G, O'Rourke D, King MD, Green A, van Kogelenberg M, Van Esch H, Gez J, Hamel BC, van Bokhoven H, de Brouwer AP (2009) Structural variation in Xq28: MECP2 duplications in 1% of patients with unexplained XLMR and in 2% of male patients with severe encephalopathy. *Eur J Hum Genet* 17: 444-453.
239. Meins M, Lehmann J, Gerresheim F, Herchenbach J, Hagedorn M, Hameister K, Epplen JT (2005) Submicroscopic duplication in Xq28 causes increased expression of the MECP2 gene in a boy with severe mental retardation and features of Rett syndrome. *J Med Genet* 42: e12.
240. Van Esch H, Bauters M, Ignatius J, Jansen M, Raynaud M, Hollanders K, Lugtenberg D, Bienvenu T, Jensen LR, Gez J, Moraine C, Marynen P, Fryns JP, Froyen G (2005) Duplication of the MECP2 region is a frequent cause of severe mental retardation and progressive neurological symptoms in males. *Am J Hum Genet* 77: 442-453.

## Chapter 7

241. Reardon W, Donoghue V, Murphy AM, King MD, Mayne PD, Horn N, Birk Moller L (2010) Progressive cerebellar degenerative changes in the severe mental retardation syndrome caused by duplication of MECP2 and adjacent loci on Xq28. *Eur J Pediatr* 169: 941-949.
242. Kirk EP, Malaty-Brevaud V, Martini N, Lacoste C, Levy N, Maclean K, Davies L, Philip N, Badens C (2009) The clinical variability of the MECP2 duplication syndrome: description of two families with duplications excluding L1CAM and FLNA. *Clin Genet* 75: 301-303.
243. Van Esch H (2012) MECP2 Duplication Syndrome. *Mol Syndromol* 2: 128-136.
244. Hanchard NA, Carvalho CM, Bader P, Thome A, Omo-Griffith L, del Gaudio D, Pehlivan D, Fang P, Schaaf CP, Ramocki MB, Lupski JR, Cheung SW (2012) A partial MECP2 duplication in a mildly affected adult male: a putative role for the 3' untranslated region in the MECP2 duplication phenotype. *BMC Med Genet* 13: 71.
245. Tang SS, Fernandez D, Lazarou LP, Singh R, Fallon P (2012) MECP2 triplication in 3 brothers - a rarely described cause of familial neurological regression in boys. *Eur J Paediatr Neurol* 16: 209-212.
246. Friez MJ, Jones JR, Clarkson K, Lubs H, Abuelo D, Bier JA, Pai S, Simensen R, Williams C, Giampietro PF, Schwartz CE, Stevenson RE (2006) Recurrent infections, hypotonia, and mental retardation caused by duplication of MECP2 and adjacent region in Xq28. *Pediatrics* 118: e1687-1695.
247. Clayton-Smith J, Walters S, Hobson E, Burkitt-Wright E, Smith R, Toutain A, Amiel J, Lyonnet S, Mansour S, Fitzpatrick D, Ciccone R, Ricca I, Zuffardi O, Donnai D (2009)

## Chapter 7

- Xq28 duplication presenting with intestinal and bladder dysfunction and a distinctive facial appearance. *Eur J Hum Genet* 17: 434-443.
248. Smyk M, Obersztyn E, Nowakowska B, Nawara M, Cheung SW, Mazurczak T, Stankiewicz P, Bocian E (2008) Different-sized duplications of Xq28, including MECP2, in three males with mental retardation, absent or delayed speech, and recurrent infections. *Am J Med Genet B Neuropsychiatr Genet* 147B: 799-806.
249. Echenne B, Roubertie A, Lugtenberg D, Kleefstra T, Hamel BC, Van Bokhoven H, Lacombe D, Philippe C, Jonveaux P, de Brouwer AP (2009) Neurologic aspects of MECP2 gene duplication in male patients. *Pediatr Neurol* 41: 187-191.
250. Prescott TE, Rodningen OK, Bjornstad A, Stray-Pedersen A (2009) Two brothers with a microduplication including the MECP2 gene: rapid head growth in infancy and resolution of susceptibility to infection. *Clin Dysmorphol* 18: 78-82.
251. Velinov M, Novelli A, Gu H, Fenko M, Dolzhanskaya N, Bernardini L, Capalbo A, Dallapiccola B, Jenkins EC, Brown WT (2009) De-novo 2.15 Mb terminal Xq duplication involving MECP2 but not L1CAM gene in a male patient with mental retardation. *Clin Dysmorphol* 18: 9-12.
252. Breman AM, Ramocki MB, Kang SH, Williams M, Freedenberg D, Patel A, Bader PI, Cheung SW (2011) MECP2 duplications in six patients with complex sex chromosome rearrangements. *Eur J Hum Genet* 19: 409-415.
253. Sanmann JN, Bishay DL, Starr LJ, Bell CA, Pickering DL, Stevens JM, Kahler SG, Olney AH, Schaefer GB, Sanger WG (2012) Characterization of six novel patients with MECP2

## Chapter 7

- duplications due to unbalanced rearrangements of the X chromosome. *Am J Med Genet A* 158A: 1285-1291.
254. Lombardi LM, Baker SA, Zoghbi HY (2015) MECP2 disorders: from the clinic to mice and back. *J Clin Invest* 125: 2914-2923.
255. Peters SU, Hundley RJ, Wilson AK, Warren Z, Vehorn A, Carvalho CM, Lupski JR, Ramocki MB (2013) The behavioral phenotype in MECP2 duplication syndrome: a comparison with idiopathic autism. *Autism Res* 6: 42-50.
256. Shimada S, Okamoto N, Ito M, Arai Y, Momosaki K, Togawa M, Maegaki Y, Sugawara M, Shimojima K, Osawa M, Yamamoto T (2013) MECP2 duplication syndrome in both genders. *Brain Dev* 35: 411-419.
257. Gottipati S, Rao NL, Fung-Leung WP (2008) IRAK1: a critical signaling mediator of innate immunity. *Cell Signal* 20: 269-276.
258. Yang T, Ramocki MB, Neul JL, Lu W, Roberts L, Knight J, Ward CS, Zoghbi HY, Kheradmand F, Corry DB (2012) Overexpression of methyl-CpG binding protein 2 impairs T(H)1 responses. *Sci Transl Med* 4: 163ra158.
259. Collins AL, Levenson JM, Vilaythong AP, Richman R, Armstrong DL, Noebels JL, David Sweatt J, Zoghbi HY (2004) Mild overexpression of MeCP2 causes a progressive neurological disorder in mice. *Hum Mol Genet* 13: 2679-2689.

## Chapter 7

260. Luikenhuis S, Giacometti E, Beard CF, Jaenisch R (2004) Expression of MeCP2 in postmitotic neurons rescues Rett syndrome in mice. *Proc Natl Acad Sci U S A* 101: 6033-6038.
261. Samaco RC, Mandel-Brehm C, McGraw CM, Shaw CA, McGill BE, Zoghbi HY (2012) Crh and Oprm1 mediate anxiety-related behavior and social approach in a mouse model of MECP2 duplication syndrome. *Nat Genet* 44: 206-211.
262. Jiang M, Ash RT, Baker SA, Suter B, Ferguson A, Park J, Rudy J, Torsky SP, Chao HT, Zoghbi HY, Smirnakis SM (2013) Dendritic arborization and spine dynamics are abnormal in the mouse model of MECP2 duplication syndrome. *J Neurosci* 33: 19518-19533.
263. Sztainberg Y, Chen HM, Swann JW, Hao S, Tang B, Wu Z, Tang J, Wan YW, Liu Z, Rigo F, Zoghbi HY (2015) Reversal of phenotypes in MECP2 duplication mice using genetic rescue or antisense oligonucleotides. *Nature* 528: 123-126.
264. Ariani F, Mari F, Pescucci C, Longo I, Bruttini M, Meloni I, Hayek G, Rocchi R, Zappella M, Renieri A (2004) Real-time quantitative PCR as a routine method for screening large rearrangements in Rett syndrome: Report of one case of MECP2 deletion and one case of MECP2 duplication. *Hum Mutat* 24: 172-177.
265. Ramocki MB, Zoghbi HY (2008) Failure of neuronal homeostasis results in common neuropsychiatric phenotypes. *Nature* 455: 912-918.
266. Cmarko D, Smigova J, Minichova L, Popov A (2008) Nucleolus: the ribosome factory. *Histol Histopathol* 23: 1291-1298.

## Chapter 7

267. Henderson AS, Warburton D, Atwood KC (1972) Location of ribosomal DNA in the human chromosome complement. *Proc Natl Acad Sci U S A* 69: 3394-3398.
268. Dev VG, Tantravahi R, Miller DA, Miller OJ (1977) Nucleolus organizers in *Mus musculus* subspecies and in the RAG mouse cell line. *Genetics* 86: 389-398.
269. Gonzalez IL, Sylvester JE (1995) Complete sequence of the 43-kb human ribosomal DNA repeat: analysis of the intergenic spacer. *Genomics* 27: 320-328.
270. Grozdanov P, Georgiev O, Karagyozov L (2003) Complete sequence of the 45-kb mouse ribosomal DNA repeat: analysis of the intergenic spacer. *Genomics* 82: 637-643.
271. McStay B, Grummt I (2008) The epigenetics of rRNA genes: from molecular to chromosome biology. *Annu Rev Cell Dev Biol* 24: 131-157.
272. Haltiner MM, Smale ST, Tjian R (1986) Two distinct promoter elements in the human rRNA gene identified by linker scanning mutagenesis. *Mol Cell Biol* 6: 227-235.
273. Learned RM, Learned TK, Haltiner MM, Tjian RT (1986) Human rRNA transcription is modulated by the coordinate binding of two factors to an upstream control element. *Cell* 45: 847-857.
274. Goodfellow SJ, Zomerdijk JC (2013) Basic mechanisms in RNA polymerase I transcription of the ribosomal RNA genes. *Subcell Biochem* 61: 211-236.
275. Lewis JD, Tollervey D (2000) Like attracts like: getting RNA processing together in the nucleus. *Science* 288: 1385-1389.

## Chapter 7

276. Grummt I (1999) Regulation of mammalian ribosomal gene transcription by RNA polymerase I. *Prog Nucleic Acid Res Mol Biol* 62: 109-154.
277. Russell J, Zomerdijk JC (2005) RNA-polymerase-I-directed rDNA transcription, life and works. *Trends Biochem Sci* 30: 87-96.
278. Hamdane N, Stefanovsky VY, Tremblay MG, Nemeth A, Paquet E, Lessard F, Sanij E, Hannan R, Moss T (2014) Conditional inactivation of Upstream Binding Factor reveals its epigenetic functions and the existence of a somatic nucleolar precursor body. *PLoS Genet* 10: e1004505.
279. Miller G, Panov KI, Friedrich JK, Trinkle-Mulcahy L, Lamond AI, Zomerdijk JC (2001) hRRN3 is essential in the SL1-mediated recruitment of RNA Polymerase I to rRNA gene promoters. *EMBO J* 20: 1373-1382.
280. Hirschler-Laszkiwicz I, Cavanaugh AH, Mirza A, Lun M, Hu Q, Smink T, Rothblum LI (2003) Rrn3 becomes inactivated in the process of ribosomal DNA transcription. *J Biol Chem* 278: 18953-18959.
281. Jansa P, Burek C, Sander EE, Grummt I (2001) The transcript release factor PTRF augments ribosomal gene transcription by facilitating reinitiation of RNA polymerase I. *Nucleic Acids Res* 29: 423-429.
282. Kobayashi T (2011) Regulation of ribosomal RNA gene copy number and its role in modulating genome integrity and evolutionary adaptability in yeast. *Cell Mol Life Sci* 68: 1395-1403.

## Chapter 7

283. Grummt I, Langst G (2013) Epigenetic control of RNA polymerase I transcription in mammalian cells. *Biochim Biophys Acta* 1829: 393-404.
284. Nemeth A, Strohner R, Grummt I, Langst G (2004) The chromatin remodeling complex NoRC and TTF-I cooperate in the regulation of the mammalian rRNA genes in vivo. *Nucleic Acids Res* 32: 4091-4099.
285. Yuan X, Feng W, Imhof A, Grummt I, Zhou Y (2007) Activation of RNA polymerase I transcription by cockayne syndrome group B protein and histone methyltransferase G9a. *Mol Cell* 27: 585-595.
286. Santoro R, Grummt I (2005) Epigenetic mechanism of rRNA gene silencing: temporal order of NoRC-mediated histone modification, chromatin remodeling, and DNA methylation. *Mol Cell Biol* 25: 2539-2546.
287. Santoro R, Grummt I (2001) Molecular mechanisms mediating methylation-dependent silencing of ribosomal gene transcription. *Mol Cell* 8: 719-725.
288. Ghoshal K, Majumder S, Datta J, Motiwala T, Bai S, Sharma SM, Frankel W, Jacob ST (2004) Role of human ribosomal RNA (rRNA) promoter methylation and of methyl-CpG-binding protein MBD2 in the suppression of rRNA gene expression. *J Biol Chem* 279: 6783-6793.
289. McGowan PO, Sasaki A, Huang TC, Unterberger A, Suderman M, Ernst C, Meaney MJ, Turecki G, Szyf M (2008) Promoter-wide hypermethylation of the ribosomal RNA gene promoter in the suicide brain. *PLoS One* 3: e2085.



## Chapter 7

290. Mayer C, Schmitz KM, Li J, Grummt I, Santoro R (2006) Intergenic transcripts regulate the epigenetic state of rRNA genes. *Mol Cell* 22: 351-361.
291. Guo P (2002) Structure and function of  $\phi$ 29 hexameric RNA that drives the viral DNA packaging motor: Review. *Prog Nucleic Acid Res Mol Biol* 72: 415-472.
292. Mayer C, Neubert M, Grummt I (2008) The structure of NoRC-associated RNA is crucial for targeting the chromatin remodelling complex NoRC to the nucleolus. *EMBO Rep* 9: 774-780.
293. Strohner R, Nemeth A, Nightingale KP, Grummt I, Becker PB, Langst G (2004) Recruitment of the nucleolar remodeling complex NoRC establishes ribosomal DNA silencing in chromatin. *Mol Cell Biol* 24: 1791-1798.
294. Henras AK, Plisson-Chastang C, O'Donohue MF, Chakraborty A, Gleizes PE (2015) An overview of pre-ribosomal RNA processing in eukaryotes. *Wiley Interdiscip Rev RNA* 6: 225-242.
295. Enright CA, Maxwell ES, Eliceiri GL, Sollner-Webb B (1996) 5'ETS rRNA processing facilitated by four small RNAs: U14, E3, U17, and U3. *RNA* 2: 1094-1099.
296. Sloan KE, Bohnsack MT, Schneider C, Watkins NJ (2014) The roles of SSU processome components and surveillance factors in the initial processing of human ribosomal RNA. *RNA* 20: 540-550.
297. Bowman LH, Goldman WE, Goldberg GI, Hebert MB, Schlessinger D (1983) Location of the initial cleavage sites in mouse pre-rRNA. *Mol Cell Biol* 3: 1501-1510.

## Chapter 7

298. Hadjiolova KV, Nicoloso M, Mazan S, Hadjiolov AA, Bachellerie JP (1993) Alternative pre-rRNA processing pathways in human cells and their alteration by cycloheximide inhibition of protein synthesis. *Eur J Biochem* 212: 211-215.
299. Dragon F, Gallagher JE, Compagnone-Post PA, Mitchell BM, Porwancher KA, Wehner KA, Wormsley S, Settlage RE, Shabanowitz J, Osheim Y, Beyer AL, Hunt DF, Baserga SJ (2002) A large nucleolar U3 ribonucleoprotein required for 18S ribosomal RNA biogenesis. *Nature* 417: 967-970.
300. Phipps KR, Charette J, Baserga SJ (2011) The small subunit processome in ribosome biogenesis-progress and prospects. *Wiley Interdiscip Rev RNA* 2: 1-21.
301. Preti M, O'Donohue MF, Montel-Lehry N, Bortolin-Cavaille ML, Choismel V, Gleizes PE (2013) Gradual processing of the ITS1 from the nucleolus to the cytoplasm during synthesis of the human 18S rRNA. *Nucleic Acids Res* 41: 4709-4723.
302. Sloan KE, Mattijssen S, Lebaron S, Tollervey D, Puijn GJ, Watkins NJ (2013) Both endonucleolytic and exonucleolytic cleavage mediate ITS1 removal during human ribosomal RNA processing. *J Cell Biol* 200: 577-588.
303. Wang M, Pestov DG (2010) 5'-end surveillance by Xrn2 acts as a shared mechanism for mammalian pre-rRNA maturation and decay. *Nucleic Acids Res*: gkq1050.
304. Reddy R, Rothblum LI, Subrahmanyam CS, Liu MH, Henning D, Cassidy B, Busch H (1983) The nucleotide sequence of 8 S RNA bound to preribosomal RNA of Novikoff hepatoma. The 5'-end of 8 S RNA is 5.8 S RNA. *J Biol Chem* 258: 584-589.

## Chapter 7

305. Michot B, Joseph N, Mazan S, Bachellerie JP (1999) Evolutionarily conserved structural features in the ITS2 of mammalian pre-rRNAs and potential interactions with the snoRNA U8 detected by comparative analysis of new mouse sequences. *Nucleic Acids Res* 27: 2271-2282.
306. Tafforeau L, Zorbas C, Langhendries JL, Mullineux ST, Stamatopoulou V, Mullier R, Wacheul L, Lafontaine DL (2013) The complexity of human ribosome biogenesis revealed by systematic nucleolar screening of Pre-rRNA processing factors. *Mol Cell* 51: 539-551.
307. Schilders G, van Dijk E, Pruijn GJ (2007) C1D and hMtr4p associate with the human exosome subunit PM/Scf-100 and are involved in pre-rRNA processing. *Nucleic Acids Res* 35: 2564-2572.
308. Ansel KM, Pastor WA, Rath N, Lapan AD, Glasmacher E, Wolf C, Smith LC, Papadopoulou N, Lamperti ED, Tahiliani M, Ellwart JW, Shi Y, Kremmer E, Rao A, Heissmeyer V (2008) Mouse Eri1 interacts with the ribosome and catalyzes 5.8S rRNA processing. *Nat Struct Mol Biol* 15: 523-530.
309. Olynik BM, Rastegar M (2012) The genetic and epigenetic journey of embryonic stem cells into mature neural cells. *Front Genet* 3: 81.
310. Fagiolini M, Jensen CL, Champagne FA (2009) Epigenetic influences on brain development and plasticity. *Curr Opin Neurobiol* 19: 207-212.
311. Fan G, Martinowich K, Chin MH, He F, Fouse SD, Hutnick L, Hattori D, Ge W, Shen Y, Wu H, ten Hoeve J, Shuai K, Sun YE (2005) DNA methylation controls the timing of

## Chapter 7

- astrogliogenesis through regulation of JAK-STAT signaling. *Development* 132: 3345-3356.
312. Nguyen S, Meletis K, Fu D, Jhaveri S, Jaenisch R (2007) Ablation of de novo DNA methyltransferase Dnmt3a in the nervous system leads to neuromuscular defects and shortened lifespan. *Dev Dyn* 236: 1663-1676.
313. Jin B, Tao Q, Peng J, Soo HM, Wu W, Ying J, Fields CR, Delmas AL, Liu X, Qiu J, Robertson KD (2008) DNA methyltransferase 3B (DNMT3B) mutations in ICF syndrome lead to altered epigenetic modifications and aberrant expression of genes regulating development, neurogenesis and immune function. *Hum Mol Genet* 17: 690-709.
314. Zhao X, Ueba T, Christie BR, Barkho B, McConnell MJ, Nakashima K, Lein ES, Eadie BD, Willhoite AR, Muotri AR, Summers RG, Chun J, Lee KF, Gage FH (2003) Mice lacking methyl-CpG binding protein 1 have deficits in adult neurogenesis and hippocampal function. *Proc Natl Acad Sci U S A* 100: 6777-6782.
315. Macdonald JL, Verster A, Berndt A, Roskams AJ (2010) MBD2 and MeCP2 regulate distinct transitions in the stage-specific differentiation of olfactory receptor neurons. *Mol Cell Neurosci* 44: 55-67.
316. Knock E, Pereira J, Lombard PD, Dimond A, Leaford D, Livesey FJ, Hendrich B (2015) The methyl binding domain 3/nucleosome remodelling and deacetylase complex regulates neural cell fate determination and terminal differentiation in the cerebral cortex. *Neural Dev* 10: 13.

## Chapter 7

317. Tsujimura K, Abematsu M, Kohyama J, Namihira M, Nakashima K (2009) Neuronal differentiation of neural precursor cells is promoted by the methyl-CpG-binding protein MeCP2. *Exp Neurol* 219: 104-111.
318. Kishi N, Macklis JD (2004) MECP2 is progressively expressed in post-migratory neurons and is involved in neuronal maturation rather than cell fate decisions. *Mol Cell Neurosci* 27: 306-321.
319. Merson TD, Dixon MP, Collin C, Rietze RL, Bartlett PF, Thomas T, Voss AK (2006) The transcriptional coactivator Querkopf controls adult neurogenesis. *J Neurosci* 26: 11359-11370.
320. Thomas T, Voss AK (2004) Querkopf, a histone acetyltransferase, is essential for embryonic neurogenesis. *Front Biosci* 9: 24-31.
321. Jawerka M, Colak D, Dimou L, Spiller C, Lager S, Montgomery RL, Olson EN, Wurst W, Gottlicher M, Gotz M (2010) The specific role of histone deacetylase 2 in adult neurogenesis. *Neuron Glia Biol* 6: 93-107.
322. Ye F, Chen Y, Hoang T, Montgomery RL, Zhao XH, Bu H, Hu T, Taketo MM, van Es JH, Clevers H, Hsieh J, Bassel-Duby R, Olson EN, Lu QR (2009) HDAC1 and HDAC2 regulate oligodendrocyte differentiation by disrupting the beta-catenin-TCF interaction. *Nat Neurosci* 12: 829-838.
323. Santoro SW, Dulac C (2015) Histone variants and cellular plasticity. *Trends in Genetics* 31: 516-527.

## Chapter 7

324. Michod D, Bartesaghi S, Khelifi A, Bellodi C, Berliocchi L, Nicotera P, Salomoni P (2012) Calcium-dependent dephosphorylation of the histone chaperone DAXX regulates H3.3 loading and transcription upon neuronal activation. *Neuron* 74: 122-135.
325. Maze I, Wenderski W, Noh KM, Bagot RC, Tzavaras N, Purushothaman I, Elsasser SJ, Guo Y, Ionete C, Hurd YL, Tamminga CA, Halene T, Farrelly L, Soshnev AA, Wen D, Rafii S, Birtwistle MR, Akbarian S, Buchholz BA, Blitzer RD, Nestler EJ, Yuan ZF, Garcia BA, Shen L, Molina H, Allis CD (2015) Critical Role of Histone Turnover in Neuronal Transcription and Plasticity. *Neuron* 87: 77-94.
326. Forneris F, Binda C, Battaglioli E, Mattevi A (2008) LSD1: oxidative chemistry for multifaceted functions in chromatin regulation. *Trends Biochem Sci* 33: 181-189.
327. Zibetti C, Adamo A, Binda C, Forneris F, Toffolo E, Verpelli C, Ginelli E, Mattevi A, Sala C, Battaglioli E (2010) Alternative splicing of the histone demethylase LSD1/KDM1 contributes to the modulation of neurite morphogenesis in the mammalian nervous system. *J Neurosci* 30: 2521-2532.
328. Toffolo E, Rusconi F, Paganini L, Tortorici M, Pilotto S, Heise C, Verpelli C, Tedeschi G, Maffioli E, Sala C, Mattevi A, Battaglioli E (2014) Phosphorylation of neuronal Lysine-Specific Demethylase 1LSD1/KDM1A impairs transcriptional repression by regulating interaction with CoREST and histone deacetylases HDAC1/2. *J Neurochem* 128: 603-616.
329. Rusconi F, Paganini L, Braida D, Ponzoni L, Toffolo E, Maroli A, Landsberger N, Bedogni F, Turco E, Pattini L, Altruda F, De Biasi S, Sala M, Battaglioli E (2015) LSD1

- Neurospecific Alternative Splicing Controls Neuronal Excitability in Mouse Models of Epilepsy. *Cereb Cortex* 25: 2729-2740.
330. Derrien T, Johnson R, Bussotti G, Tanzer A, Djebali S, Tilgner H, Guernec G, Martin D, Merkel A, Knowles DG, Lagarde J, Veeravalli L, Ruan X, Ruan Y, Lassmann T, Carninci P, Brown JB, Lipovich L, Gonzalez JM, Thomas M, Davis CA, Shiekhhattar R, Gingeras TR, Hubbard TJ, Notredame C, Harrow J, Guigo R (2012) The GENCODE v7 catalog of human long noncoding RNAs: analysis of their gene structure, evolution, and expression. *Genome Res* 22: 1775-1789.
331. Konopka W, Kiryk A, Novak M, Herwerth M, Parkitna JR, Wawrzyniak M, Kowarsch A, Michaluk P, Dzwonek J, Arnsperger T, Wilczynski G, Merckenschlager M, Theis FJ, Kohr G, Kaczmarek L, Schutz G (2010) MicroRNA loss enhances learning and memory in mice. *J Neurosci* 30: 14835-14842.
332. Su WY, Xiong H, Fang JY (2010) Natural antisense transcripts regulate gene expression in an epigenetic manner. *Biochem Biophys Res Commun* 396: 177-181.
333. Korneev S, O'Shea M (2005) Natural antisense RNAs in the nervous system. *Rev Neurosci* 16: 213-222.
334. Modarresi F, Faghihi MA, Lopez-Toledano MA, Fatemi RP, Magistri M, Brothers SP, van der Brug MP, Wahlestedt C (2012) Inhibition of natural antisense transcripts in vivo results in gene-specific transcriptional upregulation. *Nat Biotechnol* 30: 453-459.

## Chapter 7

335. Kim J, Inoue K, Ishii J, Vanti WB, Voronov SV, Murchison E, Hannon G, Abeliovich A (2007) A MicroRNA feedback circuit in midbrain dopamine neurons. *Science* 317: 1220-1224.
336. Schaefer A, O'Carroll D, Tan CL, Hillman D, Sugimori M, Llinas R, Greengard P (2007) Cerebellar neurodegeneration in the absence of microRNAs. *J Exp Med* 204: 1553-1558.
337. Davis TH, Cuellar TL, Koch SM, Barker AJ, Harfe BD, McManus MT, Ullian EM (2008) Conditional loss of Dicer disrupts cellular and tissue morphogenesis in the cortex and hippocampus. *J Neurosci* 28: 4322-4330.
338. Bian S, Hong J, Li Q, Schebelle L, Pollock A, Knauss JL, Garg V, Sun T (2013) MicroRNA cluster miR-17-92 regulates neural stem cell expansion and transition to intermediate progenitors in the developing mouse neocortex. *Cell Rep* 3: 1398-1406.
339. Akerblom M, Sachdeva R, Barde I, Verp S, Gentner B, Trono D, Jakobsson J (2012) MicroRNA-124 is a subventricular zone neuronal fate determinant. *J Neurosci* 32: 8879-8889.
340. Sanuki R, Onishi A, Koike C, Muramatsu R, Watanabe S, Muranishi Y, Irie S, Uneo S, Koyasu T, Matsui R, Cherasse Y, Urade Y, Watanabe D, Kondo M, Yamashita T, Furukawa T (2011) miR-124a is required for hippocampal axogenesis and retinal cone survival through Lhx2 suppression. *Nat Neurosci* 14: 1125-1134.
341. Lilja T, Heldring N, Hermanson O (2013) Like a rolling histone: Epigenetic regulation of neural stem cells and brain development by factors controlling histone acetylation and methylation. *Biochimica et Biophysica Acta (BBA) - General Subjects* 1830: 2354-2360.



## Chapter 7

342. Montgomery RL, Hsieh J, Barbosa AC, Richardson JA, Olson EN (2009) Histone deacetylases 1 and 2 control the progression of neural precursors to neurons during brain development. *Proc Natl Acad Sci U S A* 106: 7876-7881.
343. Norwood J, Franklin JM, Sharma D, D'Mello SR (2014) Histone deacetylase 3 is necessary for proper brain development. *J Biol Chem* 289: 34569-34582.
344. Bale TL (2015) Epigenetic and transgenerational reprogramming of brain development. *Nature Reviews Neuroscience* 16: 332-344.
345. Heard E, Martienssen RA (2014) Transgenerational epigenetic inheritance: myths and mechanisms. *Cell* 157: 95-109.
346. Knezovich JG, Ramsay M (2012) The effect of preconception paternal alcohol exposure on epigenetic remodeling of the h19 and rasgrf1 imprinting control regions in mouse offspring. *Front Genet* 3: 10.
347. Liyanage VR, Curtis K, Zachariah RM, Chudley AE, Rastegar M (2016) Overview of the Genetic Basis and Epigenetic Mechanisms that Contribute to FASD Pathobiology. *Curr Top Med Chem*.
348. Gibbons RJ, Higgs DR (2000) Molecular-clinical spectrum of the ATR-X syndrome. *Am J Med Genet* 97: 204-212.
349. Van Esch H (2006) The Fragile X premutation: new insights and clinical consequences. *Eur J Med Genet* 49: 1-8.

## Chapter 7

350. Milani D, Manzoni FM, Pezzani L, Ajmone P, Gervasini C, Menni F, Esposito S (2015) Rubinstein-Taybi syndrome: clinical features, genetic basis, diagnosis, and management. *Ital J Pediatr* 41: 4.
351. Desplats P, Spencer B, Coffee E, Patel P, Michael S, Patrick C, Adame A, Rockenstein E, Masliah E (2011) Alpha-synuclein sequesters Dnmt1 from the nucleus: a novel mechanism for epigenetic alterations in Lewy body diseases. *J Biol Chem* 286: 9031-9037.
352. Winner B, Regensburger M, Schreglmann S, Boyer L, Prots I, Rockenstein E, Mante M, Zhao C, Winkler J, Masliah E, Gage FH (2012) Role of alpha-synuclein in adult neurogenesis and neuronal maturation in the dentate gyrus. *J Neurosci* 32: 16906-16916.
353. Li J-Q, Tan L, Yu J-T (2014) The role of the LRRK2 gene in Parkinsonism. *Molecular neurodegeneration* 9: 1.
354. Winner B, Melrose HL, Zhao C, Hinkle KM, Yue M, Kent C, Braithwaite AT, Ogholikhan S, Aigner R, Winkler J, Farrer MJ, Gage FH (2011) Adult neurogenesis and neurite outgrowth are impaired in LRRK2 G2019S mice. *Neurobiol Dis* 41: 706-716.
355. Cho HJ, Liu G, Jin SM, Parisiadou L, Xie C, Yu J, Sun L, Ma B, Ding J, Vancraenenbroeck R, Lobbstaël E, Baekelandt V, Taymans JM, He P, Troncoso JC, Shen Y, Cai H (2013) MicroRNA-205 regulates the expression of Parkinson's disease-related leucine-rich repeat kinase 2 protein. *Hum Mol Genet* 22: 608-620.
356. Mouradian MM (2012) MicroRNAs in Parkinson's disease. *Neurobiol Dis* 46: 279-284.

## Chapter 7

357. Sanchez-Mut JV, Gräff J (2015) Epigenetic Alterations in Alzheimer's Disease. *Frontiers in behavioral neuroscience* 9.
358. Lord J, Cruchaga C (2014) The epigenetic landscape of Alzheimer's disease. *Nat Neurosci* 17: 1138-1140.
359. Chouliaras L, Mastroeni D, Delvaux E, Grover A, Kenis G, Hof PR, Steinbusch HW, Coleman PD, Rutten BP, van den Hove DL (2013) Consistent decrease in global DNA methylation and hydroxymethylation in the hippocampus of Alzheimer's disease patients. *Neurobiol Aging* 34: 2091-2099.
360. Kumar A, Thakur MK (2015) Epigenetic regulation of presenilin 1 and 2 in the cerebral cortex of mice during development. *Dev Neurobiol* 75: 1165-1173.
361. Singleton MK, Gonzales ML, Leung KN, Yasui DH, Schroeder DI, Dunaway K, LaSalle JM (2011) MeCP2 is required for global heterochromatic and nucleolar changes during activity-dependent neuronal maturation. *Neurobiol Dis* 43: 190-200.
362. Gabel HW, Kinde B, Stroud H, Gilbert CS, Harmin DA, Kastan NR, Hemberg M, Ebert DH, Greenberg ME (2015) Disruption of DNA-methylation-dependent long gene repression in Rett syndrome. *Nature* 522: 89-93.
363. Maezawa I, Swanberg S, Harvey D, LaSalle JM, Jin L-W (2009) Rett syndrome astrocytes are abnormal and spread MeCP2 deficiency through gap junctions. *The Journal of Neuroscience* 29: 5051-5061.

## Chapter 7

364. Lim Z, Downs J, Wong K, Ellaway C, Leonard H (2016) Expanding the clinical picture of the MECP2 Duplication syndrome. *Clin Genet*.
365. Liu Z, Li X, Zhang JT, Cai YJ, Cheng TL, Cheng C, Wang Y, Zhang CC, Nie YH, Chen ZF, Bian WJ, Zhang L, Xiao J, Lu B, Zhang YF, Zhang XD, Sang X, Wu JJ, Xu X, Xiong ZQ, Zhang F, Yu X, Gong N, Zhou WH, Sun Q, Qiu Z (2016) Autism-like behaviours and germline transmission in transgenic monkeys overexpressing MeCP2. *Nature* 530: 98-102.
366. Na ES, Nelson ED, Adachi M, Autry AE, Mahgoub MA, Kavalali ET, Monteggia LM (2012) A mouse model for MeCP2 duplication syndrome: MeCP2 overexpression impairs learning and memory and synaptic transmission. *J Neurosci* 32: 3109-3117.
367. Parlato R, Kreiner G (2013) Nucleolar activity in neurodegenerative diseases: a missing piece of the puzzle? *J Mol Med (Berl)* 91: 541-547.
368. Marquez SB (2007) Neurogenesis and Electrophysiologic Restoration of Rat Hippocampal Neurons Following Hypoxia: ProQuest.
369. Shao Z, Kamboj A, Anderson CM (2009) Functional and immunocytochemical characterization of D-serine transporters in cortical neuron and astrocyte cultures. *J Neurosci Res* 87: 2520-2530.
370. QIAGEN (2012) QIAGEN® Plasmid Purification Handbook: QIAGEN Plasmid Mini, Midi, Maxi, Mega, and Giga Kits-For purification of ultrapure, transfection-grade plasmid DNA. In: QIAGEN, editor. pp. 17-21 Accessed from <https://www.qiagen.com/literature/render.aspx?id=369>.

## Chapter 7

371. Yamaguchi S, Hong K, Liu R, Inoue A, Shen L, Zhang K, Zhang Y (2013) Dynamics of 5-methylcytosine and 5-hydroxymethylcytosine during germ cell reprogramming. *Cell Res* 23: 329-339.
372. Rastegar M, Kobrossy L, Kovacs EN, Rambaldi I, Featherstone M (2004) Sequential histone modifications at Hoxd4 regulatory regions distinguish anterior from posterior embryonic compartments. *Mol Cell Biol* 24: 8090-8103.
373. ThermoScientific (2014) NE-PER Nuclear and Cytoplasmic Extraction Reagents. In: ThermoScientific, editor. pp. 1-4 Accessed from [https://tools.thermofisher.com/content/sfs/manuals/MAN0011398\\_NEPER\\_Nuc\\_Cytoplasmic\\_Extract\\_Reag\\_UG.pdf](https://tools.thermofisher.com/content/sfs/manuals/MAN0011398_NEPER_Nuc_Cytoplasmic_Extract_Reag_UG.pdf).
374. Andersen JS, Lyon CE, Fox AH, Leung AK, Lam YW, Steen H, Mann M, Lamond AI (2002) Directed proteomic analysis of the human nucleolus. *Curr Biol* 12: 1-11.
375. Bio-Rad (1994) Bio-Rad Protein Assay. pp. 1-13 Accessed from [http://www.bio-rad.com/LifeScience/pdf/Bulletin\\_9004.pdf](http://www.bio-rad.com/LifeScience/pdf/Bulletin_9004.pdf).
376. Djuric U, Cheung AY, Zhang W, Mok RS, Lai W, Piekna A, Hendry JA, Ross PJ, Pasceri P, Kim DS, Salter MW, Ellis J (2015) MECP2e1 isoform mutation affects the form and function of neurons derived from Rett syndrome patient iPS cells. *Neurobiol Dis* 76: 37-45.
377. Chen H, Li Z, Haruna K, Semba K, Araki M, Yamamura K, Araki K (2008) Early pre-implantation lethality in mice carrying truncated mutation in the RNA polymerase 1-2 gene. *Biochem Biophys Res Commun* 365: 636-642.

## Chapter 7

378. Uemura M, Zheng Q, Koh CM, Nelson WG, Yegnasubramanian S, De Marzo AM (2012) Overexpression of ribosomal RNA in prostate cancer is common but not linked to rDNA promoter hypomethylation. *Oncogene* 31: 1254-1263.
379. Poortinga G, Wall M, Sanij E, Siwicki K, Ellul J, Brown D, Holloway TP, Hannan RD, McArthur GA (2011) c-MYC coordinately regulates ribosomal gene chromatin remodeling and Pol I availability during granulocyte differentiation. *Nucleic Acids Res* 39: 3267-3281.
380. Barber BA, Liyanage VR, Zachariah RM, Olson CO, Bailey MA, Rastegar M (2013) Dynamic expression of MEIS1 homeoprotein in E14.5 forebrain and differentiated forebrain-derived neural stem cells. *Ann Anat* 195: 431-440.
381. Sanij E, Poortinga G, Sharkey K, Hung S, Holloway TP, Quin J, Robb E, Wong LH, Thomas WG, Stefanovsky V, Moss T, Rothblum L, Hannan KM, McArthur GA, Pearson RB, Hannan RD (2008) UBF levels determine the number of active ribosomal RNA genes in mammals. *J Cell Biol* 183: 1259-1274.
382. Cohen S, Gabel HW, Hemberg M, Hutchinson AN, Sadacca LA, Ebert DH, Harmin DA, Greenberg RS, Verdine VK, Zhou Z, Wetsel WC, West AE, Greenberg ME (2011) Genome-wide activity-dependent MeCP2 phosphorylation regulates nervous system development and function. *Neuron* 72: 72-85.
383. Onishchenko N, Karpova N, Sabri F, Castren E, Ceccatelli S (2008) Long-lasting depression-like behavior and epigenetic changes of BDNF gene expression induced by perinatal exposure to methylmercury. *J Neurochem* 106: 1378-1387.

## Chapter 7

384. Buzina A, Lo MY, Moffett A, Hotta A, Fussner E, Bharadwaj RR, Pasceri P, Garcia-Martinez JV, Bazett-Jones DP, Ellis J (2008) Beta-globin LCR and intron elements cooperate and direct spatial reorganization for gene therapy. *PLoS Genet* 4: e1000051.
385. Santoro R (2014) Analysis of Chromatin Composition of Repetitive Sequences: The ChIP-Chop Assay. In: Stockert CJ, Espada J, Blázquez-Castro A, editors. *Functional Analysis of DNA and Chromatin*. Totowa, NJ: Humana Press. pp. 319-328.
386. Xu Y, Wu F, Tan L, Kong L, Xiong L, Deng J, Barbera AJ, Zheng L, Zhang H, Huang S, Min J, Nicholson T, Chen T, Xu G, Shi Y, Zhang K, Shi YG (2011) Genome-wide regulation of 5hmC, 5mC, and gene expression by Tet1 hydroxylase in mouse embryonic stem cells. *Mol Cell* 42: 451-464.
387. Baubec T, Ivanek R, Lienert F, Schubeler D (2013) Methylation-dependent and -independent genomic targeting principles of the MBD protein family. *Cell* 153: 480-492.
388. Chinelo ED (2013) A Comparative Characterization of Methyl-CpG Binding Protein 2 Isoforms in the Developing and Adult Mouse Brain: University of Manitoba.
389. Lioy DT, Garg SK, Monaghan CE, Raber J, Foust KD, Kaspar BK, Hirrlinger PG, Kirchhoff F, Bissonnette JM, Ballas N, Mandel G (2011) A role for glia in the progression of Rett's syndrome. *Nature* 475: 497-500.
390. Ballas N, Lioy DT, Grunseich C, Mandel G (2009) Non-cell autonomous influence of MeCP2-deficient glia on neuronal dendritic morphology. *Nat Neurosci* 12: 311-317.

## Chapter 7

391. Garg SK, Liou DT, Knopp SJ, Bissonnette JM (2015) Conditional depletion of methyl-CpG-binding protein 2 in astrocytes depresses the hypercapnic ventilatory response in mice. *J Appl Physiol* (1985) 119: 670-676.
392. Shahbazian MD, Antalffy B, Armstrong DL, Zoghbi HY (2002) Insight into Rett syndrome: MeCP2 levels display tissue- and cell-specific differences and correlate with neuronal maturation. *Hum Mol Genet* 11: 115-124.
393. Akbarian S, Chen RZ, Gribnau J, Rasmussen TP, Fong H, Jaenisch R, Jones EG (2001) Expression pattern of the Rett syndrome gene MeCP2 in primate prefrontal cortex. *Neurobiol Dis* 8: 784-791.
394. Brero A, Easwaran HP, Nowak D, Grunewald I, Cremer T, Leonhardt H, Cardoso MC (2005) Methyl CpG-binding proteins induce large-scale chromatin reorganization during terminal differentiation. *J Cell Biol* 169: 733-743.
395. Yasui DH, Gonzales ML, Aflatooni JO, Crary FK, Hu DJ, Gavino BJ, Golub MS, Vincent JB, Carolyn Schanen N, Olson CO, Rastegar M, Lasalle JM (2014) Mice with an isoform-ablating *Mecp2* exon 1 mutation recapitulate the neurologic deficits of Rett syndrome. *Hum Mol Genet* 23: 2447-2458.
396. Mullaney BC, Johnston MV, Blue ME (2004) Developmental expression of methyl-CpG binding protein 2 is dynamically regulated in the rodent brain. *Neuroscience* 123: 939-949.
397. Maezawa I, Jin LW (2010) Rett syndrome microglia damage dendrites and synapses by the elevated release of glutamate. *J Neurosci* 30: 5346-5356.



## Chapter 7

398. Okabe Y, Takahashi T, Mitsumasu C, Kosai K, Tanaka E, Matsuishi T (2012) Alterations of gene expression and glutamate clearance in astrocytes derived from an MeCP2-null mouse model of Rett syndrome. *PLoS One* 7: e35354.
399. Wall M, Poortinga G, Hannan KM, Pearson RB, Hannan RD, McArthur GA (2008) Translational control of c-MYC by rapamycin promotes terminal myeloid differentiation. *Blood* 112: 2305-2317.
400. Bowman LH (1987) rDNA transcription and pre-rRNA processing during the differentiation of a mouse myoblast cell line. *Dev Biol* 119: 152-163.
401. Xie W, Ling T, Zhou Y, Feng W, Zhu Q, Stunnenberg HG, Grummt I, Tao W (2012) The chromatin remodeling complex NuRD establishes the poised state of rRNA genes characterized by bivalent histone modifications and altered nucleosome positions. *Proc Natl Acad Sci U S A* 109: 8161-8166.
402. Adkins NL, Georgel PT (2011) MeCP2: structure and function. *Biochem Cell Biol* 89: 1-11.
403. Georgel PT, Horowitz-Scherer RA, Adkins N, Woodcock CL, Wade PA, Hansen JC (2003) Chromatin compaction by human MeCP2. Assembly of novel secondary chromatin structures in the absence of DNA methylation. *J Biol Chem* 278: 32181-32188.
404. Hampson DR, Blatt GJ (2015) Autism spectrum disorders and neuropathology of the cerebellum. *Front Neurosci* 9: 420.

## Chapter 7

405. Apponi LH, Corbett AH, Pavlath GK (2013) Control of mRNA stability contributes to low levels of nuclear poly(A) binding protein 1 (PABPN1) in skeletal muscle. *Skelet Muscle* 3: 23.
406. Popov A, Smirnov E, Kovacik L, Raska O, Hagen G, Stixova L, Raska I (2013) Duration of the first steps of the human rRNA processing. *Nucleus* 4: 134-141.
407. Abelson HT, Johnson LF, Penman S, Green H Changes in RNA in relation to growth of the fibroblast: II. The lifetime of mRNA, rRNA, and tRNA in resting and growing cells. *Cell* 1: 161-165.
408. Jeffery L, Nakielny S (2004) Components of the DNA methylation system of chromatin control are RNA-binding proteins. *J Biol Chem* 279: 49479-49487.
409. Yazdani M, Deogracias R, Guy J, Poot RA, Bird A, Barde YA (2012) Disease modeling using embryonic stem cells: MeCP2 regulates nuclear size and RNA synthesis in neurons. *Stem Cells* 30: 2128-2139.
410. Akhmanova A, Verkerk T, Langeveld A, Grosveld F, Galjart N (2000) Characterisation of transcriptionally active and inactive chromatin domains in neurons. *J Cell Sci* 113 Pt 24: 4463-4474.
411. Mayer R, Brero A, von Hase J, Schroeder T, Cremer T, Dietzel S (2005) Common themes and cell type specific variations of higher order chromatin arrangements in the mouse. *BMC Cell Biol* 6: 44.

## Chapter 7

412. Su H, Kodiha M, Lee S, Stochaj U (2013) Identification of novel markers that demarcate the nucleolus during severe stress and chemotherapeutic treatment. *PLoS One* 8: e80237.
413. Smetana K, Klamova H, Jiraskova I, Subrtova H, Rosa L (1998) The number of nucleoli expressed by the nucleolar coefficient in the granulopoietic bone marrow compartment in non-leukemic persons and patients suffering from chronic myeloid leukemia. *Haematologica* 83: 476.
414. Payen E, Verkerk T, Michalovich D, Dreyer SD, Winterpacht A, Lee B, De Zeeuw CI, Grosveld F, Galjart N (1998) The centromeric/nucleolar chromatin protein ZFP-37 may function to specify neuronal nuclear domains. *J Biol Chem* 273: 9099-9109.
415. Zhang S, Hemmerich P, Grosse F (2004) Nucleolar localization of the human telomeric repeat binding factor 2 (TRF2). *J Cell Sci* 117: 3935-3945.
416. Jarboui MA, Bidoia C, Woods E, Roe B, Wynne K, Elia G, Hall WW, Gautier VW (2012) Nucleolar protein trafficking in response to HIV-1 Tat: rewiring the nucleolus. *PLoS One* 7: e48702.
417. Liang YM, Wang X, Ramalingam R, So KY, Lam YW, Li ZF (2012) Novel nucleolar isolation method reveals rapid response of human nucleolar proteomes to serum stimulation. *J Proteomics* 77: 521-530.
418. Jarboui MA, Wynne K, Elia G, Hall WW, Gautier VW (2011) Proteomic profiling of the human T-cell nucleolus. *Mol Immunol* 49: 441-452.

## Chapter 7

419. Lam YW, Evans VC, Heesom KJ, Lamond AI, Matthews DA (2010) Proteomics analysis of the nucleolus in adenovirus-infected cells. *Mol Cell Proteomics* 9: 117-130.
420. Andersen JS, Lam YW, Leung AK, Ong SE, Lyon CE, Lamond AI, Mann M (2005) Nucleolar proteome dynamics. *Nature* 433: 77-83.
421. Scherl A, Coute Y, Deon C, Calle A, Kindbeiter K, Sanchez JC, Greco A, Hochstrasser D, Diaz JJ (2002) Functional proteomic analysis of human nucleolus. *Mol Biol Cell* 13: 4100-4109.
422. Santoro R, Li J, Grummt I (2002) The nucleolar remodeling complex NoRC mediates heterochromatin formation and silencing of ribosomal gene transcription. *Nat Genet* 32: 393-396.
423. Guetg C, Lienemann P, Sirri V, Grummt I, Hernandez-Verdun D, Hottiger MO, Fussenegger M, Santoro R (2010) The NoRC complex mediates the heterochromatin formation and stability of silent rRNA genes and centromeric repeats. *EMBO J* 29: 2135-2146.
424. Santoro R, Schmitz KM, Sandoval J, Grummt I (2010) Intergenic transcripts originating from a subclass of ribosomal DNA repeats silence ribosomal RNA genes in trans. *EMBO Rep* 11: 52-58.
425. Nemeth A, Guibert S, Tiwari VK, Ohlsson R, Langst G (2008) Epigenetic regulation of TTF-I-mediated promoter-terminator interactions of rRNA genes. *EMBO J* 27: 1255-1265.
426. Li J, Langst G, Grummt I (2006) NoRC-dependent nucleosome positioning silences rRNA genes. *EMBO J* 25: 5735-5741.

## Chapter 7

427. Tseng H, Chou W, Wang J, Zhang X, Zhang S, Schultz RM (2008) Mouse ribosomal RNA genes contain multiple differentially regulated variants. *PLoS One* 3: e1843.
428. Frommer M, McDonald LE, Millar DS, Collis CM, Watt F, Grigg GW, Molloy PL, Paul CL (1992) A genomic sequencing protocol that yields a positive display of 5-methylcytosine residues in individual DNA strands. *Proc Natl Acad Sci U S A* 89: 1827-1831.
429. Orlic-Milacic M, Kaufman L, Mikhailov A, Cheung AY, Mahmood H, Ellis J, Gianakopoulos PJ, Minassian BA, Vincent JB (2014) Over-expression of either MECP2\_e1 or MECP2\_e2 in neuronally differentiated cells results in different patterns of gene expression. *PLoS One* 9: e91742.
430. Tan BC, Yang CC, Hsieh CL, Chou YH, Zhong CZ, Yung BY, Liu H (2012) Epigenetic silencing of ribosomal RNA genes by Mybbp1a. *J Biomed Sci* 19: 57.
431. Smetana K, Jiraskova I, Smetana K, Jr., Cermak J (2001) A short note on micronucleoli in the course of terminal maturation of human erythroblasts. *Folia Biol (Praha)* 47: 14-17.
432. Yasui DH, Xu H, Dunaway KW, Lasalle JM, Jin LW, Maezawa I (2013) MeCP2 modulates gene expression pathways in astrocytes. *Mol Autism* 4: 3.
433. Williams EC, Zhong X, Mohamed A, Li R, Liu Y, Dong Q, Ananiev GE, Mok JC, Lin BR, Lu J, Chiao C, Cherney R, Li H, Zhang SC, Chang Q (2014) Mutant astrocytes differentiated from Rett syndrome patients-specific iPSCs have adverse effects on wild-type neurons. *Hum Mol Genet* 23: 2968-2980.

## Chapter 7

434. Volk L, Chiu SL, Sharma K, Huganir RL (2015) Glutamate synapses in human cognitive disorders. *Annu Rev Neurosci* 38: 127-149.
435. Meldrum BS (1994) The role of glutamate in epilepsy and other CNS disorders. *Neurology* 44: S14-23.
436. Handstad T, Rye M, Mocnik R, Drablos F, Saetrom P (2012) Cell-type specificity of ChIP-predicted transcription factor binding sites. *BMC Genomics* 13: 372.
437. Conboy CM, Spyrou C, Thorne NP, Wade EJ, Barbosa-Morais NL, Wilson MD, Bhattacharjee A, Young RA, Tavaré S, Lees JA, Odom DT (2007) Cell cycle genes are the evolutionarily conserved targets of the E2F4 transcription factor. *PLoS One* 2: e1061.
438. Geisberg JV, Struhl K (2004) Quantitative sequential chromatin immunoprecipitation, a method for analyzing co-occupancy of proteins at genomic regions in vivo. *Nucleic Acids Res* 32: e151.
439. Toussaint M, Levasseur G, Tremblay M, Paquette M, Conconi A (2005) Psoralen photocrosslinking, a tool to study the chromatin structure of RNA polymerase I-transcribed ribosomal genes. *Biochem Cell Biol* 83: 449-459.
440. Guy J, Gan J, Selfridge J, Cobb S, Bird A (2007) Reversal of neurological defects in a mouse model of Rett syndrome. *Science* 315: 1143-1147.
441. Davis T, Vaisvila R (2011) High sensitivity 5-hydroxymethylcytosine detection in Balb/C brain tissue. *J Vis Exp*.

## Chapter 7

442. Santiago M, Antunes C, Guedes M, Sousa N, Marques CJ (2014) TET enzymes and DNA hydroxymethylation in neural development and function - how critical are they? *Genomics* 104: 334-340.
443. Mellen M, Ayata P, Dewell S, Kriaucionis S, Heintz N (2012) MeCP2 binds to 5hmC enriched within active genes and accessible chromatin in the nervous system. *Cell* 151: 1417-1430.
444. Brown K, Selfridge J, Lagger S, Connelly J, De Sousa D, Kerr A, Webb S, Guy J, Merusi C, Koerner MV, Bird A (2016) The molecular basis of variable phenotypic severity among common missense mutations causing Rett syndrome. *Hum Mol Genet* 25: 558-570.
445. Shen L, Zhang Y (2013) 5-Hydroxymethylcytosine: generation, fate, and genomic distribution. *Curr Opin Cell Biol* 25: 289-296.
446. Peedicayil J, Grayson DR, Avramopoulos D (2014) *Epigenetics in Psychiatry*: Elsevier Science.
447. Gavin DP, Kusumo H, Sharma RP, Guizzetti M, Guidotti A, Pandey SC (2015) Gadd45b and N-methyl-D-aspartate induced DNA demethylation in postmitotic neurons. *Epigenomics* 7: 567-579.
448. Sweatt JD (2013) The emerging field of neuroepigenetics. *Neuron* 80: 624-632.
449. Lister R, Mukamel EA (2015) Turning over DNA methylation in the mind. *Front Neurosci* 9: 252.

## Chapter 7

450. Heyward FD, Sweatt JD (2015) DNA Methylation in Memory Formation: Emerging Insights. *Neuroscientist* 21: 475-489.
451. Morris MJ, Monteggia LM (2014) Role of DNA methylation and the DNA methyltransferases in learning and memory. *Dialogues Clin Neurosci* 16: 359-371.
452. Gavin DP, Chase KA, Sharma RP (2013) Active DNA demethylation in post-mitotic neurons: a reason for optimism. *Neuropharmacology* 75: 233-245.
453. Wang KY, Chen CC, Shen CK (2014) Active DNA demethylation of the vertebrate genomes by DNA methyltransferases: deaminase, dehydroxymethylase or demethylase? *Epigenomics* 6: 353-363.
454. Becker A, Allmann L, Hofstatter M, Casa V, Weber P, Lehmkuhl A, Herve HD, Cardoso MC (2013) Direct homo- and hetero-interactions of MeCP2 and MBD2. *PLoS One* 8: e53730.
455. Cartron PF, Nadaradjane A, Lepape F, Lalier L, Gardie B, Vallette FM (2013) Identification of TET1 Partners That Control Its DNA-Demethylating Function. *Genes Cancer* 4: 235-241.
456. Kleiman R, Banker G, Steward O (1993) Inhibition of protein synthesis alters the subcellular distribution of mRNA in neurons but does not prevent dendritic transport of RNA. *Proc Natl Acad Sci U S A* 90: 11192-11196.
457. Zemp JW, Wilson JE, Schlesinger K, Boggan WO, Glassman E (1966) Brain function and macromolecules. I. Incorporation of uridine into RNA of mouse brain during short-term training experience. *Proc Natl Acad Sci U S A* 55: 1423-1431.



## Chapter 7

458. Krokowski D, Gaccioli F, Majumder M, Mullins MR, Yuan CL, Papadopoulou B, Merrick WC, Komar AA, Taylor D, Hatzoglou M (2011) Characterization of hibernating ribosomes in mammalian cells. *Cell Cycle* 10: 2691-2702.
459. Bai D, Zhang J, Li T, Hang R, Liu Y, Tian Y, Huang D, Qu L, Cao X, Ji J, Zheng X (2016) The ATPase hCINAP regulates 18S rRNA processing and is essential for embryogenesis and tumour growth. *Nat Commun* 7: 12310.
460. Schwanhausser B, Gossen M, Dittmar G, Selbach M (2009) Global analysis of cellular protein translation by pulsed SILAC. *Proteomics* 9: 205-209.
461. Kelleher RJ, 3rd, Govindarajan A, Jung HY, Kang H, Tonegawa S (2004) Translational control by MAPK signaling in long-term synaptic plasticity and memory. *Cell* 116: 467-479.
462. Aakalu G, Smith WB, Nguyen N, Jiang C, Schuman EM (2001) Dynamic visualization of local protein synthesis in hippocampal neurons. *Neuron* 30: 489-502.
463. Bramham CR, Wells DG (2007) Dendritic mRNA: transport, translation and function. *Nat Rev Neurosci* 8: 776-789.

## Appendix A: Reagents and Materials List

### A1. Cortical Neuron Isolation

#### Materials used

<b>Table A1. Reagents used in cortical neuron isolation</b>		
<b>Reagent Name</b>	<b>Company</b>	<b>Catalog Number</b>
Poly – D lysine	BD Biosciences	354210
Poly-L-ornithine	Sigma	P4957
Neurobasal Media	Life Technologies	21103-049
Pen/Strep*	Gibco	10378-016
B27	Gibco	17504-044
L-Glutamine*	Gibco	25030-081
CA	Sigma	C1768
Cysteine	Sigma	C-1276
EDTA	Gibco	15575-038
Papain	Worthington	3126
Ovomucoid	Sigma	T-9253
BSA (WB grade)	EMD	2930
Earle's Balanced Salt Solution (EBSS)	Gibco	14155-063
Hank's Balanced Salt Solution (HBSS)	Gibco	14025-092
DNase	Sigma	DN25

## Appendix

\*The Pen/Strep that we use already has Glutamine in it, therefore we do not add extra L-Glutamine in the Neurobasal media

### Other Materials

<b>Table A2. Other materials used in cortical neuron isolation</b>		
<b>Name</b>	<b>Company</b>	<b>Catalog Number</b>
Coverslips (12 mm)	Fisher	12-545-82
Fine scissors	FST	14058-11
Large forceps	FST	1108-15
Fine straight forceps	Dumont (or) FST	55 11255 - 29
Fine curved forceps	Dumont (or) FST	5-45 112531-35

### Reagent Preparation

#### **Poly-D-Lysine:**

Prepare 1% v/v (500 $\mu$ l in 50 ml) in sterile water.

## Appendix

### **Neuronal Culture Media**

Neurobasal media, 1% v/v Pen/Strep, 2% B27 supplement, 500 $\mu$ M L-Glutamine. For 50 ml media add 1 ml B27, 500 $\mu$ l Pen/Strep, 125 $\mu$ l L-glutamine.

### **Neuronal Selection Media**

Neuronal Culture Media + 7 $\mu$ M Cytosine Arabinoside (0.07% final CA concentration)

### **Papain Solution**

Add 1mg of Cysteine in 9ml of EBSS and 22.5 $\mu$ l of 200mM EDTA

Take 3 ml of the solution prepared in the previous step and add 43 $\mu$ l of 877U/ml papain suspension (final papain concentration about 10 U/ml)

Incubate at 37°C for at least 30 minutes to activate the papain.

### **10/10 Solution**

50 mg of BSA (WB grade) + 50 mg of ovomucoid in 5ml of EBSS

Let dissolve at 37°C and sterile filter before use.

### **1/10 Solution**

10/10 solution diluted 1:10 with EBSS (1ml of 10/10 solution + 9ml EBSS)

## Appendix

### DNase

Powder: 2000-3000 U/mg. 10mg of DNase in 10ml of 0.15M NaCl, store at -20°C.

### Cytosine Arabinoside

Stock solution: 1mM (store at -20°C)

Working Solution: Make a 12 $\mu$ M solution (4X)

### ACSF for dissection

<b>Component</b>	<b>Amount (for 100ml)</b>
2M NaCl	6.2 ml
1M KCl	0.5 ml
1M MgCl <sub>2</sub>	0.13 ml
155mM NaHCO <sub>3</sub>	16.9 ml
1M Glucose	1 ml
108 mM CaCl <sub>2</sub>	1.84 ml
1X antibiotic/antimycotic	1 ml

## A2. Primary astrocyte isolation and culture

### Materials Used

Appendix

<b>Table A4. Reagents used in primary astrocyte isolation and culture</b>		
<b>Reagent Name</b>	<b>Company</b>	<b>Catalog Number</b>
Poly – D lysine	BD Biosciences	354210
MEM	GIBCO	12360-038
Pen/Strep	GIBCO	10378-016
Papain	Worthington	3126
EBSS	GIBCO	14155-063
DNase	Sigma	DN25
HBSS	GIBCO	14025-092
Antibiotic-Antimycotic	GIBCO	15240-062

**Other Materials**

<b>Table A5. Other materials used in astrocyte culture</b>		
<b>Name</b>	<b>Company</b>	<b>Catalog Number</b>
Coverslips (12 mm)	Fisher	12-545-82
Fine Scissors	FST	14058-11
Large forceps	FST	1108-15

## Appendix

Fine straight forceps	Dumont (or)  FST	55   11255 - 29
Fine curved forceps	Dumont  (or)  FST	5-45   112531-35

### **Preparation of solutions and media**

#### **Astrocyte Media (10% FBS in MEM)**

MEM 500ml

FBS 50ml

Pen/Strep 5ml

#### **Papain**

Dissolve papain 40units/ml in HBSS-A (2mg/ml).

100mg in 50ml HBSS-A

Place in warm bath until dissolved

Filtered (0.22 $\mu$ m), divide into 1ml aliquots, store at  $-20^{\circ}\text{C}$

## Appendix

### **DNase (100mg/bottle, sigma cat# DN-25)**

Dissolve DNase (2mg/ml) in HBSS

100mg in 50ml HBSS

Place in warm bath until dissolved

Filter, divide into 1ml aliquots, store at -20°C.

### **A3. Salt shock total cell extraction buffer**

50 mM tris pH 8.0

150 mM NaCl

5 mM EDTA, pH 8.0

0.2% sodium deoxycholate

1% NP-40

50 mM NaF

1 mM sodium orthovanadate

Roche Complete Cocktail protease inhibitor